Cancer cell killing using engineered intracellular antibody fragments



Jennifer Susan Chambers

St. Peter's College

University of Oxford

A thesis submitted for the degree of

Doctor of Philosophy

Trinity 2018

(Word count 40,051)

The candidate confirms that the work submitted is her own and that appropriate credit has been given where reference has been made to the work of others.

Jennifer Susan Chambers

2018

University of Oxford

Acknowledgements

I would like to express my gratitude to the WIMM and the MRC for funding my work, and for giving me the opportunity to continue my scientific training. I would like to thank my thesis committee, Prof Tom Milne and Prof Alison Simmons, for their constructive and enthusiastic advice. I would also like to thank the members of the Rabbitts laboratory, past and present, who have been a source of support, advice and laughter along the way. In particular, I would like to acknowledge Dr Carole Bataille, Dr Osama Al-Assar and Dr Tim Brend for their input with parts of this project, and I am grateful to Dr Ami Miller for sharing reagents and for offering cheerful encouragement during the stressful moments. I would also like to acknowledge our clinical collaborators for providing research samples, and Kevin Clark and Sally-Ann Clark of the WIMM FACS facility for assistance with cell sorting.

I am thankful for the love and support of those closest to me over these last few years. There are too many to mention individually, but I am grateful to you all. My particular thanks go to my good friend Dr Rebecca Miller for providing encouragement and advice, and to my boyfriend Duncan for providing love, patience, comfort and humour in equal measure. I would also like to thank my mother Carolyn for being with me along this journey, and for her unconditional love and never-ending support.

Lastly, but most importantly, I would like to express my sincerest thanks and deepest gratitude to my supervisor, Prof Terry Rabbitts. This thesis would not have been possible without your guidance and support, your enthusiasm and your belief in me. You have taught me so much over the years and I am lucky to have worked with you. I will always remember you and your laboratory with fondness. Thank you for everything.

Abstract

Cancer is one of the leading causes of morbidity and death worldwide, with many either refractory to current therapy regimens or subsequently developing resistance. Novel targeted therapies are therefore needed. Acute T cell leukaemia (T-ALL) is an example of a malignancy without targeted therapies. It has a poor prognosis in adult patients and relapsed disease patients have only a 10% survival rate. T-ALL oncogenes include mutant RAS and aberrantly expressed LMO2, occurring in approximately 10-20% and 50% of cases respectively. There are currently no treatments specific for these oncogenes.

Intracellular expression of single domain VH antibodies raised against these targets has been shown to inhibit tumour growth in leukaemic models. These antibody fragments can target and disrupt the effect of oncogenic proteins and their downstream complexes. The aim of this thesis was to potentiate the effect of these antibodies by linking them to a cytotoxic domain to destroy tumour cells upon antibody-antigen interaction. This thesis describes a novel adaptation to a method of targeted cancer cell killing known as Antibody-antigen Interaction Dependent Apoptosis (AIDA). The results of this study show the ability of two single domain antibodies (VH and VL) linked to the inactive apoptotic enzyme proCaspase 3 to elicit RAS antigen-specific, antibody-mediated cancer cell death. This effect requires both antibody fragments to bind at close epitopes for proximity auto-activation of the caspase 3 enzyme. This thesis also describes the development of a mammalian screening strategy for isolation of VL antibody fragments complementary to antigen-binding VH, and a method of *in vitro* culture and testing of AIDA in T cell lines and primary tumours. Subject to further progress in therapeutic delivery methods, this approach is anticipated to be widely applicable to cancers caused by many different oncogenic proteins, following the development of synergistic antigen-specific antibody fragments.

Table of Contents

Acknowledgements ..... **i**

Abstract ..... **ii**

Table of Contents ..... **iii**

List of Figures ..... **vii**

List of Tables ..... **ix**

List of Abbreviations ..... **x**

List of amino acids ..... **xv**

List of DNA bases ..... **xvi**

Chapter 1 Introduction **1**

1.1 Human Cancers 2

1.1.1 Leukaemia *2*

1.1.2 Acute Lymphoblastic Leukaemia *4*

1.1.3 Acute T Cell Lymphoblastic Leukaemia *4*

1.1.3.1 Molecular causes of T-ALL *6*

1.2 LMO2 6

1.3.1 LMO2 structure *8*

1.3.2 LMO2 forms a DNA-binding complex *9*

1.3.3 LMO2 in haematopoiesis *13*

1.3.4 LMO2 in development *15*

1.3.5 LMO2 is an oncogene *15*

1.3.5.1 LMO2 causes clonal T cell tumours *15*

1.3.5.2 LMO2 in other cancers *17*

1.3.6 Mechanisms of LMO2 activation in T-ALL *17*

1.3.6.1 LMO2 activation by chromosomal translocation *18*

1.3.6.2 LMO2 activation by chromosomal deletion *18*

1.3.6.3 LMO2 activation by cryptic aberrations *20*

1.3.6.4 LMO2 activation following retroviral insertion *20*

1.3.7 LMO2 is a chromosomal translocation master gene *21*

1.3.8 Model of LMO2 oncogenesis *21*

1.4 RAS 24

1.4.1 RAS structure *24*

1.4.2 RAS in growth and development *25*

1.4.3 RAS mutations in cancer *27*

1.4.3.1 RAS mutations in T-ALL *29*

1.5 T-ALL Therapies 29

1.5.1 Potential anti-LMO2 therapies for T-ALL *30*

1.5.2 Potential anti-RAS therapies for T-ALL *31*

1.6 Antibodies and antibody fragments 32

1.6.1 Antibody Structure *32*

1.6.2 Isolation of intracellular VH and VL domain antibodies *35*

1.6.3 Linking single domain antibodies to effector functions *39*

1.7 Role of caspases in apoptosis 41

1.7.1 Caspase 3 as a cytotoxic effector domain *45*

1.8 Thesis aims 46

Chapter 2 Materials and Methods **50**

2.1 General methods 51

2.1.1 DNA and RNA Methods *51*

2.1.1.1 Agarose gel casting and electrophoresis *51*
2.1.1.2 RNA isolation *51*
2.1.1.3 cDNA Production *51*
2.1.2 Cloning Methods *52*
2.1.2.1 Preparation of plasmid vectors for cloning *52*
2.1.2.2 Calculation of pmol DNA ends *53*
2.1.2.3 Preparation of insert fragments for cloning *53*
2.1.2.4 Molecular cloning *55*
2.1.2.5 Plasmid propagation and purification *55*
2.1.2.6 Preparation of chemical competent E. coli *56*
2.1.2.7 Bacterial chemical transformation *56*
2.1.2.8 Bacterial electroporation *57*
2.1.2.9 Bacterial LB Growth Medium and Agar *57*
2.1.3 Protein Analysis Methods *58*
2.1.3.1 SDS-PAGE Gel Casting *58*
2.1.3.2 SDS-PAGE Gel Running *59*
2.1.3.3 SDS-PAGE Coomassie staining *60*
2.1.3.4 Western Blotting *60*
2.1.3.5 Bicinchoninic Acid (BCA) Assay of Protein Concentration *61*
2.2 Mammalian Cell Culture 63
2.2.1 Cell line growth medium *63*
2.2.2 Adherent cell line culture *63*
2.2.3 Non-adherent cell line culture *63*
2.2.4 Mouse and T-ALL tumour culture *64*
2.2.5 Cell Counting *64*
2.2.6 Cell cryopreservation *64*
2.2.7 Antibiotic selection titration *65*
2.2.8 General mammalian transfection *65*
2.2.8.1 Transient transfection *65*
2.2.8.2 Stable transfection *65*
2.2.9 Tetracycline (Tet) induction of TetOn constructs *66*
2.3 AIDA Assessment Methods 67
2.3.1 Construction of AIDA plasmids *67*
2.3.2 RAS mutation analysis *67*
2.3.3 Clonogenic assay *68*
2.3.4 Caspase 3 inhibitor assay *69*
2.3.5 PhiPhiLux Fluorogenic substrate assay *69*
2.3.6 PrestoBlue viability assay *70*
2.3.7 Annexin-V and 7-AAD flow cytometric profiling *70*
2.3.8 ApoToxGlo assay *71*
2.3.9 Cell cycle analysis *71*
2.3.10 Spheroid culture *72*
2.3.11 Luciferase assay *73*
2.4 Protein expression methods 74
2.4.1 Bacterial expression plasmids *74*
2.4.2 Bacterial expression of recombinant proteins *74*
2.4.3 Large-scale bacterial lysis *75*
2.4.4 Purification of Histidine-tagged proteins *76*
2.4.5 Loading $KRAS_{166}$G12V protein with guanosine 5'-[β,γ-imido] triphosphate (GMP.PNP) *77*
2.4.6 Size Exclusion Chromatography (SEC) of $KRAS_{166}$G12V protein *78*
2.4.7 Dialysis of VH-proCASP3 and VL-proCASP3 proteins *79*
2.4.8 Mammalian expression of VH-proCASP3 and VL-proCASP3 ..... *80*
2.4.9 FLAG affinity purification of VH-proCASP3 and VL-proCASP3 ..... *80*
2.5 *In vivo* experiments 81

2.5.1 AIDA clone xenografts 81
2.5.2 Human T-ALL propagation 82
2.6 Anti-LMO2 VL isolation experiments 82
2.6.1 Tumour cell flow cytometry 82
2.6.2 T cell line Fluorescence Activated Cell Sorting (FACS) 83
2.6.3 Lentivirus Methods 83
2.6.3.1 Lentivirus Constructs 83
2.6.3.2 Lentivirus Packaging 83
2.6.3.3 Lentivirus Titration 84
2.6.3.4 Lentivirus Transduction 84
2.6.4 Tripartite GFP Assay 84
2.6.5 VL Randomised CDR3 Library 85

Chapter 3 Initial assessment of AIDA against mutant RAS 86
3.1 Introduction 87
3.1.1 Aim 90
3.2 Confirmation of RAS mutation 90
3.3 AIDA stable cell lines 91
3.4 Assessment of clone phenotype 94
3.5 Cell viability changes 96
3.6 Apoptosis-associated cell membrane changes 96
3.7 Direct evidence of CASP3 activation 99
3.7.1 Fluorogenic substrate analysis 99
3.7.2 CASP3 inhibition 99
3.8 Protein purification for cell-free AIDA 102
3.8.1 Bacterial KRAS expression and purification 102
3.8.2 Mammalian Expression of VH- and VL-proCASP3 105
3.8.3 Improving VH-proCASP3 cytosolic yield 109
3.8.4 Large-scale mammalian expression of VH- and VL-proCASP3 112
3.8.5 Affinity Purification of VH- and VL-proCASP3 112
3.8.6 Bacterial expression of VH- and VL-proCASP3 115
3.8.7 Optimisation of VH- and VL-proCASP3 expression 117
3.8.8 Affinity purification of His-tagged VH- and VL-proCASP3 121
3.9 Discussion 126
3.10 Conclusion 128

Chapter 4 Testing AIDA antigen dependency and efficacy in tumour models… ……130
4.1 Introduction 131
4.1.1 Aim 134
4.2 Creation of mutant vectors and stable cell line characterisation 135
4.3 Apoptosis-related cell surface changes 137
4.4 Multiparameter assessment of apoptosis 139
4.4.1 ApoTox Glo cell viability measurements 139
4.4.2 ApoTox Glo cytotoxicity measurements 142
4.4.3 ApoToxGlo active CASP3 measurements 144
4.5 Effect upon the cell cycle and DNA degradation 144
4.6 Luciferase reporter confirmation of RAS-specific binding 148
4.7 Tumour recapitulation assays 150
4.7.1 Clonogenic assay 150
4.7.2 Tumour spheroid assessment 154
4.7.3 Preliminary in vivo study 158
4.8 Discussion 160
4.9 Conclusion 162

Chapter 5 Development of an *in vitro* VL screening method 163
5.1 Introduction 164
5.1.1 Aim 168
5.2 Initial assessment of screening by the tripartite GFP method 168
5.3 Modification of the tripartite GFP vectors 172
5.4 Expansion of the tripartite GFP screening test 174
5.5 Preparation of CDR3 randomised VL libraries 178
5.6 Discussion 182
5.7 Conclusion 183

Chapter 6 Development of a method for testing AIDA in T-ALL 184
6.1 Introduction 185
6.1.1 Aim 187
6.2 Culture of *Lmo2*-driven mouse T cell tumours 187
6.3 Propagation of T-ALL leukaemic samples *in vivo* 195
6.4 Trial *ex vivo* culture of T-ALL samples 197
6.5 Lentiviral vector cloning 203
6.6 Lentivirus transduction efficiency testing 205
6.7 Discussion 213
6.8 Conclusion….. 215

Chapter 7 General discussion and future work 216
7.1 General Discussion 217
7.1.1 The AIDA System targeting mutant RAS 217
7.1.2 Developing AIDA against LMO2 219
7.1.3 AIDA against other oncogenic targets 221
7.1.4 Potential Improvements to AIDA 223
7.1.5 AIDA as a clinical therapy 224
7.2 Conclusion 227

References 229

Appendix A 247

Appendix B 250

Appendix C 251

Appendix D 253

Appendix E 255

Appendix F 258

Appendix G 260

Appendix H 264

Appendix I 268

Appendix J 270

Appendix K 271

Appendix L 272

Appendix M 274

List of Figures

FIGURE 1.1 HAEMATOPOIETIC HIERARCHY 3
FIGURE 1.2 LMO2 AND THE LIM DOMAIN STRUCTURE 10
FIGURE 1.3 LMO2 TRANSCRIPTION FACTOR COMPLEX 11
FIGURE 1.4 LMO2 IN MOUSE DEVELOPMENT 14
FIGURE 1.5 *LMO2* ACTIVATION BY CHROMOSOMAL TRANSLOCATION 19
FIGURE 1.6 LMO2 ACTIVATION DURING X-SCID THERAPY TRIALS 22
FIGURE 1.7 MODEL OF LMO2-INDUCED T-ALL 23
FIGURE 1.8 RAS SIGNALLING 26
FIGURE 1.9 RAS MUTATION BIAS 28
FIGURE 1.10 ANTIBODY AND ANTIBODY FRAGMENT STRUCTURE 33
FIGURE 1.11 VH AND VL DOMAIN GENERAL SEQUENCE 36
FIGURE 1.12 VH#Y6 AND VL#204 IN COMPLEX WITH MUTANT RAS 40
FIGURE 1.13 EXTRINSIC AND INSTRINSIC APOPTOSIS PATHWAYS 43
FIGURE 1.14 STRUCTURAL COMPARISON OF THE PROCASPASES 44
FIGURE 1.15 SCHEMATIC DIAGRAM OF THE HYPOTHESISED AIDA METHOD 49
FIGURE 3.1 ILLUSTRATIONS OF THE CELL SURFACE CHANGES ASSOCIATED WITH CELL DEATH 89
FIGURE 3.2 CONFIRMATION OF HT1080TETON RAS MUTATION 92
FIGURE 3.3 ILLUSTRATION OF THE AIDA EXPRESSION CONSTRUCTS DESIGN 93
FIGURE 3.4 WESTERN BLOT ANALYSIS OF STABLE CLONE EXPRESSION 95
FIGURE 3.5 CELL VIABILITY CHANGES UPON EXPRESSION 97
FIGURE 3.6 ANNEXIN V AND 7-AAD MEMBRANE PROFILE ASSOCIATED WITH CELL DEATH 98
FIGURE 3.7 FLUOROGENIC SUBSTRATE ANALYSIS OF CASP3 ACTIVATION 100
FIGURE 3.8 EFFECT OF CASP3 INHIBITION UPON APOPTOTIC CELL MEMBRANE CHANGES 101
FIGURE 3.9 EFFECT OF CASP3 INHIBITION ON CELL VIABILITY 103
FIGURE 3.10 NICKEL PURIFICATION OF HIS-TEV-AVI-$KRAS_{166}$(G12V) 104
FIGURE 3.11 GMP.PNP LOADED KRAS SIZE EXCLUSION CHROMATOGRAPHY 106
FIGURE 3.12 CONFIRMATION OF KRAS PURIFICATION BY COOMASSIE STAINING 107
FIGURE 3.13 CONFIRMATION OF KRAS PURIFICATION BY WESTERN BLOT 108
FIGURE 3.14 CONFIRMATION OF MAMMALIAN VH- AND VL-PROCASP3 EXPRESSION 110
FIGURE 3.15 IMPROVING VH-PROCASP3 SOLUBILITY WITH NACL 111
FIGURE 3.16 LARGE-SCALE MAMMALIAN VH- AND VL-PROCASP3 PROTEINS 113
FIGURE 3.17 AFFINITY PURIFICATION OF VH- AND VL-PROCASP3 PROTEINS 114
FIGURE 3.18 BACTERIAL EXPRESSION TEST OF VH- AND VL-PROCASP3 116
FIGURE 3.19 BACTERIAL EXPRESSION TEST WITH REVERSIBLE CASP3 INHIBITOR 118
FIGURE 3.20 OPTIMISATION OF BACTERIAL VH-PROCASP3 EXPRESSION 119
FIGURE 3.21 OPTIMISATION OF BACTERIAL VL-PROCASP3 EXPRESSION 120
FIGURE 3.22 FURTHER OPTIMISATION OF BACTERIAL VH-PROCASP3 EXPRESSION 122
FIGURE 3.23 FURTHER OPTIMISATION OF BACTERIAL VL-PROCASP3 EXPRESSION 123
FIGURE 3.24 LARGE-SCALE PURIFICATION OF VH-PROCASP3 124
FIGURE 3.25 LARGE-SCALE PURIFICATION OF VL-PROCASP3 125
FIGURE 4.1 ILLUSTRATION OF THE AIDA CONSTRUCT MUTATIONS 132
FIGURE 4.2 CONFIRMATION OF VARIANT AIDA CONSTRUCT EXPRESSION 136
FIGURE 4.3 APOPTOSIS-ASSOCIATED CELL SURFACE CHANGES 138
FIGURE 4.4 APOTOXGLO CELL VIABILITY ASSAY 141
FIGURE 4.5 APOTOXGLO CYTOTOXICITY ASSAY 143
FIGURE 4.6 APOTOXGLO CASP3 ACTIVITY ASSAY 145
FIGURE 4.7 EFFECT OF CLONE EXPRESSION ON THE CELL CYCLE 147
FIGURE 4.8 LUCIFERASE REPORTER ASSAY 149
FIGURE 4.9 TRIPLEX PLASMID AND RAS ANTIGEN EXPRESSION CONFIRMATION 151
FIGURE 4.10 CLONOGENIC ASSAY 153
FIGURE 4.11 COLONY NUMBER DATA FROM THE CLONOGENIC ASSAY 155
FIGURE 4.12 REPRESENTATIVE TUMOUR SPHEROID IMAGES 156
FIGURE 4.13 TUMOUR SPHEROIDS FOR *IN VITRO* TUMOUR CAPITULATION 157
FIGURE 4.14 PRELIMINARY *IN VIVO* TUMOUR GROWTH ASSAY 159
FIGURE 5.1 SINGLE DOMAIN ANTIBODY LIBRARY SELECTION PROCESS 166

FIGURE 5.2 TRIPARTITE GFP RECONSTITUTION DIAGRAM 167
FIGURE 5.3 INITIAL TEST OF THE TRIPARTITE PLASMIDS 170
FIGURE 5.4 TRIPARTITE TEST WITH STABLE LMO2 EXPRESSION 171
FIGURE 5.5 COMPARISON OF GFP RECONSTITUTION IN DIFFERENT CELL LINES 173
FIGURE 5.6 CONFIRMATION OF TRIPARTITE PLASMID VH AND VL EXPRESSION 176
FIGURE 5.7 EXPANDED TRIPARTITE GFP ASSAY 177
FIGURE 5.8 GRAPHICAL REPRESENTATION OF THE TRIPARTITE ASSAY DATA 179
FIGURE 5.9 CDR3 RANDOMISED VL LIBRARIES 181
FIGURE 6.1 TRANSPLANTED *LCK-LMO2* T CELL TUMOUR PHENOTYPE 188
FIGURE 6.2 CULTURED *LCK-LMO2* CELL DIFFERENTIATION ANALYSIS: CD44/CD25 191
FIGURE 6.3 CULTURED *LCK-LMO2* CELL DIFFERENTIATION ANALYSIS: CD4/CD8 192
FIGURE 6.4 CELL COUNTS OF EXPANDED *LCK-LMO2* CULTURE 193
FIGURE 6.5 EXPANDED *LCK-LMO2* CULTURE DIFFERENTIATION ANALYSIS 194
FIGURE 6.6 PROPAGATION OF T-ALL SAMPLES 196
FIGURE 6.7 *EX VIVO* CULTURED T-ALL GROWTH CURVES 199
FIGURE 6.8 H1 SAMPLE DIFFERENTIATION ANALYSIS 200
FIGURE 6.9 4P SAMPLE DIFFERENTIATION ANALYSIS 201
FIGURE 6.10 CD8/CD44 ANALYSIS OF *EX VIVO* CULTURED T-ALL SAMPLES 202
FIGURE 6.11 LENTIVIRAL CONSTRUCT EXPRESSION TEST 204
FIGURE 6.12 MRUBY2 LENTIVIRAL VECTOR EXPRESSION TEST 206
FIGURE 6.13 FLUORESCENT IMAGES OF LENTIVIRAL REPORTER EXPRESSION 207
FIGURE 6.14 TITRATION OF LENTIVIRUS-LIKE PARTICLES INTO HEK293T CELLS 209
FIGURE 6.15 LENTIVIRAL TRANSDUCTION OF T CELL LINES 210
FIGURE 6.16 ASSESSMENT OF LONG-TERM MRUBY2 EXPRESSION 211
FIGURE 6.17 RT-PCR CONFIRMATION OF MRUBY2 EXPRESSION 212

List of Tables

TABLE 1.1 COMMON MUTATIONS IN T-ALL 7
TABLE 1.2 ENGINEERED VH AND SCFV KINETIC DATA 38
TABLE 2.1 PHUSION POLYMERASE PCR REACTION SET UP 54
TABLE 2.2 KOD POLYMERASE PCR REACTION SET UP 54
TABLE 2.3 TOUCHDOWN PCR PROGRAM 55
TABLE 2.4 RESOLVING GEL CASTING SET UP 58
TABLE 2.5 STACKING GEL CASTING SET UP 59
TABLE 2.6 ANTIBODIES FOR WESTERN BLOT 61
TABLE 2.7 BSA DILUTIONS FOR BCA ASSAY STANDARDS 62
TABLE 4.1 VH#Y6 VARIANT SEQUENCES 133
TABLE 4.2 SUMMARISED DATA OF APOPTOSIS-RELATED CELL SURFACE CHANGES 140
TABLE 6.1 CULTURED *LCK-LMO2* TUMOUR CELL COUNTS 189
TABLE 6.2 T-ALL TRANSPLANT POST-MORTEM CELL COUNTS 198

List of Abbreviations

7-AAD	7-Amino actinomycin D
AAV	Adeno-associated virus
AD	Activation domain
AFC	7-Amino-4-trifluoromethyl coumarin
AIDA	Antibody interaction dependent apoptosis
ALL	Acute lymphoblastic leukaemia
APS	Ammonium persulphate
ATP	Adenosine triphosphate
BCA	Bicinchoninic acid
βGal	βGalactosidase
BiFC	Bimolecular fluorescence complementation
bp	base pair
BSA	Bovine serum albumin
CAD	Caspase activated Dnase
CAR	Chimaeric antigen receptor
CARD	Caspase recruitment domain
CASP3	Caspase 3
cDNA	complementary DNA
CDR	Complementarity determining region
CLP	Common lymphoid progenitor
DARPin	Directed ankyrin repeat protein
DBD	DNA binding domain
DED	Death effector domain
DEPC	Diethlypyrocarbonate
DL1	Delta-like 1

DMEM	Dulbecco's Modified Eagle Medium
DMSO	Dimethyl sulphoxide
DN	Double negative
DNA	Deoxyribonucleic acid
dNTP	Deoxyribonucleotide triphosphate
DP	Double positive
DTT	Dithiothreitol
E. coli	Escherichia coli
EDTA	Ethylenediamine tetraacetic acid
ES	Embryonic stem
EtOH	Ethanol
ETP	Early T cell progenitor
Fab	Fragment antigen binding
FBS	Foetal bovine serum
Fc	Fragment crystallisable
FITC	Fluorescein isothiocyanate
FSC	Forward scatter
Ftase	Farnesyltransferase
g	Grams
g	Gravity
GDP	Guanosine diphosphate
GFP	Green fluorescent protein
GGTase	Geranylgeranyltransferase
GMP.PNP	5'-Guanylyl imidodiphosphate
GTP	Guanosine triphosphate
GTPase	Guanosine triphosphatase
HA	Haemagglutinin

HCl	Hydrochloric acid
HEPES	4-(2-Hydroxyethyl)-1-piperazineethanesulfonic acid
HRP	Horseradish peroxidase
HSC	Haematopoietic stem cell
IAC	Intracellular antibody capture
Ig, IG	Immunoglobulin (protein, gene)
IL	Interleukin
IMDM	Icove's Modified Dulbecco's Medium
IPTG	Isopropyl β-D-1-thiogalactopyranoside
KCM	Potassium, calcium, magnesium
Kd	Dissociation constant
kDa	Kilo Daltons
L	Litre
LB	Luria Bertani
LMO	LIM domain only
m	Metre
M	Molar
MEM	Minimal essential medium
MOI	Multiplicity of infection
mRNA	messenger RNA
MWCO	Molecular weight cut off
NaCl	Sodium Chloride
NaOH	Sodium hydroxide
Nfarn	N-terminal farnesylation
Ni	Nickel
Ni-NTA	Nickel nitrotriacetic
NSG	NOD SCID Gamma

O.D.	Optical density
PBS	Phosphate-buffered saline
PCR	Polymerase chain reaction
PE	Phycoerythrin
Psi	Pounds per square inch
PVDF	Polyvinylidene fluoride
R110	Rhodamine 100
RAG	Recombination activating gene
RNA	Ribonucleic acid
Rpm	Revolutions per minute
RPMI medium	Roswell Park Memorial Institute medium
RT	Room temperature
RT-PCR	Reverse transcription PCR
rtTA	reverse tetracycline transactivator
scFv	single chain Fragment variable
SDS	Sodium dodecyl sulphate
SDS-PAGE	Sodium dodecyl sulphate polyacrylamide gel electrophoresis
SEC	Size exclusion chromatography
SP	Single positive
SSC	Side scatter
TAE	Tris-acetate EDTA
TBE	Tris-borate EDTA
TBS	Tris-buffered saline
TR	T cell receptor
TEMED	N,N,N',N'-tetramethylene-1,2-diamine
Tet	Tetracycline
TU	Transducing units

U.V.	Ultraviolet
VH	Variable heavy domain
VL	Variable light domain
WHO	World Health Organisation
X-SCID	X-linked severe combined immunodeficiency
YFP	Yellow fluorescent protein
Z-DEVD-FMK	Benzyloxycaronyl-Asp(OMe)-Glu(OMe)-Val-Asp(OMe)-fluoromethylketone

List of amino acids

Amino Acid	Three letter code	Single letter code
Alanine	Ala	A
Cysteine	Cys	C
Aspartic Acid	Asp	D
Glutamic Acid	Glu	E
Phenylalanine	Phe	F
Glycine	Gly	G
Histidine	His	H
Isoleucine	Ile	I
Leucine	Leu	L
Methionine	Met	M
Asparagine	Asn	N
Proline	Pro	P
Glutamine	Gln	Q
Arginine	Arg	R
Serine	Ser	S
Threonine	Thr	T
Valine	Val	V
Tryptophan	Trp	W
Tyrosine	Tyr	Y

N.B. The one letter code ‘X’ refers to any amino acid reside.

List of DNA bases

Single Letter Code	Base	Description
A	Adenine	purine, amino
C	Cytosine	pyrimidine, amino
G	Guanine	purine, ketone
T	Thymine	pyrimidine, ketone
R	A or G	any purine base
Y	C or T	any pyrimidine base
S	G or C	‘strong’ bonding
W	A or T	‘weak’ bonding
K	G or T	any ketone base
M	A or C	any amino base
B	not A	(C, G or T/U)
D	not C	(A, G or T/U)
H	not G	(A, C or T/U)
V	not T (or U)	(A, C or G)
N	any base	(A, C, G or T/U)
-	gap	no base

Chapter 1 Introduction

1.1 Human Cancers

Collectively, cancer is the second leading cause of mortality worldwide (World Health Organization, 2015). Cancers may arise in almost any somatic cell, occurring when the tightly controlled process of cell division and apoptosis are deregulated or dysfunctional, permitting unchecked malignant growth (Hanahan and Weinberg, 2011). The cellular defects leading to overt tumour formation are many and varied. As such, cancers are typically reported as separate diseases according to their original tissue type, growth characteristics and molecular alterations (O'Sullivan et al., 2017). Indeed, most cancers form solid tumours but malignancies of the blood are commonly diffuse owing to the nature of the cells. Blood cancers encompass various diseases, including leukaemia, lymphoma and myeloma (Allart-Vorelli et al., 2015).

1.1.1 Leukaemia

Leukaemia is a malignancy of the blood, which originates in the bone marrow or at extramedullary sites. It is the most common type of blood cancer (Allart-Vorelli et al., 2015) and can be subdivided into myeloid or lymphoid leukaemia depending upon the originating cell-type (Hamerschlak, 2008). The haematopoietic hierarchy (Figure 1.1) illustrates the lineage of the lymphoid and myeloid cells. The accepted model shows differential specification of haematopoietic stem cells (HSCs) along either the myeloid or lymphoid pathways, with the final mature cells occupying distinct roles within the blood system (Zhang et al., 2018).

Myeloid leukaemia can develop from red blood cell precursors, platelet-making megakaryocytes or myeloid-biased leukocytes (white blood cells) such as neutrophils, basophils or monocytes. In contrast, lymphoid leukaemia arises from lymphocyte progenitor cells, and can be further sub-categorised into B or T cell lymphoid (or lymphoblastic) leukaemia. Both types of leukaemia may be either acute or chronic in nature. Acute leukaemia derives from immature progenitor cells retaining stem-like characteristics, whereas chronic leukaemias tend to have more of

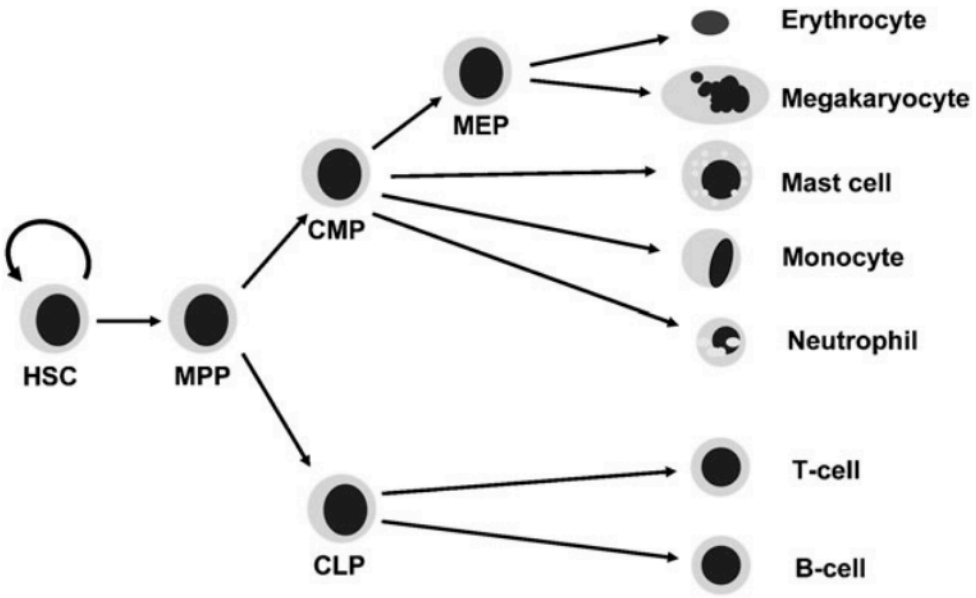

Figure 1.1 Haematopoietic hierarchy

Simplified diagram to represent mature blood cell specification into myeloid and lymphoid lineages. The haematopoietic stem cell (HSC) is situated at the apex of the hierarchy. It has self-renewing properties to maintain the stem cell pool within the bone marrow. Blood cell production initiates from HSCs giving rise to multipotent progenitors (MPPs). The MPP further differentiate into myeloid or lymphoid restricted progenitor populations, either the common myeloid progenitor (CMP) or common lymphoid progenitor (CLP). The myeloid pathway bifurcates from the CMP into either the megakaryocyte and erythroid lineages via the megakaryocyte-erythroid progenitor (MEP), or into the granulocytic pathway to produce granulocytes including mast cells, monocytes, neutrophils. The lymphoid specification from the CLP leads to the mature B and T lymphocytes. T cells undergo a multistep maturation process in the thymus. B cells can further differentiate into antibody secreting plasma cells or memory cells within the germinal centres. Figure reproduced from (Foster et al., 2009) with permission from The Royal Society of Chemistry.

a matured phenotype, and can often partially function as normal, mature blood cells (Kipps et al., 2017). Chronic leukaemia is typified by a slow disease progression, which can affect patients for many years. However, acute leukaemia has much faster disease progression, often proving fatal within months if left untreated (Khwaja et al., 2016).

1.1.2 Acute Lymphoblastic Leukaemia

Acute Lymphoblastic Leukaemia (ALL) is not a single disease but rather a family of related malignancies (Terwilliger and Abdul-Hay, 2017). As such, they can possess differences in disease outlook and progression, leading to variation in their response to conventional therapies. The WHO classification of ALL types first segregates them according to the type of lymphocyte affected (Arber et al., 2016); precursor B cell or precursor T cell ALL (B-ALL and T-ALL respectively) are the most common. B-ALL can be further sub-divided into possession of recurrent cytogenetic abnormalities versus non-specified abnormalities. T-ALL is not sub-divided for clinical classification, except for the provisional classification of early T cell progenitor T-ALL (ETP-ALL) due to it aligning more closely with B-ALL.

1.1.3 Acute T Cell Lymphoblastic Leukaemia

Acute T cell lymphoblastic leukaemia (T-ALL) is an aggressive neoplastic proliferation of immature lymphoid progenitors, affecting the bone marrow, thymus and lymph nodes. It comprises approximately 20-25% of total ALL cases (Marks et al., 2009). It is usually regarded as a paediatric disease as the majority of cases occur in children of late childhood to early adolescence, with T-ALL encompassing 12-15% of total paediatric ALL cases (Schneider et al., 2000). However, 25% of T-ALL cases occur in adults, usually after the age of 50. The risk of childhood and adult T-ALL is slightly higher in males and Caucasian populations (Dores et al., 2012, Crist et al., 1988).

B-ALL and T-ALL prevalence and survival statistics are usually combined in reported figures, and both leukaemias are subject to the same treatment regimen, with the exception of some B-ALL targeted therapies (Terwilliger and Abdul-Hay, 2017). Recent investigations are only just beginning to unravel the clinical and prognostic differences between subtypes of ALL (Marks et al., 2009, Van Vlierberghe and Ferrando, 2012). Adult-onset T-ALL has a poorer disease prognosis than childhood T-ALL; while 80-90% of patients initially respond to treatment, approximately half of the adult cohort relapse within 5-10 years. Of these relapsed cases, only 7-10% survive (Pui et al., 2004, Marks and Rowntree, 2017). The reason for this disjuncture between adult and childhood T-ALL is unknown, although it is postulated that they may be separate diseases, with adult T-ALL blast cells more resistant to therapy (Plasschaert et al., 2004).

Diagnosis of T-ALL is dependent on a combination of morphologic, immunophenotypic and genetic characteristics of the neoplasm (Jevremovic et al., 2016). Upon histological analysis, T-ALL morphology is exemplified by an infiltration of small to medium-sized precursors (also known as blast) cells into the bone marrow, thymus, and sometimes with involvement of the lymph nodes and spleen. These cells show their immature stage with a network mesh of fine chromatin (Jevremovic et al., 2016) rather than the distinct, condensed chromatin of more mature cells. T-ALL can also be defined by the presence of immunophenotypic markers such as the pan-T cell marker CD3, markers of cell immaturity such as CD34, CD99 and CD1a, and even by the abnormal presence of myeloid markers CD13 and CD33 (Jevremovic et al., 2016). Lastly, recurrent cytogenetic features are linked with T-ALL, such as clonal T cell receptor (TR) rearrangements indicating a transformed population in addition to many other gross genetic abnormalities, such as chromosomal translocations.

1.1.3.1 Molecular causes of T-ALL

T-ALL is the result of malignant transformation events occurring in haematopoietic cells undergoing thymocyte development (Crist et al., 1988, Van Vlierberghe and Ferrando, 2012). These events encompass chromosome translocations, deletions and inversions or gene mutations. These typically result in either the activation of oncogenes or the inactivation of tumour suppressor genes. However, the development of frank neoplasia is often the result of multiple, cooperative events (Van Vlierberghe and Ferrando, 2012). Indeed, it has been estimated that 10 or more such genomic lesions may act in concert to result in a fully transformed thymocyte (Girardi et al., 2017).

Many common recurrent abnormalities have been found in T-ALL cases (Girardi et al., 2017) (Table 1.1). These include mutations in NOTCH1, NRAS and KRAS, resulting in their constitutive activation and signalling, chromosomal deletions that result in the loss of the cyclin dependent kinase inhibitor 2A (*CDKN2A*) tumour suppressor gene, and aberrant expression of oncogenic transcription factors such as the LIM-domain-only 2 (LMO2) master transcriptional regulator following chromosomal translocations or deletions.

This thesis will focus on T-ALL associated with aberrant LMO2 expression and mutant RAS. LMO2 has been found in almost 50% of T-ALL cases (Ferrando et al., 2002) whilst *RAS* mutations are present in 10-20% of T-ALL cases (Girardi et al., 2017). The biology and aetiology of LMO2 and mutant RAS mediated leukaemogenesis will be discussed in following sections of this introductory chapter, in addition to the status of current therapies and the rationale for further targeted treatments.

1.2 LMO2

LIM-Domain Only 2 (LMO2, formerly Rhombotin-2, RBTN2, Ttg-2) belongs to the LIM-domain-only (LMO) gene family of transcriptional activators, so-called

Gene	Classification	Type of genetic aberration	% Frequency in T-ALL	
			Paediatric	Adult
LMO2	Transcription factor	Chromosomal translocation/ rearrangement, deletions Expression	13	21
TAL1		Chromosomal translocation/ rearrangement, deletions Expression	30	34
NOTCH1	Signaling	Chromosomal rearrangement Inactivating mutations	50	57
KRAS		Activating mutations	6	0
NRAS		Activating mutations	14	9
CDKN2A	Cell Cycle	Locus deletion	61	55

Table 1.1 Common mutations in T-ALL

Common, recurrent abnormalities have been found to occur in T-ALL. The mutations listed are representative of some of the affected genes relevant to this thesis. The type of mutation affecting each gene is indicated, alongside the frequency of their involvement in adult and paediatric cohorts. The data displayed was compiled by Girardi et al (Girardi et al., 2017), referencing chromosomal rearrangements, copy number variation and gene mutations, in addition to gene expression data (transcription factors only). Table adapted from (Girardi et al., 2017) with permission from the American Society of Hematology.

because their protein structure contains just two LIM-domains. The nuclear LMO-family consists of four, highly homologous members (LMO1, 2, 3 and 4) (Matthews et al., 2013).

Human LMO2 is a 158 amino acid protein coded from the last three exons of a 6 exon gene located on the short arm of chromosome 11 at band 13p. As with *LMO1* (Boehm et al., 1990, Boehm et al., 1991b), *LMO2* has two major transcriptional promoters resulting in two alternative transcripts (Royer-Pokora et al., 1995) with a third 'intermediate' promoter that has been shown to sustain leukaemogenesis via a feedback loop (Oram et al., 2010). LMO2 acts as a master transcriptional activator, and is essential for nucleating a multimeric transcription factor complex to drive gene expression (Valge-Archer et al., 1994, Wadman et al., 1997, Wadman et al., 1994, Osada et al., 1995). Early gene expression analyses showed LMO2 is widely expressed during development (Foroni et al., 1992, Boehm et al., 1991b, Neale et al., 1995) and is essential during primitive (Warren 1994 Cell) and definitive (Yamada et al., 1998) haematopoiesis. LMO2 is also a key factor during vascular remodelling as part of angiogenesis (Yamada et al., 2000) and is found in developing CNS tissue (Foroni et al., 1992). LMO2 has no essential function during lymphopoiesis (McCormack et al., 2003) and has very low expression levels in the thymus (Kenny et al., 1998, Neale et al., 1995, Foroni et al., 1992) and in very early CD4 and CD8 double negative (DN1, DN2 stage) T cell populations (Herblot et al., 2000). LMO2 is absent from mature thymocytes except transformed T cells (Royer-Pokora et al., 1995, Foroni et al., 1992) thus indicating that activation mechanisms such as chromosomal translocations, deletions or insertions are necessary to induce LMO2 expression.

1.3.1 LMO2 structure

The LIM domain, named after the Cysteine-Histidine region of the transcription factors Lin-11, Isl-1 and Mec-3 (Freyd et al., 1990, Karlsson et al., 1990,

Way and Chalfie, 1988), are cysteine-rich motifs which fold into two finger-like projections. Each finger coordinates one zinc (Zn) atom (Archer et al., 1994) which stabilises the finger structure and is therefore crucial for the formation and maintenance of protein interactions. LMO2 posses two of these regions, arranged in tandem, known as the LIM1 and LIM2 domains (Figure 1.2). The zinc atoms are coordinated by the side-chains of four amino acids; three cysteine resides and one histidine (Finger 1) or three cysteine residues with one aspartic acid residue (Finger 2). The polypeptide chain between these complexed residues fold as two perpendicular anti-parallel β-sheets, which are thrust outward to form the LIM fingers (Perez-Alvarado et al., 1996). The two amino acid linker region between the two fingers of each domain is crucial for conferring the target specificity of the LMO-protein (Schmeichel and Beckerle, 1997). The LIM domains zinc-finger-like structures are distinct from the DNA-binding zinc finger motifs possessed by many transcription factors, as the LIM fingers participate in protein interactions rather than directly binding DNA (Sadler et al., 1992, Valge-Archer et al., 1994, Schmeichel and Beckerle, 1997, Wadman et al., 1997).

1.3.2 LMO2 forms a DNA-binding complex

As LMO2 contains only LIM domains, it is unable to elicit effect through direct DNA binding. Rather, LMO2 bridges a bipartite, multiprotein DNA-binding complex nucleated through the protein:protein interactions of the LIM fingers (Figure 1.3). This LMO2-nucleated complex contains several transcription factors, in addition to a stabilising protein, LIM-domain-binding protein 1 (LDB1, also known as CLIM2, NLI) (Agulnick et al., 1996, Jurata et al., 1996). LDB1 is part of the LMO2-complex in both erythroid cells (Wadman et al., 1997, Agulnick et al., 1996) and in LMO2-transgenic thymocytes (Grutz et al., 1998). LDB1 has no known enzymatic function or DNA-binding ability, rather it is thought to act as a protein binding adapter (Matthews and Visvader, 2003), being able to homodimerise to bring together two LMO2 complexes

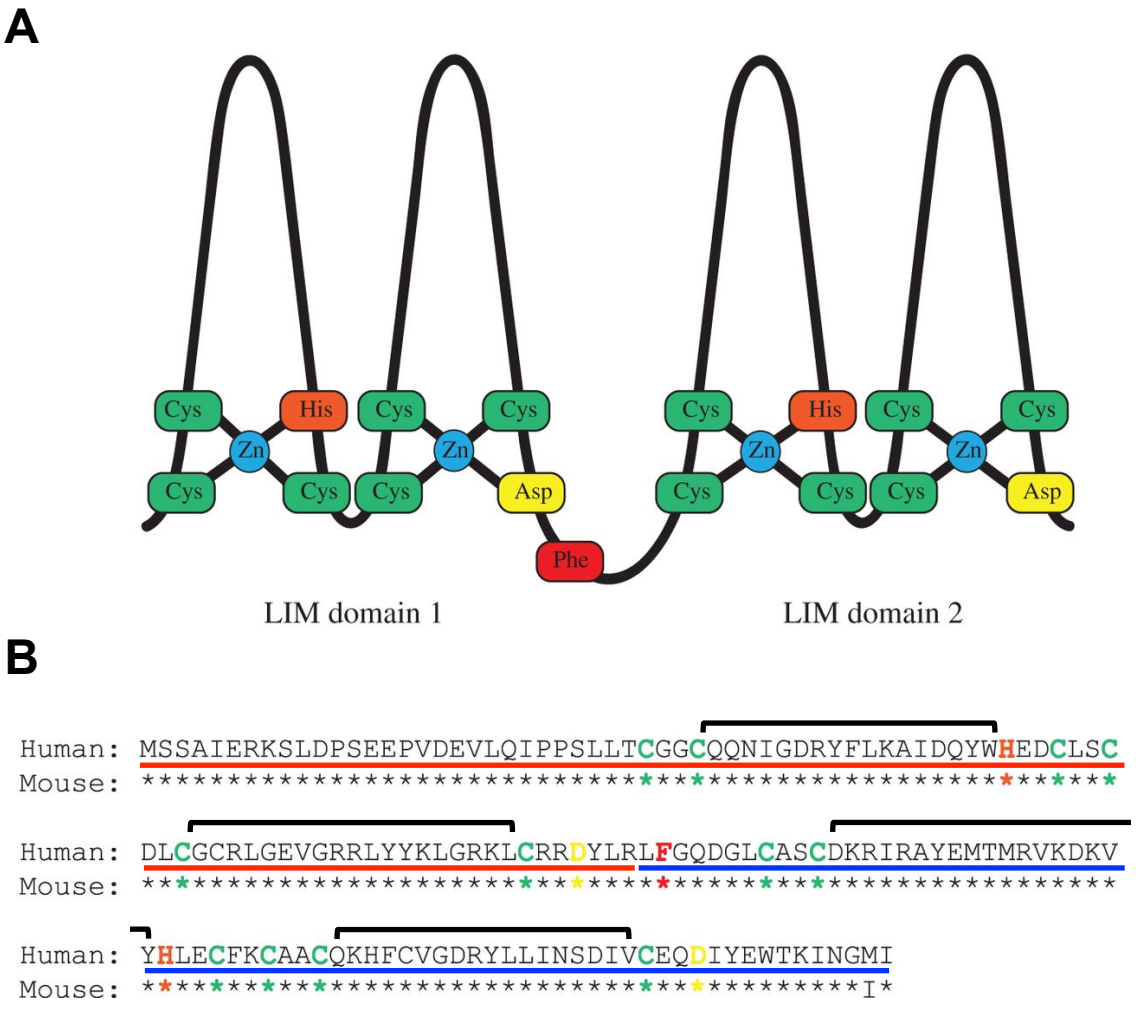

Figure 1.2 LMO2 and the LIM domain structure

A: Cartoon illustration of the LIM domains of LMO2. LMO2 contains two tandemly arranged LIM domains, separated by a flexible hinge region containing phenylalanine (El Omari et al., 2011). The two LIM domains are thought to be evolutionarily conserved to confer functional specificity, as each domain shows greater homology with the equivalent LIM domain in orthologues than they do with additional LIM domains within the same protein (Gill, 1995). The LIM domains each possess two LIM fingers, each coordinating a zinc atom between four residues. The peptide sequence of the linker region between the LIM fingers of each domain is critical for specification of subsequent protein-protein interaction. B: Alignment of human and mouse LMO2 amino acid sequence. The 158 residue sequence shows near identical homology between the two species. The key structural residues from A are highlighted in the same colour. Green, cysteine; Orange, histidine; yellow, aspartate; red, phenylalanine. The two LIM domains are shown underlining the human amino acid sequence (LIM1, red line, LIM2, blue line). The four LIM fingers are shown as black brackets above the sequence. Figure reproduced and adapted from (Chambers and Rabbitts, 2015) under the creative commons licence CC BY 4.0.

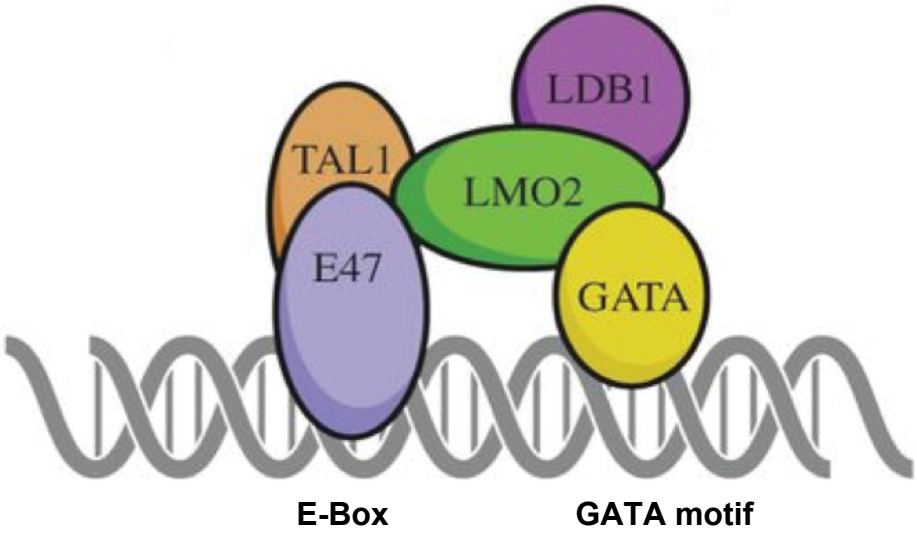

Figure 1.3 LMO2 transcription factor complex

LMO2 nucleates a transcription factor complex by forming protein-protein interactions. LDB1 binding to LMO2 acts to stabilise the LMO2 structure, leaving the LIM fingers available to mediate further protein interactions with TAL1 and GATA zinc-finger transcription factors. LMO2 does not contact DNA directly, but rather acts to bridge the TAL1/E47 dimer and GATA factor, allowing the complex to recognise the bipartite E-box-GATA motif, with each sequence separated by approximately 9 base pairs. Leukaemic cells have demonstrated an altered version of this complex, nucleating two TAL1/E47 dimers which in turn recognise an E-box-E-box motif. Reproduced from (Chambers and Rabbitts, 2015) under the creative commons licence CC BY 4.0.

at promoters and distal enhancers into proximity (Krivega et al., 2014). LDB1 provides structural stability to LMO2, binding across both LIM domains (LIM1 and LIM2) but on the opposite face to the LIM fingers (El Omari et al., 2013, El Omari et al., 2011, Matthews et al., 2001, Deane et al., 2001), leaving them unoccupied to permit the other protein interactions of the complex (El Omari et al., 2011). Moreover, the region between both the LIM domains of LMO2 and the corresponding region in the LDB1 act as a hinge, allowing the LIM domains to maintain their secondary structure but with the ability to adopt conformational flexibility (El Omari et al., 2011).

LMO2 has been shown to directly interact with class II basic Helix-Loop-Helix (bHLH) transcription factors including TAL1 (TCL5, SCL) in erythroid cells (Valge-Archer et al., 1994) and with TAL1, TAL2 and LYL1 in leukaemic cells (Wadman et al., 1994). Interestingly, TAL1 is also a T-cell oncogene (Begley et al., 1989, Finger et al., 1989, Baer, 1993, Larson et al., 1996, Ono et al., 1997). The E2A gene product proteins E12 and E47 have been found within the LMO2-multiprotein complex (Wadman et al., 1997). TAL1 forms heterodimers with the E protein transcription factors (Hsu et al., 1991, Hsu et al., 1994), explaining their presence in the LMO2-complex without direct LMO2 binding (Wadman et al., 1994).

The LMO2-complex also includes GATA-family transcription factors (Valge-Archer et al., 1994, Wadman et al., 1997, Osada et al., 1995, Ono et al., 1998, Manaia et al., 2000). The GATA-family of transcription factors are zinc finger DNA-binding proteins, their name derived from their consensus recognition sequence (Evans et al., 1988, Wall et al., 1988, Orkin, 1992). GATA-1, GATA-2 and GATA-3 are expressed during blood, CNS and endothelial specification and development (Simon, 1995, Lentjes et al., 2016). Only GATA-3 expression occurs in T lymphocytes (Ho et al., 1991, Marine and Winoto, 1991, Ko and Engel, 1993) making it the likely GATA factor bound in LMO2-expressing leukaemias (Ono et al., 1998).

Taken together, these basic elements of the LMO2-complex mediate recognition of a bipartite DNA sequence, comprising of an E box (via the TAL1/E47

heterodimer) and a GATA motif (through the binding of GATA-1/GATA-2/GATA-3). The LMO2-complex has been demonstrated to be capable of substituting the GATA-factor for a second TAL1/E protein heterodimer in erythroid cells at the cKit promoter (Vitelli et al., 2000) and in LMO2-transgenic tumours (Grutz et al., 1998) to recognise an E box-E box motif. This suggests that LMO2 is capable of nucleating different complexes to suit different cellular and developmental situations.

1.3.3 LMO2 in haematopoiesis

LMO2 is critical for haematopoiesis. Homozygous *Lmo2*-null mutations proved lethal in utero at embryonic stage E9-E10.5, with a complete lack of erythroid cells despite normal yolk sac architecture (Warren et al., 1994) (Figure 1.4A). This demonstrated that *Lmo2* was essential in mouse primitive erythropoiesis. A similar phenotype had already been demonstrated in *Gata1* and *Gata-2*-null embryos (Pevny et al., 1991, Simon et al., 1992, Tsai et al., 1994) and was later also shown in *Tal1*-null embryos (Shivdasani et al., 1995, Robb et al., 1995), paralleling with the LMO2 transcription factor complex containing both TAL1 and GATA factors (Wadman et al., 1997, Wadman et al., 1994, Osada et al., 1995). Experiments with chimaeric mice showed that *Lmo2*-null ES cells could not differentiate into any of the blood lineage (Yamada et al., 1998), indicating *Lmo2* is also necessary for definitive haematopoiesis (Figure 1.4B) and the creation of HSCs. In support of these findings, *Lmo2* expression been confirmed in mouse embryos in both primitive (Silver 1997 Blood) and definitive haematopoietic stages (Manaia et al., 2000). It was also noted in human foetal liver samples (Royer-Pokora et al., 1991) and in early blood progenitors representing HSCs (Akashi et al., 2003). Furthermore, overexpression of *LMO2* in erythroblast cell lines produced immature red cell precursors (Visvader et al., 1997) demonstrating that LMO2 can confer a negative effect on cellular differentiation, hinting at the importance of LMO2 in HSC creation and maintenance.

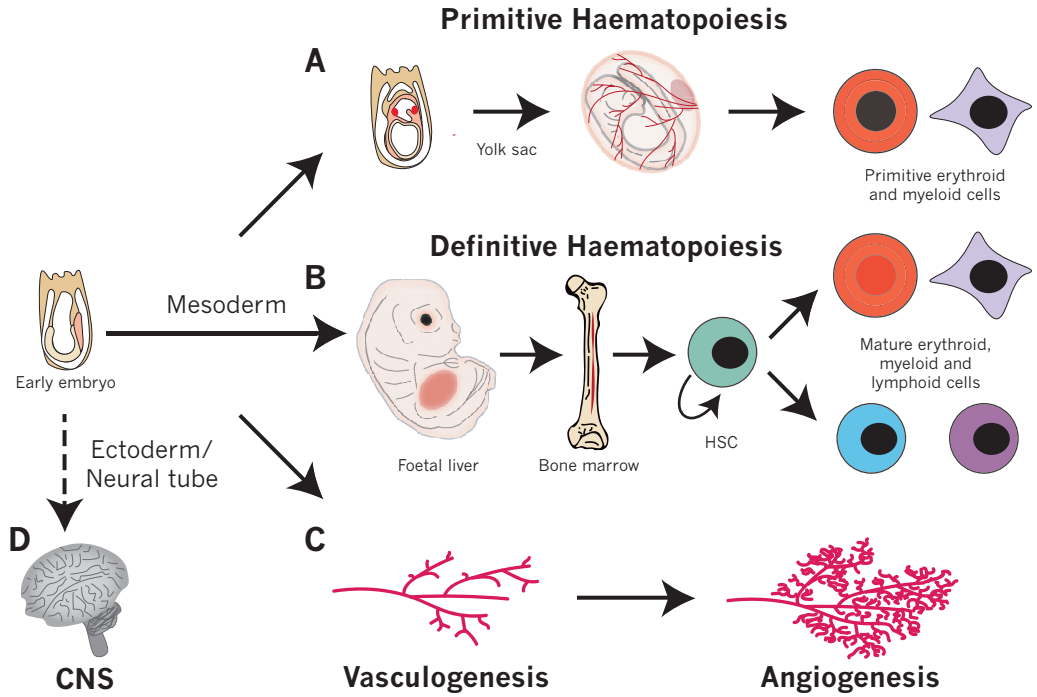

Figure 1.4 LMO2 in mouse development

Cartoon illustration of the roles of LMO2 in mouse development. LMO2 is required for *A*) primitive (Warren et al., 1994) and *B*) definitive (Yamada et al., 1998) haematopoiesis. LMO2 has also been shown to be vital for C) vascular remodelling during angiogenesis (Yamada et al., 2000). Moreover, LMO2 expression has been noted in the hindbrain regions (Hinks et al., 1997)(D) although no knock-out phenotype has been described. Figure reproduced from (Chambers and Rabbitts, 2015) under the creative commons licence CC BY 4.0.

1.3.4 LMO2 in development

The vital role played by *Lmo2* in definitive blood development led to investigation of its role in the formation of blood vessel endothelium, also derived from the embryonic mesodermal layer, as both processes are known to be connected (Lacaud et al., 2004). Chimaeric mouse embryos showed a complete lack of contribution of *Lmo2*-null ES cells in the mature blood vessel network (Yamada et al., 2002) (Figure 1.4C). Lmo2 is therefore not required in early embryonic vasculature formation but is essential for network remodelling during later angiogenic processes. Lymphangiogenesis, the formation of new lymph vessels, is similar to angiogenesis, and in both types of vessel, the endothelial lining cells possess raised levels of LMO2 and GATA2 (Coma et al., 2013). Similarly, *LMO2* is involved with tumour neovascularisation, with LMO2 detected in human tumour blood vessels (Yamada et al., 2002, Gratzinger et al., 2009), while chimaeric mouse models of teratocarcinoma showed a distinct lack of *Lmo2*-null ES cell contribution to the newly-formed tumour blood vessels (Yamada et al., 2002).

Early work identified *Lmo2* expression in developing mouse brain tissue (Foroni et al., 1992, Boehm et al., 1991a) (Figure 1.4D) that persists in adult mouse forebrain regions (Hinks et al., 1997), with changes in expression levels following limbic seizures. Although the role of LMO2 in the CNS remains unclear, this may indicate involvement as part of a repair mechanism, and may also have a possible role in glioma formation (Kim et al., 2015).

1.3.5 *LMO2* is an oncogene

1.3.5.1 LMO2 causes clonal T cell tumours

LMO2 is a T cell specific oncogene, as widespread *Lmo2* expression under the ubiquitous, inducible metallothionine promoter produced only T-ALL-like neoplasias in mice (Neale et al., 1995), with no other tumour formation apparent. Additionally, these clonal T cell tumours appeared only after a long latency period of

up to 10 months, independent of the promoter used to drive the expression (Fisch et al., 1992, Larson et al., 1995, Larson et al., 1994, Ruggero et al., 2016). This latent period suggested that the acquisition of additional oncogenic factors were necessary for full transformation (Larson et al., 1994). This was exemplified with *Lmo2* and *Tal1* transgenic mice possessing an accelerated disease progression (Larson et al., 1996) compared with *Lmo2*-only mice (Larson et al., 1994) and a complete absence of tumours in *Tal1* transgenics (Robb et al., 1995). Analysis of the latent, asymptomatic phase in *Lmo2*-only transgenic mice showed an expansion of CD4 and CD8 double negative (DN) progenitor T cells in the thymus (Larson et al., 1995), specifically those of DN3 stage (McCormack et al., 2003, Cleveland et al., 2013) despite the overt tumours possessing both markers (Larson et al., 1994). This differentiation block at the DN3 stage of maturation correlates with *Lmo2* expression in the DN1 and DN2 progenitor T cell populations of wild-type mice before down regulation (McCormack et al., 2003) and the ability of only the *Lmo2*-transgenic DN3 cells to serially repopulate thymocyte-depleted mice with a normal repertoire of T cells (McCormack et al., 2010). Therefore these DN3 thymocytes possess self-renewal properties (McCormack et al., 2010), a stem cell-like property, priming a pool of cells for the accumulation of secondary oncogenic mutations, implying that LMO2 is necessary but not sufficient to fully transform thymocytes. These findings in mouse models of the disease have led to a model of LMO2-driven human T-ALL, which is discussed further in section 1.3.8.

The persistence of *Lmo2*-transgenic thymocytes after sub-lethal irradiation indicates that Lmo2 induction of stem cell-like qualities affords a level of resistance (McCormack et al., 2010). This feature correlates with a recently identified, highly aggressive and treatment-resistant form of childhood T-ALL called Early T cell precursor-like ALL (ETP-ALL) (Coustan-Smith et al., 2009). These leukaemias are characterised by having oncogenic activation of signalling cascades such as the RAS pathway, although they also have increased levels of LMO2 and the

transcription factor Lymphoblastic leukaemia associated haematopoiesis regulator 1 (LYL1) (Zhang et al., 2012, McCormack et al., 2013).

1.3.5.2 LMO2 in other cancers

Recently it has been suggested that LMO2 has a role in other, non-T cell cancers. LMO2 has been linked with glioblastoma and the glioma cancer stem cells deriving from them (Kim et al., 2015). This correlates with *LMO2* expression in brain tissue (Boehm et al., 1991a, Foroni et al., 1992, Hinks et al., 1997), and with the identification of an LMO2-complex with neuronal-specific binding partners (Han et al., 2005). *LMO2* expression has also been demonstrated in the normal B cells occupying the germinal centres and in diffuse large B cell lymphoma (DLBCL) derived from the same region (Natkunam et al., 2007, Cubedo et al., 2012). Interestingly, *LMO2* expression in DLBCL samples correlates with improved prognosis (Natkunam et al., 2008, Lossos et al., 2004). Lastly, LMO2 has been implicated in 80-90% of epithelial neoplasias and in 60% of pancreatic cancers (Nakata et al., 2009) although this finding disagrees with another study, which only found LMO2 in the surrounding blood vessels (Gratzinger et al., 2009), as part of tumour angiogenesis (Yamada et al., 2002).

1.3.6 Mechanisms of *LMO2* activation in T-ALL

LMO2 is largely unexpressed in normal T lymphocytes (Herblot et al., 2000) and has no mandatory role in their development (McCormack et al., 2003), although it is upregulated in tumourigenic T cells (Royer-Pokora et al., 1991, Foroni et al., 1992). Gross chromosomal aberrations such as translocations or deletions are implicated to induce *LMO2* expression in approximately 9% of paediatric T-ALL (Van Vlierberghe and Ferrando, 2012, Wu et al., 2015). However *LMO2* is expressed in up to 45% of these tumours (Ferrando et al., 2002) and therefore implies gene activation by alternative mechanisms. Lastly, *LMO2* activation by retroviral insertion has resulted in T-ALL-like leukaemias in gene therapy trials (Hacein-Bey-Abina et al.,

2008, Hacein-Bey-Abina et al., 2003b, Hacein-Bey-Abina et al., 2003a, Howe et al., 2008).

1.3.6.1 LMO2 activation by chromosomal translocation

Chromosomal translocations are often associated with cancers, particularly haematological tumours. These gross changes in chromosome architecture produce one of two outcomes; the creation of a *de novo* fusion protein possessing chimaeric effects or they juxtapose immunoglobulin or TR loci with oncogenes (Rabbitts, 1991). Study of the TR gene locations and rearrangement mechanisms led to the correct postulation that the oncogenicity of recurrent translocation-positive T cell tumours would be the result of oncogene activation (Lefranc and Rabbitts, 1985, Rabbitts et al., 1985).

LMO2, located on chromosome 11 at band p13 (11p13), has been found at the junction of chromosomal translocations involving the T cell receptor alpha/delta (*TRA/TRD*) locus at 14q11 (Royer-Pokora et al., 1991, Boehm et al., 1991a) and the T cell receptor beta (*TRB)* locus at 7q35 (Garcia et al., 1991), resulting in the t(11;14)(p13;q11) and t(7;11)(q35;p13) rearrangements (Figure 1.5). These translocations account for approximately 5% of paediatric T-ALL (Wu et al., 2015). It was originally thought that these translocations brought strong enhancer or promoter elements proximal to *LMO2*. However, a negative regulatory element has been defined upstream of the first exon of *LMO2*, which is typically removed through these translocations (Hammond et al., 2005).

1.3.6.2 LMO2 activation by chromosomal deletion

Four percent of T-ALL patients possess a large deletion upstream of *LMO2* at bands p12 and p13. The del(11)(p12p13) abnormality (Van Vlierberghe and Ferrando, 2012) permits *LMO2* expression through deletion of the same negative regulatory element that is removed during the t(11;14) and t(7;11) translocations (Hammond et al., 2005). Interestingly, the del(11)(p12p13) breakpoints in one

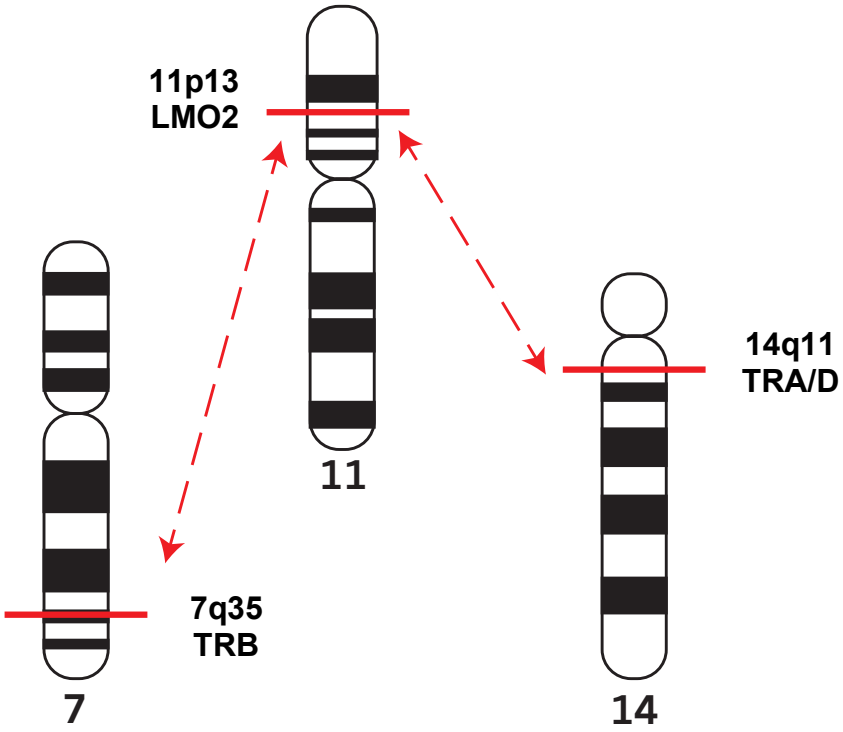

Figure 1.5 LMO2 activation by chromosomal translocation

Expression of *LMO2* in T-ALL was first discovered to be activated by chromosomal translocation with T cell receptor (TR) loci (Boehm et al., 1991a), which are now known to occur in approximately 5% of paediatric T-ALL cases. TR translocations occur following mistakes during the receptor recombination process, mediated by recombination activating genes 1 and 2 (RAG1/2), for T cell maturation in the thymus. Rearrangements with the *TRA/D* locus at 14q11 occur most frequently, with a less common *TRB* translocation at 7q35. The *LMO2-TR* translocations are indicated by red dashed arrows, and the location of the join by solid red lines. Reproduced and adapted from (Chambers & Rabbitts, 2015) under the creative commons licence CC BY 4.0.

sample completely removed *RAG1* and the coding region of *RAG2*, juxtaposing the *RAG2* promoter with exon 1 of *LMO2*. Given that immature thymocytes express *RAG1/RAG2* during maturation for *TR* recombination, this could suggest interplay between the active promoter and deleted inhibitory sequence in aberrant *LMO2* expression.

1.3.6.3 LMO2 activation by cryptic aberrations

Aberrant *LMO2* expression occurs in almost 50% of all T-ALL cases (Ferrando et al., 2002) yet only 9% harbour the gross lesions described in the previous sections (Van Vlierberghe and Ferrando, 2012). In such cases, cryptic abnormalities may be present or additional *LMO2* activation mechanisms may exist. Two novel, non-*TR*;*LMO2* translocations have been identified in T-ALL relapse cell lines at t(3;11)(q25;p13) and t(X;11)(q25;p13) (Chen et al., 2011), suggesting that previously undefined *LMO2* translocations may occur. Additionally, recent work has found small indels within the first *LMO2* intron in T-ALL cell lines and patient samples that may bestow neomorphic properties (Rahman et al., 2017) to the intermediate *LMO2* promoter (Oram et al., 2010), whilst non-mutant promoter activity may be through feedback loops generated by the association of TAL1, LYL1 and/or ERG (Oram et al., 2010).

1.3.6.4 LMO2 activation following retroviral insertion

X chromosome-linked severe combined immunodeficiency syndrome (X-SCID) is a rare disease caused by mutations in the Interleukin-2 receptor gamma common chain gene (*IL2RG*), and characterised by a lack of mature T cells and natural killer (NK) cells resulting in highly compromised immune system. During gene therapy trials for X-SCID (Hacein-Bey-Abina et al., 2002), *LMO2* expression was activated following insertion of a retroviral gene therapy vector, resulting in a T-ALL-like leukaemia in four of the paediatric patients (Howe et al., 2008, Hacein-Bey-Abina et al., 2008, Hacein-Bey-Abina et al., 2003b, Hacein-Bey-Abina et al., 2003a). In four

of the leukaemias, the virus had integrated at sites within or just upstream of the *LMO2* locus (Figure 1.6). The strong, constitutive promoter and enhancer elements of the viral vector resulted in activated expression of *LMO2*. Furthermore, recent work demonstrates the synergistic nature of combined *LMO2* and *IL2RG* expression (Ruggero et al., 2016, Dave et al., 2009) which, when compared with *LMO2* expression alone, results in accelerated tumour formation in transgenic models.

1.3.7 LMO2 is a chromosomal translocation master gene

The theory of the chromosomal translocation master gene model was proposed to account for the normal and leukaemogenic role of translocated genes in ALL (Rabbitts, 1991). To be classified as a master gene, the translocated loci were required to play a normal, pivotal involvement in cell lineage or tissue specification in addition to tumourigenic effect upon deregulated expression following translocation events. Moreover, these qualities should be exacted through either protein-protein interaction or DNA binding. *LMO2* fits this model; it nucleates a DNA-binding complex via protein interactions, its expression is necessary for haematopoietic and angiogenic development, whilst aberrant expression causes malignant tumour formation.

1.3.8 Model of LMO2 oncogenesis

Studies of Lmo2 expression in mouse T cell tumour formation provide an insight into the aetiology of T-ALL following chromosomal translocation. This has allowed the formulation of a model of the disease progression (McCormack and Rabbitts, 2004) (Figure 1.7A). Normal T lymphopoiesis originates with a common lymphoid progenitor (CLP) maturing through defined developmental stages before becoming a fully mature T cell. The transgenic *Lmo2* models show perturbation of this scheme of development, with a differentiation block, usually at the CD44/CD25 double negative (DN) 3 stage. Although some cells can overcome this block to maintain the normal thymic cellularity, most are held here, abrogating regular thymic

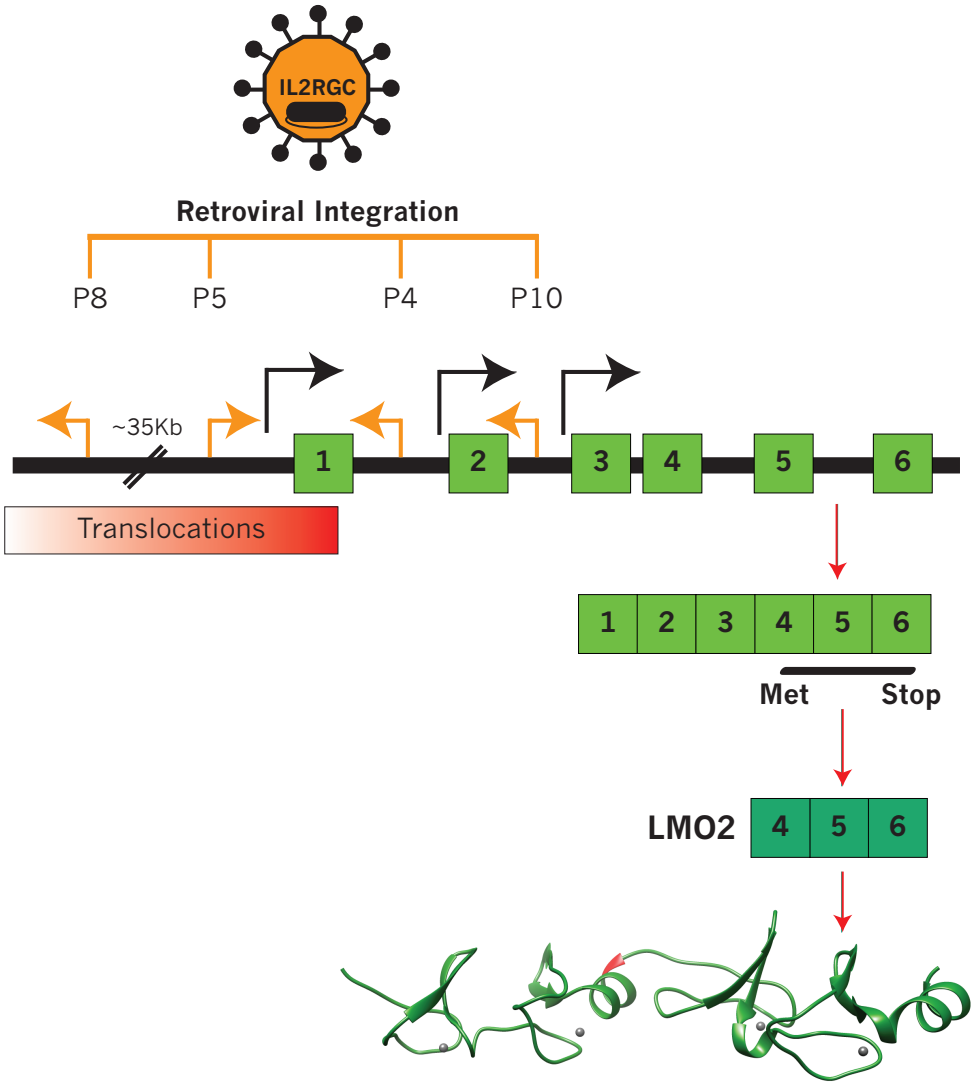

Figure 1.6 LMO2 activation during X-SCID therapy trials

Schematic representation of the therapeutic retrovirus insertions (orange lines) which led to T-ALL-like leukaemias in four X-SCID gene therapy trial patients. *Ex vivo* retroviral therapy to replace the *IL2RG* common chain was successful in reconstituting a normal immune system repertoire, although therapy-related leukaemia developed following insertional mutagenesis of the virus (Hacein-Bey-Abina et al., 2008). Direction of the viral promoter insertion is indicated (orange arrows) along the *LMO2* locus. Black arrows represent the three *LMO2* promoter elements in relation to the coding region (light green boxes, exons). The full-length LMO2 protein (dark green boxes, translated exons) comprises of exons 4-6, with the ribbon diagram of LMO2 shown below (green ribbon) coordinating zinc atoms in the LIM fingers (grey spheres). Figure adapted from (Chambers & Rabbitts, 2015) under the creative commons licence CC BY 4.0.

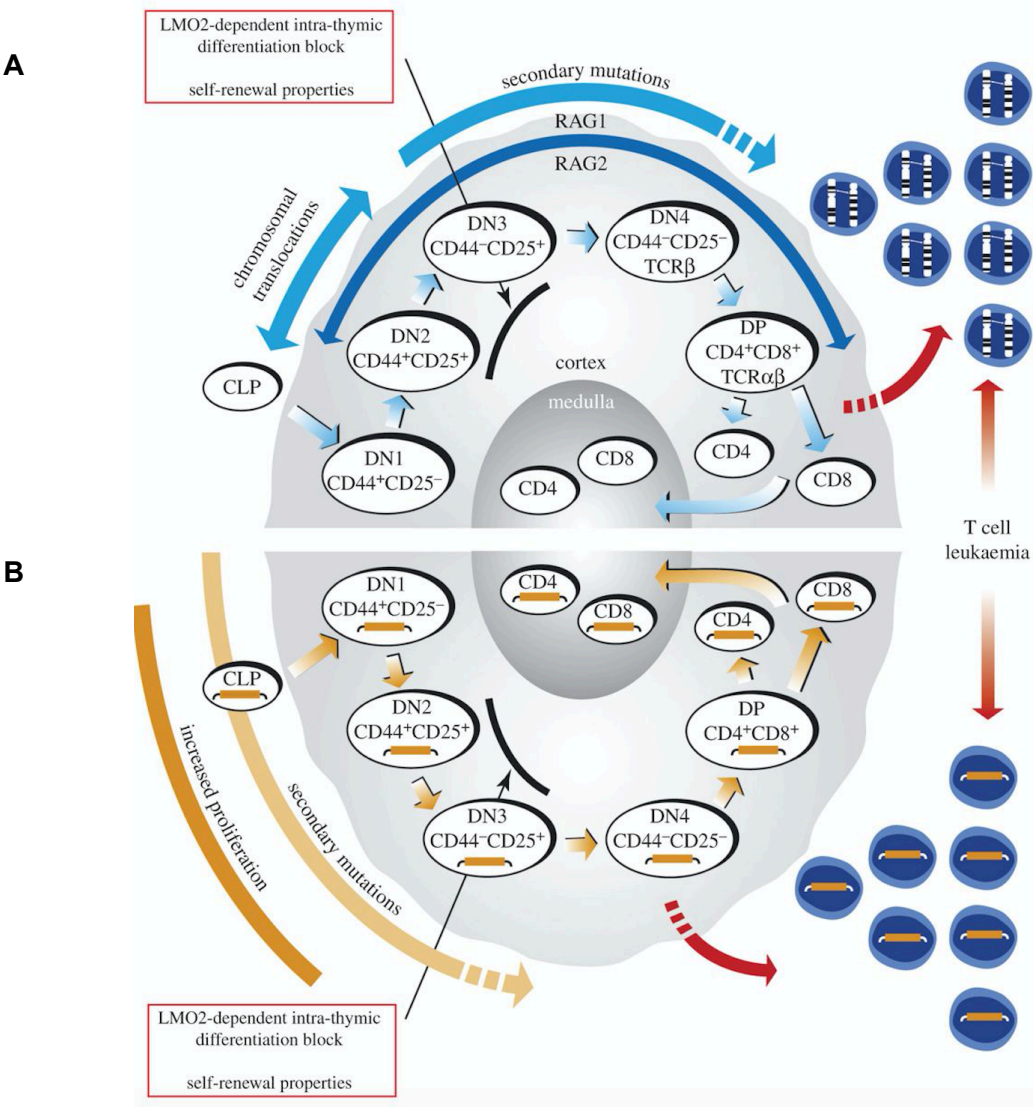

Figure 1.7 Model of LMO2-induced T-ALL

The parallel between the oncogenicity of A: *LMO2* translocations and B: retroviral mutagenesis encountered during the X-SCID gene therapy trials is represented following transgenic animal studies. Normal T cell maturation occurs in the thymus, with functional CD4/CD8 single positive cells developing from double negative (DN) and double positive (DP) stages. The DN stages (1-4) are defined by differential changes in CD25 and CD44 marker expression. T cell receptor (TR) gene rearrangements require expression of the recombination activating genes (RAG) 1 and 2, which begin at the DN2 stage of development. A: *LMO2* translocations occur concomitant with RAG expression. LMO2 acts to confer a differentiation block at the DN2/DN3 stage and an accumulation of thymocytes representing the asymptomatic phase (Larson et al., 1995, Larson et al., 1994, Cleveland et al., 2013) whereby overt, clonal T cell tumours develop following the acquisition of further mutations (Larson et al., 1996). Self-renewal seen in ETP-ALL is mimicked by the Lmo2 transgenics, which can be serially transplanted (McCormack et al., 2010). B: Therapeutic retroviral insertions within the *LMO2* locus and activated its expression (Hacein-Bey-Abina et al., 2008, Howe et al., 2008). Paralleling the translocation model, transduced lymphoid progenitors aberrantly expressing *LMO2* experience a differentiation block and accumulation of cells at the DN2/DN3 stage, acquiring self-renewal properties and ultimately lthe observed leukaemias following the development of further mutations. Figure reproduced from (Chambers and Rabbitts, 2015) under the creative commons licence CC BY 4.0 having been adapted from the original figure which is reproduced with permission from (McCormack and Rabbitts, 2004), Copyright Massachusetts Medical Society.

import of additional early progenitors (McCormack et al., 2010), until the acquisition of further mutations, such as NOTCH1 abnormalities (Ruggero et al., 2016). These additional oncogenic changes permit differentiation and increased cycling for overt tumour formation. This process likely mimics the human disease and implies LMO2 activation occurs at or before DN3, as *RAG1/2* expression (essential for *TR* recombination events and implicated as a mediator of the *LMO2*-activating chromosomal translocations) occurs from the DN2 to the CD4/CD8 double positive (DP) stage of T cell maturation. This model also parallels the leukaemias initiated in the X chromosome-linked severve combined immunodeficiency syndrome (X-SCID) (Figure 1.7B).

1.4 RAS

1.4.1 RAS structure

The *RAS* gene family encompass *HRAS*, *NRAS* and *KRAS*. The RAS family are members of a vast small guanosine triphosphate hydrolase (small GTPase) superfamily (Bourne et al., 1990). HRAS and KRAS were first identified by homology to the Harvey and Kirsten rat sarcoma virus oncogenes (Der et al., 1982), and NRAS later identified in a neuroblastoma cell line (Shimizu et al., 1983, Hall et al., 1983). The *RAS* genes encode small proteins of approximately 21kDa. *KRAS* has two alternatively spliced isoforms, 4A and 4B. The HRAS, NRAS and KRAS 4B proteins are ubiquitously expressed (Fiorucci and Hall, 1988), whilst KRAS 4A expression is restricted to differentiation during embryonic stem cell development (Pells et al., 1997). The RAS proteins are composed of a N-terminal G domain for binding and hydrolysis of the guanine nucleotides, and a short C-terminal membrane localisation domain (Vetter and Wittinghofer, 2001). Sequence homology between the RAS family proteins is high within the G domain, but highly diverse in the C-terminal region, specifying the mechanism of membrane localisation (Simanshu et al., 2017). RAS proteins have two flexible ‘switch’ regions within the G domain (Milburn et al.,

1990) which undergo conformational changes upon nucleotide binding. Switch-I and switch-II regions encompass residues 30-38 and 59-67 respectively (Vetter and Wittinghofer, 2001). Residues from both switch regions make hydrogen bonds with the γ-phosphate of the GTP molecule, holding RAS in the active conformation. Upon hydrolysis, release of the free γ-phosphate returns the switch region to the inactive conformation (Simanshu et al., 2017). The process of GTP/GDP binding been referred to as resembling a spring-loaded mechanism (Vetter and Wittinghofer, 2001). These conformational changes allow RAS proteins to act as binary signalling switches through guanidine nucleotide binding, with GDP bound in the 'off' state and GTP bound in the 'on' state. Exchange of these nucleotides is mediated through RAS association with guanine nucleotide exchange factors (GEFs) and GTPase activating proteins (GAPs) (Scheffzek et al., 1997, Boriack-Sjodin et al., 1998). The C-terminal region is subject to post-translational modifications to target RAS proteins to the cell membrane. Prenylation at CAAX (where A is any alphatic residue), CXC or CC amino acid motifs occurs through the action of farnesyltransferase (FTase) or geranylgeranyltransferase (GGTase) types I and II adding lipid chains to the cysteine residues (Hancock et al., 1989). HRAS and NRAS proteins may also be palmitoylated through the action of a palmitoyltransferase (Liu et al., 1996). KRAS also has a poly-lysine tract which aids membrane localisation through complementary charge interaction with the phospholipid bilayer (Hancock et al., 1991).

1.4.2 RAS in growth and development

RAS proteins are essential for signal transduction, playing a role in cell growth and proliferations resulting from activation of the ERK, JNK and p38 mitogen-activated protein kinase (MAPK) cascades and the AKT pathway (Karnoub and Weinberg, 2008) (Figure 1.8). RAS mediates signals from tyrosine kinase receptors to downstream RAS effector proteins. RAF kinase is a major effector of RAS

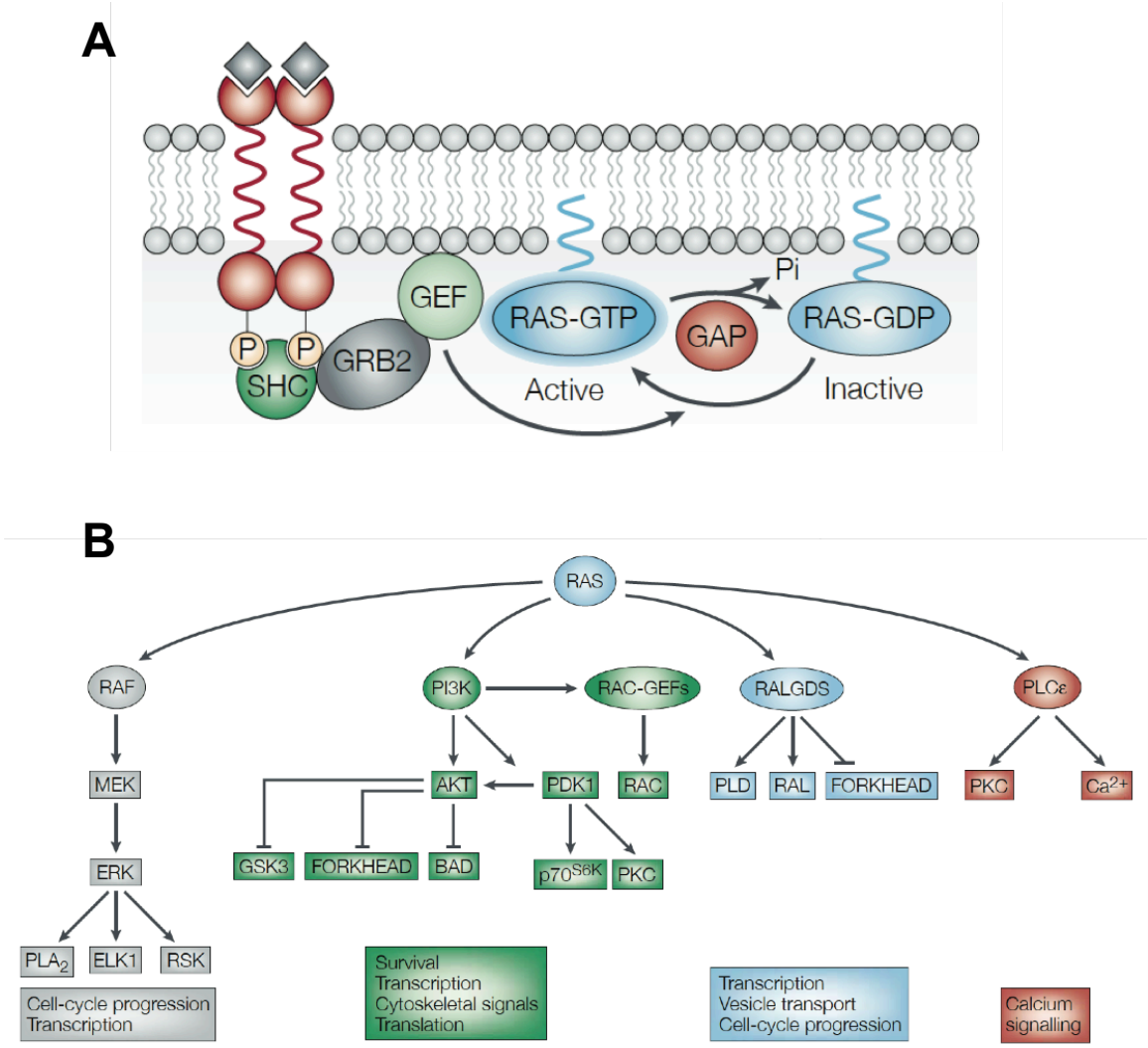

Figure 1.8 RAS signalling

Simplified diagram to represent RAS signalling. A: Representation of normal RAS activation, beginning with receptor tyrosine kinase dimerization in the presence of ligand. The phosphorylated intracellular domains recruit guanidine exchange factors (GEFs) to the plasma membrane for direct association with RAS. The GEFs promote RAS binding GTP. The hydrolysis of GTP to GDP to inactivate RAS signalling is mediated by association of GTPase activating proteins (GAPs) to increase the rate of reaction. B: GTP-bound RAS signals through many effector proteins, the most common are shown alongside the effect of the activated pathways. The mitogen activated protein kinase (MAPK) path is initiated by RAF, whereas phosphatidyl inositol 3 kinase (PI3K) activation forms lipid second messenger molecules which activate AKT. The RAL pathway is activated by RAS-mediated RALGDS activation, whilst the phospholipase C effector begins intracellular calcium mobilisation for signalling. Figure parts A and B reproduced from (Downward, 2003) with permission from Springer Nature publishers.

(Drosten et al., 2010), which acts on the ERK pathway which potentiates cellular proliferation and differentiation. Other effectors include RAL guanidine dissociation stimulator (RALGDS) (Kikuchi et al., 1994) which acts as a GEF of RAL, whose pathway is implicated in membrane trafficking and organisation of the cytoskeleton (Cully et al., 2006). Phosphatidylinositol-3 kinase (PI3K) (Gupta et al., 2007) produce lipid messenger molecules which are part of the AKT pathway, responsible for survival signalling. RAS has also been shown to interact with phospholipase C, which may link RAS signalling to calcium mobilisation (Kelley et al., 2001). These effectors bind to all RAS isoforms at their switch regions (Simanshu et al., 2017).

The essential function of RAS in these pathways was investigated in inducible RAS-less mouse embryonic fibroblasts, where lack of the RAS family proteins resulted in a loss proliferation in viable cells, and also inhibited cell motility and migration (Drosten et al., 2010). Morphological changes included enlarged, flattened cellular appearance and an increase in the number of actin stress fibres (Drosten et al., 2010).

1.4.3 RAS mutations in cancer

RAS proteins are frequently mutated in a variety of human cancers (Forbes et al., 2006), The oncogenicity of these mutations has been documented extensively, from mouse models (Shih et al., 1981, Adams and Cory, 1991) to characterisation of RAS mutations in human tumours (Bos et al., 1987, Fujita et al., 1984, Visvanathan et al., 1988). KRAS mutations occur the most frequently, in approximately 85% of mutant RAS positive tumours, followed by NRAS and HRAS mutations (11-12% and 3-4% of all cases respectively) (Simanshu et al., 2017, Hobbs et al., 2016). The most common mutations occur at amino acid positions G12, G13 and Q61, although each RAS isoform displays different mutation bias (Figure 1.9) (Prior et al., 2012). These mutations impair the intrinsic GTPase activity of RAS, despite GAP binding (Adjei, 2001). On average, RAS mutations occur in approximately 30% of all human cancers

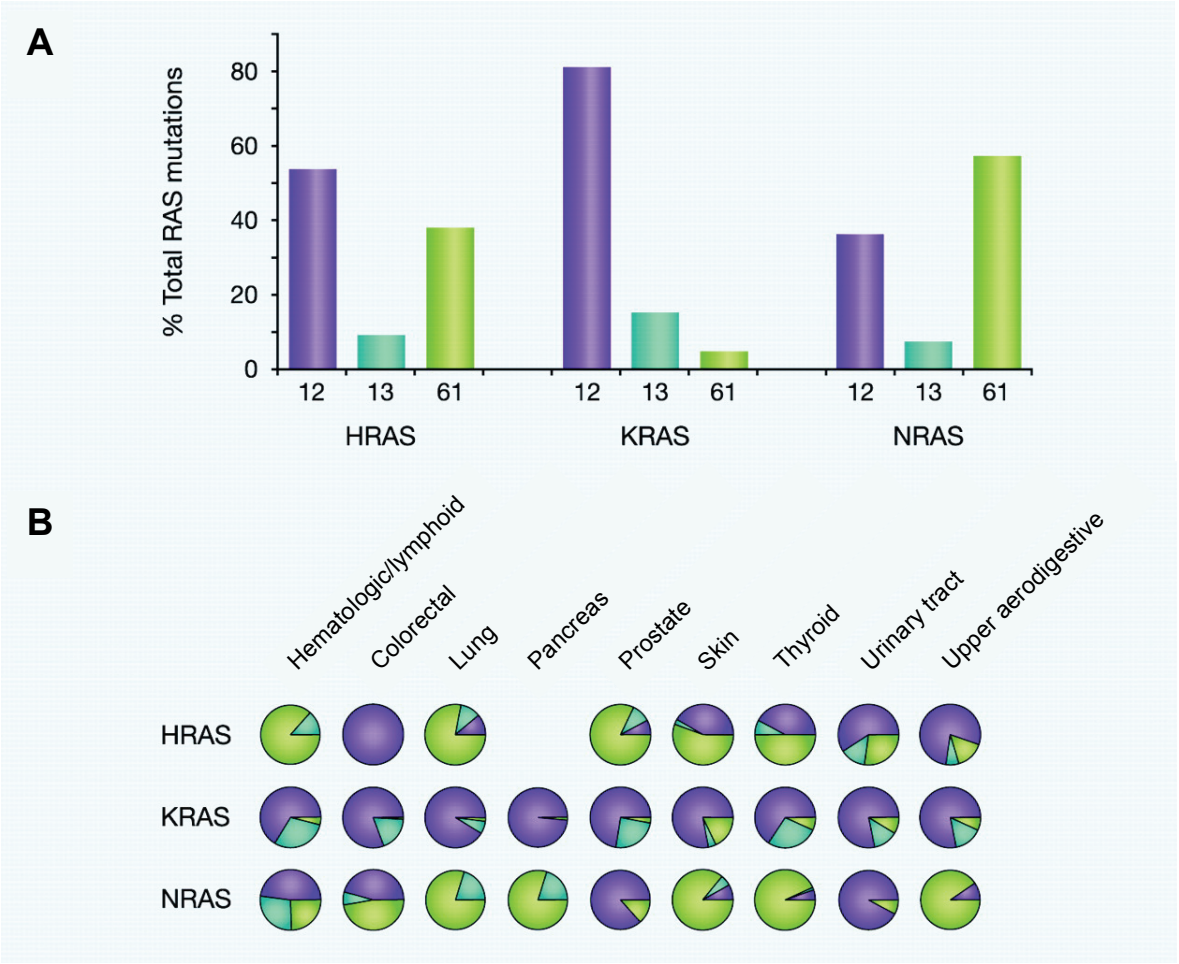

Figure 1.9 RAS mutation bias

The RAS isoforms are commonly mutated at codons 12, 13 and 61. Each isoform has shown bias in the particular codon mutation. A: Averaged data from total cancers investigated show the preferences of each isoform. KRAS has a strong preference for codon 12 mutations which occur in approximately 80% of mutant KRAS tumours. NRAS has a slight preference (60% of mutant NRAS tumours) for codon 61 alterations. HRAS has a more split preference, but predominates with codon 12 mutation. B: The RAS isoforms also show codon mutation preference within specific tumour types. The pie charts indicate the mutated codon preferences of each isoform across different cancers, where codon 12 is represented by purple segments, codon 13 by turquoise and codon 61 mutations by light green. The figure is created from data collated by the Catalog of Somatic Mutations in Cancer (COSMIC) database. Figure reproduced from (Prior et al., 2012) with permission from the American Association for Cancer Research publishers.

(Hobbs et al., 2016), although the frequency and individual mutation varies amongst tumour types (Bos et al., 1987). For example, adenocarcinoma of the pancreas and colon possess the highest incidence of RAS mutations, 90% and 50% respectively. These mutations are predominantly of the KRAS isoform, whereas only 8% of head and neck cancers are mutant RAS positive and are mostly of the HRAS isoform (Hobbs et al., 2016). NRAS mutations are most common in thyroid and haematological malignancies (Hobbs et al., 2016).

1.4.3.1 RAS mutations in T-ALL

RAS mutations are also found in up to 10-20% of T-ALL cases at diagnosis, with the predominant mutation being NRAS, with half as many possessing KRAS mutations (Girardi et al., 2017). However, relapsed disease has a greater incidence of RAS mutations, being identified in up to 40% of matched diagnosis-relapse samples, of which 27% possess NRAS mutations, indicating the subclonal nature of the disease (Oshima et al., 2016). Interestingly, RAS mutations in T-ALL were associated with altered sensitivity to standard chemotherapeutic drugs, with vincristine sensitivity and methotrexate resistance increased compared to wildtype RAS T-ALL cases (Oshima et al., 2016).

1.5 T-ALL Therapies

Typical T-ALL treatment regimens continue to comprise of multi-agent chemotherapeutics, including vincristine, corticosteroids and anthracyclines such as doxorubicin (Marks et al., 2009). Other therapies include allogeneic stem cell transplants and administration of the enzyme L-Asparaginase to starve the tumour cells (Amylon et al., 1999). However, these agents are not specific to the tumour mutations, and provide systemic toxicity and unpleasant side effects by being active in non-target tissues. The high mortality of relapsed T-ALL disease, particularly in adults (Pui et al., 2004), necessitates additional, tumour-specific therapies.

Immunotherapy applications are promising targeted cancer treatments and

include autologous chimaeric antigen receptor (CAR) T cell therapy (Almasbak et al., 2016), and monoclonal therapeutic antibodies that prevent receptor activation or eliminate signalling molecules from the tumour microenvironment (Stern and Herrmann, 2005). These treatment modalities are currently limited to recognising B cell tumours, usually targeting CD19 (CAR-T cells) or CD20, such as Rituximab (Mabthera) (Boross and Leusen, 2012). T-ALL is therefore still under-represented with regard to targeted therapies. Moreover, these approaches are limited to recognising extracellular antigens. Typically cancer is caused by intracellular aberrations, and tumour-restricted cell surface molecules are limited. As such, oncogene-specific anti-tumour agents that can operate within the cell would be advantageous.

1.5.1 Potential anti-LMO2 therapies for T-ALL

As LMO2 is aberrantly expressed in up to 50% of T-ALL cases, it represents an excellent target for specific T-ALL therapy. Currently there are no LMO2-targeted anti-cancer therapies in clinical use. Small molecule inhibitor drugs would be ideal for crossing the cell membrane and ease of use, although their systemic use would likely cause anaemia owing to LMO2 being necessary for erythroid cell development (Warren et al., 1994, Yamada et al., 1998). Indeed, such small molecules will be challenging to isolate given LMO2 has a rather flat secondary structure.

An alternative would be the use of larger, biological macromolecules or ‘macrodrugs’ (Tanaka and Rabbitts, 2008b). Examples of these types of protein drugs can take the form of peptide aptamers (Appert et al., 2009), and intracellular antibody fragments (Nam et al., 2008, Tanaka et al., 2011). These structures not only provide a scaffold for rational small molecule drug design but could also be used as therapeutics in their own right. Previous work in the laboratory has isolated LMO2-specific macrodrugs in the form of an scFv (Nam et al., 2008), a peptide aptamer (Appert et al., 2009) and an intracellular single domain antibody fragment (Tanaka et

al., 2003a). The anti-LMO2 single domain variable heavy (VH) chain fragment, VH#576, has been demonstrated to inhibit both LMO2 function *in vitro* and LMO2-mediated oncogenesis *in vivo* (Tanaka et al., 2011). The inhibitory mechanism is thought to be caused by VH binding distorting the structure of LMO2, making it unavailable for nucleation of the LMO2-transcription factor complex (Sewell et al., 2014).

1.5.2 Potential anti-RAS therapies for T-ALL

Development of mutant RAS inhibitors has been challenging, with many considering it an 'undruggable' target due to it lacking an active site-type binding pocket (Cox et al., 2014). Low affinity RAS inhibitors have been developed (Taveras et al., 1997, Peri et al., 2005, Herrmann et al., 1998) but lack the necessary potency to be of clinical value. Inhibitors tend to focus on other components of the RAS signalling pathway instead, such as prevention of membrane localization. FTase inhibition showed some efficacy in reducing HRAS oncogenicity (James et al., 1994) but not against KRAS (James et al., 1996), as GGTase activity can compensate for the lack of farnesylation (Whyte et al., 1997). GGTase inhibitors alone are ineffective at abrogating mutant RAS activity (Berndt et al., 2011), whilst GGTase inhibitors used in combination with FTase inhibitors showed a high level of toxicity (Lobell et al., 2001). More recent approaches aim to inhibit MAPK and PI3K effector protein activation, either by blocking their binding site on RAS or by directly inhibiting the effector itself. BRAF inhibitior vemurafenib has given promising results in early clinical trials (Kopetz et al., 2015) as has combination of PI3K inhibition alongside MEK inhibition (Engelman et al., 2008). Recently several biological affinity molecules such as antibodies (Shin et al., 2017) and single domain antibody fragments (Tanaka et al., 2007) have been developed against active RAS, the latter of which have enabled implementation of a unique anti-RAS drug screening strategy (Quevedo et al., 2018). The single domain antibodies have also been shown to impart an anti-

tumour effect in mouse models of mutant RAS-driven cancer by disrupting RAS effector binding (Tanaka and Rabbitts, 2003, Tanaka et al., 2007, Tanaka and Rabbitts, 2010a).

1.6 Antibodies and antibody fragments

1.6.1 Antibody Structure

Antibodies, or immunoglobulins, are large affinity molecules naturally produced by B cells as part of the adaptive immune system. Antibodies exist as five distinct classes or isotypes (IgA, IgD, IgE, IgG and IgM), categorised on the type of heavy chain they contain (α, δ, ε, γ and μ respectively). IgG antibodies are the predominant antibody type found on the B cell surface and in blood plasma, being released from memory B cells in the second wave response to foreign antigens (Schroeder and Cavacini, 2010). IgG antibodies comprise of four sub-classes, IgG1-4, which differ in the constant regions of their heavy chains. IgG1 is the most predominant and has increased effector potency and as such, therapeutic antibodies are mostly IgG1 (Irani et al., 2015).

The IgG antibody is a monomer comprised of two heavy chains and two light chains (kappa, κ, or lambda, λ), linked by disulphide bonds (Figure 1.10). The heavy chain consists of one variable (VH) and three constant (CH) domains (CH1, CH2 and CH3), whilst light chains only possess one variable (VL) and one constant (CL) domain. These discrete domains share a similar structure, the immunoglobulin fold, which comprises two antiparallel β sheets linked by a disulphide bond to create a β sandwich structure. Moreover, the overall IgG structure is stabilised by the presence of interchain disulphide bonds, resulting in a Y-shaped structure comprising of two distinct regions; the Fragment antigen binding (Fab) and Fragment crystallisable (Fc) regions. The two Fab regions contain the VH and VL domains that confer antigen specificity through their hypervariable loops, or complementarity determining regions (CDRs) (Sela-Culang et al., 2013). The Fc regions, consisting of only CH2 and CH3

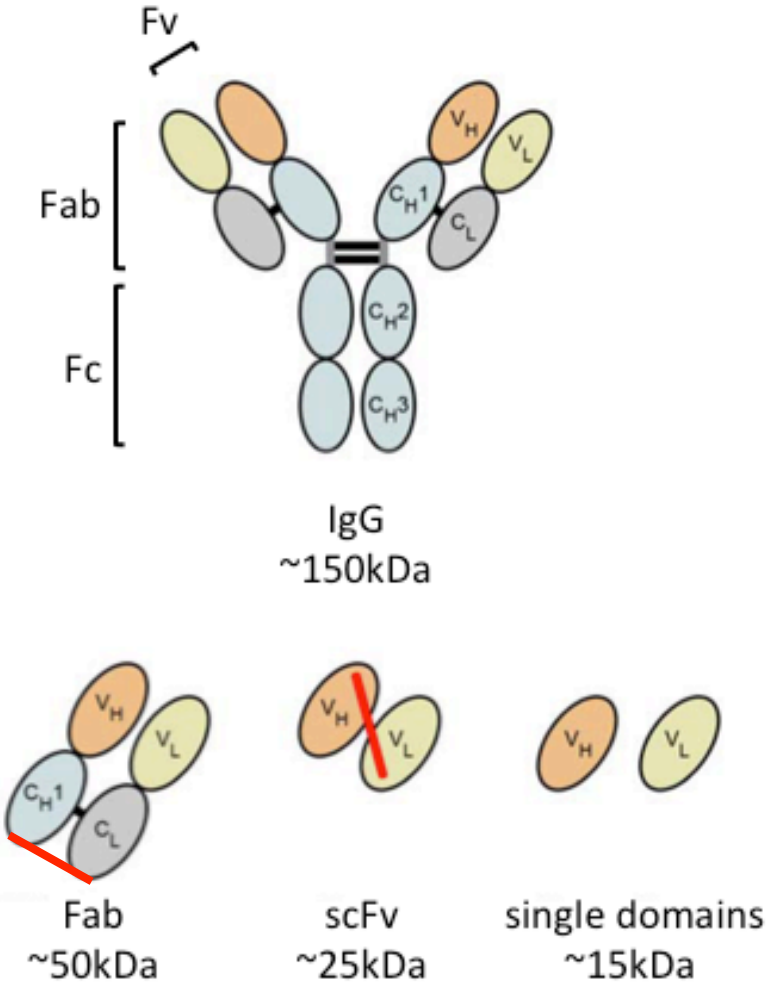

Figure 1.10 Antibody and antibody fragment structure

IgG1 antibodies are the predominant antibody class found in blood plasma, and represent the most developed type for antibody therapy. IgG1 antibodies are arranged in a Y-shaped configuration, comprising four peptide chains, two heavy and two light chains, linked by disulphide bonds, although the number of disulphide bridges between the two heavy chains varies according to the IgG subtype. Light chains contain two domains, a constant (CL) (grey) and a variable (VL) domain (lemon), whereas heavy chains possess three constant domains (CH1-3) (pale blue) and one variable (VH) domain (orange). Enzymatic digest showed the IgG structure to consist of three globular regions, two of which are distinct, separated by a flexible hinge region. The fragment crystallisable (Fc) region is made of the paired CH2 and CH3 domains, and acts to recruit immune system effector cells to destroy the bound antigenic target molecule. The fragment antigen binding (Fab) mediates antigen interaction through the complementarity determining regions (CDRs) of the variable regions (VH and VL, fragment variable domain (Fv)), linked via their constant domains. Antibody engineering has developed singe chain fragment variable (scFv) which lack the constant domain of the Fab fragment. Identification of functional antibodies containing only heavy chain (e.g. camel, shark antibodies) has led to the study of single variable domains as therapeutic antibodies. Figure adapted from (Hussack and Tanha, 2010) under the creative commons licence CC BY 3.0.

domains, mediates effector functions. The flexible hinge region between the Fab and Fc regions allows the molecule to adapt for antigen binding.

Study of antibody structure has led to the engineering of smaller fragments of whole IgG antibodies which lack the Fc region (Holliger and Hudson, 2005) (Figure 1.10). These fragments may be mono- or multivalent, allowing the recognition of one or more antigen units respectively. Monovalent fragments such as the Fab regions and single chain variable fragments (scFv, VH and VL domains linked by a short peptide chain) possess enhanced tissue penetrance compared with full-length IgG (Adams et al., 2001) although they possess much lower circulatory half-lives (Wu and Yazaki, 2000). However, the minimal, functional antigen-binding fragment is that of the individual VH and VL domains (domain antibodies, DAbs) (Ward et al., 1989). The discovery that shark and camelid (camel and llama) antibodies comprise of only a heavy chain, which have an amino terminal VH region for high-affinity antigen binding bound to a constant region (Nuttall et al., 2001, Hamers-Casterman et al., 1993, Roux et al., 1998), implied that VH domains do not require a VL domain for antigen interaction. However, VH domains are hydrophobic due to unmasked framework residues (Ward et al., 1989), resulting in poor solubility, whilst camelid antibodies are highly soluble (Hamers-Casterman et al., 1993). VH domain solubility may be improved by mutation of framework residues to resemble that of the camelid domain (Davies and Riechmann, 1994) or by selection (Tanaka et al., 2003b) to counteract their hydrophobicity and achieve highly soluble fragments, yet retain the human scaffold for reduced immunogenicity.

These single domains can reach ‘hidden’ epitopes that are unavailable to full-length antibodies and larger fragments owing to their small size. Additionally, single domain fragments do not require intra-domain disulphide bonds for functionality (Tanaka and Rabbitts, 2008a). This quality makes single domain VH and VL antibody fragments suitable for expression within the reducing environment of the cell, and therefore allows direct interaction with the intracellular oncogene.

1.6.2 Isolation of intracellular VH and VL domain antibodies

Single domain antibodies have the advantage of being more easily engineered and isolated than scFv antibodies. Advances in yeast two-hybrid genetic screening methods have simplified the generation of specific antigen-binding domains (Tanaka and Rabbitts, 2010b). Intracellular VH domains against LMO2 (VH#576) (Tanaka and Rabbitts, 2009, Tanaka et al., 2011) and mutant (G12V) RAS (VH#Y6) (Tanaka et al., 2003a, Tanaka and Rabbitts, 2009) have been isolated or characterised with this method of third generation intracellular antibody capture, screened from diverse CDR3-randomised human VH and VL libraries (Tanaka and Rabbitts, 2010b). These libraries were developed from two synthetic scFv libraries (I and J) containing human V region framework (Figure 1.11), derived from heavy chain genes IGHV3-23 (DP-47) and IGHJ4 (J_H4b), and κ light chain genes IGKV1-39/IGKV1D-39 (O12/O2/DPK9) and IGKJ1 (de Wildt et al., 2000). These initial I and J libraries had CDR diversity encoded by DVT or NNK nucleic acid codon specification respectively, to avoid redundancy of the genetic code whilst minimising the introduction of translational stop codons.

Protein:protein interaction between the 'bait' oncogene, fused to the DNA binding domain of either the yeast Gal4 transcription factor or the bacterial LexA repressor, and the 'prey' VH, fused to the activation domain of Herpes simplex VP16 transcription factor, permits reporter gene expression through the reconstitution of a functional, chimaeric transcription factor. Reporter genes include the Histidine biosynthesis gene, to allow yeast growth on dropout media, or the β-galactosidase gene for blue/white screening (Tanaka and Rabbitts, 2010b). Positive VH domain binder plasmids were subsequently recovered and used to create sequential sub libraries with CDR2 and CDR1 randomisation by polymerase chain reaction (PCR). Fully matured domains could then be characterised further.

The CatcherAb method was a supplementary approach, developed for

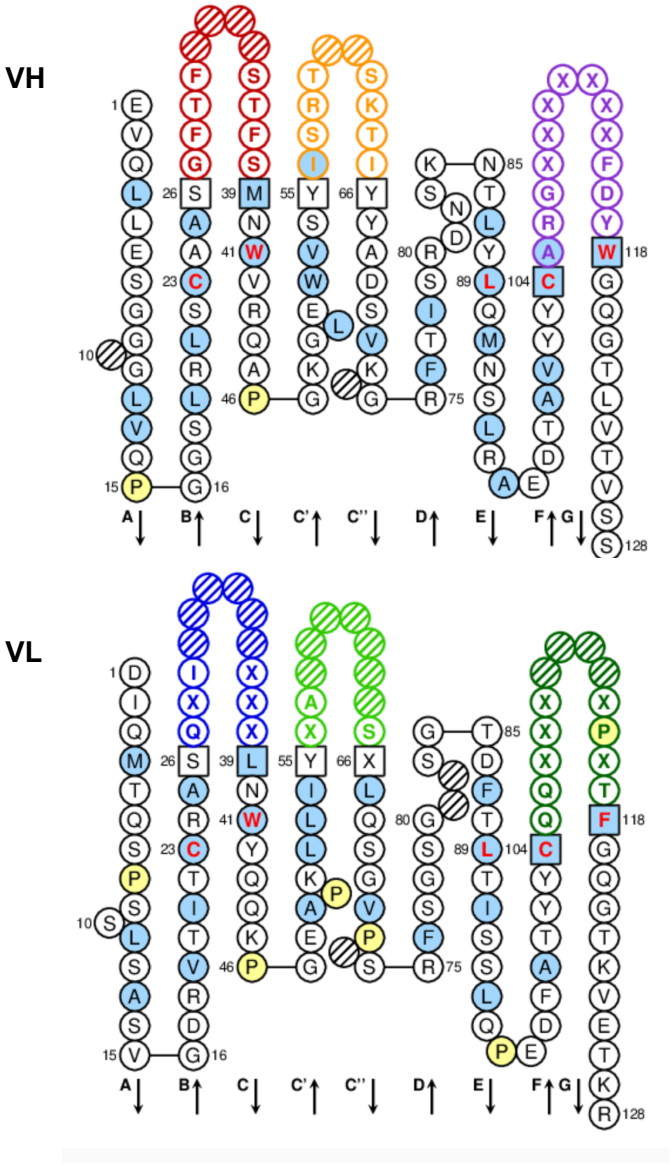

Figure 1.11 VH and VL domain general sequence

ImMunoGeneTics (IMGT) Collier de Perles two-dimensional representation of the VH (top) and VL (bottom) protein sequence used for library screening with the IAC (Tanaka and Rabbitts, 2010b) and CatcherAb (Tanaka and Rabbitts, 2009) methods. Single-letter code residues are numbered according to the IMGT system. Framework is represented as black outlined circles whilst CDRs are shown in coloured outline circles; VH: CDR1 red, CDR2 orange, CDR3 purple; VL: CDR1 blue, CDR2 bright green, CDR3 dark green. Hatched circles indicates missing residues from the database consensus. Proline (yellow filled circles) and hydrophobic (blue filled circles) and conserved (red font) residues shown. X denotes randomised amino acids within the CDR regions. Black arrows below the diagram indicate β strands and their orientation. Figures produced using the IMGT database Collier de Perles tool (Ruiz and Lefranc, 2002, Kaas et al., 2007, Ehrenmann et al., 2011).

isolation of VL domains that bind the same epitopic region as the VH (Tanaka and Rabbitts, 2009). As scFv VL domains do not necessarily contribute complementary antigen binding due to the construction of scFv from separate randomised fragments, this method allowed the identification of VL domains which could increase affinity of the scFv. Because VL domains do not possess sufficient antigen affinity to be selected alone, screens were performed with the antigen-specific VH supplied to strengthen the VL:antigen interaction. These screens have selected VL antibodies against LMO2 and RAS (Tanaka and Rabbitts, 2009). Affinities of the antigen-specific VH domains, linked in scFv format with their cognate VL (anti-mutant RAS VL#204, or anti-LMO2 VL#826) versus a non-specific VL (VL#I21, derived from scFv#I21 which displayed no enhanced RAS binding in mammalian cells (Tanaka and Rabbitts, 2003), were determined with dissociation constants (Kd) in the nanomolar range (Table 1.2).

The anti-LMO2 VH, VH#576, can successfully inhibit LMO2 function *in vitro* by preventing mouse erythroid cell differentiation (Tanaka et al., 2011). Furthermore, VH#576 demonstrated an anti-tumour effect *in vivo* (Tanaka et al., 2011), when expressed in malignant *Lck-Lmo2* transgenic T cells (Ruggero et al., 2016). The mechanism of LMO2 inhibition by VH#576 was investigated by epitope mapping and competitive binding (Tanaka et al., 2011), where VH#576 was found to bind across the LIM1 and LIM2 domains, and be able to compete with LDB1, though not TAL1, in competitive two-hybrid experiments. However, when LMO2 was expressed fused with part of LDB1, VH#576 could not displace the LDB1 domain (Sewell et al., 2014), recapitulating the Kd differences (LMO2:VH#576 had a measured Kd of 94nM, whilst the LMO2:LDB1 interaction Kd was reported as 20nM (Tanaka and Rabbitts, 2009, Tanaka et al., 2011). Crystal structure determination (Sewell et al., 2014) found all three CDR loops to be in contact with LMO2 across both LIM domains, in addition to VH framework interaction with LIM2. Binding of VH#576 to LMO2 causes a 23° bend

Antigen	Antibody	K_d (nM)	K_{on} ($M^{-1}S^{-1}$)	K_{off} (S^{-1})
RAS	VH#Y6	6.2	2.9×10^{5}	1.8×10^{-3}
	VH#Y6-VL#204 scFv	0.3	4.2×10^{6}	1.3×10^{-3}
	VH#Y6-VL#I21 scFv	11	1.1×10^{5}	1.2×10^{-3}
LMO2	VH#576-VL#826 scFv	4.3	2.2×10^{3}	9.6×10^{-6}
	VH#576-VL#I21 scFv	94	7.8×10^{3}	7.4×10^{-4}

Table 1.2 Engineered VH and scFv kinetic data

The binding affinities of the anti-RAS and anti-LMO2 scFv and single domain VH antibodies were assessed by surface plasmon resonance (SPR) (Tanaka and Rabbitts, 2009, Tanaka et al., 2011, Tanaka et al., 2007). The scFv join either the antigen-specific VL domains (isolated by CatcherAb screening) or the non-relevant VL#I21 (Tanaka and Rabbitts, 2003). Dissociation constant (Kd) affinities show the pairing of a complementary, antigen-specific VH and VL domain increases affinity over scFv antibodies involving non-specific VL domains. The affinity of single anti-RAS VH domain is between that of the two scFvs.

in LMO2 conformation when superimposed with the structure of LMO2 bound to its usual partner, LDB1 (El Omari et al., 2011), and thus inhibiting the assembly of the transcription factor complex. Taken together, the data implied the mechanism of LMO2 inhibition by VH#576 was due to sequestration of newly synthesised LMO2 protein prior to the LMO2:LDB1 association, preventing nucleation of the LMO2 transcription factor complex (Sewell et al., 2014).

An anti-LMO2 VL domain (VL#826) was assessed for antigen-specific binding by incorporating it into an scFv antibody alongside VH#576. A greater than 20-fold increase in affinity was observed compared with the scFv containing VH#576 with the non-relevant VL#I21 (Tanaka and Rabbitts, 2009), with a final Kd measured at 4.3nM. However, the location of VL#826 (and other CatcherAb anti-LMO2 VL fragments) binding on the LMO2 protein has not been established. This contrasts with the anti-mutant RAS single domain pair (VH#Y6 and VL#204), which both bound the same residue, Tyr 64, via CDR3 contacts (Tanaka et al., 2007) (Figure 1.12). In keeping with these results, the VH#Y6 single domain has a 20-fold higher Kd with mutant RAS than does the VH#Y6-VL#204 scFv (Tanaka et al., 2007), yet interestingly VH#Y6 alone has an almost 2-fold higher affinity than when paired with the non-relevant VL#I21 (Tanaka and Rabbitts, 2009) (Table 1.2).

1.6.3 Linking single domain antibodies to effector functions

In vivo experiments have established that intracellular expression of VH#576 and VH#Y6 inhibits LMO2 and mutant RAS induced tumours respectively (Tanaka et al., 2007, Tanaka et al., 2011). In the case of mutant RAS inhibition, tumour suppression was only effective whilst VH#Y6 was expressed, with removal of VH#Y6 expression resulting in a return of malignant growth (Tanaka and Rabbitts, 2010a). This implies that oncogene inhibition alone does not result in cancer cell death, going against the ‘oncogene addiction’ model (Weinstein, 2002), and seems likely given that neoplasias tend to acquire multiple detectable mutations (Girardi et al., 2017)

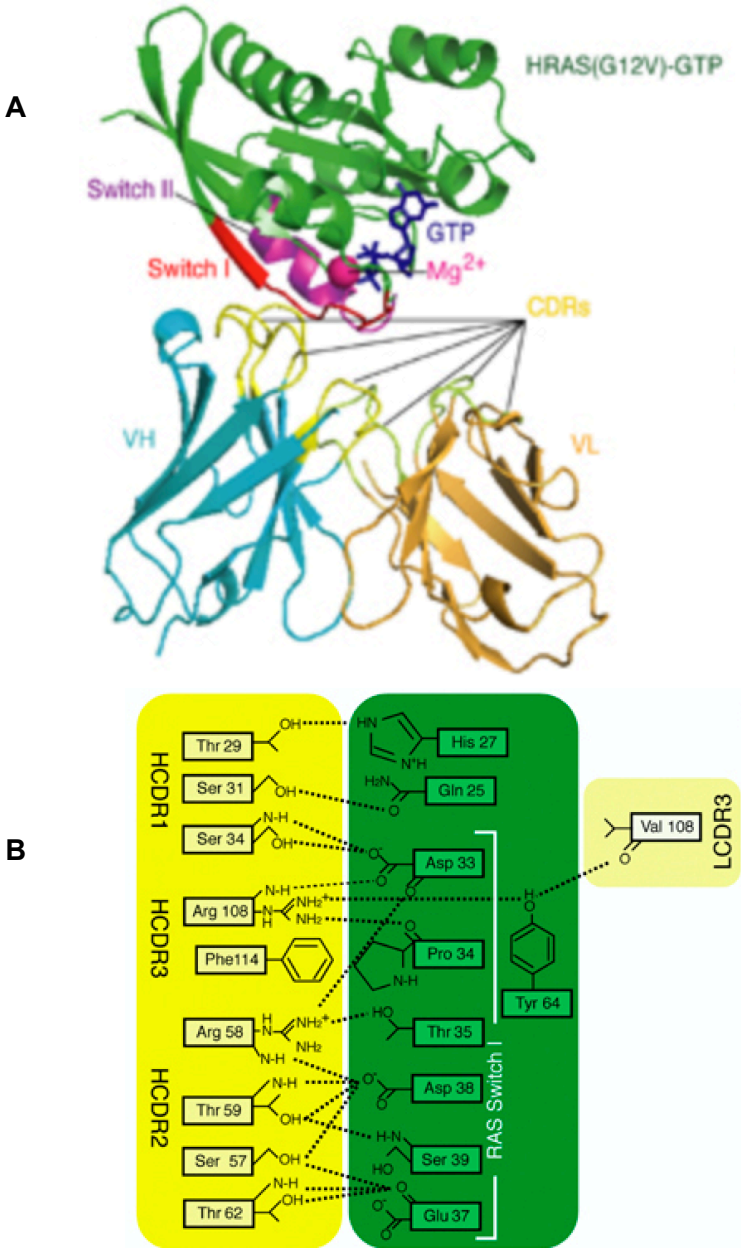

Figure 1.12 VH#Y6 and VL#204 in complex with mutant RAS

A: Ribbon diagram of the crystal structure of the anti-RAS VH#Y6 (cyan) and VL#204 (orange) as an scFv bound to the mutant HRAS(G12V) protein (green) in complex with GTP (blue) and coordinating a magnesium ion (magenta). The CDR loops of the VH and VL (yellow and lemon respectively) are highlighted, which interact with the switch I region (red) of RAS. The switch II region is shown in purple. B: Schematic diagram of the scFv interactions with GTP-bound HRAS(G12V) (green). The hydrogen bonds (dashed lines) of specific VH#Y6 (yellow) and VL#204 (lemon) residue sidechain and peptide bond interactions with RAS are indicated. Note that most of the contacts occur between the VH#Y6 and the switch I region, with all three CDRs interacting with the antigen. One residue of VL#204 CDR3 contacts RAS at the same amino acid as VH#Y6 (Tyr 64). Figure adapted and reproduced from (Tanaka et al., 2007) with permission from John Wiley and Sons publishers.

although the true number may be far higher (Tomlinson et al., 2002). As such, linkage of cytotoxic effector domains to the single domain antibodies could potentiate the antibody's inhibitory effect by directly killing the cancer cells rather than simply suppressing their growth.

Full-length antibodies have been linked to anti-cancer therapeutic agents such as radioactive isotopes (e.g. yttrium-linked antibody Ibritumomab (Zevalin)) (Stern and Herrmann, 2005) or to drug compounds such as doxorubicin (Trail et al., 1993). These work by internalisation of the antibody-drug conjugate following their binding to the cognate epitope on the cell surface. However, as intracellular domain antibodies offer the advantage of being expressed within the cell, they would necessitate the fusion of a cell death-inducing protein to their coding sequence. Ideally, these proteins would require specific cancer antigen binding of the intracellular antibody to activate the toxic protein. Previous studies have employed membrane soluble chemicals to dimerise conditional alleles, each comprised of a chemical binding domain and a pro-apoptotic protein domain (Spencer et al., 1996). These pro-apoptotic domains are chosen for their ability to signal or self-activate upon dimerisation, allowing artificial induction of apoptosis, examples of which include the cysteinyl aspartate proteases (caspases), caspase 8 (Muzio et al., 1998), caspase 1 and caspase 3 (MacCorkle et al., 1998).

1.7 Role of caspases in apoptosis

Apoptosis is a normal yet tightly controlled process of cell death (Kerr et al., 1972) with roles in tissue development and homeostasis as well as a protective response following the detection of irreparable cellular damage (Elmore, 2007). Deregulation of apoptosis is implicated in human disease, such as autoimmune conditions and cancer (Zhang et al., 2005, Brown and Attardi, 2005). Induction of apoptosis occurs via extrinisic and intrinsic pathways, depending upon the cellular assault, although the common process invokes a proteolytic caspase cascade

(Figure 1.13). Caspase enzymes are present in the cells as inactive precursors or zymogens (Creagh et al., 2003) and those involved in apoptosis may be classified as 'initiator' or 'executioner' enzymes, according to their role within the process. As their name suggests, initiator caspases (caspases 2, 8, 9 and 10) begin apoptosis through dimerisation-induced auto-activation (Muzio et al., 1998), whilst executioner caspases (caspases 3, 6 and 7) require cleavage by the upstream initiators to become active (Stennicke et al., 1998). Activation of the executioner enzymes irreversibly commits the cell to destruction.

The caspase family share a common protein structure, with all possessing a variable length N-terminal pro-domain and two catalytic subunits, one large (p17) and one small (p12) (Figure 1.14). During catalytic activation, procaspases undergo several proteolytic cleavage events, to liberate the pro-domain and cleave the intersubunit linker. Mature, active caspases are tetrameric, comprising of two p17 and two p12 subunits derived from two procaspase chains, being regarded as being 'dimers of heterodimers' (Taylor et al., 2008).

Initiator caspases possess one of two types of pro-domain, the caspase recruitment domain (CARD) or death effector domain (DED), which interact with the same domains in adaptor proteins to facilitate proximity auto-activation of the initiator enzymes. By contrast, the executioner enzymes possess a short pro-domain, lacking an interaction domain. Instead of being recruited into a dimeric state, the executioner caspases exist naturally as inactive dimers (Pop et al., 2001), predominantly stabilised by hydrophobic interactions between the two chains (Bose and Clark, 2001). The short pro-domain may help maintain the zymogen in its inactive state (Meergans et al., 2000), although the major mechanism of auto-activation suppression in procaspase 3 (proCASP3) is postulated to be the tri-aspartate (Asp-Asp-Asp or DDD) 'safety catch' motif (Roy et al., 2001). The protective effect relies on the negatively charged residues of the motif interacting with positively charged amino acids within the main structure of the proenzyme, possibly those

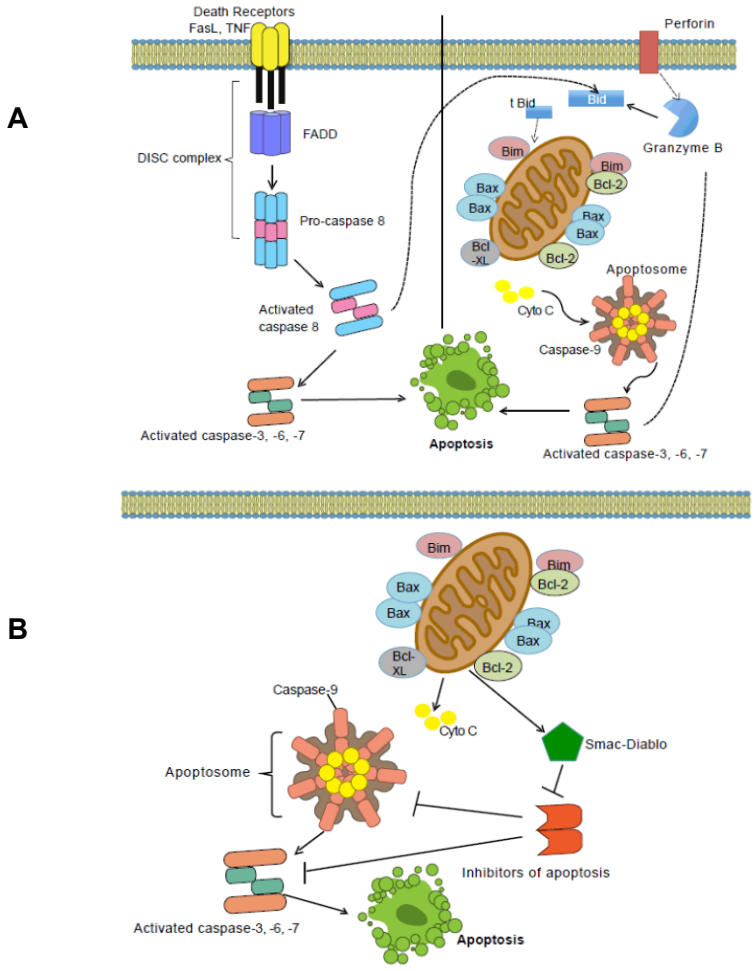

Figure 1.13 Extrinsic and intrinsic apoptosis pathways

Diagrams of the major pathways activating apoptosis. A: The extrinsic pathway is initiated by factors external to the cell, by death receptor (left) or by granzyme B/perforin (right) mediated pathways. Binding of ligands (Fas ligand (FasL) or tumour necrosis factor (TNF)) permits trimerisation of death receptors (e.g. Fas receptor, TNF receptor) which in turn bind the Fas activated death domain (FADD) adaptor proteins. These initiate formation of the death-inducing signalling complex (DISC) through recruitment and activation of procaspase 8. Active caspase 8 can either initiate the caspase 9-mediate intrinsic apoptotic pathway via Bid protein cleavage or by direct procaspase3/7 activation. The granzyme B/perforin extrinsic pathway is initiated by natural killer and cytotoxic T cells, which release both molecules upon target recognition. Perforin protein forms pores in the cell membrane which allow granzyme B permeation into the cytoplasm, whereby it cleaves Bid to promote caspase 9 activation. Granzyme B can also directly activate the executioner procaspases.B: The intrinsic pathway provides a mechanism of apoptosis initiation following internal cellular damage. Changes in mitochondrial permeability are facilitated balancing the ratio of pro- and anti-apoptotic Bcl2 protein family members. Permeabilisation of the mitochondrial membrane permits cytochrome c release and association with apoptotic protease activating factor 1 (Apaf1) to activate and complex with procaspase 9, forming the apoptosome complex. The apoptosome subsequently activates executioner caspases to complete apoptosis. Figure reproduced from (Cooper, 2012) under the creative commons licence.

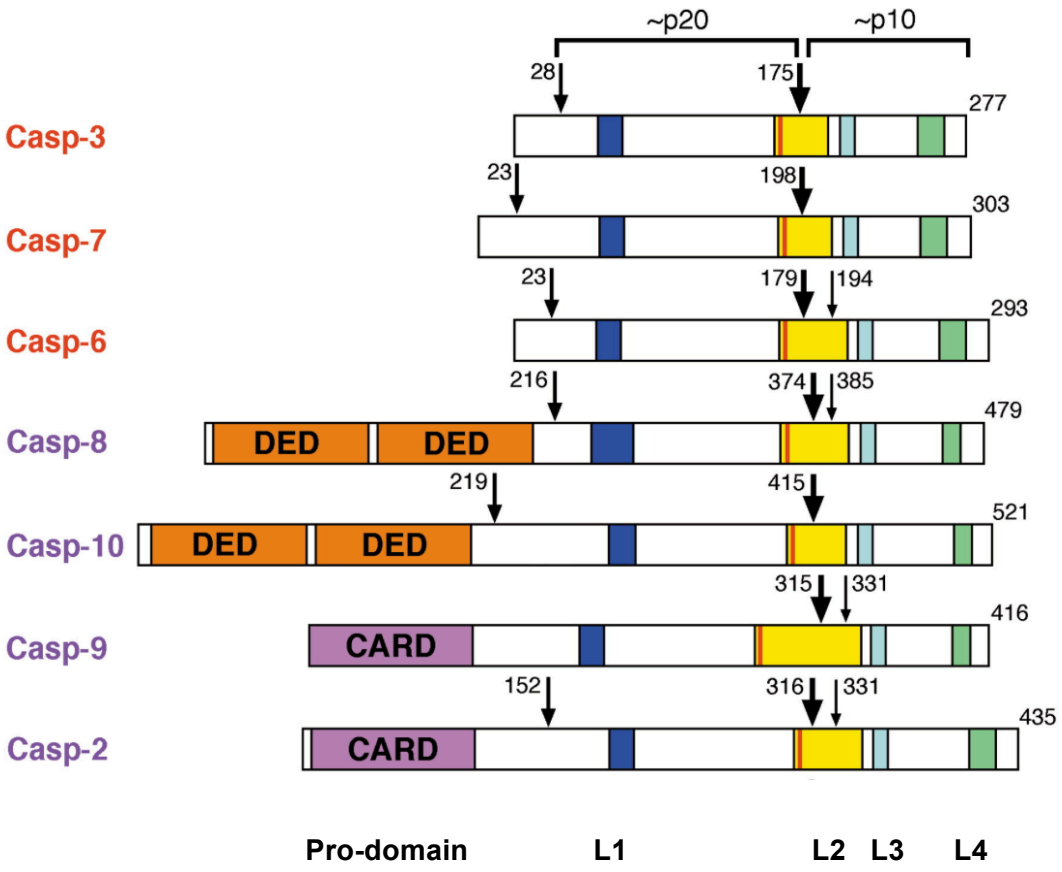

Figure 1.14 Structural comparison of procaspases

Representation of the executioner (red) and initiator (purple) procaspase monomer protein structure. The pro-domains are shown, and indicate the presence of the two types of dimerisation domain present in the initiator procaspases; the death effector domain (DED, orange box) or the caspase recruitment domain (CARD, purple box). The aspartate residues where cleavage occurs are denoted by black arrows, with numbers referring to the amino acid residue position. The thicker arrow indicates the initial cleavage event which in the linker region between the large and small subunit. The four loop regions (L1-4) are drawn as coloured boxes (dark blue, yellow, pale blue and green respectively). The catalytic Cys residue is shown as a red line within L2. The length of each procaspase signifies their size. Figure adapted and reproduced from (Shi, 2002) with permission from Elsevier publishers.

encompassing the active site, to occlude the intersubunit cleavage site. Moreover, evidence of interplay between two additional tripeptide sequences, the RGD and DDM motifs, may result in additional blockage at the key proteolytic activation sites (Buckley et al., 1999). Interestingly, the DDD and DDM motif overlap, which highlights the importance of this region in proCASP3 activation.

Owing to their propensity to form inactive dimers, proCASP3 proteins can be exogenously expressed within mammalian cells without inducing apoptosis (Hasegawa et al., 1996, Yamabe et al., 1999). However, they can auto-activate expressed at very high levels in bacterial (Mittl et al., 1997) yeast (Ryser et al., 1999) and mammalian cells (Fernandes-Alnemri et al., 1994), albeit with less efficiency than the initiator caspases do in the same scenario. This may result from acidified conditions in the expression cultures mimicking the cellular acidification encountered during onset of apoptosis, and acting to protonate and subsequently destabilise the DDD peptide safety catch (Roy et al., 2001). Similarly, single dimeric proCASP3 chains can auto-activate when held in proximity (Colussi et al., 1998, MacCorkle et al., 1998), presumably due to inhibition of the RGD and DDM motif interaction (Buckley et al., 1999).

1.7.1 Caspase 3 as a cytotoxic effector domain

Studies of exogenous proCASP3 expression, alone or as artificial death switch domains, have shown that the presence of single dimeric chains result in only basal levels auto-activation (Colussi et al., 1998, Hasegawa et al., 1996, Yamabe et al., 1999, Fan et al., 1999, MacCorkle et al., 1998). Full auto-activation of the proCASP3 domains is only resolved upon proximal positioning, achieved by chemical induced dimerisation (MacCorkle et al., 1998, Fan et al., 1999, Shariat et al., 2001) or by chimaeric addition of initiator caspase pro-domains (Colussi et al., 1998). Recently, leucine zipper domains have been demonstrated to engage proximity-induced auto-activation of proCASP3 to the fully mature, catalytically active caspase 3 (CASP3)

enzyme in the nematode (Chelur and Chalfie, 2007). Although these studies reveal the exciting potential of CASP3 as an inducible apoptotic agent, the mechanisms of proCASP3 dimerisation they describe do not demonstrate CASP3 auto-activation to be specific in a biological target-dependent context. However, this has been achieved by linking proCASP3 domains to scFv antibodies raised against the bacterial enzyme β galactosidase (βGal) (Tse and Rabbitts, 2000). As βGal is a tetrameric protein, four scFv binding sites enabled proximity-induced auto-activation of the fused C-terminal proCASP3 domains. The proCASP3 domain auto-activation and ensuing apoptosis was dependent upon the antigen-specific association of the scFv with the βGal antigen. This mechanism of antibody-mediated cell killing, known as Antibody Interaction Dependent Apoptosis (AIDA) (Tse and Rabbitts, 2000), illustrates a potential, novel method of antigen-dependent cell killing.

1.8 Thesis aims

Despite research efforts and improved therapy regimes leading to increased survival and reduced morbidity, cancer remains one of the leading causes of death (World Health Organization, 2015). As such, there is a clinical need for new treatment modalities. One example of a malignancy where relapsed disease has a poor prognosis, yet has few disease-specific targeted therapies, is T-ALL (Terwilliger and Abdul-Hay, 2017). Although a variety of oncogenes have been implicated in T-ALL (Girardi et al., 2017), LMO2 and the mutant RAS-family proteins are two interesting targets for therapeutic development. LMO2 represents a unique anti-T-ALL target, due to its expression being documented in almost 50% of cases (Girardi et al., 2017, Ferrando and Look, 2003, Wu et al., 2015), yet proving absent in normal cellular counterparts (Herblot et al., 2000, Foroni et al., 1992, Kenny et al., 1998). By contrast, RAS is a ubiquitously expressed protein whose mutant forms are implicated in up to 30% of human cancers (Hobbs et al., 2016). Therefore, therapies directed

against mutant RAS-driven cancer would have a broad applicability to other malignancies in addition to T-ALL.

Isolation of small molecule drug inhibitors of LMO2 will likely prove difficult as a consequence of the inherent lack of secondary structure possessed by LMO2. Furthermore, LMO2 has normal roles in angiogenesis (Yamada et al., 2000) and erythroid cell specification (Warren et al., 1994) which may become deregulated in the event of systemic drug administration. The search for RAS inhibitors has already been problematic, with low affinity, non-specific candidate drugs (Peri et al., 2005, Herrmann et al., 1998) supporting the idea of RAS being "undruggable" (Cox et al., 2014). Our laboratory has developed high-affinity intracellular VH antibodies against two common oncogenes, LMO2 and mutant RAS, that have both demonstrated tumour inhibition effect *in vivo* (Tanaka et al., 2007, Tanaka and Rabbitts, 2010a, Tanaka et al., 2011). However, tumour inhibition with the anti-RAS VH only affected cancer growth whilst antibody expression was maintained (Tanaka and Rabbitts, 2010a), which may also prove true in the LMO2 context particularly given the complexity of mutations within human tumours. Maintaining VH expression in a therapeutic scenario could be challenging, but may be resolved by linking the intracellular antibodies with a cytotoxic effector domain. Use of proCASP3 as the effector domain is validated by its history of use as a death domain following chemical and antibody binding-induced proximity activation (Tse and Rabbitts, 2000, MacCorkle et al., 1998, Fan et al., 1999). Therefore, the aim of this study is to evaluate the potential of AIDA as a targeted anti-tumour therapy. To date, AIDA has only been shown in the context of an exogenous, non-mammalian protein (Tse and Rabbitts, 2000). This thesis will investigate the manifestation of AIDA against clinically relevant T-ALL oncogenes in human tumour cells. Moreover, intracellular single domain antibodies will be used rather than scFv. The single domains express more easily than scFv and can access a greater repertoire of antigenic regions when single domain antibodies are not linked.

To recapitulate scFv binding, two intracellular single domain antibodies would be required. These should bind the same antigen at close epitopic regions to bring the fused proCASP3 domains into proximity for their auto-activation. A schematic overview of the proposed single domain AIDA against both LMO2 and mutant RAS antigens is shown in Figure 1.15. Use of complementary VH and VL domain antibodies, isolated by the CatcherAb method (Tanaka and Rabbitts, 2009), should allow the formation of an antigen-dependent Fv inside the cell. Complementarity of the anti-RAS VH and VL pair has been established (Tanaka et al., 2007) (Figure 1.12) and so these antibodies will be used to ascertain whether the AIDA approach is relevant as a method of cancer cell killing. As LMO2 exemplifies an ideal oncogenic target, this thesis will also explore the characterisation and isolation of LMO2-specific, VH#576-complementary VL domains, and develop strategies for screening anti-LMO2 AIDA in tumourigenic T cells.

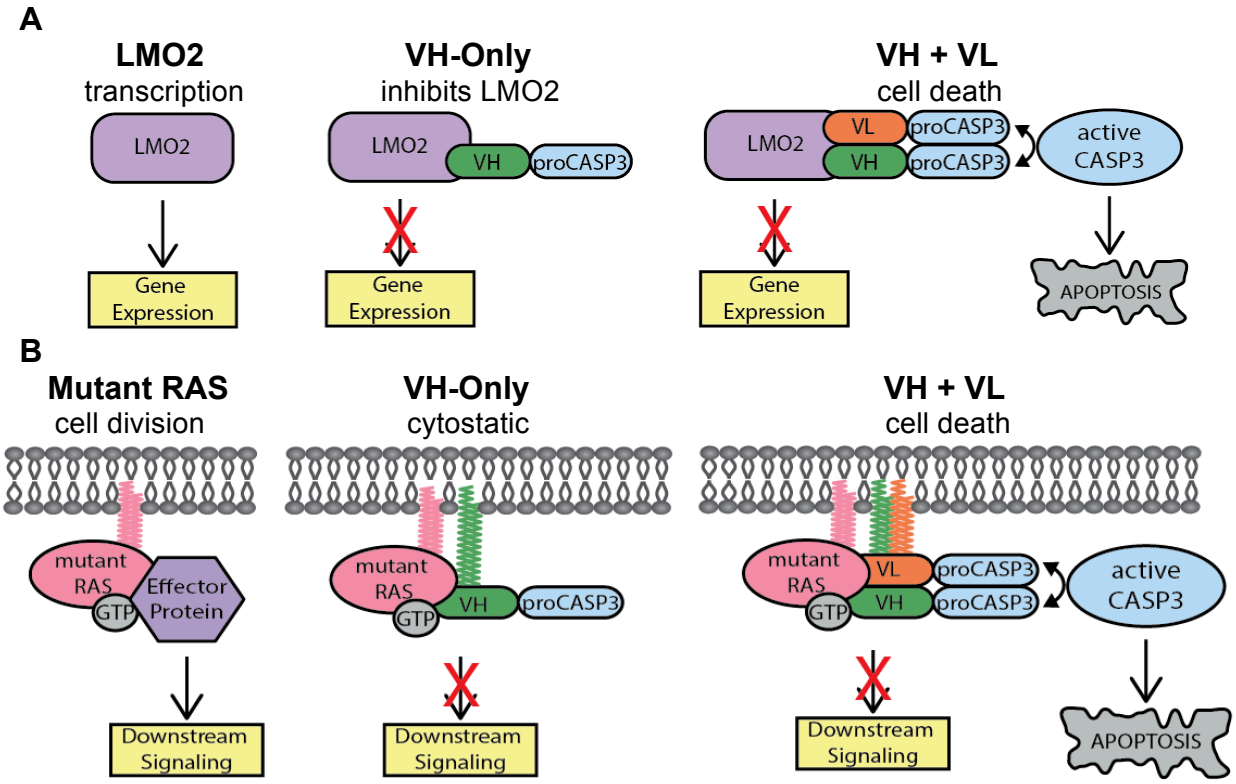

Figure 1.15 Schematic diagram of hypothesised AIDA method

Overview of the AIDA cancer cell killing method, based upon the initial description of AIDA technology (Tse and Rabbitts, 2000), showing the anticipated effects of the system against two oncogenes, A: LMO2 and B: mutant RAS. The diagrams show the hypothesized effect of expressing the VH-proCASP3 fusion alone (green and light blue rounded oblongs) (herein referred to as VH-Only) and when expressed alongside the VL-proCASP3 fusion (orange and light blue rounded oblongs) (herein referred to as VH+VL). Expression of VH-Only should not result in activation of the CASP3 moiety despite antigen binding, as dimerisation of the VH-proCASP3 fusion should not occur. Expression of VH+VL should form a trimeric complex of the fusion proteins with their cognate oncogenic antigen (A: LMO2, lilac oval, B: RAS, pink oval). This would place both proCASP3 domains in close proximity to permit their auto activation, resulting in active CASP3 enzyme (light blue oval) and induction of cell apoptosis (puckered grey rectangle). The VL fragment contained within the VL-proCASP3 fusion (herein referred to as VL-Only) is of too low affinity to bind antigen without partnering with the complementary VH and is therefore not shown as a separate diagram. A: Anti-LMO2 AIDA. The aberrant expression of LMO2 in T cells leads to an altered transcriptional programme. The LMO2-specific VH obviates nucleation of the LMO2 transcription factor complex, reversing the effect of LMO2 but should not elicit CASP3 activation as no VL-proCASP3 protein is present. Cell death as a result of CASP3 activation should only occur upon VH+VL binding to LMO2. Currently only an anti-LMO2 VH has been isolated by the laboratory. B: Anti-mutant RAS AIDA. Initial testing of this technology will be performed with VH and VL domains specific for active, GTP-bound (grey circle) RAS. RAS is a membrane-bound small G-protein, targeted to the cell membrane through post-translational modification with hydrophobic lipid moieties (pink jagged lines). For optimal interaction with RAS, the VH- and VL-proCASP3 fusion proteins in this scenario are targeted to the cell membrane by the addition of a farnesylation signal (green (VH) and orange (VL) jagged lines). Mutant RAS constitutively signals through conserved effector proteins such as RAF and RAL (lilac hexagon) to generate mitogenic responses following signal transduction. Expression of the anti-RAS VH single domain fragment has been shown to prevent tumour growth by preventing normal RAS signaling (Tanaka and Rabbitts, 2010a, Tanaka et al., 2007). VH-Only is thus hypothesised to elicit the same effect as the unconjugated VH, and impart a cytostatic effect on the tumour cells, with VH+VL required for antigen-specific cell death.

Chapter 2 Materials and Methods

2.1 General methods

2.1.1 DNA and RNA Methods

2.1.1.1 Agarose gel casting and electrophoresis

DNA preparations were analysed by agarose gel electrophoresis. Briefly, appropriate percentage w/v agarose in 1x buffer was prepared by boiling the solution until the powdered agarose has fully dissolved. For best resolution of DNA bands, 1x TAE buffer (40mM Tris, 20mM acetic acid, 1mM EDTA) was used for long gels whilst 1x TBE buffer (89mM Tris, 89mM Boric acid, 2mM EDTA) was used for mini gels. For DNA staining during electrophoresis, 1µg/ml Ethidium Bromide (Fisher Scientific, Loughborough, UK) was added before pouring.

2.1.1.2 RNA isolation

RNA was isolated using Trizol (Invitrogen, Paisley, UK) as per the manufacturer's instructions. Briefly, 10^7 cells were lysed in 0.75ml Trizol reagent and incubated at room temperature for 5 minutes then 0.2ml chloroform (Fisher Scientific, Loughborough, UK) was added and samples mixed vigorously for 15 seconds. After a further 2-3 minutes incubation at room temperature, samples were centrifuged for 10 minutes at 12,000 x g, 4°C. The RNA pellet was washed with 1ml 75% ethanol in diethylpyrocarbonate (DEPC)-treated water and re-pelleted. The pellet was air dried and resuspended in 50µl DEPC-treated water. RNA was heated to 55°C for 10-15 minutes to aid resuspension. RNA quality was assessed by absorbance ratio A260/280nm ratio and by gel electrophoresis.

2.1.1.3 cDNA Production

First strand cDNA synthesis was prepared from RNA samples using the SuperScript II RT-PCR kit (Invitrogen, Paisley, UK) according to manufacturer's instructions. Briefly, 1.5µg RNA was added to a reaction mix containing oligo d(T) primers and dNTPs. This mix was heated to 65°C then chilled on ice. Buffer

components were added followed by SuperScript II enzyme, with a total reaction volume of 20µl. Samples were incubated at 42°C for 50 minutes, and heat-inactivated for 15 minutes at 70°C. RNase H was added to degrade the RNA template at 37°C for 20 minutes. The cDNA was subsequently used at 2µl per 50µl PCR reaction.

2.1.2 Cloning Methods

2.1.2.1 Preparation of plasmid vectors for cloning

Plasmids were linearised in either single or double restriction endonuclease digest reactions. Typically, 1µg of plasmid DNA was digested in a total reaction volume of 50µl. Restriction enzymes (NEB, Hitchin, UK) were added at a final concentration of 5-20 Units per µg DNA, usually 1µl of per enzyme. Digests were performed in the proprietary buffers recommended and supplied by the manufacturer (NEB, Hitchin, UK), and incubated in a heated water bath at 37°C for at least 1 hour, with the exception of SfiI reactions which were performed at 50°C and SmaI reactions which were performed at 25°C. If required, buffer exchange was performed using the Nucleotide Removal Kit (Qiagen, Crawley, UK), by passing the reaction through a purification column and eluting the singly digested DNA with water. Where 'blunt end' cloning was required, the vector would be treated with 1µl (5 Units) of (DNA Polymerase I, Large (Klenow) Fragment (NEB, Hitchin, UK) per µg DNA. Removal of the 3' overhang and in-fill of the 5' overhang was performed in T4 DNA Ligase buffer (NEB) (50mM Tris-HCl, pH 7.5, 10mM $MgCl_2$, 1mM ATP, 10mM DTT) supplemented with 33µM dNTP mix (NEB, Hitchin, UK) and incubated for 15 minutes at 25°C. Single digest and blunt ended preparations were treated with Shrimp Alkaline Phosphatase (rSAP) (NEB, Hitchin, UK) to remove 5' phosphate groups by adding 1 unit of rSAP per pmol of DNA ends and incubated at 37°C for 30 minutes. The linearised vectors were then visualised by agarose gel electrophoresis on a 0.8% w/v agarose gel made in 1x TAE buffer, run at a constant current of 35mA

overnight. Next day, the gel was stained in 1xTAE buffer containing a final concentration of 1µg/ml Ethidium Bromide (Fisher Scientific, Loughbrough, UK) for approximately 30 minutes. Excess staining solution was discarded and the gel rinsed under running water. The gel was visualised and appropriate bands were excised on a U.V. transilluminator, and then an image was taken on a Gel Doc system (BioRAD, Hertfordshire, UK). Bands excised from the gel were purified with the QIAquick Gel Extraction Kit (Qiagen, Crawley, UK), and eluted from the column in 20µl of water. Spectrophotometric DNA concentration of the eluate was determined using a Nanodrop 8000 spectrophotometer (Thermo Scientific, MA, USA).

2.1.2.2 Calculation of pmol DNA ends

The following equation was used to calculate the quantity of DNA ends for 5' phosphate removal, where n is the number of nucleotide pairs. The result is then multiplied by two to determine number of DNA ends.

$$\mu g\ DNA \times \frac{1\ pmol}{660\ pg} \times \frac{10^6\ pg}{1\ \mu g} \times \frac{1}{n} = pmol\ DNA$$

2.1.2.3 Preparation of insert fragments for cloning

Fragments for cloning were prepared by either directly by subcloning from another vector through restriction endonuclease digestion, or by PCR-amplification with custom oligonucleotide primers, incorporating suitable restriction endonuclease sites. For PCR amplified fragments, high-fidelity polymerases (Phusion (NEB, Hitchin, UK) or KOD polymerase (Novagen, WI, USA) were used which possess 3' to 5' exonuclease activity in addition to the 5' to 3' polymerase activity. Reaction and thermal cycling conditions varied according to which polymerase was being used; see tables 2.1 and 2.2 for example reaction set up. Both polymerase PCR amplifications were run on 'touchdown' protocols, as indicated in table 2.3.

Component	Volume	Final Concentration
5x HF Buffer	10µl	1x
dNTP Mix, 10mM each	1µl	200µM each
10µM Forward Primer	2.5µl	0.5µM
10µM Reverse Primer	2.5µl	0.5µM
Template DNA, ≤250ng	Variable	≤5ng/µl
Phusion polymerase, 2 Units/µl	0.5µl	1 Unit per reaction
Water	to volume	
Total reaction volume	50µl	

Table 2.1 Phusion polymerase PCR reaction set up

Component	Volume	Final Concentration
10x Reaction Buffer	5µl	1x
dNTP Mix, 2mM each	5µl	200µM each
10µM Forward Primer	1.5µl	0.3µM
10µM Reverse Primer	1.5µl	0.3µM
Template DNA: ≤250ng genomic/cDNA 10ng plasmid DNA	Variable	≤5ng/µl
KOD polymerase, 1 Unit/µl	1µl	1 Unit per reaction
25mM $MgSO_4$	3µl	1.5mM
Water	to volume	
Total reaction volume	50µl	

Table 2.2 KOD polymerase PCR reaction set up

Step	Phusion	KOD
Initial denaturation	98°C x 30 seconds	95°C x 2 minutes
Cycle 1: Denaturation	98°C x 10 seconds	95°C x 20 seconds
Cycle 1: Annealing	68°C x 10 seconds (-1°C/repeat)	68°C x 20 seconds (-1°C/repeat)
Cycle 1: Extension	72°C x 15-30 seconds	70°C x 10-25 seconds
Repeat Cycle 1	Further 14 times	Further 14 times
Cycle 2: Denaturation	98°C x 10 seconds	95°C x 20 seconds
Cycle 2: Annealing	54°C x 10 seconds	54°C x 20 seconds
Cycle 2: Extension	72°C x 15-30 seconds	70°C x 10-25 seconds
Repeat Cycle 2	Further 19 times	Further 19 times
Final Extension	72°C x 5 minutes	70°C x 5 minutes

Table 2.3 Touchdown PCR program

2.1.2.4 Molecular cloning

All DNA cloning steps were performed with an insert to vector molar ratio of 3:1, determined by the calculation:

$$Insert\ mass\ (ng) = \frac{Vector\ mass\ (ng) \times Insert\ size\ (Kb)}{Vector\ size\ (Kb)} \times \frac{3}{1}$$

Ligation reactions contained the calculated insert amount, 100ng of linearised vector plasmid, 1µl (400U) T4 DNA Ligase (NEB), 1µl 10x T4 DNA Ligase buffer (10mM $MgCl_2$, 50mM Tris-HCl, 1mM ATP, 10mM dithiothreitol (DTT), pH 7.5) (NEB, Hitchin, UK) in a 10µl total reaction volume. Reactions were incubated at RT for at least 2 hours, with 2µl of the reaction used for bacterial transformation.

2.1.2.5 Plasmid propagation and purification

Plasmids resulting from ligations were miniprepared from 1ml of overnight culture, grown at 37°C, 225rpm. Bacteria were harvested at 10,000 x g for 5 minutes at room temperature. The pellets were prepared using the QIAPrep Spin Miniprep kit (Qiagen, Crawley, UK) according to the manufacturer's instructions. Plasmid DNA was eluted in 30µl sterile water. A diagnostic restriction digest was performed and visualised by gel electrophoresis to screen for ligation-positive clones. Cloning

junctions were confirmed by DNA sequencing (Source Bioscence, Nottingham, UK). Confirmed clone miniprep DNA was retransformed into chemical competent DH5α. A single colony was cultured in overnight in 50ml LB medium at 37°C with shaking at 225rpm. Plasmid DNA was midiprepared using the Plasmid Plus Midiprep kit (Qiagen, Crawley, UK) according to the manufacturer's instructions, and eluted in 200µl sterile water.

2.1.2.6 Preparation of chemical competent E. coli

Transformation competent E.coli bacteria were prepared according to the method of Chung and Miller for chemical transformants (Chung and Miller, 1988). A starter culture of E. Coli strains (DH5α or C41) were grown overnight at 37°C at 220rpm in Luria-Bertani (LB) nutrient broth. Next day, the starter culture was used to inoculate 100ml of fresh LB broth. The growth of the culture was monitored by measuring absorbance changes in optical density (O.D.) at 600nm. Once the culture had reached 0.5-0.6 (corresponding to early log phase of growth), bacterial cells were pelleted in a benchtop centrifuge (Eppendorf, Stevenage, UK) for 5 minutes at 300 x g, 4°C and resuspended in 9ml of Transformation/Storage Buffer (TSB) (10mM $MgCl_2$, 10mM $CaCl_2$, 10% PEG, 5% DMSO) and incubated on ice for 10 minutes. For freezing, 10% (1ml) sterile glycerol (Sigma Aldrich, Dorset, UK) was added and mixed thoroughly thorough the cell suspension. 100µl aliquots were snap frozen in a mix of dry ice and 100% Ethanol (EtOH) (VWR, Leicestershire, UK), then stored at -80°C until use.

2.1.2.7 Bacterial chemical transformation

The chemical transformation competent E.coli were thawed. Plasmid DNA for bacterial transformation (typically 2µl of ligation reactions or 100ng of plasmid) was mixed with 20µl 5x KCM (500mM KCl, 150mM $CaCl_2$, 250mM $MgCl_2$) and sterile water to a final volume of 100µl and chilled on ice. 100µl aliquots of transformation competent E. Coli (made and frozen previously) were thawed on ice and then

combined with the DNA mix. The competent cell:DNA mix was incubated on ice for 20 minutes then at RT for a further 10 minutes. Cells were allowed to recover by addition of 1ml LB broth and incubated at 37°C for 1 hour and then pelleted at 1000 x g for 5minutes in a microfuge (Eppendorf, Stevenage, UK). Pellets were resuspended and diluted in appropriate volumes of LB broth and spread onto selective LB agar plates. Plates were allowed to dry, inverted and grown overnight at 37°C. Next day, colonies were counted and typically 6-24 were picked for further analysis.

2.1.2.8 Bacterial electroporation

High-competency electrocompetent DH10β E.coli (NEB, Hitchin, UK) were transformed by electroporation. Briefly, 25µl of bacteria were mixed with DNA in a microtube, then transferred to a pre-chilled 0.1cm electrode gap cuvette. Electroporation was performed at 2000 Volts, 200 Ohms, 25 µFarads, using a Gene Pulser II electroporator (BioRAD, Hertfordshire, UK). Cells were recovered for 1 hour at 37°C in Outgrowth Media (NEB, Hitchin, UK) to a final volume of 1ml. Cells were then pelleted at 1000 x g for 5minutes in a microfuge (Eppendorf, Stevenage, UK), then resuspended and diluted in appropriate volumes of LB broth and spread onto selective LB agar plates. Plates were allowed to dry, inverted and grown overnight at 37°C. Next day, colonies were counted and harvested for further analysis.

2.1.2.9 Bacterial LB Growth Medium and Agar

A solution of 10g/L Tryptone (Oxoid, Basingstoke, UK), 5g/L Yeast Extract (Oxoid) and 10g/L NaCl (Sigma Aldrich, Dorset, UK) was mixed, and corrected to pH 7.0 with 5N Sodium Hydroxide (NaOH) (Sigma Aldrich). The medium sterilised by autoclaving at 121°C for 20mins with steam at 15 psi. LB agar was prepared as for LB Broth but with an additional 15g/L agar (Oxoid, Basingstoke, UK). The agar solution was sterilised by autoclave, and cooled to 50°C. Selective plates for antibiotic resistant bacterial transformants were made at the following

concentrations; 100µg/ml Ampicillin (Amp), 15µg/ml Chloramphenicol (Cam) or 50µg/ml Kanamycin (Kan) (all Sigma Aldrich, Dorset, UK). All antibiotics were made as 1000x concentrated stock solutions, filter sterilised, and stored frozen at -20°C in aliquots. Plates were then poured using asceptic technique, with approximately 25ml agar per 10cm petri dish, or 250ml per 25cm^{2} Nunc bio-assay dish (Fisher Scientific, Loughborough, UK).

2.1.3 Protein Analysis Methods

2.1.3.1 SDS-PAGE Gel Casting

Polyacrylamide gels were cast in 1 or 1.5mm glass spacer plates, with either 10- or 15-well combs, depending upon sample number and volume. Depending upon the protein of interest's size (kDa), for optimal separation resolving gel layers contained either 10, 12 or 15% acrylamide. Typically 5ml was prepared for each mini gel (approx. 9cm x 7cm) or doubled for large gels (approx. 18cm x 7cm) as shown in table 2.4.

Resolving Gel Component	10%	12%	15%
Deionised Water	1.9ml	1.6ml	1.1ml
Resolving Buffer (1.5M Tris, pH8.8)	1.3ml	1.3ml	1.3ml
30% Acrylamide:Bis-acrylamide (37.5:1 mix) (BIORAD, Hertfordshire, UK)	1.7ml	2.0ml	2.5ml
10% w/v Sodium Dodecyl Sulphate (SDS) (Severn Biotech, Kidderminster, UK)	50µl	50µl	50µl
10% w/v Ammonium Persulphate (APS) (Sigma Aldrich, Dorset, UK)	50µl	50µl	50µl
TEMED (N,N,N',N'-Tetramethylethylenediamine) (MP Biomedicals, MA, USA)	5µl	5µl	5µl

Table 2.4 Resolving gel casting set up

Resolving gels were poured immediately after mixing, and overlaid with 0.5ml isopropanol to prevent overdrying of the gel and ensure a level layer. Once set, the

isopropanol overlay was rinsed from the resolving gel and, depending on gel size, 2.5-5ml of 5% acrylamide stacking gel (table 2.5) was poured over the resolving gel and the sample comb inserted and left to set.

Stacking Gel Component	5%
Deionised Water	900µl
Stacking Buffer (0.5M Tris, pH6.8)	750µl
30% Acrylamide:Bis-acrylamide (37.5:1 mix) (BioRAD)	330µl
10% w/v Sodium Dodecyl Sulphate (SDS) (Severn Biotech)	20µl
10% w/v Ammonium Persulphate (APS) (Sigma Aldrich)	20µl
TEMED (N,N,N',N'-Tetramethylethylenediamine) (MP Biomedicals)	2µl

Table 2.5 Stacking gel casting set up

2.1.3.2 SDS-PAGE Gel Running

Once set, gel plates were rinsed in deionised water to remove excess acrylamide and then assembled into the Mini-Protean Tetra Cell electrophoresis units (BioRad, Hertfordshire, UK). Tanks were filled with SDS-PAGE Running buffer (20mM Tris, 190mM Glycine, 0.1% SDS, pH8.3) and samples loaded. All samples were denatured in a final 1x Laemmli Sample buffer (62.5mM Tris, pH6.8 (Sigma Alridch, Dorset, UK), 2% w/v SDS (Severn Biotech, Kiddermminster, UK), 10% v/v glycerol (Sigma Aldrich), 715mM 2-Mercaptoethanol (Sigma Aldrich), 0.025% Bromophenol Blue (Sigma Aldrich)) by boiling for 5 minutes at 100°C. For size determination from 10 to 240kDa, 3µl of BluEYE prestained protein ladder (GeneFlow, Litchfield, UK) was loaded in an empty lane. Gels were run at 100 volts until the bromophenol blue dye front reached the bottom of the gel. Once finished, the apparatus was disassembled and the gel released form the glass sandwich plates for further use, either with Coomassie staining or Western blotting.

2.1.3.3 SDS-PAGE Coomassie staining

To visualise protein bands, gels were covered with Coomassie stain (0.1% w/v Brilliant Blue G-250 (MP Biomedicals, CA, USA), 10% v/v Acetic Acid (Sigma Aldrich, Dorset, UK), 50% v/v Methanol (VWR, Leicestershire, UK)) for 1 hour, with shaking on a rocking platform (VWR). The staining solution was discarded, and the gel rinsed briefly with Coomassie Destain solution (10% v/v Acetic Acid (Sigma Aldrich, Dorset, UK), 50% Methanol (VWR)). Several washes were performed with fresh with Coomassie Destain solution until the protein bands were visible. Gels were imaged with a Gel Doc XR System (BioRad, Hertfordshire, UK).

2.1.3.4 Western Blotting

Gels were equilibrated in Transfer buffer (20mM Tris (Sigma), 190mM Glycine (Fisher Scientific, Loughborough, UK), pH8.3) for 20 minutes at room temperature. Meanwhile, Hybond 0.2µm polyvinylidene difluoride (PVDF) membrane (GE Healthcare, Amersham, UK) was cut to size and activated in Methanol (Sigma Aldrich, Dorset, UK) for 15 seconds. The methanol was discarded and the membrane washed three times in deionised water, before being equilibrated in Transfer buffer for 5 minutes. The gel/PVDF membrane sandwich was assembled with gel-sized foam pads and 3MM Grade Chromatography Filter paper (Whatman, Buckinghamshire, UK), pre-soaked in Transfer buffer. The proteins in the gel were transferred to the PVDF membrane at a constant 350mA for 1 hour. The sandwich was disassembled and the membrane marked for orientation, before being rinsed in Tris-buffered Saline with Tween (TBS-T) buffer (20mM Tris, pH 7.4, 150mM NaCl (readymade by Severn Biotech, Kidderminster, UK), 0.1% Tween-20 (Sigma Aldrich, Dorset, UK)). A milk-based blocking solution (TBS-T, 5% w/v skimmed milk powder (Sigma Aldrich)) was applied to the membrane to discourage non-specific antibody binding, for 1 hour with rotation on a roller mixer (VWR, Leicestershire, UK) at room temperature. The blocking solution was discarded and the membrane rinsed three

times with fresh TBS-T. Primary antibodies were diluted to an appropriate concentration (see table 2.6) in TBS-T containing 1% w/v skimmed milk powder (Sigma Aldrich), and incubated overnight, with rotation, at 4°C.

Primary Antibody	Supplier	Host Species	Dilution
Anti-CASP3	Cell Signalling	Rabbit	1:1000
Anti-Cleaved CASP3	Cell Signalling	Rabbit	1:1000
Anti-FLAG (M2)	Sigma Aldrich	Mouse	1:1000
Anti-PARP	Cell Signalling	Rabbit	1:1000
Anti-β-Actin	Sigma Aldrich	Mouse	1:4000
Anti-HA-HRP	AbCam	Rabbit	1:5000
Anti-His-HRP	Sigma Aldrich	Mouse	1:1000

Table 2.6 Antibodies for Western blot

Next day, membranes were rinsed three times with fresh TBS-T, before a solution containing secondary, Horseradish peroxidase (HRP)-linked antibodies (Cell Signalling, MA, USA) was applied. The secondary antibodies were diluted 1:1000 in TBS-T containing 1% w/v skimmed milk powder (Sigma Aldrich, Dorset, UK) and incubated with the membrane for 1 hour at room temperature with rotation. The antibody solution was discarded and unbound antibody was removed by rinsing the membrane three times, followed by three, 15 minute washes in TBS-T. Antibody binding was detected by application of HRP substrate, Pierce Enhanced Chemiluminescent (ECL) reagent (Thermo Scientific, MA, USA), to the membrane and incubating for 5 minutes. The membrane was drained of excess reagent, then covered with Saran wrap (SC Johnson & Sons, WI, USA) before being exposed to photographic film (Thermo Scientific, MA, USA). Films were developed with an X-O-Graph developer (Xograph Healthcare, Gloucestershire, UK).

2.1.3.5 Bicinchoninic Acid (BCA) Assay of Protein Concentration

To determine the concentration of protein solutions (cell lysates or purified

protein), the Pierce BCA Protein Assay Kit (Thermo Scientific, MA, USA) was used. Briefly, a calibration curve was prepared using known concentration standards. These standards were prepared from the supplied 2mg/ml Bovine serum albumin (BSA), by dilution with sterile water as described in the table 2.7.

BSA Concentration (mg/ml)	Dilution
0	No BSA
0.125	1:16
0.25	1:8
0.5	1:4
0.75	1:2.67
1	1:2
2	Undiluted

Table 2.7 BSA dilutions for BCA assay standards

In a 96-well flat-bottomed plate (Corning, New York, USA), 10µl of BSA standard was added per well, with each concentration in duplicate or triplicate wells. An equivalent volume of the unknown samples were added to empty wells, in triplicate. The supplied reagents, “A” and “B” were mixed at a 50:1 ratio to produce the working reagent. 200µl of the working reagent were added to each standard or sample-containing well, and mixed. Plates were wrapped in foil to protect the reagent from light, and incubated at 37°C for 30 minutes. Absorbance measurements were taken at 562nm with either an Envision (Perkin Elmer, MA, USA) or SpectraMax M2e (Molecular Devices, CA, USA) plate reader. The standard well readings were averaged and a calibration curve was plotted in an Excel (Microsoft, CA, USA) spreadsheet. Concentrations (in mg/ml) of the unknown samples were determined against the calibration curve, having first subtracted the buffer background from the averaged absorbance readings.

2.2 Mammalian Cell Culture

2.2.1 Cell line growth medium

Adherent cell lines (HT1080, CHO, HEK293T) were cultured in Dulbecco's Modified Eagle's Medium (DMEM) (Gibco, MA USA) base medium, whilst non-adherent cell lines (Jurkat, KOPT-K1, MOLT4, MEL585) were cultured in Roswell Park Memorial Institute 1640 medium (RPMI 1640) (Gibco). Both types of complete growth media contained 10% v/v Foetal Bovine Serum (FBS) (Sigma Aldrich, Dorset, UK) and 1x Penicillin/Streptomycin (Pen/Strep) antibiotic supplement (Gibco). OP9-*DI1* cells were maintained in Minimum Essential Medium Eagle with alpha modification (αMEM) medium (Gibco) containing 20% v/v FBS and 1x Pen/Strep.

2.2.2 Adherent cell line culture

Cells were expanded from a starting density of 2 x 10^4 cells per cm^2, and grown to a maximum of 90% confluence at 37°C, 5% CO_2. Routine sub-culturing was achieved by first washing the cell layer with 1x PBS pH 7.4 (Gibco, MA, USA) and then applying 0.05% Trypsin-EDTA (Gibco) for 5 minutes at 37°C, 5%CO_2. The trypsin was then triturated for a single cell suspension and quenched with an excess of growth medium. Cells were pelleted at 200 x g for 5mins, RT to remove the trypsin, and resuspended in a suitable volume of growth medium. Viable cells were counted by Trypan Blue (Invitrogen, Paisley, UK) dye exclusion and replated at an appropriate cell density.

2.2.3 Non-adherent cell line culture

Cells were expanded from a starting density of 2 x 10^4 cells per ml, and grown to a maximum of 90% confluence at 37°C, 5% CO_2. Routine sub-culturing was achieved by counting viable cells by Trypan Blue (Invitrogen, Paisely, UK) dye exclusion. Appropriate dilutions of cells were performed to replate cells at the correct starting cell density.

2.2.4 Mouse and T-ALL tumour culture

Mouse and passaged human T-ALL cells were co-cultured on an OP9-*Dl1* cell layer, plated at a starting density of 2.5 x 10^4 cells/cm^2. Tumour cells were plated at initial densitites of either 10^5, 10^6 or 10^7 cells/ml. Culture media formulations tested were as follows;

RPMI: RPMI base medium (Gibco, MA, USA), 10% v/v FBS, 1x mercaptoethanol (Gibco), 50U/ml interleukin-2 (IL-2) (Roche, Basel, Swtizerland), 25ng/ml interleukin-7 (IL7) (Peprotech, London, UK), 1x Pen/Strep.

IMDM: IMDM base medium (Gibco), 10% v/v FBS, 1x mercaptoethanol, 1x Glutamine, 1x Non-essential amino acids, 1x Sodium Pyruvate, 1x HEPES (all Gibco) 50U/ml interleukin-2 (IL-2), 25ng/ml interleukin-7 (IL7). Medium composition protocol from personal communication with Dr Katia Ruggero, former member of the Rabbitts laboratory, WIMM, University of Oxford.

MEM: αMEM base medium (Gibco), 10% v/v FBS, 1x mercaptoethanol, 50U/ml interleukin-2 (IL-2), 25ng/ml interleukin-7 (IL7), 1x Pen/Strep. Medium composition protocol adapted from personal communication with Dr Katia Ruggero, former member of the Rabbitts laboratory, WIMM, University of Oxford.

2.2.5 Cell Counting

Cell number was determined by Trypan Blue (Invitrogen, Paisely, UK) dye exclusion, which was performed with a 1:1 cell to dye dilution for 5 minutes before loading onto an Improved Neubauer haemocytometer (Reichert Ltd, Munich, Germany).

2.2.6 Cell cryopreservation

Cell lines and tumour samples were frozen in a cryoprotective medium with a final concentration of 90% v/v FBS (Sigma Aldrich, Dorset, UK), 10% v/v Dimethyl sulphoxide (DMSO) (Sigma Aldrich). Cells were immediately placed at -80^oC for 24hrs and then relocated to liquid nitrogen for long-term storage.

2.2.7 Antibiotic selection titration

Cells were assessed for their antiobiotic sensitivitiy prior to stable transfection to gauge the most suitable selection concentration. G418 was assayed between 0-800µg/ml, Hygromycin assayed between 0-350µg/ml and Puromycin 0-4µg/ml (all Invitrogen, Paisley, UK). The lowest concentration to kill non-resistant cells was chosen. Dual selection was similarly tested to ensure no cross-reactivity of the antibiotics.

2.2.8 General mammalian transfection

The initial procedure for both transient and stable transfection was identical. Cells were plated in 6-well plates at a density of 4 $x10^4$ (HT1080) or 6 $x10^4$ (CHO) cells/cm^2 the night before transfection to allow adherence overnight. The following day, 10µl of Lipofectamine 2000 (Invitrogen, Paisley, UK) was added to 90µl Opti-MEM reduced serum medium (Gibco, MA, USA) and incubated at room temperature for 5 minutes for initial liposome formation. Meanwhile, 1-3µg of plasmid was diluted into Opti-MEM medium to a 100µl total volume. The Lipofectamine and plasmid solutions were then combined and incubated at RT for a further 20 minutes, to allow the DNA-complexed liposomes to form then diluted into 2ml of complete growth medium and overlaid onto the cell layer overnight.

2.2.8.1 Transient transfection

After overnight liposome incubation, growth medium was aspirated and cells washed with 1x PBS pH7.4 (Gibco, MA, USA). Growth medium was then either replaced for extended culture or cells were harvested for analysis with 0.05% Trypsin-EDTA (Gibco).

2.2.8.2 Stable transfection

After overnight liposome incubation, growth medium was aspirated and cells washed with 1x PBS pH7.4 (Gibco, MA, USA). Fresh growth medium was applied

and cells were cultured for a further 24 hours. At 48 hours post-transfection, cells were washed with 1x PBS pH7.4 (Gibco) and then detached from the culture vessel with 1ml of 0.05% Trypsin-EDTA (Gibco) for 5 minutes at 37°C, 5% CO_2. Trypsinisation was quenched with 5ml growth medium, and cells were pelleted in a bench top centrifuge (Eppendorf, Stevenage, UK) at 200 x g for 5 minutes at RT. The supernatant was discarded and cells were resuspended in 10ml of growth medium. Cells were then plated onto 10cm dishes (Corning, New York, USA) in 12ml total volumes at the following ratios; 1/2, 1/5, 1/10, 1/20 and 1/40. An untransfected well was prepared in parallel at the lowest and highest cell dilutions (1/2 and 1/40) to act as a selection control. The next day (72 hours post lipofection) antibiotic marker selection was begun at the following final concentrations; 200µg/ml Hygromycin B (Invitrogen), 500-600µg/ml G418 (Invitrogen) or 3.5µg/ml Puromycin (Invitrogen). Selection medium was replaced every two days. After approximately 7-12 days in selection (or when the control plates were devoid of viable cells), single transfected colonies were picked with by pipette into a single well of a 96-well plate (Corning) and grown until 90% confluence. At this point, cells were harvested with 50µl of 0.05% Trypsin-EDTA for 5 minutes at 37°C, 5% CO_2 and trypsinisation quenched with 50µl growth medium. Half of the cell suspension was transferred to a replica 96-well plate, to which an equal volume of 2x Freezing medium was applied and mixed. The replica plate was then wrapped in Parafilm (Bemis, USA), placed in a polystyrene box for insulation and frozen at -80°C. The remaining cells were then expanded for appropriate assessment of transgene expression.

2.2.9 Tetracycline (Tet) induction of TetOn constructs

A 1mg/ml stock solution of Tetracycline (Doxycycline Hyclate) (Sigma Aldrich, Dorset, UK) was prepared in milliQ H_2O (Millipore, Hertfordshire, UK), and filter sterilised through a 0.2µm syringe filter (Sartorius, Göttingen, Germany). Stock solutions were protected from light and stored at 4°C for a maximum of two weeks.

For use, stock solutions were diluted 1/1000 in cell growth medium to a final working concentration of 1µg/ml.

2.3 AIDA Assessment Methods

2.3.1 Construction of AIDA plasmids

Cloning was performed according to the scheme devised by Dr Tim Brend (former member of the Rabbitts laboratory, WIMM, Univeristy of Oxford) and Prof. T.H. Rabbitts (WIMM, University of Oxford). A single FLAG tag was added via SacII/BamHI restriction cloning to the Hygromycin-resistant vector pUHD10-3H which contains a 7x Tet-response element. The proCASP3 cDNA sequence was PCR amplified and cloned via NotI/BglII. VH#Y6 or VL#204 was added via NotI/SfiI, Annealed oligos encoding F2A and HA tag sequences were digested with BglII and ClaI and cloned into the same sites in the vector. The VH+VL vector was created from the single VH#Y6 vector, with VL#204 added via ClaI/XbaI and a second proCASP3 element introduced downstream of the HA-tag via XbaI/BamHI. All three vectors were subsequently modified to contain an N-terminal Farnesylation sequence, PCR amplified form Neuromodulin/GAP43 cDNA, which was cloned via SalI/NheI upstream of the FLAG tag, and blunt cloned into the EcoRV site upstream of the HA-tag in the VH+VL vector. VH variants were cloned by amplification of the fragments and cloning into the NotI/SfiI sites as before. (Maps and primers in Appendix A)

2.3.2 RAS mutation analysis

HT1080TetOn cDNA was amplified with primers designed for human HRAS, KRAS and NRAS cDNA (obtained for Dr Ami Miller, Rabbitts laboratory, WIMM, University of Oxford) with Phusion polymerase using a ‘touchdown’ protocol (described in section 2.1.2.3 and tables 2.1-2.3). PCR products were gel extracted, digested and cloned into pBluescript SKII+ (Stratagene, CA, USA). Positive insert clones were sent for sequencing (Source Bioscience, Nottingham, UK). (Primers in

Appendix B)

2.3.3 Clonogenic assay

The following method was adapted from Franken et al (Franken et al., 2006). Cells were harvested from a T75 flask (Corning, New York, USA) with 3ml 0.05% Trypsin-EDTA (Gibco, MA, USA) for 5 minutes at 37°C, 5% CO_2. Trypsinisation was quenched with the addition of 5ml growth medium, and cells were pelleted in a bench top centrifuge (Eppendorf, Stevenage, UK) at 200 x g for 5 minutes at room temperature. The supernatant was discarded and cells were resuspended in 10ml of growth medium and viable cells were counted. A working cell suspension of $2x10^2$ cells/ml for plating was prepared by serial dilution. Appropriate volumes of the working suspension were mixed with medium to achieve i) 20, ii) 50 and iii) 100 cells in a total volume of 4ml per 6cm diameter plate (Corning). Six replica plates were made per cell density to allow triplicate plates of both growth conditions (with and without tetracycline), having been prepared from a mastermix for reproducibility, and left overnight to adhere to the dish. Next day, medium was removed and replaced with either fresh medium (three plates) or medium containing tetracycline (three plates). Cells were incubated at 37°C, 5% CO_2 for the next nine days, replacing medium every three days. On day nine, the growth medium was removed and the cell layer washed with 2ml 1x PBS, pH7.4 (Gibco). Colonies were stained for 30 minutes with 3ml staining solution (6% v/v glutaraldehyde (Sigma Aldrich, Dorset, UK), 0.5% w/v Crystal Violet (Sigma Aldrich)), and then washed twice with deionised water. Plates were then gently submerged in deionised water to remove the last traces of dye, and left to air dry on the bench. Cell patches of greater than 10 cells were deemed to be a colony for this assay (due to the anticipated growth impedance effect of the anti-Ras VH). Colonies were visualised on a large-view field stereomicroscope (Leica MZFLIII, Leica, Milton Keynes, UK) and counted using a colony counting pen (VWR, Leicestershire, UK). The Plating Efficiency (PE) of each

clone was calculated from combined average colony counts of all cell densities tested of the uninduced (no Tet) plates. The Surviving Fraction (SF) was similarly determined from the tetracycline-induced plates and compared with the plating efficiency. Formulae are as follows;

$$PE = \frac{Average\ colony\ number\ (no\ Tet)}{Number\ of\ cells\ plated} \div Number\ of\ densities\ tested$$

$$SF = \frac{Average\ colony\ number\ (Tet)}{Number\ of\ cells\ plated} \div (Number\ of\ densities\ tested \times PE)$$

Statistical analyses performed were unpaired two-tailed student t tests and a one way ANOVA and calculated by GraphPad Prism 7.0 software (GraphPad Software, CA, USA).

2.3.4 Caspase 3 inhibitor assay

One VH+VL and one VH-Only clone were plated at $4x10^4$ cells per well of a 24-well plate and left to adhere overnight. Next day, growth medium was replaced with either regular medium (no tetracycline, uninduced), medium containing 1µg/ml tetracycline, or medium containing 1µg/ml tetracycline and varying titres of the irreversible CASP3 inhibitor, Z-DEVD-FMK (Santa Cruz Biotechnology, Heidlelberg, Germany). Each condition was performed on six 24-wells, for analysis by two methods, both with triplicate wells. The inhibitor was reconstituted in sterile DMSO to 20mM, and experimental titres tested were 5, 10, 15, 20 and 40µM. The DMSO concentration was normalised to 0.2% v/v across all samples to account for any possible effect on cell viability. After incubation for 48 hours, cells were analysed by i) PrestoBlue (Invitrogen, Paisley, UK) viability assay and ii) Annexin-V, 7-AAD flow cytometric profiling.

2.3.5 PhiPhiLux Fluorogenic substrate assay

Cells were plated at $2x10^4$ cells per cm^2. Next day, cells were either uninduced or induced with tetracycline at 1µg/ml for 48 hours. For an apoptosis

control, etoposide was added to a final concentration to 100μM for the last 8 hours of the growth period. Cells were harvested by trypsinisation and counted. $5x10^5$ cells were aliquoted into microtubes and pelleted at 200 x g for 5mins at room temperature. Pellets were subjected to the PhiPhiLux assay (OncoImmunin, Maryland, USA) to test for active CASP3. Briefly, cells were resuspended in 75μl of the PhiPhiLux substrate solution or 'FC Dilution Buffer' for the no substrate control, each supplemented with 8μl FBS (Sigma, Dorset, UK). Cells were incubated at 37°C for 30-60 minutes, protected from the light. Excess reagent was then removed by washing cells with 1ml of 'FC Dilution Buffer' and pelleted as before. Finally, cells were resuspended in 1ml of 'FC Dilution Buffer' and analysed by flow cytometry (488nm laser, FITC channel).

2.3.6 PrestoBlue viability assay

Following appropriate treatment of cells, growth medium was aspirated and replaced with an equal volume of PrestoBlue reagent (Invitrogen, Paisley, UK), dilulted 1:10 with growth medium. Cells were incubated for 20 minutes at 37°C, 5% CO_2. Conversion of the reagent to a fluorescent product by metabolically-active cells was measured using an M2e SpectraMax plate reader (Molecular Devices, CA, USA), at the following wavelengths: 544nm excitation, 590nm emission, 570nm cut-off.

2.3.7 Annexin-V and 7-AAD flow cytometric profiling

Following appropriate treatment, cells were trypsinised from their culture vessel and counted as described previously, with $5x10^4$ cells aliquoted per staining reaction. Each cell aliquot was washed in 3ml of Annexin-V Staining buffer (10mM HEPES, pH7.4, 140mM NaCl, 2.5mM $CaCl_2$). Cells were pelleted at 200 x g for 5 minutes at 4°C and resuspended in 100μl of Annexin-V Staining buffer containing 5μl fluorescein isothiocyante (FITC)-conjugated Annexin-V (BD, New Jersey, USA). Cells were stained on ice for 15 minutes, protected from strong light to prevent FITC

bleaching. Unbound Annexin-V was washed from the cells with 3ml Annexin-V Staining buffer, and cells pelleted as before. Cells were resuspended in 500µl of fresh Annexin-V staining buffer containing 5µl of 50µg/ml 7-Aminoactinomycin D (7-AAD) solution (BD), and left to stain for 10 minutes. Cells were immediately taken for analysis on an Attune NxT flow cytometer (Invitrogen, Paisley, UK), with data analysis performed with FlowJo software (Tree Star Inc., OR, USA).

2.3.8 ApoToxGlo assay

Original and mutant clones were plated in 96-well plates at an initial density of $2x10^4/cm^2$ in two triplicate sets (for -/+Tetracycline) and left to adhere overnight. Growth medium was replaced the following day, and tetracycline induction begun. Etoposide (Sigma Aldrich, Dorset, UK) was added to control wells at a final concentration of 100µM for 8hrs. The ApoToxGlo assay (Promega, WI, USA) was measured at 18 and 48hrs post-tetracycline addition and performed according to the manufacturer's instructions. Briefly, 20µl of viability substrate was added, mixed and incubated at 37^oC for 30mins. Viability fluorescence was simultaneously measured at 400nm excitation, 505nm emission (the spectra for 7-Amino-4-trifluoromethylcoumarin (AFC)) and cytotoxicity was read at 485nm excitation, 520nm emission (the spectra for Rhodamine 110 (R110)) on an M2e Spectramax plate reader (Molecular Devices, CA, USA). Following this, 100µl of the Caspase reagent was added to each well, mixed and incubated for 30mins at RT, before reading luminescence on the same plate reader. Raw data was analysed by first subtracting the averaged blank well readings from all data points. Results were then converted to either percentage value (Viabililty) or fold increase (Cytotoxicity and CASP3) relative to the respective clone's uninduced reading.

2.3.9 Cell cycle analysis

Original and mutant clones were plated in 6-well plates at an initial density of $2x10^4/cm^2$ in two triplicate sets (for -/+ tetracycline) and left to adhere overnight.

Growth medium was replaced the following day, and induction was performed with 1µg/ml tetracycline (Sigma Aldrich, Dorset, UK). Etoposide (Sigma Aldrich, Dorset, UK) was added to control wells at a final concentration of 100µM for 8hrs. After 48hrs cells were harvested with 0.05% Trypsin (Gibco, MA, USA) and pelleted at 200 x g for 5mins, room temperature. $5x10^4$ cells were washed in PBS then fixed and permeabilised in 2ml of ice-cold 70% ethanol and incubated at -20°C for at least one hour. Cells were pelleted as before, washed twice in PBS and resuspended in 50µl of 50µg/ml 7-AAD staining solution (BD, New Jersey, USA), supplemented with 0.1% Triton X-100 (Sigma Aldrich, Dorset, UK), 2.5 units of RNase A (Thermo Scientific, MA, USA). Cellular DNA was stained for 30mins at room temperature, protected from the light. Samples were then diluted with PBS immediately before collecting area fluorescence measurements on a linear scale with an Attune flow cytometer (Invitrogen, Paisley, UK). Data was analysed using FlowJo software (TreeStar, OR, USA) where cell cycle gates (Sub G1, G1, S and G2/M phases) were set on the uninduced (no tetracycline) sample of each clone, and the copied across to the respective induced (with tetracycline) sample for comparison.

2.3.10 Spheroid culture

The following method was adapted from the Cultrex 3-D Spheroid Fluorometric Proliferation/Viability assay (Trevigen, MD, USA) (Ivascu and Kubbies, 2006, Vinci et al., 2012). Cells were harvested with 0.05% Trypsin (Gibco, MA, USA) and pelleted at 200 x g for 5mins, at room temperature. After counting, cells were kept on ice to ensure they were chilled ready for matrigel addition, as matrigel solidifies rapidly above 4°C. Cells were washed once in PBS (Gibco), and resuspended in a 1:10 mix of ice-cold matrigel (BD, New Jersey, USA) to growth medium at a density of $2x10^4$/ml. 50µl of cell mixture was added to each well of a ultra low adhesion round-bottom 96-well plate (Corning, New York, USA) and centrifuged at 200 x g, 5mins, 4°C. Plates were transferred to a 37°C, 5% CO_2

incubator for 30mins to allow the matrigel layer to set. Once solidified, 50µl of growth medium was overlaid, with those wells receiving tetracycline beginning treatment when spheroids reached ~0.5mm diameter. Induction of tetracycline-inducible transgene expression was performed with 1µg/ml tetracycline (Sigma Aldrich, Dorset, UK). Plates were cultured for the next 14 days, with light microscope images taken every two days. Extra growth medium was added at regular intervals to avoid accidental damage to the spheroids. At the end of the experiment, area changes were calculated using FIJI image analysis software (Schindelin et al., 2012) and spheroid viability was measured using PrestoBlue reagent (Invitrogen, Paisley, UK) as previously described. Unpaired two-tailed student t tests were performed on the viability assay results to investigate whether there was significant variation between the treated and untreated spheroid types. These results were calculated using GraphPad Prism 7.0 software (GraphPad Software, CA, USA).

2.3.11 Luciferase assay

Combinations of VH and VL variants (anti-RAS VH#Y6, VH#Y6dm and VH#Y6mut, anti-RAS VL#204, non-specific VL#I21 and anti-LMO2 VLs #819, #826 and #827 were cloned into the triplex vector (Tanaka and Rabbitts, 2010b). PCR amplified fragments were gel extracted and introduced via NotI/SfiI (VH) or BamHI/EcoRV (VL) restriction sites. Primer sequences and maps are shown in Appendix C. HEK293T cells were transiently co-transfected in triplicate in 12-well plates, with the 400ng triplex plasmids encoding the various combinations of both VH-VP16 and VL-Gal4DBD, alongside 200ng pG5-Luc reporter and 200ng pPGK-$KRAS_{166}$(G12V)-2A-Puro RAS antigen plasmid. After 48 hours, cells were harvested and transferred to a white walled luminescence 96-well plate. Luciferase activity was measured using the Dual-Glo Luciferase assay (Promega, WI, USA), performed according to manufacturer's instructions. Luminescence measurements were read by a M2e Spectramax plate reader (Molecular Devices, CA, USA). The ratio of Renilla

to Firefly luciferase was calculated, and used to derive the fold luciferase activity relative to the empty vector control.

2.4 Protein expression methods

2.4.1 Bacterial expression plasmids

The KRAS expression plasmid pRK-HisTev-Avi-KRas$_{166}$(G12V) was cloned by and obtained from Dr Ami Miller (Rabbitts Laboratory, WIMM, University of Oxford). It was used for KRAS expression and modified for bacterial AIDA construct expression. KRAS166(G12V) was excised via BamHI/HindIII and an oligonucleotide stuffer fragment was introduced containing appropriate restricution sites. The resulting clone was digested with SfiI/BglII to receive the FLAG-VH#Y6/VL#204-proCASP3 insert, liberated from the pUHD10-based AIDA vector. Primers and maps are shown in Appendix D.

2.4.2 Bacterial expression of recombinant proteins

Chemical transformation competent C41 E.coli were produced and transformed with the respective protein expression plasmid (plasmid backbone pRK vector), according to the previously described methods. Transformants were selected on LB agar ampicillin antibiotic resistance plates, and grown overnight at 37°C. The next day, one colony was picked into a 50ml starter culture containing 100µg/ml Ampicillin and grown overnight in an orbital shaking incubator (Infors, Surrey, UK) set to 225 revolutions per minute (rpm) at 37°C. The following morning, eight 1 Litre (L) LB flasks containing 100µg/ml ampicillin were each inoculated with 5ml of the overnight starter culture. A starting optical density absorbance measurement at 600nm (O.D.$_{600nm}$) was taken in 1ml disposable cuvettes (Fisher Scientific, Loughborough, UK) using an Ultrospec 10 cell density meter (Amersham Biosciences, Buckinghamshire, UK). Cultures typically started growth at O.D.$_{600nm}$ readings between 0.05-0.1. The cultures were grown as before, at 225rpm, 37°C with O.D.$_{600nm}$ measurements taken periodically, until the cultures reached 0.6

corresponding to mid log phase, approximately 4-5 hours after inoculation. Protein expression was then induced by the addition of Isopropyl β-D-1-thiogalactopyranoside (IPTG) (Sigma Aldrich, Dorset, UK) to a final concentration of 0.5mM. Expression times and temperature varied depending upon the protein in question; $KRAS_{166}G12V$ was expressed overnight at 16°C, whereas the VH-proCASP3 and VL-proCASP3 fusion proteins were expressed at 37°C for 2 hours to minimise CASP3 activation due to high localised concentrations within the bacterial cells. To aid minimisation of CASP3 activation, the VH-proCASP3 and VL-proCASP3 expression cultures were also supplemented with 25mg/ml (77.1mM) reversible CASP3 inhibitor, 5-[[2-(methoxymethyl)-1-pyrrolidinyl]-sulfonyl]-1H-indole-2,3-dione (chemical abstracts service registry number 1110670-49-9) (Lee et al., 2001, Lee et al., 2000), which was synthesised by Dr Carole Bataille, Rabbitts laboratory, Dept. of Chemistry, University of Oxford (synthesis method is described in Appendix E). Following expression, cultures transferred to 1L centrifuge flasks (Beckman Coulter, CA, USA) and were centrifuged for 15 minutes at 3315 x g (or 4000rpm) set to 4°C with a JLA 9.1000 rotor (Beckman Coulter) in an Avanti J25 high-speed centrifuge (Beckman Coulter). Pelleted cells were combined and either lysed immediately or frozen at -20°C until further use.

2.4.3 Large-scale bacterial lysis

Following protein expression, bacterial cell pellets were lysed to liberate cytosolic protein for downstream purification. Pellets were resuspended in bacterial lysis buffer (50mM HEPES pH7.4, 500mM NaCl, 5% v/v glycerol, 10mM imidazole containing 1x protease inhibitor cocktail (Roche, Basel, Switzerland)), with 20ml lysis buffer used per 1L original culture volume. The bacterial lysate was then stirred rapidly for 10 minutes at room temperature to ensure a homogeneous lysate. Cells were then lysed at high pressure with a cell disruptor (Constant Systems, Daventry, UK) set to 25 kilo pounds per square inch (kPsi) at 4°C. Extra buffer was passed

through the cell disruptor and collected to ensure full recovery of the lysate. To reduce the viscosity of the lysate, 6 Units (6µl) of DNase I (Invitrogen, Paisley, UK) were added per 100ml lysate, supplemented with $MgSO_4$ to a final concentration of 2mM. DNase I digestion was performed for 30 minutes at RT with constant agitation. Lysates were then clarified by centrifugation at 53,000 x g (21,000 rpm) at 4°C with a JA 25.5 rotor (Beckman Coulter, CA, USA) in an Avanti J25 high-speed centrifuge (Beckman Coulter). Small samples of both the supernatant and pellet were kept for SDS-PAGE analysis, whilst the rest of the supernatant was carried forward for purification.

2.4.4 Purification of Histidine-tagged proteins

Recombinant proteins with 6x Histidine (His) residue tags were purified at neutral pH (pH7.4) through charge interaction with immobilised Nickel (Ni) divalent ions (Ni^{2+}). For purification of lysate derived from 8L total expression culture, 12ml of 50% Ni-NTA agarose slurry (Qiagen, Crawley, UK) was used, corresponding to a 6ml bead volume. The Ni-NTA agarose was washed and resuspended in equilibration buffer (50mM HEPES, pH7.4, 500mM NaCl, 5% v/v glycerol, 10mM Imidazole), and then added to the clarified bacterial lysate. For maximal binding of the His-tagged proteins to the Ni-NTA agarose beads, the lysate:bead mixture was incubated overnight at 4°C with gentle agitation. The next day, the lysate:bead mixture was applied to a 20ml polypropylene gravity flow column (BioRAD, Hertfordshire, UK), and passed through to allow the resin to settle at the base of the column, with an aliquot kept for subsequent SDS-PAGE anaylsis. The column was washed twice with 4x bed volumes (4x 6ml agarose resin) of equilibration buffer, followed by washing in the same manner with wash buffer (50mM HEPES, pH7.4, 500mM NaCl, 5% v/v glycerol, 25mM Imidazole). Immobilised proteins were then eluted in three stages with rising Imidazole concentrations from 50mM to 250mM; Elution buffer 1 (50mM HEPES, pH7.4, 500mM NaCl, 5% v/v glycerol, 50mM

Imidazole), Elution buffer 2 (50mM HEPES, pH7.4, 500mM NaCl, 5% v/v glycerol, 100mM Imidazole), and Elution buffer 3 (50mM HEPES, pH7.4, 500mM NaCl, 5% v/v glycerol, 250mM Imidazole). Each elution was performed 3-4 times with 3ml (1x bead bed volume) of the respective elution buffer. Flow-through of the wash and first two elution concentrations (50mM and 100mM Imidazole were pooled, whilst the 250mM Imidazole elutions were kept as separate fractions. Aliquots of the wash and elution fractions were kept for subsequent SDS-PAGE or Western blot anaylsis, where 10µl of each sample were loaded onto appropriate percentage acrylamide gels to confirm expression of the correct protein and determine which fraction(s) held the highest and purest yield. Those deemed most suitable were carried forward for GTP analogue loading and further purification by size exclusion chromatography (SEC) ($KRAS_{166}$G12V protein) or dialysed for use without further purification (VH-proCASP3 and VL-proCASP3 proteins).

2.4.5 Loading $KRAS_{166}$G12V protein with guanosine 5'-[β,γ-imido] triphosphate (GMP.PNP)

Protocol adapted from Quevedo et al (Quevedo et al., 2018). IMAC-purified $KRAS_{166}$G12V was loaded with the non-hydrolysable GTP nucleotide analogue guanosine 5'-[β,γ-imido]triphosphate (GMP.PNP) (Sigma Aldrich, Dorset, UK) to ensure the protein was in the GTP-bound "on" or active state. Protein eluate from the IMAC purification was concentrated in to a final volume of 2.5ml using a 15ml 10kDa molecular weight cut-off (MWCO) Amicon centrifugal concentrator units (Millipore, MA, USA), that had been pre-rinsed with deionised water to remove traces of glycerol from manufacture, in a bench top centrifuge operated at 3220 x g (4000 rpm) at 4°C until the lysate had been concentrated to the desired volume. Buffer exchange of the protein sample was then achieved by running the sample through a PD-10 Sephadex desalting column (GE Healthcare, Amersham, UK), as per the manufacturer's instructions, and eluting in 3.5ml of GMP.PMP Loading buffer (1x

PBS, pH7.4, 5mM $MgSO_4$). The sample was concentrated as before to a suitable volume, and the protein concentration was calculated by reading absorbance at 280nm (A280) in triplicate with a NanoDrop spectrophotomer (Thermo Scientific, MA, USA). The A280 value was converted to mg/ml concentration by dividing the averaged reading with the protein's estimated absorbance at 1mg/ml, generated by the MacVector software (MacVector Inc., NC, USA) protein analysis tool. Further conversion to molarity was performed by dividing the mass per volume by the molar mass of the protein, and multiplying by the volume. A 1ml GMP.PNP loading reaction was performed, with KRAS166G12V at a final concentration of 0.63mM, with a 10x molar excess of GMP.PMP (6.3mM final concentration) and 30 Units of Alkaline Phosphatase (Roche, Basel, Switzerland) in a 1x Alkaline Phosphatase reaction buffer (50mM Tris, pH8.5, 1mM EDTA, 200mM $(NH_4)_2SO_4$. The reaction was allowed to proceed at room temperature for 2 hours, and then quenched by the addition of $MgCl_2$ to a final concentration of 50mM. The GMP.PNP-loaded protein was then taken forward for purification by size exclusion chromatography.

2.4.6 Size Exclusion Chromatography (SEC) of $KRAS_{166}$G12V protein

The GMP.PNP-loaded $KRAS_{166}$G12V protein were pooled and concentrated as necessary to a final volume of 1.5ml using a 15ml 10kDa molecular weight cut-off (MWCO) Amicon centrifugal concentrator units (Millipore, MA, USA), that had been pre-rinsed with deionised water to remove traces of glycerol from manufacture. Centrifugation was performed in a bench top centrifuge (Eppendorf) at 3220 x g (4000 rpm) at 4°C until the lysate had been concentrated to the desired volume, periodically triturating to keep the lysate homogenised. Once at volume, the lysate was transferred to a microtube and any aggregates or impurities were pelleted out of solution by centrifuging twice in a refrigerated microfuge at 16,100 x g (13,200 rpm) at 4°C for 10 minutes. Meanwhile, the SEC column was set up. A HiLoad Superdex 75 prep grade prepacked 16/600 column (GE Healthcare, Amersham, UK), attached

to an ÄKTA automated fast protein liquid chromatography (FPLC) system (GE Healthcare), was prepared for chromatography by exchanging the storage buffer (20% v/v EtOH) for deionised water, followed by equilibration with column running buffer (1x PBS, pH7.4, 5mM $MgCl_2$), that had previously been filtered through a 0.2µm cellulose nitrate membrane (Whatman, Buckinghamshire, UK) and degassed by stirring for 10 minutes at RT. The protein sample was loaded onto the ÄKTA system by injection into a 2ml loop port through a Millex PVDF 0.22µm syringe-driven filter unit (Millipore, MA USA). The column was run at a flow rate of 1ml per minute, and fractions of approximately 1.5ml were collected in polypropylene deep (2ml) 96-well plates (Greiner Bio-One, Gloucestershire, UK). Fractions with 280nm absorbance protein peaks eluting at the expected molecular weight (determined from previous column calibration with known standards) were chosen from the chromatogram, and 10µl of these fractions were analysed for correct protein size and purity by SDS-PAGE. Those fractions deemed of suitable quality were concentrated in a 4ml 10kDa Amicon MWCO centrifugal filter unit (Millipore). The protein concentration of the sample was determined by reading absorbance at 280nm (A280) in triplicate with a NanoDrop spectrophotomer (Thermo Scientific, MA, USA). The A280 value was converted to mg/ml concentration by dividing the averaged reading with the protein's estimated absorbance at 1mg/ml, generated by the MacVector software protein analysis tool (MacVector Inc., NC, USA). Further conversion to molarity was performed by dividing the mass per volume by the molecular mass of the protein, and multiplying by the volume. $KRAS_{166}$G12V protein was aliquoted and frozen at -80°C until use.

2.4.7 Dialysis of VH-proCASP3 and VL-proCASP3 proteins

Small volumes of Ni-NTA agarose purified protein (350µl or less) were dialysed into 1x PBS, pH7.4, 5mM $MgCl_2$ using 3.5kDa MWCO mini dialysis units (Pierce, Thermo Scientific, MA, USA). Briefly, the units were washed in 1L of

deionised water for 15mins to remove traces of glycerol from the membrane before addition of the protein sample. The sample was dialysed at 4°C for 2 hours in 4L of dialysate (1x PBS, pH7.4, 5mM $MgCl_2$), which was replaced with fresh dialysate for overnight dialysis. The concentration of the dialysed protein was determined with a NanoDrop spectrophotomer (Thermo Scientific) as previously described, then aliquoted and frozen at -80°C until further use.

2.4.8 Mammalian expression of VH-proCASP3 and VL-proCASP3

Clones stably expressing the non-N-terminal farnesylated versions of VH/VL-proCASP3 proteins were plated at 2x10^{7} cells per Hyperflask (Corning, New York, USA). Next day, Tetracycline induction was begun and allowed to proceed for 18 hours. Cells were harvested and pelleted in 250ml centrifuge tubes (Corning) at 200 x g for 10 minutes at 4°C with a JS 4.2 rotor (Beckman Coulter, CA, USA) in a J6-MI high-capacity centrifuge (Beckman Coulter). Cells were washed in 1x PBS, pH7.4 (GIBCO) and lysed in 40ml Lysis buffer (50mM Tris, pH7.4, 150mM NaCl, 0.1% v/v Triton X-100,1mM EDTA) for 30 minutes, rotating at 4°C. A small aliquot was retained for later SDS-PAGE or Western blot analysis. The lysate was cleared by centrifugation at 3220 x g (4000 rpm) for 25 minutes at 4°C in a bench top centrifuge, and then sequentially passed through a 1.2μm and a 0.45μm syringe-driven filter unit (Sartorius, Göttingen, Germany). The lysate was then ready for anti-FLAG-tag affinity chromatography.

2.4.9 FLAG affinity purification of VH-proCASP3 and VL-proCASP3

Protein lysates were subsequently purified with L5 Anti-FLAG affinity gel (BioLegend, CA, USA). Two milliliters of the 50% slurry (1ml resin) was washed in equilibration buffer (1x PBS, pH7.4, 0.5M NaCl), then added to the lysates and incubated overnight for efficient binding, at 4°C with constant rotation. Next day, the lysate:resin mix was applied to a 5ml polypropylene gravity flow column (BioRAD, Hertfordshire, UK), and passed through twice. The column was washed three times

with 5x resin volumes (5ml) of equilibration buffer. Bound protein was then eluted with three 2ml volumes of glycine elution buffer (200mM glycine, pH2.2, 150mM NaCl) directly into tubes containing 165µl 2M Tris, pH8 to neutralise the elution buffer. To assess the purification, 10µl of each fraction was kept for SDS-PAGE or Western blot analysis, and the rest of the elution fractions were pooled and concentrated then frozen at -20°C until further use.

2.5 *In vivo* experiments

All animal experimentation was performed according to Home Office and University of Oxford welfare standards and guidelines. Transplants were performed by Dr Osama Al-Assar, former member of the Rabbitts laboratory, University of Oxford.

2.5.1 AIDA clone xenografts

Clones were trypsinised, passed through a 70µm cell strainer (BD, New Jersey, USA) to remove clumps, and pelleted at 200xG for 5 minutes. Pellets were washed twice in ice-cold PBS. Viable cells were counted and cells were resuspended to 10^{7} cells/ml in sterile PBS. Cells were kept on ice until transplanted subcutaneously into athymic CD1-Nude mice (*nu/nu*) (Charles River, Harlow, UK). Mice were anesthetised with isoflurane vapour and injected with 100µl of cell suspension on both flanks. Tumour growth was monitored by daily measurement with digital calipers. Once tumours reached ~5mm in diameter, tetracycline was administered through diet (200g/kg Doxycycline diet, Bio-Serv, NJ, USA) and drinking water (2mg/ml, Sigma Aldrich) supplemented with 10% (v/v) blackcurrant cordial (Ribena, Suntory Ltd., Uxbridge, UK) to mask the taste and prevent dehydration.

2.5.2 Human T-ALL propagation

Human T-ALL cells were thawed briefly in a 37°C waterbath, and diluted into RPMI culture medium, supplemented with 10% (v/v) FBS to remove residual DMSO. Cells were then passed through a 70uM cell strainer (BD, NJ, USA) to remove clumps and pelleted at 200xG for 5 minutes. Cell pellets were subsequently washed twice in ice-cold PBS. Viable cells were determined via trypan blue (Invitrogen, Paisley, UK) exclusion and counted. Cells were resuspended to a final concentration of 10^7/ml and kept on ice until injection, approximately 30 minutes. Two NSG mice were prepared for transplant per T-ALL sample. Briefly, mice were warmed in a 37°C box for twenty minutes to promote dilation of the tail vein and restrained in an appropriate apparatus. Tails were sanitized with 70% ethanol and 10^6 cells (100µl) were injected using a fine gauge insulin needle (BD). Engraftment of the hT-ALL transplants was gauged through fortnightly blood sampling.

2.6 Anti-LMO2 VL isolation experiments

2.6.1 Tumour cell flow cytometry

10^5 cells were washed in 1x PBS (Gibco, MA, USA) and resuspended in 100µl of 1x PBS supplemented with 1% FBS (Sigma Aldrich, Dorset, UK). Antibody cocktails were made for a final dilution of 1:300. Cells were incubated with the antibodies for 1 hour on ice, protected from light, and then washed and resuspended in PBS, 1% FBS for analysis. Flow cytometry was performed on a CyAn ADP analyser (Beckman Coulter, CA, USA) with data analysis performed with FlowJo software (Tree Star Inc., OR, USA). Antibodies: Anti-mouse: CD4-PE, CD44-PE, CD8-FITC, CD25-FITC (all BD, NJ, USA), CD45.1-AlexaFluor488, CD45.2-BrilliantViolet421 (both BioLegend, CA, USA). Anti-human: CD45-Violet450, CD4-APC, CD44-APC, CD25-PE, CD8-PE (all BioLegend).

2.6.2 T cell line Fluorescence Activated Cell Sorting (FACS)

FACS cell sorting was performed by Dr S Clark and Dr K Clark (WIMM Flow Cytometry Facility, WIMM, University of Oxford) on a FACSARIA FUSION cell sorter (BD, NJ, USA).

2.6.3 Lentivirus Methods

All lentivirus work was performed in Category II containment facilities. Waste was decontaminated by disinfection in 2% w/v Virkon solution (Day-Impex Ltd, Essex, UK) for 30 minutes or by autoclave sterilisation at 121-125°C for at least 15 minutes.

2.6.3.1 Lentivirus Constructs

The TetOn lentiviral transfer vector pLVX-TetOne was purchased from Clontech (Clontech Laboratories, CA, USA). The mRuby2 fluorescent reporter cassette was constructed by PCR assembly of an F2A peptide and mRuby2, which was cloned into the vector via SmaI. The VH576-P2A-YFP cassette was subcloned from pFUW-VH576-P2A-YFP via BamHI/HindIII into pLVX-TetOne/pLVX-TetOne-mRuby2 via the blunted EcoRI site. Plasmids and primers shown in Appendix F.

2.6.3.2 Lentivirus Packaging

HEK293T cells were plated at 2x10^{6} cells/T75 flask. Next day, cells were transiently co-transfected. The transfection mix comprised 1.5µg psPax2 packaging plasmid, 1.5µg pMD2.G envelope plasmid and 2.3µg transfer plasmid in 750µl Opti-MEM medium (Gibco, MA, USA) combined with 40µl Lipofectamine 2000 (Invitrogen, Paisley, UK) in 750µl total volume with Opti-MEM medium (Gibco). After 20 minutes, the mix was applied to cells, and virus production proceeded for 72 hours, at 37°C 5% CO_2. Medium was then centrifuged at 1000 x g for 5 minutes, then passed through a 0.45µm syringe filter (Sartorius, Göttingen, Germany). Recombinant virus was concentrated by centrifugation for 2 hours at 4°C at 20,000rpm with a JA 25.50 rotor (Beckman Coulter, CA, USA) in an Avanti J25 high-speed centrifuge (Beckman

Coulter). Pellets were resuspended in 200µl sterile PBS and frozen at -80°C until further use.

2.6.3.3 Lentivirus Titration

HEK293T cells were plated at $2x10^4$ cells/cm^2 in 6-well plates. Next day, serial dilutions of virus stock equating to 20, 10, 3, 1, 0.3 and 0.1µl were applied in a total volume of 0.5ml. After 48 hours, cells were harvested and analysed for fluorescent reporter expression. The viral titre of transducing units (TU) per ml was calculated from the number of fluorescent cells according to the following formula;

$$TU\ per\ ml = \frac{Number\ of\ cells \times Fluorescent\ positive\ cells\ (\%)}{Virus\ volume\ (ml)}$$

2.6.3.4 Lentivirus Transduction

Lentiviral T cell line and tumour cells were transduction was aided by spinoculation. 10^5 cells were plated in 50µl growth medium were seeded per well of a 96-well plate, supplemented with 4µg/ml final concentration of Polybrene (Sigma Aldrich, Dorset, UK). Plates were centrifuged at 1250 x g, 34°C for 1.5 hours. Cells were incubated for 48 hours, then washed three times in PBS (Gibco, MA, USA), and resuspended in 250µl PBS, 1% FBS (Sigma Aldrich) prior to assessing fluorescent reporter expression by flow cytometry and/or cell sorting.

2.6.4 Tripartite GFP Assay

The tripartite GFP assay plasmids pEF-NFarn-VH#576-GFP11, and pEF-NFarn-VL#I21-GFP10 were obtained from Dr Ami Miller (Rabbitts Laboratory, WIMM, University of Oxford). The N-terminal Farnesylation (NFarn) sequence was removed by restriction digest with PmlI/SalI and an oligonucleotide stuffer fragment replaced it. The VH variants (VH#Y6, VH#Y6dm and VH#Y6mut, VH#576) were cloned into pEF-FLAG-GFP11, and VL fragments (anti-RAS VL#204, non-specific VL#I21 and anti-LMO2 VLs #819, #826 and #827) were cloned into pEF-FLAG-GFP10, both via XhoI/NcoI restriction sites. Primers and maps are shown in Appendix G.

Combinations of these plasmids were assayed in duplicate, with $2x10^4$ HEK293T cells transiently co-transfected with 1µg of each plasmid (pEF-FLAG-VH-GFP11, pEF-FLAG-VL-GFP10, pEF-GFP1-9 and pPGK-$KRAS_{166}$(G12V)-2A-Puro) using Lipofectamine2000 (Invitrogen). After 48hours cell were harvested and analysed for GFP fluorescence with an Attune flow cytometer (Invitrogen, Paisley, UK). Data was analysed using FlowJo software (TreeStar Inc., OR, USA).

2.6.5 VL Randomised CDR3 Library

The randomised VL library was produced by adapting the method published by Tanaka and Rabbitts (Tanaka and Rabbitts 2010). VL#204 and VL#l21 were used as templates for PCR amplification with KOD polymerase (Novagen, Millipore, MA, USA) using the touchdown protocol using degenerate primers to introduce mutations into CDR3. Products were gel extracted and digested with XhoI and NcoI restriction enzymes (NEB, Hitchin, UK), and ligated into the pEF-GFP10 vector cut with the same enzymes (having removed VL#l21). Ligation reactions were purified by ethanol precipitation and DNA resuspended in 10µl TE buffer, pH8. Pilot transformations were performed with 0.5µl DNA into chemical competent DH5α E.coli. Colonies were picked, miniprepared and sequenced (Source Bioscience, Nottingham, UK) to check for randomised sequences. Large-scale transformations were performed by electroporation, and plated onto selective agar in 25cm x 25cm square plates (Fisher Scientific, Loughborough, UK). Colonies were grown overnight at 37°C, and transformants harvested from the plates and pooled into one pellet. Plasmid DNA was prepared by maxipreparation using the Plasmid Plus Mega Kit (Qiagen, Crawley, UK) as per the manufacturer's instructions.

Chapter 3 Initial assessment of AIDA against mutant RAS

3.1 Introduction

Single variable domain antibody fragments may be considered as 'macrodrugs' (Tanaka and Rabbitts, 2008b), combining advantages of both small molecule drugs and full-length antibodies. These variable domain fragments retain the minimal region of the full-length antibody necessary for the high specificity and affinity antigen interaction (Tanaka et al., 2003b). Although they cannot cross the cell membrane, the variable domain fragments may be expressed and fold correctly within the cell and, unlike conventional drug discovery, these fragments may be isolated and engineered following relatively rapid protocols (Tanaka and Rabbitts, 2010b). Pre-clinical anti-tumour efficacy of these fragments has been demonstrated in mice (Tanaka and Rabbitts, 2010a, Tanaka et al., 2011, Tanaka et al., 2007), where the anti-RAS VH successfully inhibited mutant RAS-driven tumour growth. Whilst this tumour inhibition was striking, it was only in effect if expression of the fragment was maintained (Tanaka and Rabbitts, 2010a).

It may be that this transient anti-tumour effect would also hold true for other oncogenes. Achieving sustained, high level expression in a therapeutic setting may be difficult. Linking a cytotoxic effector domain to the single domain antibodies could circumvent the problem of persistent expression, whilst potentiating the therapeutic outcome through destruction of the tumour cells. Our chosen cytotoxic effector domain is proCaspase 3 (proCASP3), the zymogenic (inactive) precursor of the apoptotic enzyme CASP3, following from the previously described method of Antibody Interaction Dependent Apoptosis (AIDA) (Tse and Rabbitts, 2000). AIDA was first demonstrated with a single proCASP3 element linked to an scFv fragment (VH and VL domains joined by a short peptide linker) raised against the bacterial enzyme β-Galactosidase (β-Gal). As β-Gal is a homotetrameric protein, four scFv antigenic sites were present per molecule, permitting proximity activation of the proCASP3 domains.

It is envisaged that AIDA technology could be a novel, targeted therapy method for T-ALL. Figure 1.15 in Chapter 1 shows the hypothesised functioning of this system against both LMO2 and RAS antigens, two oncogenes associated with T-ALL. It is predicted that the use and requirement of two separate antigen-binding variable domains (one VH and one VL fragment), rather than an scFv (Tse and Rabbitts, 2000), would confer a safety mechanism in the unlikely event of 'off-target' binding or cellular uptake. Although clinical application of this method would be dependent upon advances in cell-specific delivery of the components, it is not a focus of this thesis. Instead, this work concentrates on the development and efficacy of this novel AIDA technology within the cancer cell.

This system will first be validated against mutant RAS as the oncogene target because a VH (VH#Y6) and a VL (VL#204) have already been isolated which are specific for both mutant RAS and active, GTP-bound wild-type RAS (Tanaka et al., 2007). VH#Y6 has been shown to bind to both HRAS and KRAS (Tanaka and Rabbitts, 2010a, Tanaka et al., 2007), whereas VL#204 will only bind to the RAS molecule in the presence of VH#Y6, due to just one amino acid residue of the VL directly binding RAS. Importantly, these two fragments bind RAS as close epitopic regions. The availability of these reagents affords an initial feasibility study of the AIDA system in human cancer cells, with single domain fragments specific to a human oncogenic protein. Due to the location and normal biology of RAS signalling, the AIDA antibodies will be targeted to the cell membrane using a membrane localisation sequence derived from Neuromodulin (GAP43). The anti-RAS AIDA will be characterised in a human tumour cell line, by cellular assays to detect apoptosis and activation of CASP3.

Apoptosis can be monitored by flow cytometry for changes in the integrity of the cell membrane and exposure of phosphatidylserine on the outer membrane (Figure 3.1), whilst fluorescent dyes can indicate the viability of the cells. CASP3 activation can be assessed by visualising the CASP3 subunits which are cleaved as

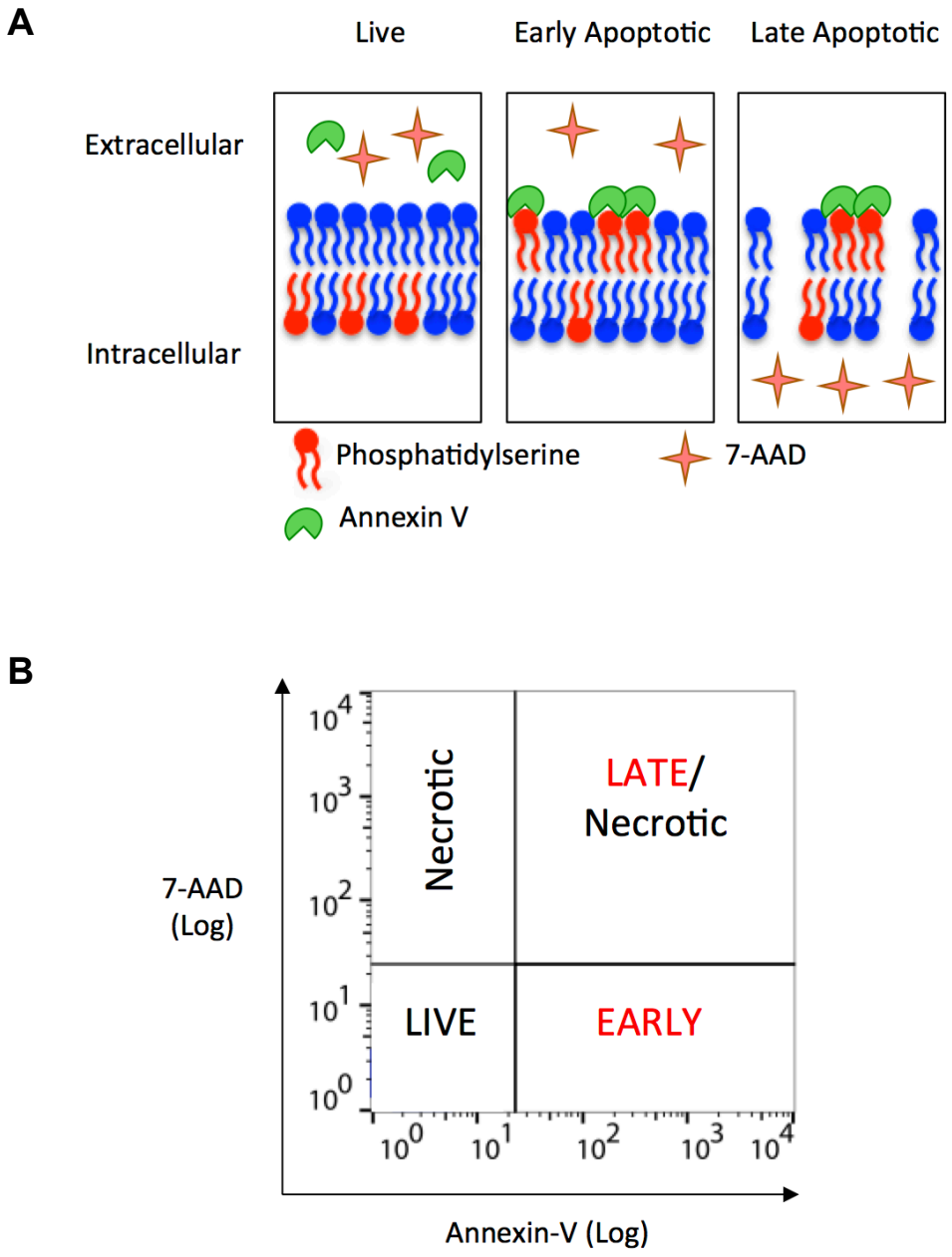

Figure 3.1 Illustrations of the cell surface changes associated with cell death

Cell death can be assessed by characteristic changes to the integrity of the cell surface membrane. A: Cartoon representation of phosphatidylserine exposure on the outer leaflet of the cell membrane following deregulation of the 'flip flop' transportation mechanism during early stages of apoptosis can be detected by Annexin V protein. Cells in the later stages of apoptosis lose membrane integrity, allowing permeation of vital dyes into the cytoplasm. B: Example flow cytometry plot indicating the segregation of Annexin V and 7-AAD stained cells into their respective stages of cell death.

part of its activation process, and by CASP3 cleavage of fluorochrome-linked, synthetic substrates containing the canonical peptide recognition motif, DEVD.

As antigen dependency is the critical concept behind the AIDA method of cancer cell destruction, testing this requires assaying the method with and without antigen. An *in vitro* or 'cell-free' method could provide a fast method to study antigen-dependency and to calculate the efficiency of the system. Moreover, this approach would be advantageous for efficient characterisation of AIDA with VH and VL domains raised against other oncogenic targets, such as those hoped for LMO2. To investigate if this would be possible, recombinant proteins will need to be expressed.

This chapter describes the initial testing of anti-RAS AIDA and the development of an expression and purification strategy for the preparation of both VH- and VL-proCASP3 proteins for subsequent cell-free assays.

3.1.1 Aim

The aim of this chapter was to test the applicability of a novel AIDA system with single domain antibodies (rather than scFv) as a potential targeted T-ALL cancer therapy. As the system has not been trialled against a human oncogene, the feasibility was to first be investigated using mutant RAS as model oncogenic protein, owing to the availability of reagents. The requirement of both VH and VL to initiate apoptosis is shown in this chapter as is the potential to express and purify the AIDA proteins for subsequent development of an *in vitro* assay.

3.2 Confirmation of RAS mutation

The human fibrosarcoma cell line HT1080 was chosen as the model system, as the literature indicates it expresses Q61K mutant NRAS (Benedict et al., 1984) and because it had previously been used by the laboratory for testing the anti-RAS VH (Tanaka et al., 2007, Tanaka and Rabbitts, 2010a). The laboratory already had a clone of this cell line expressing the Tetracycline reverse transactivator (rtTA) or 'TetOn' protein, which would be necessary for the Tetracycline inducible constructs.

This clone, herein referred to as HT1080TetOn or Parent cells, had been made previously by Dr. Tomoyuki Tanaka, a former member of the Rabbitts laboratory (Tanaka and Rabbitts, 2010a).

The RAS mutation status of these cells was checked by sequencing. *HRAS*, *KRAS* and *NRAS* were amplified from cDNA with *RAS* family gene-specific primers (Appendix B), designed by Dr Ami Miller, Rabbitts laboratory, WIMM, University of Oxford. PCR products were visualised by agarose gel electrophoresis and extracted. Digested products were cloned via HindIII and BamHI restriction sites and resulting clones were sequenced. *HRAS* and *KRAS* sequences were as wild-type, but *NRAS* sequences contained a mixture of wild-type and Q61K mutants, indicating the presence of heterozygous alleles (Figure 3.2).

As the HT1080TetOn Parent line would be transfected with the AIDA plasmid constructs, an antibiotic titration was performed to determine the most appropriate concentrations at which to select transfectants. The prior 'TetOn' creation had inserted the pUHD172-1Neo plasmid (Gossen et al., 1995) encoding the Neomycin resistance marker (Appendix A). Therefore G418 sensitivity was titrated on HT1080 cells, and was determined to be 500µg/ml. Hygromycin was titrated on both HT1080 and HT1080TetOn cells, with 200µg/ml chosen for selection of the subsequent transfectants.

3.3 AIDA stable cell lines

Three basic plasmid constructs were cloned prior to the commencement of the DPhil program and modified during. These are illustrated in Figure 3.3 (plasmid maps in Appendix A). Expression of the VH- and VL-proCASP3 fusion polypeptides is under the control of the Tetracycline-inducible ('TetOn') promoter (Gossen et al., 1995), and each fusion has an N-terminal farnesylation sequence for membrane localisation added to target the proteins near RAS. The plasmids were linearised with SspI and ethanol precipitated for a sterile DNA preparation. Stable transfection of the



Figure 3.2 Confirmation of HT1080TetOn RAS mutation

The HT1080TetOn cells stably transfected with the AIDA constructs were confirmed as possessing the NRAS Q61K mutation. RNA was extracted and cDNA produced by reverse transcription with Oligo(dT) primers. The NRAS primer set was used to amplify transcripts of each gene. PCR products were purified by gel electrophoresis, cloned into pBluescript SKII+ and sequenced. Clones of HRAS and KRAS were wildtype, whereas NRAS clones were identified as wildtype and Q61K mutation positive, indicating the HT1080TetON cell line is heterozygous for the NRAS Q61K mutation. The red star indicates the position of the mutation. Matched amino acid residues are shaded in grey, mismatched residues are unshaded. Sequencing of additional cDNA clones, or genomic sequencing of the cell line itself, may also have been employed to corroborate this finding. However, because this result showed that the cell line possessed the same NRAS mutation as described in the literature (Benedict et al., 1984) further characterisation was not performed.

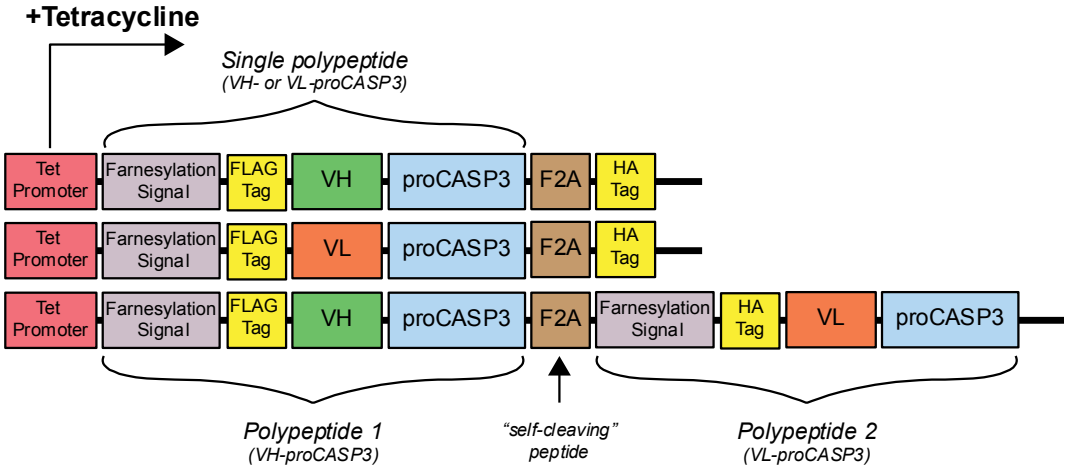

Figure 3.3 Illustration of the AIDA expression constructs design

The AIDA cassettes were cloned into a Tetracycline-dependent expression plasmid, pUHD10, containing a hygromycin selectable marker. Each AIDA cassette contains an N-terminal farnesylation sequence to target both elements to the cell membrane. Single cassette vectors are FLAG-tagged for affinity recognition of the VH/VL-proCASP3 polypeptide. The viral F2A sequence follows to cleave the proteins. Vectors containing both AIDA cassettes possess a second polypeptide after the F2A sequence. This codes the VL-proCASP3 fusion which is haemagglutinin (HA)-tagged for identification. All vectors were linearised with SspI restriction endonuclease for stable transfection.

HT1080TetOn Parental cell line yielded colonies. The resulting colonies were expanded and assessed by Western blot for Tetracycline (Tet)-specific induction of the VH-, VL- and VH+VL-proCASP3 fusion proteins. The three clones of each type that were deemed to have the most consistent protein level expression were carried forward for *in vitro* testing (Figure 3.4). Cell death resulting from the AIDA system should involve activation of CASP3. Following tetracycline induction of the fusion protein expression, each clone type was assessed for CASP3 activation by Western blot. CASP3 activation involves cleavage of the proCASP3 zymogen, which may be detected with an antibody specific for cleaved (activated) CASP3, producing bands resolving at 17-19kDa. VL-Only clone blots showed that no bands corresponding to cleaved CASP3 were detected, indicating that CASP3 activation has not occurred in these clones. In the VH-Only clones, two clones showed cleaved CASP3 bands indicating some CASP3 activation had occurred. In the VH+VL clones, all clones showed bands corresponding to cleaved, or active, CASP3. Interestingly, the antibody (specific for the cleaved form of the CASP3 enzyme) detected the same bands seen on the blots with the full-length CASP3 antibody at sizes corresponding with breakdown products of the fusion proteins.

3.4 Assessment of clone phenotype

Upon screening the colonies by Western blot, positive clones were noted to exhibit particular clone type dependent phenotypes upon tetracycline induction (Appendix H). Expanded cultures were compared with the control Parental cell line. The VL-Only positive clones appeared normal upon induction, with no apparent morphological changes when compared with the Parent line. In contrast, the VH-Only and VH+VL clones showed obvious changes upon Tet induction. The VH-Only clones were still attached to the culture vessel, displaying an enlarged and flattened morphology. Additionally, the cells lacked membrane definition, and seemed to stop dividing. The VH+VL clones possessed a strong cell death effect, with cells beginning to detach

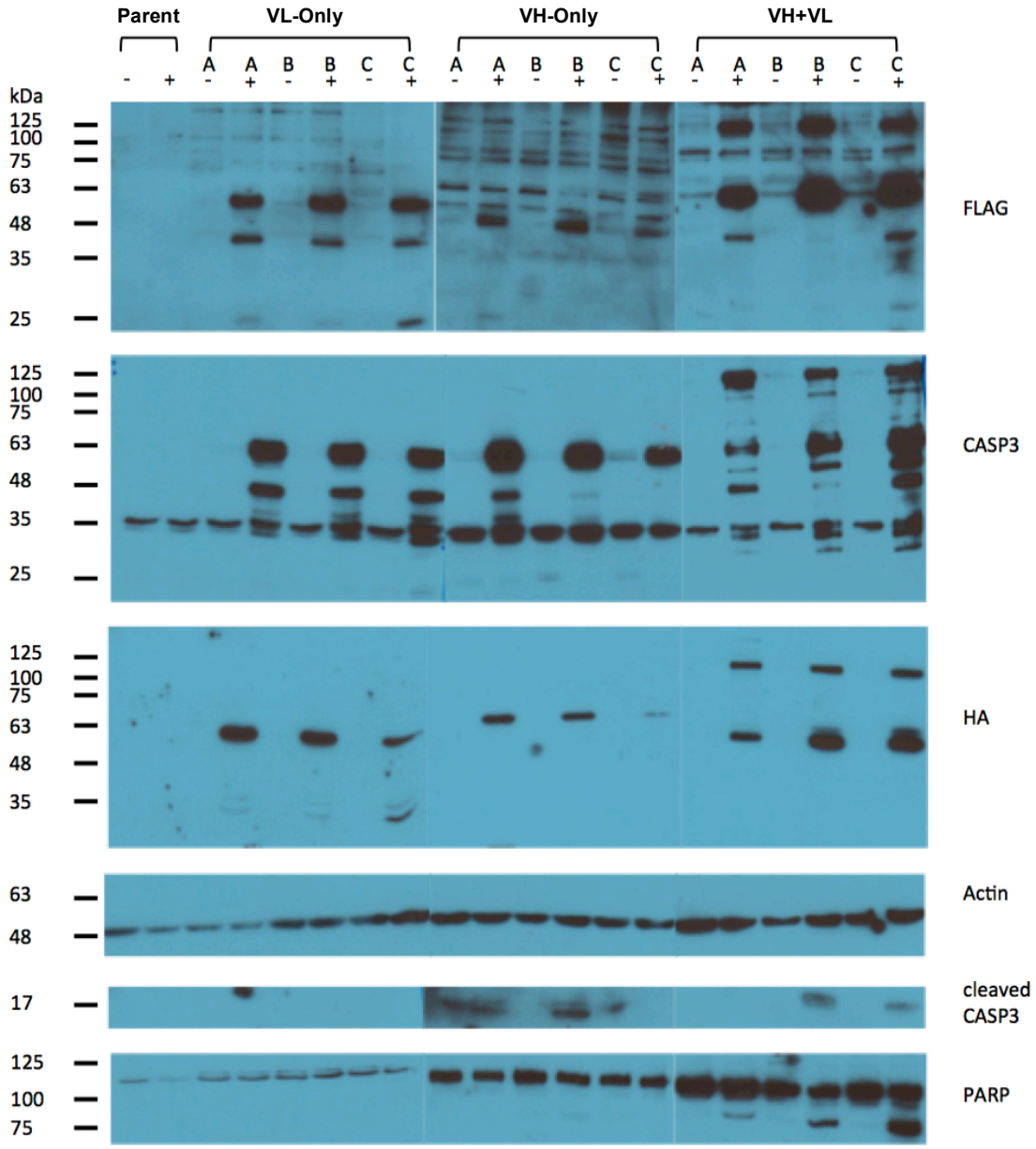

Figure 3.4 Western blot analysis of stable clone expression

Western blot analysis of three clones (clones A-C) of each AIDA construct type, to assess respective VH+VL protein expression. Cells were grown for 48hrs with (+) and without (-) tetracycline induction, then lysed and sonicated. Total protein concentration was determined by bicinchoninic acid (BCA) assay, and 10µg protein was loaded per lane. Strong expression of the fragments were confirmed by three different primary antibodies, anti-FLAG, anti-HA tag and anti-CASP3. The CASP3 antibody also identified the endogenous protein band. β-Actin was included as a loading control. The VH- and VL-proCASP3 fusion proteins resolve at various sizes dues to breakdown of the polypeptides, although the major, intact protein resolves at approximately 50kDa. FLAG-tagged expression of the VH-proCASP3 moiety is difficult to visualise consistently although it can be detected with the CASP3 antibody. Furthermore the HA tag is not always cleaved from the single chains indicated some inefficiency of the F2A 'cleavage'. Direct evidence of CASP3 activation is evident by antibody detection of cleaved CASP3 large (p20/p17) subunit at ~17kDa. PARP is a cellular protein target of active CASP3. CASP3-mediated cleavage of its C-terminal catalytic domain is observed in the VH+VL samples, with an extra band resolving at 89kDa compared with the endogenous full-length band observed at 116kDa.

from 24 hours post Tet induction, and disintegrated debris visible between 48 and 72 hours.

3.5 Cell viability changes

Cell viability changes upon the Tet induction of the VH- and VL-proCASP3 fusions were measured with a Prestoblue resazurin-based dye, whereby the initial dye molecule is converted to fluorescent product in live cells. The resulting fluorescence can therefore be considered as a proportional measure of live cells. This assay showed no appreciable effect of tetracycline induction of the VL-Only cells, with these clones mimicking the Parent line (Figure 3.5A). VH-Only cells displayed a reduced viability upon induction to nearly half that of the uninduced sample by day 3. Strikingly, VH+VL clones retained less than 20% viability relative to their uninduced control samples. A breakdown of each clone's viability measurements is shown graphically in Figure 3.5B. The absolute results of individual clones vary, but follow the same pattern overall.

3.6 Apoptosis-associated cell membrane changes

It is hypothesised that the AIDA system would induce apoptosis but viability measurements can only assess live cells. Therefore, flow cytometric profiling of cell surface changes associated with apoptosis was performed. Annexin-V and 7-AAD staining was employed to assess the presence and extent of cell death within the induced and uninduced clone types (Figure 3.6). There is a very slight shift in the VH-Only Annexin-V, 7-AAD double negative population toward early apoptotic Annexin-V postive, 7-AAD negative quadrant upon induction of the VH-proCASP3 fusion. However, the actual difference in the gated populations is minor, with less than 1% increase in the early and late apoptotic stages. VH+VL clone double expression shows 30% of viable cells are in the late stages of apoptosis (Annexin-V, 7-AAD double positive cells), with almost a 13-fold increase in cells in the early

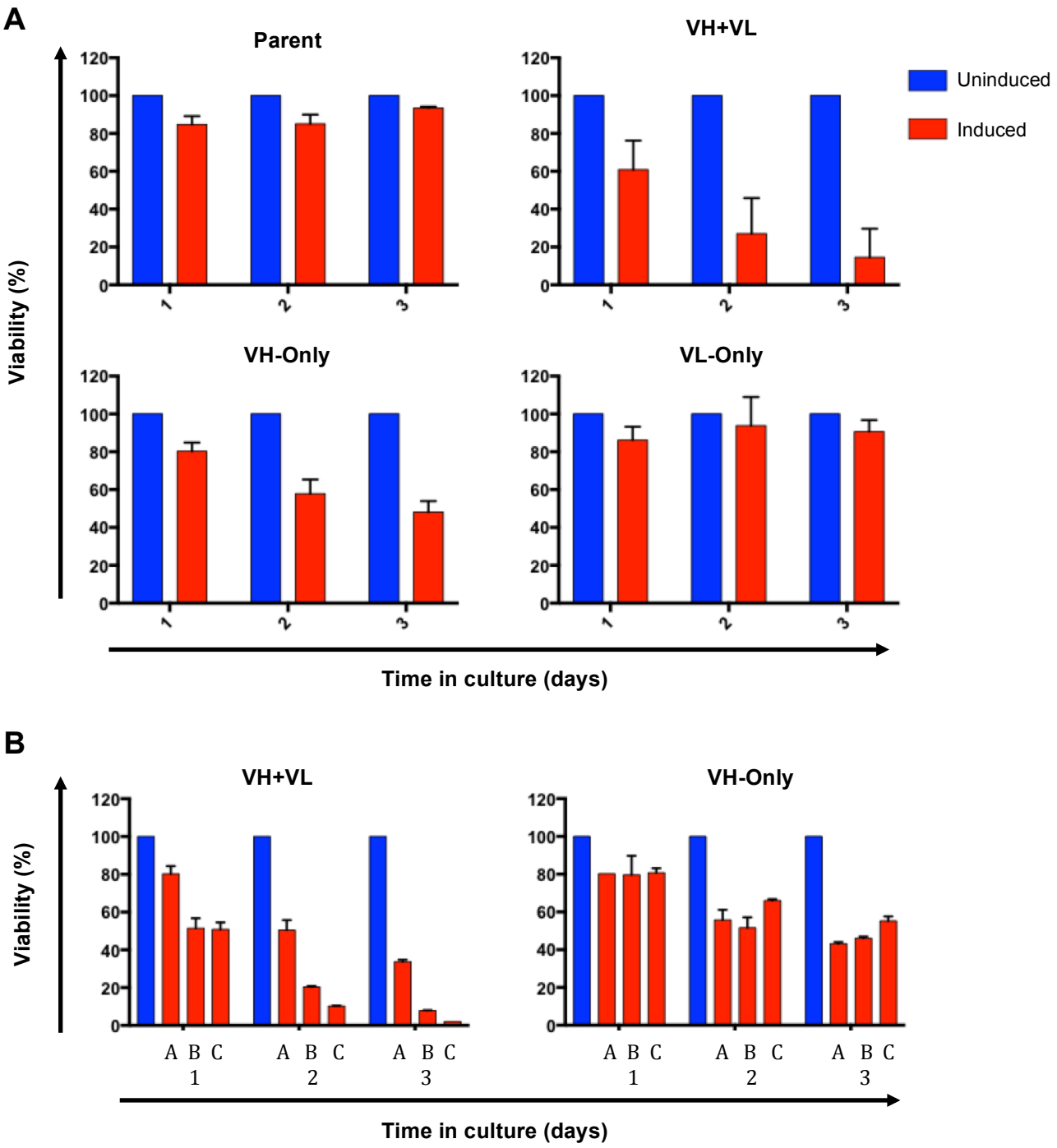

Figure 3.5 Cell viability changes upon expression

Three clones (A-C) of each type (VH-Only, VL-Only and VH+VL) were assessed for the effect of AIDA construct expression on cell viability over three days with and without tetracycline induction. The parent line was included as a control. Cells were incubated with PrestoBlue resazurin-based viability dye then fluorescence was measured at 544nm excitation, 590nm emission. Background signal was determined with a no cell control well, and subtracted from each measurement. Fluorescence measurements were averaged and converted to a percentage of the uninduced samples, with the uninduced samples being regarded as 100% viable as a reference point to allow comparison between clones. Each data point is therefore relative to the uninduced clone control. A: Averaged data of the three clones (A-C) per type, represented as a bar chart. B: Full clone data of the VH+VL and VH-Only clones, with clone numbers indicated below the x axis. Blue bars, uninduced; Red bars, induced. Error bars represent standard deviation from the mean.

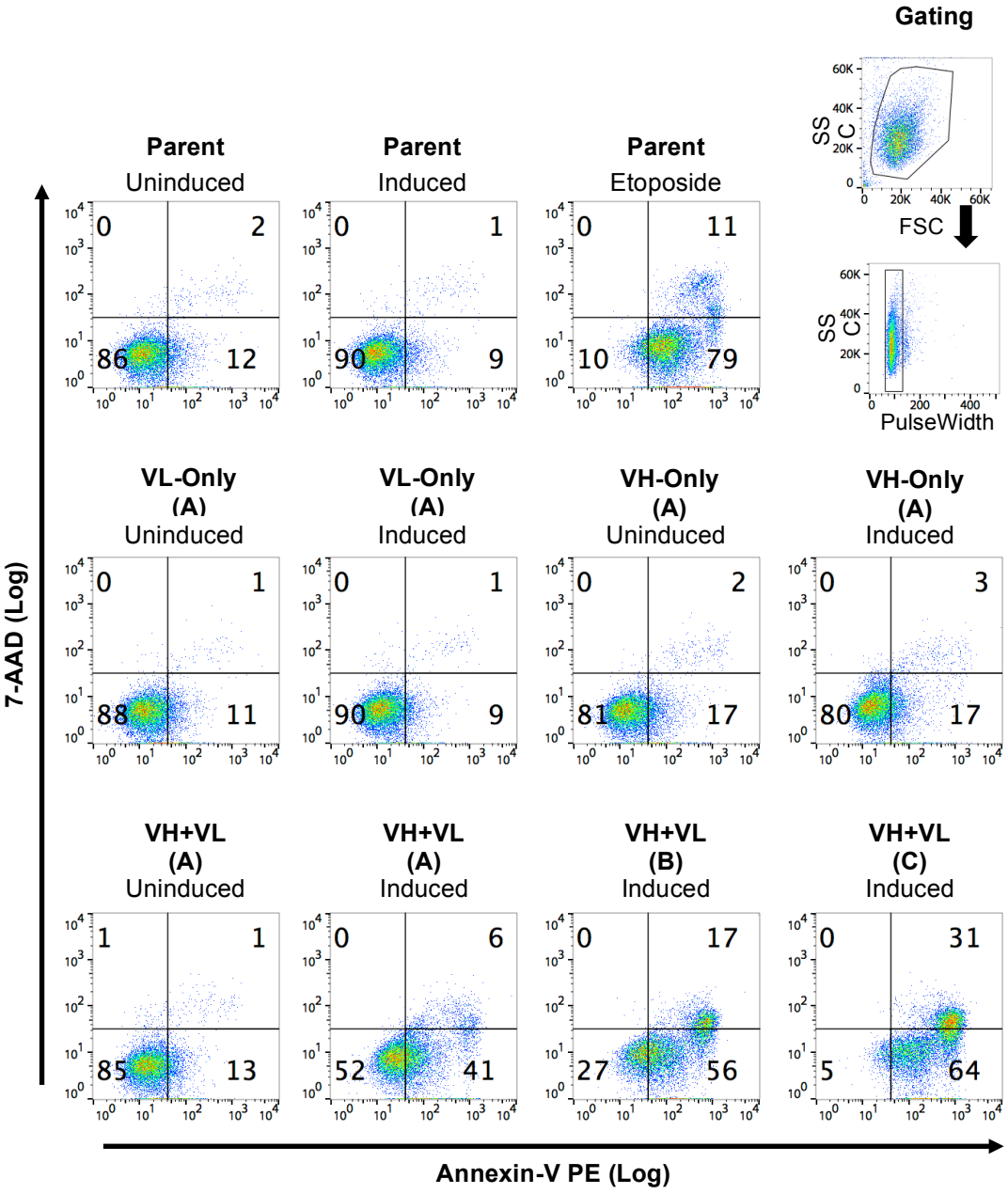

Figure 3.6 Annexin V and 7-AAD membrane profile associated with cell death

Analysis of the apoptotic cell surface changes upon induction of AIDA construct expression was monitored by flow cytometry. One clone of VL-Only and VH-Only (both clone A) and three clones of VH+VL (clones A-C) were grown with and without tetracycline induction (induced vs. uninduced) for 48 hours, with an 8 hour etoposide positive control for apoptosis performed on the parental line. Clone type, number and growth condition are indicated above the plots. Forward scatter (FSC) and Side scatter (SSC) parameters gated the cells (ring gate) and then single cells selected according to Pulse Width and SSC parameters (box gate). A quadrant gate was set to divide the cells into the respective Annexin-V/7-AAD populations. The percentage of the single cell gated population occupying each of the quadrants are shown, rounded to whole numbers. Compensation was performed with single stained colour controls. Annexin-V PE was monitored on the FL2 channel, 7-AAD on the FL4 channel.

stages of cell death (Annexin-V positive, 7-AAD negative). The Parental line and VL-Only cells produce no discernible change in cell membrane integrity upon application of Tet or induction of the VL-proCASP3 fragment respectively.

3.7 Direct evidence of CASP3 activation

3.7.1 Fluorogenic substrate analysis

To ascertain whether the cleaved CASP3 proteins detected by Western blot were active, the fluorogenic peptide assay PhiPhiLux was employed. Active CASP3 would proteolytically cleave the commercial peptide at the consensus CASP3 substrate motif separating fluorescent domains. Upon cleavage, these domains are liberated from their dimerised state, permitting higher levels of fluorescence upon excitation. Similar to the previous assays, the Parent cell line and the VL Only clones produce no increase in fluorescence when treated with Tet (Figure 3.7). Etoposide-treated Parent cells acted as an apoptosis control, although this sample only showed 24% of cells above background fluorescence imparted by the uncleaved substrate. Approximately 75-80% of the VH+VL cells possess increased fluorescence, with the population peak almost one log above background levels. A more modest fluorescence increase in 30% of VH Only cells shows substrate cleavage has occurred.

3.7.2 CASP3 inhibition

To confirm whether the observed CASP3 activation was responsible for the changes in membrane integrity and cell viability, an irreversible CASP3 inhibitor was applied to tetracycline induced samples of both VH Only and VH+VL cells. The effect of the inhibitor was assessed over a series of rising concentrations by flow cytometry and viability assay. Figure 3.8 shows representative flow cytometry plots of Annexin-V and 7-AAD staining at no inhibitor and with the highest concentration of inhibitor (40μM). Even at the highest titre of inhibitor VH Only cells remained largely unchanged, relative to the induced sample with no inhibitor. By contrast, with 40μM

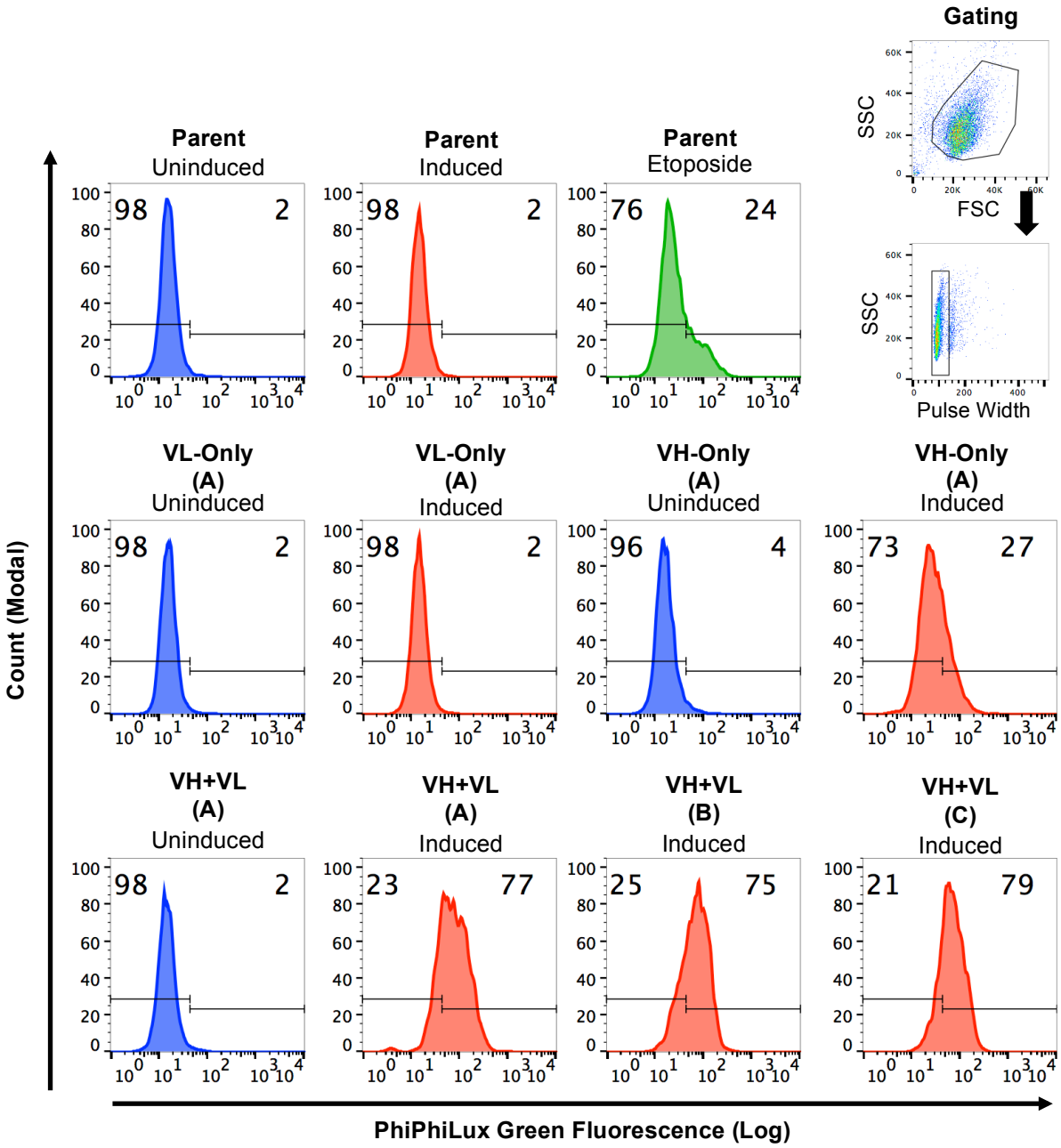

Figure 3.7 Fluorogenic substrate analysis of CASP3 activation

Univariate intensity plot representation of fluorescence resulting from active CASP3 mediated cleavage of a fluorogenic substrate. One clone of VL-Only and VH-Only (both clone A) and three clones of VH+VL (clones A-C) were grown for 48 hours with and without tetracycline induction of AIDA construct expression, and incubated with the PhiPhiLux (OncoImmunin) substrate for one hour prior to analysis. The parental line was incubated with etoposide for 8 hours as a positive apoptosis control. Forward scatter (FSC) and Side scatter (SSC) parameters gated the cells (ring gate) and then single cells selected according to Pulse Width and SSC parameters (box gate). Fluorescence was measured on the FITC (FL1) channel. Negative (left) and positive (right) bisector fluorescence gates were set relative to the fluorescence of the uninduced parental cells. Percentage fluorescence in each gate is shown on the plots. Clone type, number and growth condition are indicated above the plots. Traces were coloured for identification; uninduced (blue), induced (red), etoposide-treated apoptosis control (green).

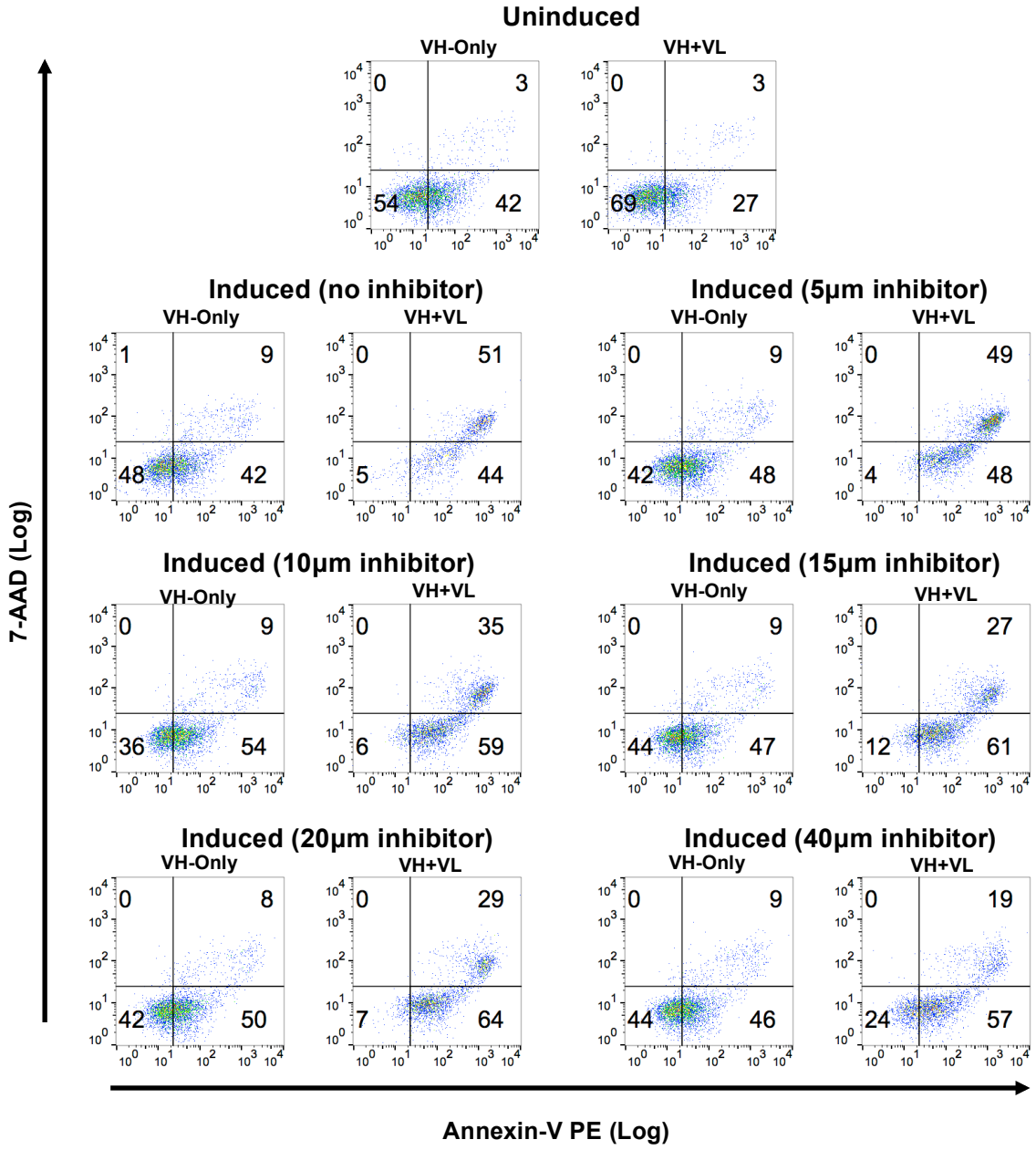

Figure 3.8 Effect of CASP3 inhibition upon apoptotic cell membrane changes

Analysis of whether the cell surface changes associated with the AIDA construct expression could be obviated by addition of an irreversible CASP3 inhibitor compound was monitored by flow cytometry. One clone of VH-Only (clone A) and VH+VL (clone C) types were investigated after 48 hours culture in their respective conditions. Irreversible inhibitor (Z-DEVD-FMK) concentrations ranged from 0-40µM. Single cells were gated according to size and granularity parameters on the uninduced VH-Only clone, as was the quadrant fluorescence gate. Annexin-V PE was monitored on the FL2 channel, 7-AAD on the FL4 channel. Compensation was performed with single stained colour controls. Percentage of cell population occupying the quadrants are shown rounded to whole numbers.

inhibitor added to the induced VH+VL cells, a partial reversal of cell membrane phenotype was detected, with 60% less cells in the late stages of cell death (Annexin-V, 7AAD double positive quadrant) and almost a 5-fold increase in the number of cells classed as live (Annexin-V, 7AAD double negative quadrant). Moreover, a large shift in the population occurs, resulting in the majority of cells being classified in early stages of cell death (Annexin-V positive, 7-AAD negative). This partial reversal of cell surface changes in the VH+VL cells was observed at the lower titres of inhibitor, albeit to a lesser extent. These findings were recapitulated with the cell viability assay (Figure 3.9) where VH Only cells posses a constant viability of around 65% that of the uninduced control sample which is independent of CASP3 inhibition. VH+VL cells show increasing viability over the dose escalation, from 10% of uniduced sample without CASP3 inhibition, to a maximum of approximately 45% with the highest inhibitor concentration.

3.8 Protein purification for cell-free AIDA

3.8.1 Bacterial KRAS expression and purification

The bacterial expression plasmid pRK-His-TEV-Avi-$KRAS_{166}$G12V, obtained from Dr. Ami Miller, Rabbitts Laboratory, WIMM, University of Oxford (for the plasmid maps see appendix D), was chosen as protocols for efficient expression and purification already existed within the laboratory. The plasmid encodes the truncated form of mutant KRAS protein, lacking the poly-lysine tract associated with membrane targeting. VH#Y6 was originally isolated with mutant (G12V) KRAS at the antigen (Tanaka et al., 2003a), and all subsequent affinity measurements had involved KRAS G12V mutants as the RAS antigen (Tanaka et al., 2007, Tanaka and Rabbitts, 2009) which further rationalised this choice of plasmid.

The plasmid was used to transform C41 E.coli. Expression was initiated with IPTG and continued overnight, with purification performed as described. The resulting fractions are shown by Coomassie gel staining (Figure 3.10), where $KRAS_{166}$G12V

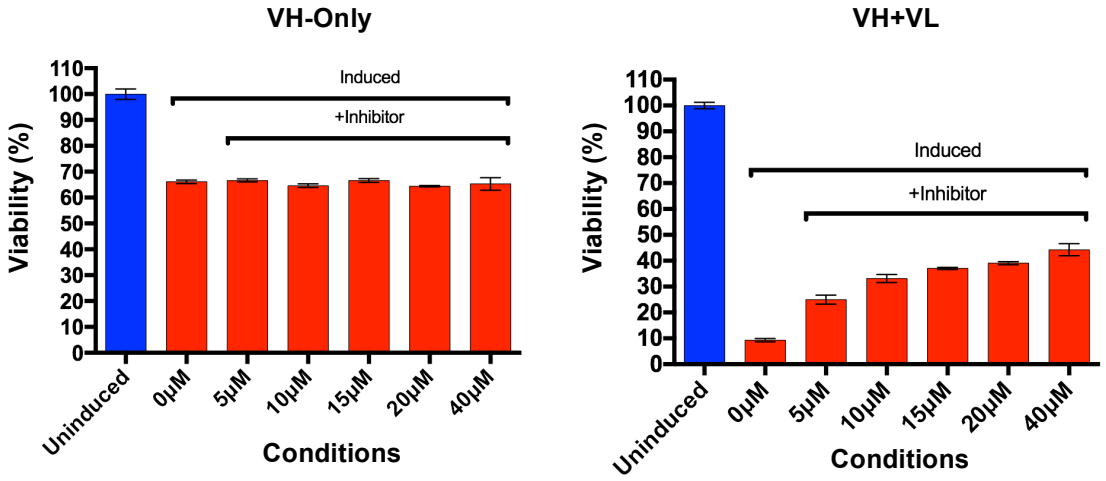

Figure 3.9 Effect of CASP3 inhibition on cell viability

Viability measurements with PrestoBlue reagent were performed to assess the effect of an irreversible CASP3 inhibitor, Z-DEVD-FMK on cell viability following 48 hours of tetracycline induction of the AIDA fusion proteins. One clone of VH-Only (clone A) and VH+VL (clone C) types were investigated, with inhibitor concentrations ranging from 0-40μM. Cells were incubated with PrestoBlue reazurin-based viability dye then fluorescence was measured at 544nm excitation, 590nm excitation. Background signal was determined with a no cell control well, and subtracted from each measurement. Fluorescence measurements were averaged and converted to a percentage of the uninduced samples, with the uninduced samples being regarded as 100% viable as a reference point to allow comparison between clones. Each data point is therefore relative to the uninduced clone control. Blue bars, uninduced; Red bars, induced, with and without inhibitor as marked. Error bars represent standard deviation.

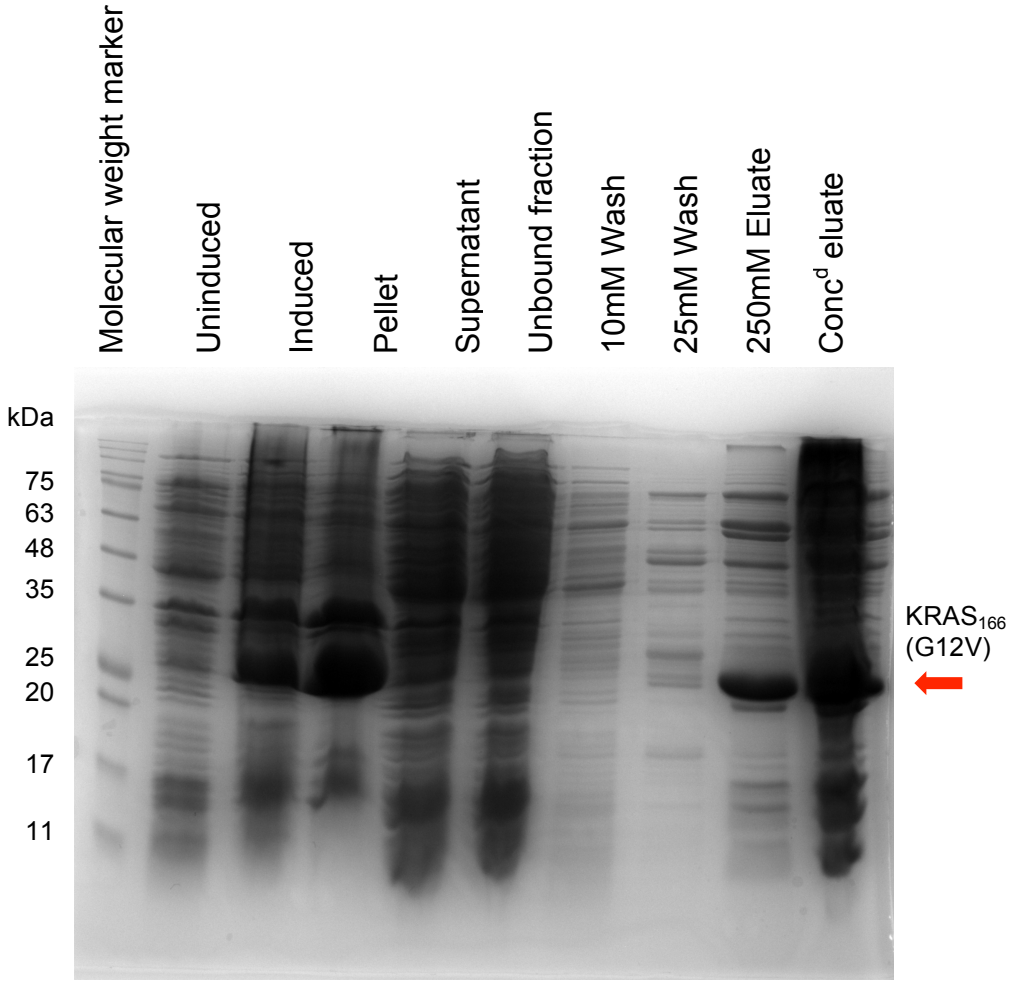

Figure 3.10 Nickel purification of His-Tev-Avi-KRAS$_{166}$(G12V)

Coomassie stained 12% SDS-PAGE gel of C41 E.coli bacteria expressed His-TEV-Avi-KRAS$_{166}$(G12V) and initial nickel (Ni-NTA) agarose purification fractions. Bacteria were grown to O.D.600 0.6 (early log phase) and induced with IPTG and expressed overnight. Cells were lysed and clarified by centrifugation before performing the Ni-NTA affinity chromatography. Aliquots were taken at stages throughout purification (uninduced bacteria, induced bacteria, pellet, supernatant unbound fraction, 10mM imidazole wash, 25mM imidazole wash, 250mM imidazole elution and concentrated eluate). Equal volumes of the samples were denatured and loaded. The band size corresponding to the mutant KRAS protein is indicated by the red arrow, approximately 23kDa.

elutes strongly from nickel (Ni) agarose in the final elution with 250mM Imidazole, and can be seen at the expected size of 23kDa. Some bacterial proteins can be seen to have eluted alongside the His-tagged antigen. Concentration of the recombinant protein was determined to be 13.5mg/ml at A280nm. Approximately half of the final eluate (3.5ml corresponding to 47mg protein) was taken forward for loading with a 10x molar excess of guanosine 5'-[β,γ-imido]triphosphate (GMP.PNP, a non-hydrolysable GTP analogue). The GMP.PNP-loaded $KRAS_{166}$G12V protein was then re-purified by size exclusion chromatography (SEC), to remove the contaminant bacterial proteins and unbound GMP.PNP analogue (Figure 3.11). The peak eluting at fractions C5 to C12 corresponded to that of $KRAS_{166.}$ The peak at fraction E10 correlates to 'free' GMP.PNP analogue. The peak of larger molecular mass at fraction B2 is aggregated $KRAS_{166}$ protein. The presence of KRAS166 in the eluted samples was confirmed by Coomassie staining of SDS-PAGE gels (Figure 3.12). Fraction C7 and C10 contained the highest density of $KRAS_{166}$ protein and were pooled. The identity of the 23kDa band was verified as $KRAS_{166}$ by Western blot with a Pan-RAS antibody (Figure 3.13). The final concentration was determined by BCA assay to be 3.16 mg/ml.

3.8.2 Mammalian Expression of VH- and VL-proCASP3

Expression of the anti-RAS VH- and VL-proCASP3 proteins was first assessed in mammalian cells as the fragments had already shown themselves to be active and well expressed in the HT1080TetOn clones. However, cytosolic protein was desired and the previous VH-Only and VL-Only clones (Chapter 3) were targeted to the cell membrane for more efficient localisation with RAS. To circumvent this, single VH or VL-proCASP3 AIDA plasmids were taken from an earlier part of their construction, which lacked the N-terminal farnesylation sequence and used to transfect the parental HT1080TetOn line. One 96-well plate of each non-farnesylated (non-NF) construct were picked and expanded for assessment. Approximately half of

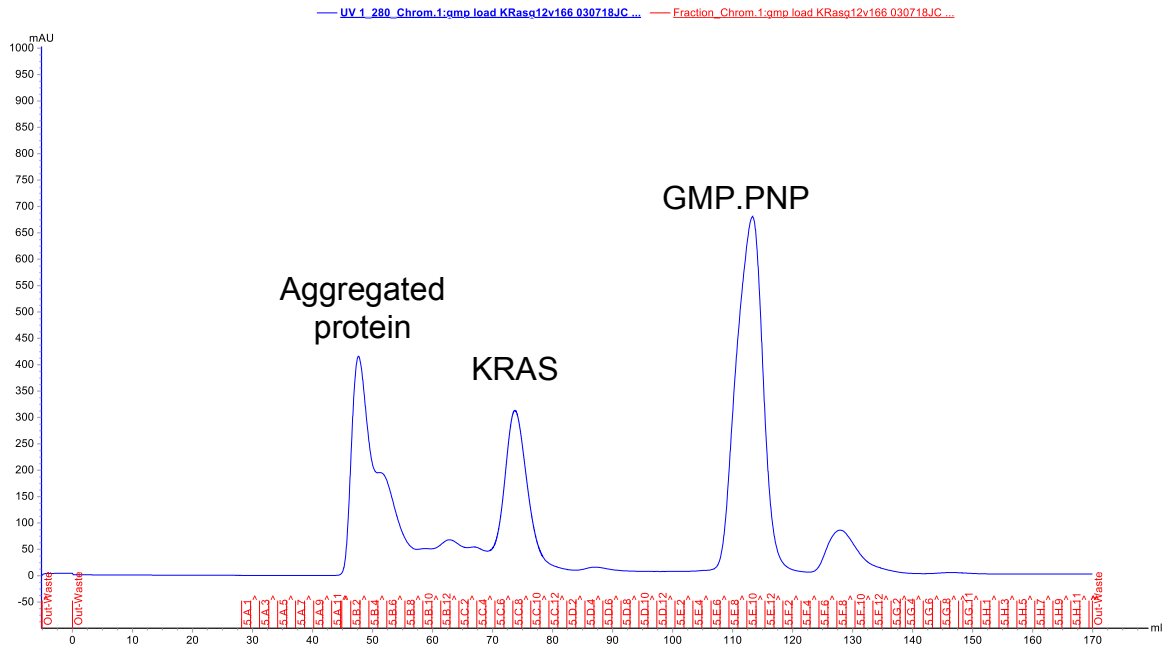

Figure 3.11 GMP.PNP loaded KRAS size exclusion chromatography

RAS proteins require GTP nucleotide binding to adopt the active conformation. Although the oncogenic mutations remove GTPase activity, GTP nucleotides may become hydrolysed to GDP. Loading of a non-hydrolysable GTP analogue prevents this. Size exclusion chromatography (SEC) to further purify the GMP.PNP-loaded KRAS protein for use in the assay. The chromatogram shows the elution profile of KRAS and unbound GMP.PNP (indicated). Protein purification was performed on an AKTA fast protein liquid chromatography unit (GE).

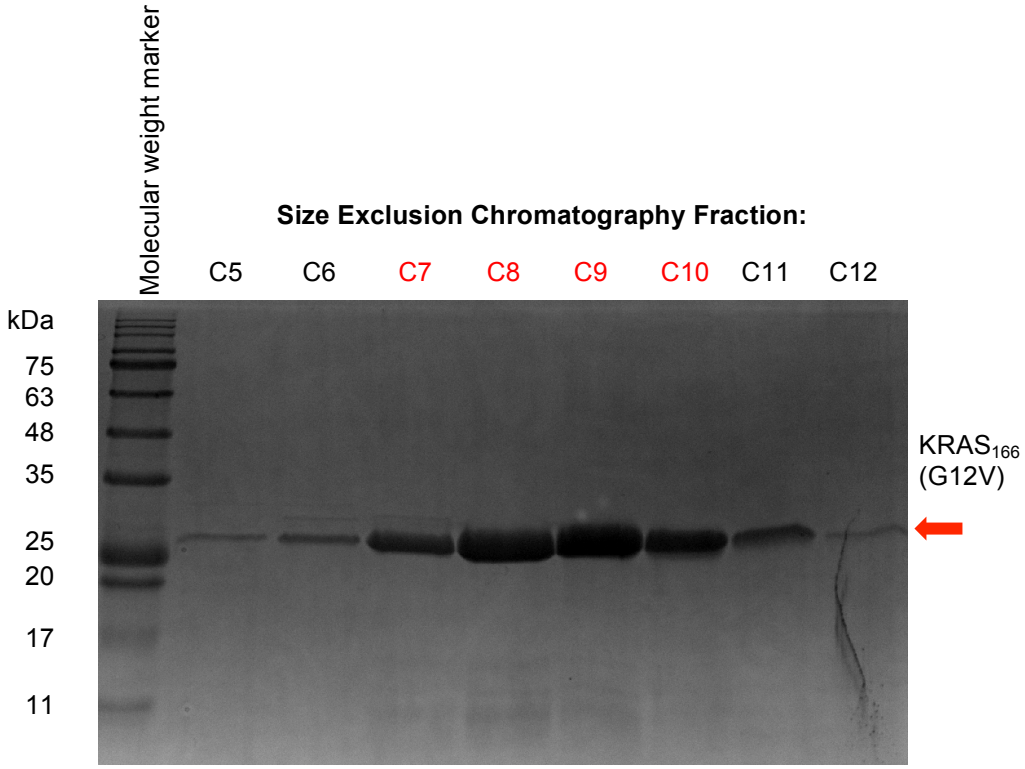

Figure 3.12 Confirmation of KRAS purification by Coomassie staining

The fractions from the SEC purification that corresponded to the KRAS elution were confirmed for their identity and purity by SDS-PAGE. Protein was visualised by Coomassie staining. Ten microlitres of the 1.5ml elutions were loaded. Fractions C7 to C10 (red text) were subsequently pooled and concentrated for stock.

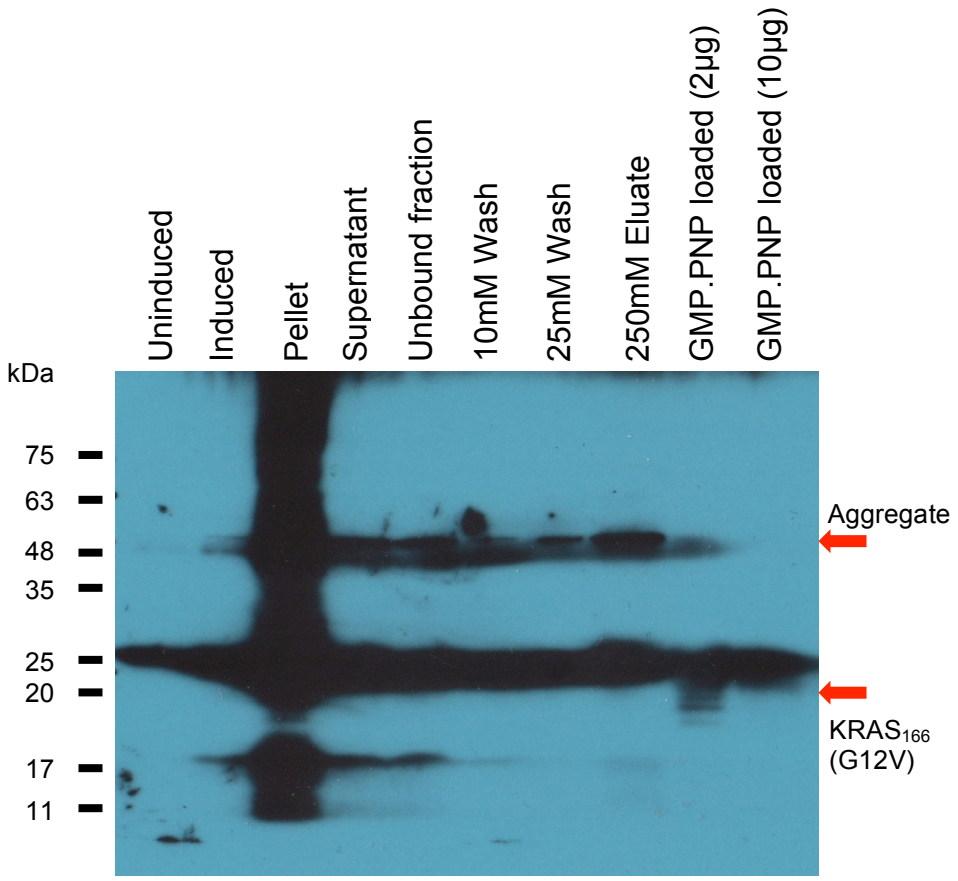

Figure 3.13 Confirmation of KRAS purification by Western blot

The purified protein has previously identified as His-TEV-Avi-$KRAS_{166}$(G12V) by localisation at the expected molecular mass by SDS-PAGE analysis. The identity of the protein was subsequently confirmed by Western blot with a pan-RAS antibody, being observed to resolve at the expected 26kDa molecular weight.

each expressed the non-NF VH- or VL-proCASP3 moieties. From these clones, the two highest expressers were carried forward for assessment. After expression cells were crudely fractionated into a soluble (supernatant) and insoluble (pellet) fraction. Location of the expressed proteins was assessed by Western blot, with the Parental line as a control. The FLAG-tagged moieties were detected at their expected ~50kDa masses, although the VH-proCASP3 protein appeared insoluble as it was located entirely within the pellet fraction (Figure 3.14). The VL-proCASP3 protein was mostly cytosolic, with only a small quantity of the correctly sized product being found in the pellet. Importantly, whilst only present in low concentrations, cellular RAS located to the pellet, allowing removal from the sample by fractionation. Endogenous CASP3 was found predominantly in the supernatant with only a slight band representing cleaved (activated) CASP3 visible in the pellet of the non-NF VH-proCASP3 preparation, implying this form of expression was suitable for large scale purification as little autoactivation was detected. The β-actin control blot was variable across the samples but indicates that it can localise to either fraction.

3.8.3 Improving VH-proCASP3 cytosolic yield

Resolubilisation of proteins found in the pellet fraction is possible, but it is a long and inefficient process involving denaturation and refolding of the recombinant protein (Yamaguchi and Miyazaki, 2014). The harsh conditions employed during the process may also be detrimental to the functionality of the proCASP3 zymogen in later experiments. Ways of improving the solubility of the non-NF VH-proCASP3 were investigated, although addition of detergent was avoided to reduce potential disruption of the membrane-localised RAS proteins. Instead, increasing ionic strength with rising concentrations of salt (as sodium chloride, NaCl) was tested, as it was reasoned that the VH-proCASP3 protein may have been pulled out of solution through its interaction with cellular RAS during the extraction process. Of the three concentrations tested, addition of 200mM NaCl to the lysis buffer increased the level

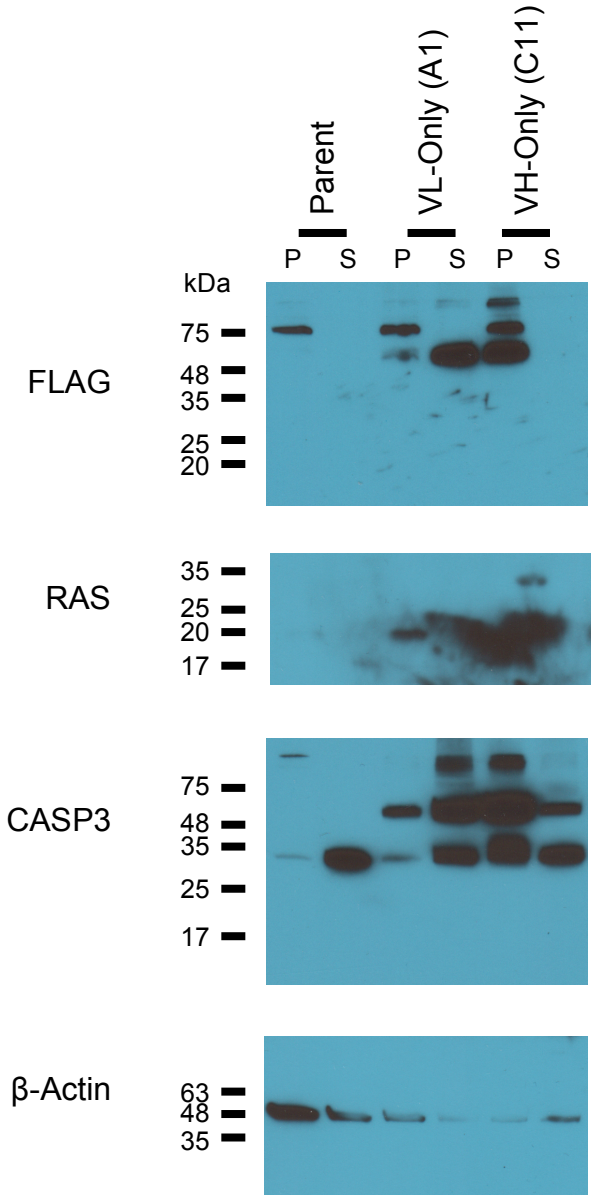

Figure 3.14 Confirmation of mammalian VH- and VL-proCASP3 expression

HT1080TetOn cells stably transfected with the non-farnesylated VH- and VL-proCASP3 plasmids were induced to express the proteins with tetracycline addition for 48 hours. Cells were harvested and protein lysates of the soluble (supernatant, S) and insoluble (pellet, P) fractions were prepared. Equivalent volumes (10µl) of samples were loaded per lane. A: Expression of the non-farnesylated VH- and VL-proCASP3 proteins was shown by Western blot for the FLAG-tagged moieties, which resolve at approximately 50kDa as expected. B: Endogenous RAS localises to the pellet. C: Endogenous CASP3 protein (35kDa) is found in both fractions. D: β-actin loading control.

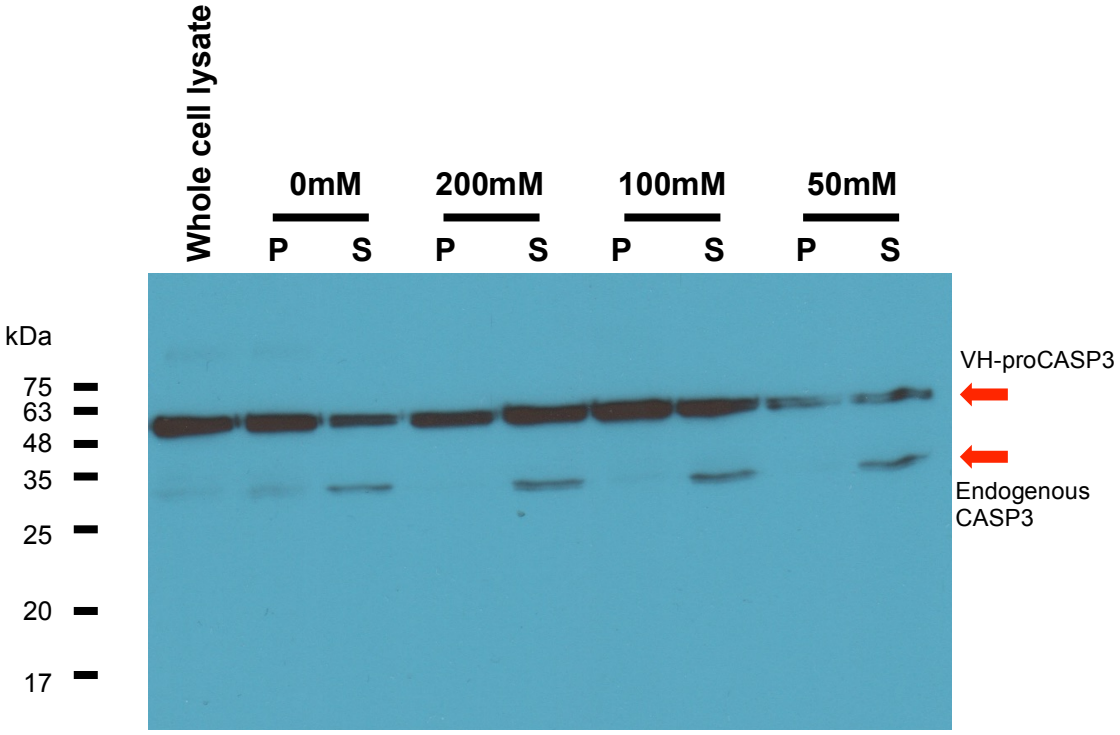

Figure 3.15 Improving VH-proCASP3 solubility with NaCl

The tetracycline-induced non-N-farnesylated VH-proCASP3 clone was harvested and lysed in buffers containing increased NaCl concentration, from no salt up to 200mM. Protein concentration was determined by BCA assay, with 20µg of total protein was loaded per lane. Gels were transferred to membrane for Western blot detection. The CASP3 antibody was used to allow endogenous CASP3 to act as a loading control. Fractions denoted as P for pellet and S for supernatant. More VH-proCASP3 protein is present in the supernatant with 200mM NaCl.

of non-NF VH-proCASP3 in the supernatant the most (Figure 3.15). Of note, upon addition of 100mM and 200mM NaCl to the lysis buffer, cell lysis appeared inhibited, with samples at these concentrations requiring extra time for lysis to reach completion. The lysis buffer was therefore kept at the same composition until confirmation that ≥90% of cells were dead by Trypan blue uptake, with NaCl added to a final concentration of 200mM after initial lysis but before fractionation.

3.8.4 Large-scale mammalian expression of VH- and VL-proCASP3

The first large-scale preparation of the non-NF proteins was performed from cell lysates derived from one hyperflask after 18 hours of tetracycline induction. Extraction and initial fractionation was performed as before. Western blot analysis showed good expression of each full-length protein, and presence of each in the cytosolic fraction (Figure 3.16). The lower band of ~35kDa was also observed in the cytosolic fractions across all three samples. Whilst these bands correspond with the expected size of endogenous CASP3, the intensity of the band is far greater on the expressed lanes when compared with the Parent line. This may reflect the presence of some cleaved recombinant protein, although levels of the fully cleaved large subunit (17-19kDa) are very low. The corresponding β-actin blot shows a uniform distribution across all cytosolic and insoluble fractions.

3.8.5 Affinity Purification of VH- and VL-proCASP3

The protocol for anti-FLAG affinity chromatography was adapted from laboratory protocols (Sewell et al., 2014). Eluates were subsequently pooled and concentrated to approximately 150µl. The fractions and eluates (single and pooled) were subjected to Western blot to confirm presence of the FLAG-tagged proteins (Figure 3.17) and the fused proCASP3 protein. The FLAG antibody identifies both of the FLAG-tagged proteins in the eluated fractions, with most protein eluting in the first pass of elution buffer. It struggles to show the presence of the VL-proCASP3 protein in the initial cells lysates, but the protein is detected later in the purification. In contrast, an

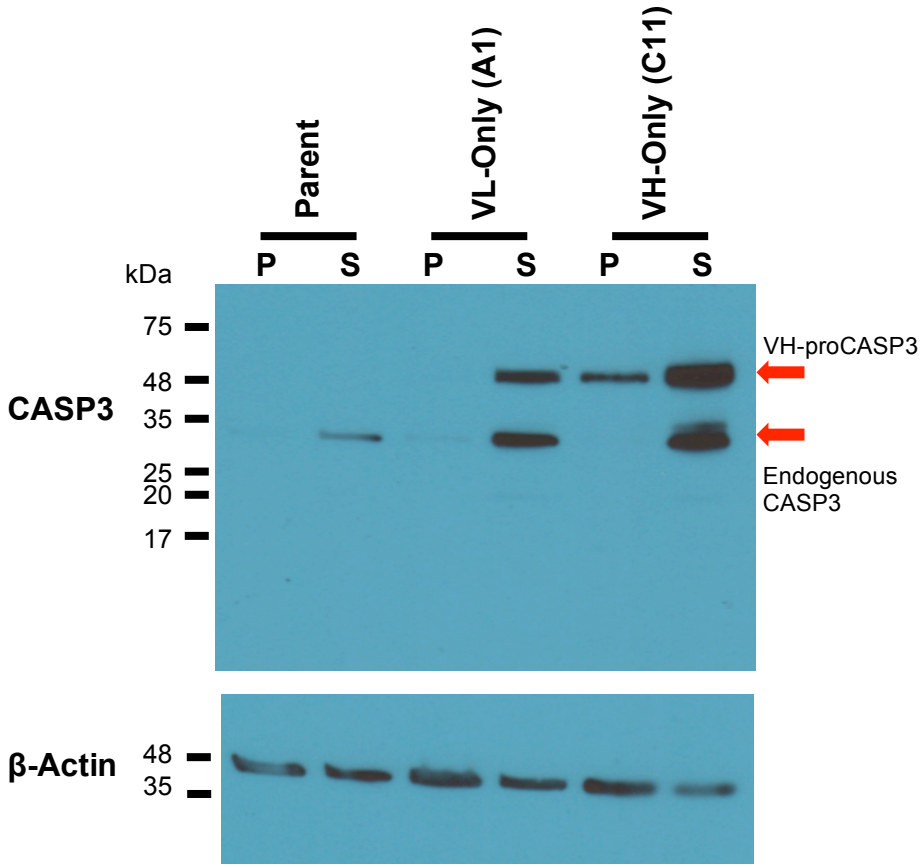

Figure 3.16 Large-scale mammalian VH- and VL-proCASP3 proteins

After 48 hours expression, large-scale preparation of proteins from the tetracycline induced clones and parental cells were harvested and lysed in buffer containing 200mM NaCl. The whole cell lysate is compared with the soluble fraction of each clone type. Equivalent volumes were loaded per lane. Gels were run and subsequently transferred to membrane for Western blot detection. Actin levels were assessed to confirm equal protein loading. Fractions denoted as P for pellet and S for supernatant. Full-length VH- and VL-proCASP3 proteins are detected in the soluble fraction (supernatant).

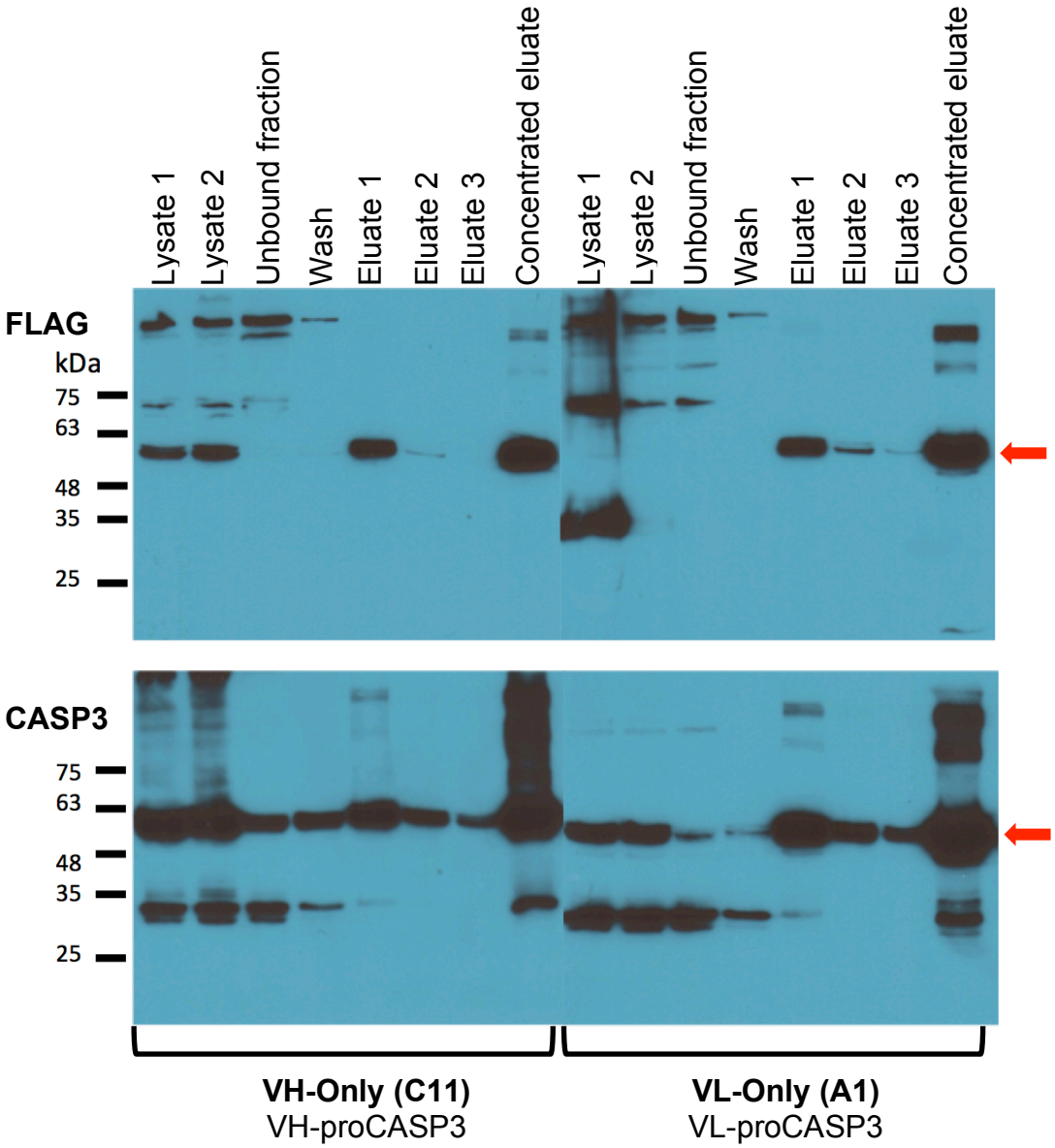

Figure 3.17 Affinity purification of VH- and VL-proCASP3 proteins

Large-scale preparation of the soluble fractions from the tetracycline induced clones and parental cells were harvested and lysed. Lysate was then purified over FLAG affinity agarose, and eluted with 2M Glycine. Equal volumes (20µl) of each purification fraction were loaded onto a 12% acrylamide gel. Gels were transferred to membrane for Western blot detection. Actin levels were assessed to confirm equal protein loading. A: VH anti-FLAG blot, B: anti-CASP3 blot. The bands corresponding to the full-length VH/VL-proCASP3 protein is indicated by red arrows.

equivalent gel, blotted and exposed to the anti-CASP3 antibody, shows very strong bands across the membrane at the same molecular weight. The 35kDa band which is seen on the CASP3 blots first appears a double band in the crude lysates, then reduces to a single band of lower intensity during purification, reappearing more strongly in the concentrated eluate. This implies presence of endogenous CASP3 and cleaved recombinant protein in the lysate and unbound fraction, and some concentration induced activation of the proCASP3 moieties in the eluates. The concentration of the VH- and VL-proCASP3 eluates were determined to be 77 and 73ng/µl respectively, with a total purified yield of 11.5µg and 11µg each. Further purification by SEC was considered, but each round of purification and concentration results in loss of material. The overall poor yield of recombinant protein limits the range of reactions and controls that would be desirable, without which establishment of the reaction parameters would be impossible.

3.8.6 Bacterial expression of VH- and VL-proCASP3

Following the poor VH- and VL-proCASP3 protein yields by mammalian expression, bacterial protein expression was investigated as a final alternative protein production method. As recombinant $KRAS_{166}$(G12V) had expressed well in the C41 E.coli transformed with the pRK expression vector, this same system was modified for the AIDA protein expression.

Plasmid constructs of i) pRK-His-Tev-Avi-VH-proCASP3 and ii) pRK-His-Tev-Avi-VL-proCASP3 were generated (Appendix D) and used to transform C41 E.coli. Expression levels were analysed by Western blot after 18 hours induction by IPTG with CASP3 and His-tag antibodies (Figure 3.18). Both blots show high level of fully cleaved proCASP3 domains in both protein expressions. The CASP3 antibody detects the ‘free’ cleaved large subunit at 17-19kDa, and the His-tag antibody detects His-tagged VH and His-tagged VL devoid of both CASP3 subunits at a similar size. However, contradictory results are seen when examining the higher

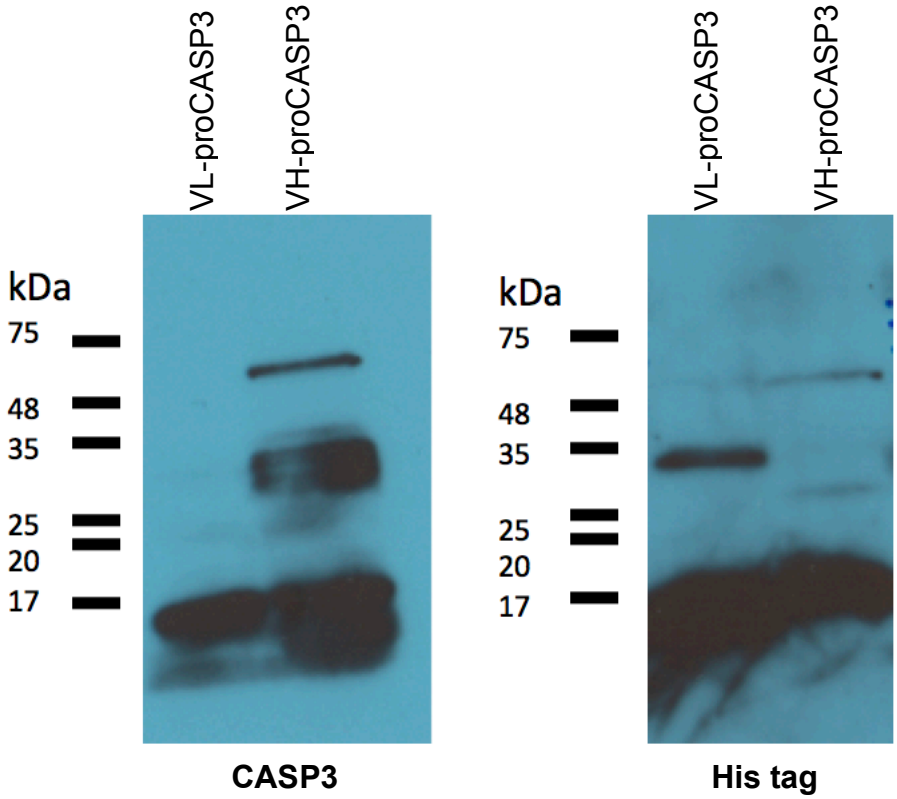

Figure 3.18 Bacterial expression test of VH- and VL-proCASP3

Small-scale cultures of transformed bacterial cells were induced to express the His tagged VH/VL-proCASP3 proteins by addition of IPTG for 18 hours at 37°C. Pelleted bacteria were lysed directly in Laemmli buffer and loaded onto 12% acrylamide gels and later transferred to membrane for Western blotting. Protein was detected with both A: CASP3 and B:His-tag specific antibodies. High concentrations of cleaved (active) CASP3 is visible at 17kDa.

mass products. The CASP3 antibody shows a higher ~35kDa band corresponding to VH-proCASP3 protein that has lost the small subunit and a lower intensity full-length band at ~50kDa, yet detects no, or very little, protein in the VL-proCASP3 lane. By contrast, the His-tag antibody binds to a strong ~35kDa band only on the VL-proCASP3 lane, yet on the VH-proCASP3 lane only faintly to the full-length protein. In spite of this, expression seemed efficient, and these problems may relate to non-optimal expression conditions.

3.8.7 Optimisation of VH- and VL-proCASP3 expression

Industrial expression of proCASP3 is difficult (Kang et al., 2008), owing to the spontaneous auto-activation of the zymogen at the high levels produced in bacteria (Stennicke and Salvesen, 1997) and yeast (Sun et al., 1997). Indeed, commercial CASP3 is only available as the active enzyme, presumably as a result of the proximity-induced cleavage of the zymogen during production. Whilst most recombinant protein was observed to be fully cleaved when assessed at 18 hours of expression (Figure 3.18), a lower expression time may enable purification of full-length protein before reaching the critical concentration within the bacterial cell. Moreover, it was postulated that addition of a reversible CASP3 inhibitor to the bacterial culture may reduce CASP3 activation, in a similar manner to the irreversible inhibitor used in Chapter 3. The inhibitor (Lee et al., 2001, Lee et al., 2000) was synthesised by Dr Carole Bataille, Rabbitts Laboratory, Dept. of Chemistry, University of Oxford (Appendix E).

Bacterial expression of VH- and VL-proCASP3 proteins was assessed at 18, 30 and 37°C for 2, 4 and 18 hours (18°C only) post-IPTG induction, with and without the addition of a reversible CASP3 inhibitor (Figures 3.19, 3.20 and 3.21). Two hour expressions at 37°C produced the most full-length protein in the soluble fraction, with the lowest level of breakdown product visualised when analysed by Western blot. Expression of VL-proCASP3 was particularly aided by addition of the inhibitor. This

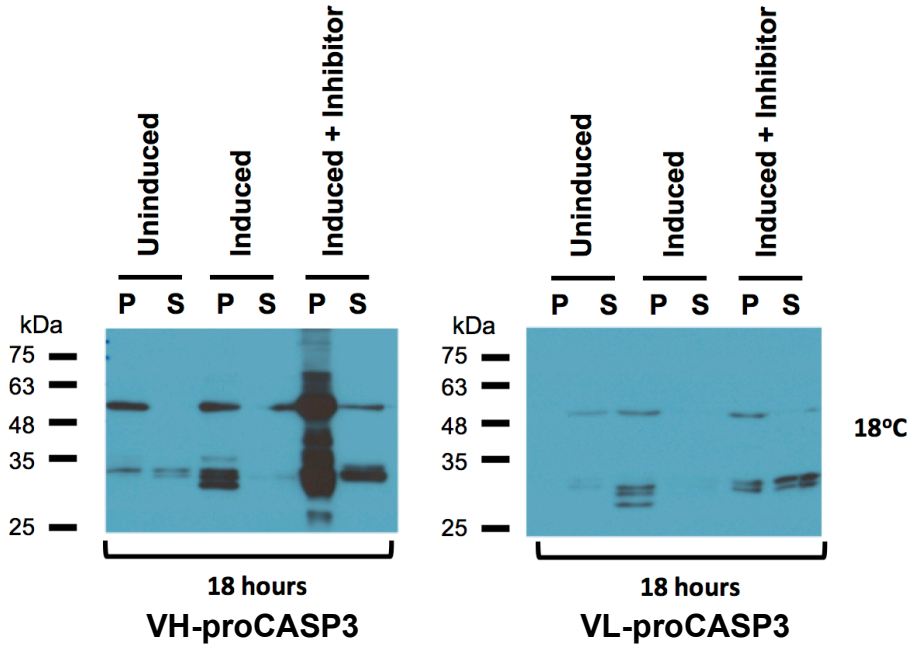

Figure 3.19 Bacterial expression test with reversible CASP3 inhibitor

Small-scale cultures of transformed bacterial cells were induced to express the tagged VH- and VL-proCASP3 proteins by addition of IPTG, with or without 154μM reversible CASP3 inhibitor. The CASP3 inhibitor (Lee et al., 2001, Lee et al., 2000) was made on my behalf by Dr. Carole Bataille, Rabbitts laboratory, Dept. of Chemistry, University of Oxford. Expression was performed overnight at 18°C. Bacteria were lysed by sonication, and soluble (supernatant, S) and insoluble (pellet, P) fractions were separated by centrifugation. Equivalent volumes were loaded onto 12% acrylamide gels for Western blot transfer. VH/VL-proCASP3 proteins were detected with the CASP3 antibody. VH-proCASP3 expressed well with CASP3 inhibition, although full-length protein was yield was low in the soluble fraction. VL-proCASP3 expression was low.

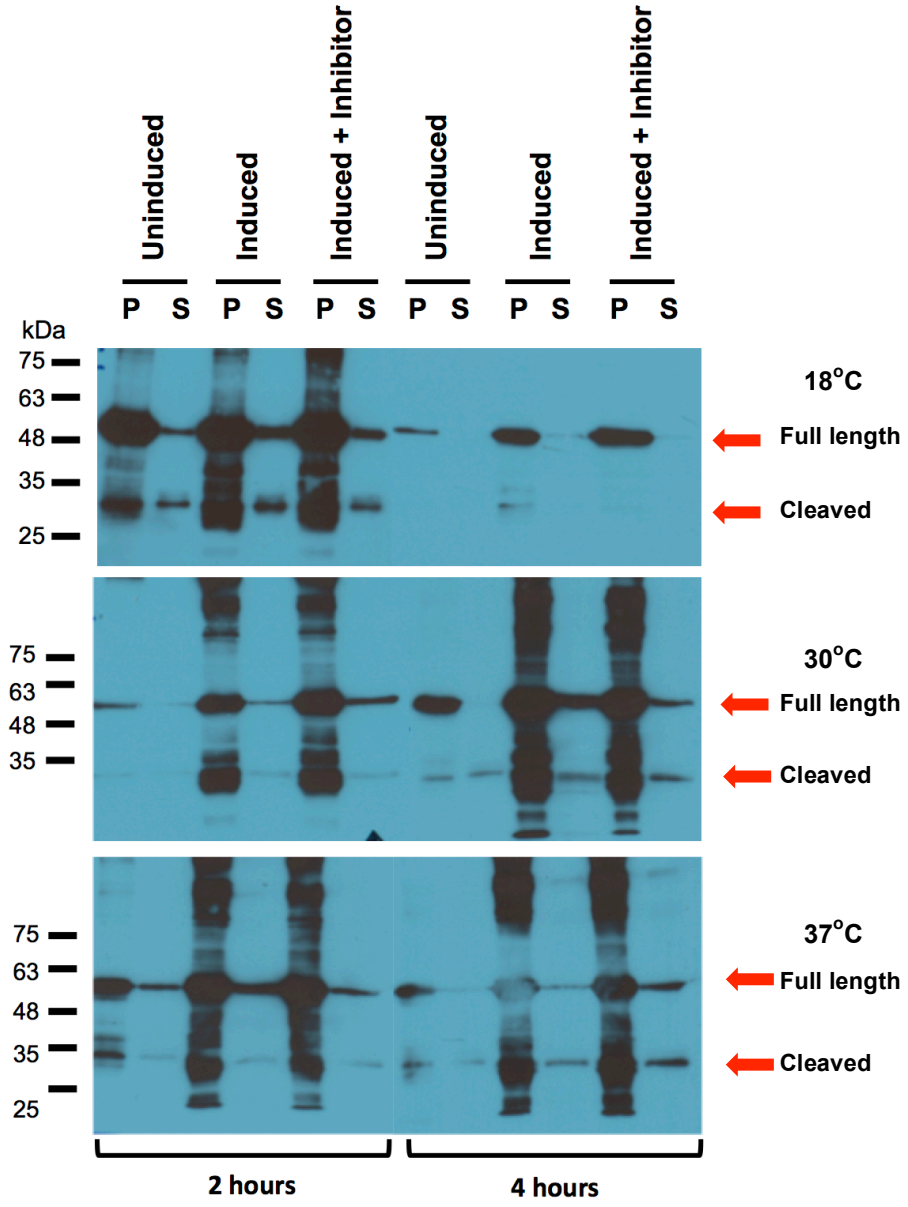

Figure 3.20 Optimisation of bacterial VH-proCASP3 expression

Small-scale cultures of transformed bacterial cells were induced to express the tagged VH-proCASP3 protein by addition of IPTG, with or without 154μM reversible CASP3 inhibitor. Expression conditions were tested over three temperatures (18, 30 and 37°C) and for three different expression times (2 and 4 hours). Bacteria were lysed by sonication, and soluble (supernatant, S) and insoluble (pellet, P) fractions were separated. Equivalent volumes were loaded onto 12% acrylamide gels for Western blot transfer. Protein was detected by with the CASP3 antibody. Positions of the full-length and cleaved recombinant protein are marked with red arrows. A higher expression temperature results in more full-length protein in the soluble fraction.

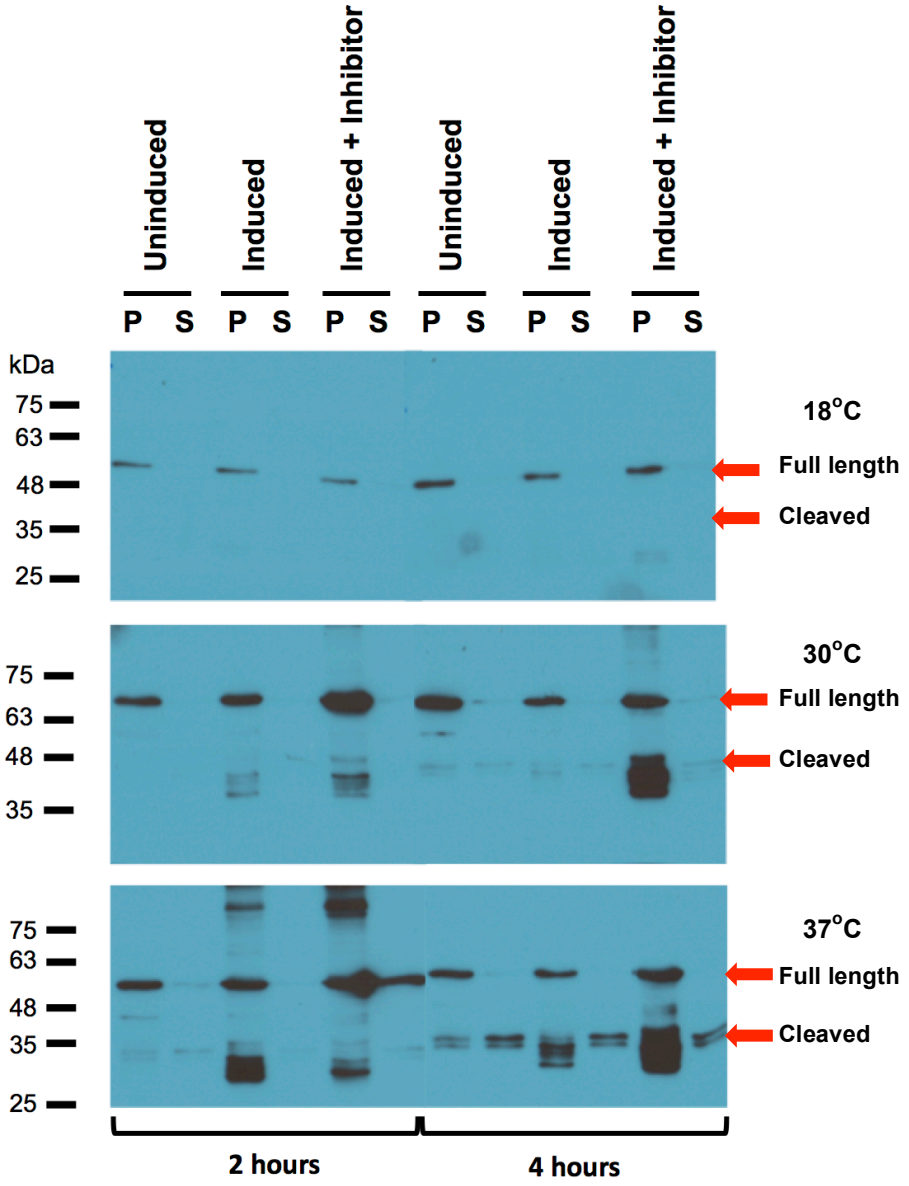

Figure 3.21 Optimisation of bacterial VL-proCASP3 expression

Small-scale cultures of transformed bacterial cells were induced to express the tagged VL-proCASP3 protein by addition of IPTG, with or without 154μM reversible CASP3 inhibitor. Expression conditions were tested over three temperatures (18, 30 and 37°C) and for three different expression times (2 and 4 hours). Bacteria were lysed by sonication, and soluble (supernatant, S) and insoluble (pellet, P) fractions were separated. Equivalent volumes were loaded onto 12% acrylamide gels for Western blot transfer. Protein was detected by with the CASP3 antibody. Positions of the full-length and cleaved recombinant protein are marked with red arrows. Expression at 37°C for two hours with CASP3 inhibitor is the only condition that results in more full-length protein in the soluble fraction.

finding was confirmed with a second round of expression optimisation, this time investigating expression times of 1 to 4 hours, with two concentrations of inhibitor – the previously tested 154μM versus 500μM (Figures 3.22 and 3.23). Again, two hour expression at 37°C produced the highest level of soluble, full-length protein, with VL-proCASP3 benefitting from the higher inhibitor concentration. The final bacterial expression conditions were therefore chosen to be 37°C for two hours, supplemented with 500μM reversible inhibitor (VL-proCASP3) and either 154μM or 500μM inhibitor (VH-proCASP3).

3.8.8 Affinity purification of His-tagged VH- and VL-proCASP3

The protocol used for the Ni-NTA agarose purification of His-tagged $KRAS_{166}$(G12V) was employed. Fractions were loaded onto acrylamide gels and subjected to Coomassie staining and Western blotting for the detection CASP3 antibody binding to the recombinant proteins (Figures 3.24 and 3.25). Large expression cultures of VL-proCASP3 and VH-proCASP3 were subjected to the purification protocol. Although full-length protein can be seen to elute across fraction of the rising imidazole concentrations, the eluate possessing the lowest level of cleaved protein is observed at the fourth elution of buffer containing 250mM imidazole. When the same fractions were visualised by Coomassie staining of SDS-PAGE gels, it was apparent that the protein concentration of each full-length band was fairly low, although some recombinant protein could be discerned, particularly in the 50mM Imidazole elutions. Undeterred, attempts at protein quantification were made, although the protein concentration of the eluates was too low to be measured within the limits of the BCA assay. Instead, reading the concentration at A280nm gave a concentration of 9.1μg/ml VL-proCASP3 and 21.2μg/ml VH-proCASP3.

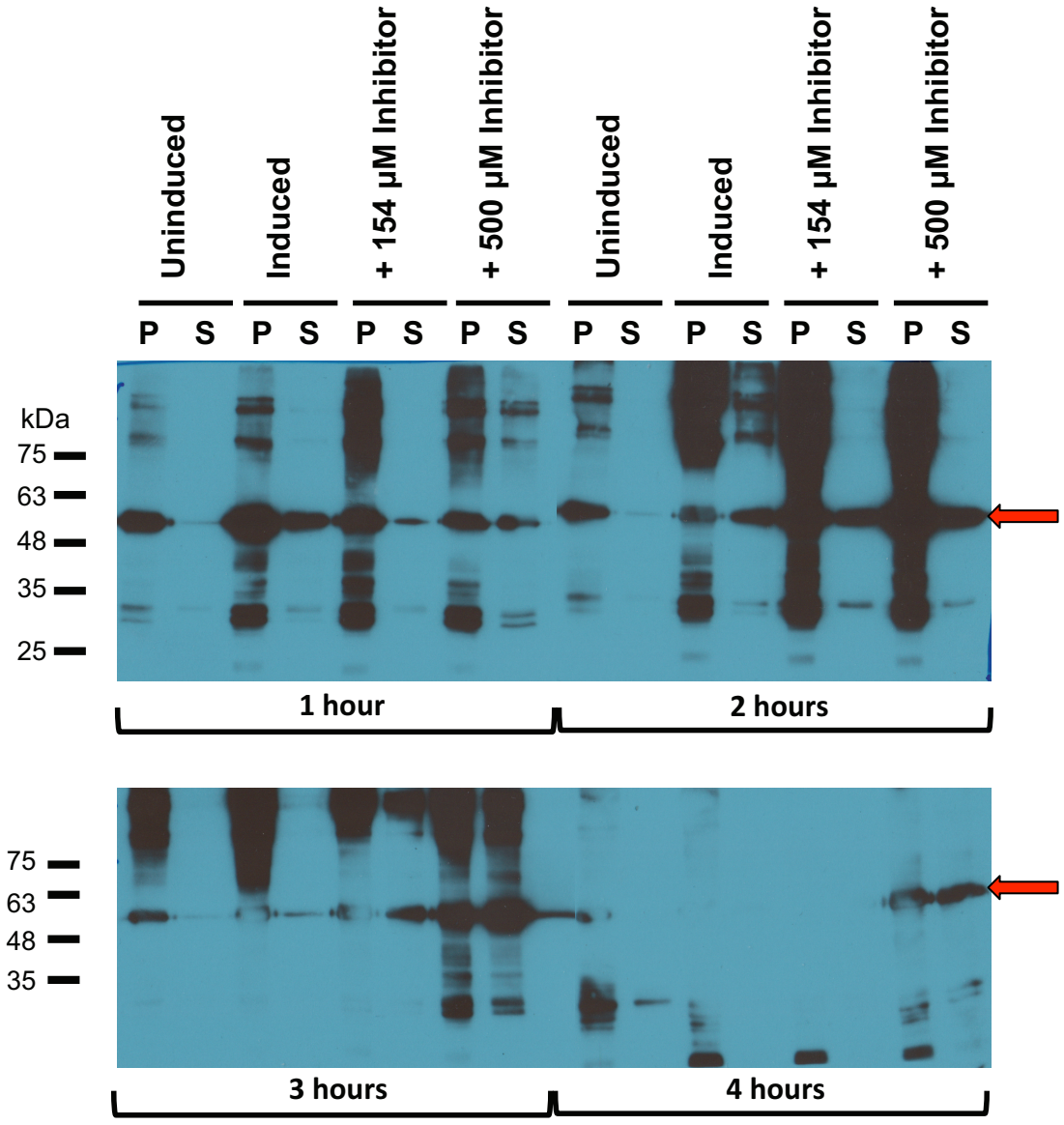

Figure 3.22 Further optimisation of bacterial VH-proCASP3 expression

Small-scale cultures of transformed bacterial cells were induced to express the tagged VH-proCASP3 protein by addition of IPTG, with or without reversible CASP3 inhibitor at two concentrations, 154 and 500µM. Expression was performed at 37°C, with expression time compared from 1-4 hours. Equal volumes of bacteria were lysed by sonication and fractions separated by centrifugation. Equivalent volumes were loaded per lane of a 12% acrylamide gel, which was later transferred to membrane for Western blotting. Protein was detected by with the CASP3 antibody. The highest level of intact protein (red arrow) is found in the soluble fraction when VH-proCASP3 expression is allowed to proceed for two hours. Presence of the inhibitor increases levels of VH-proCASP3, although increasing the inhibitor concentration from 154 to 500µM has minimal effect.

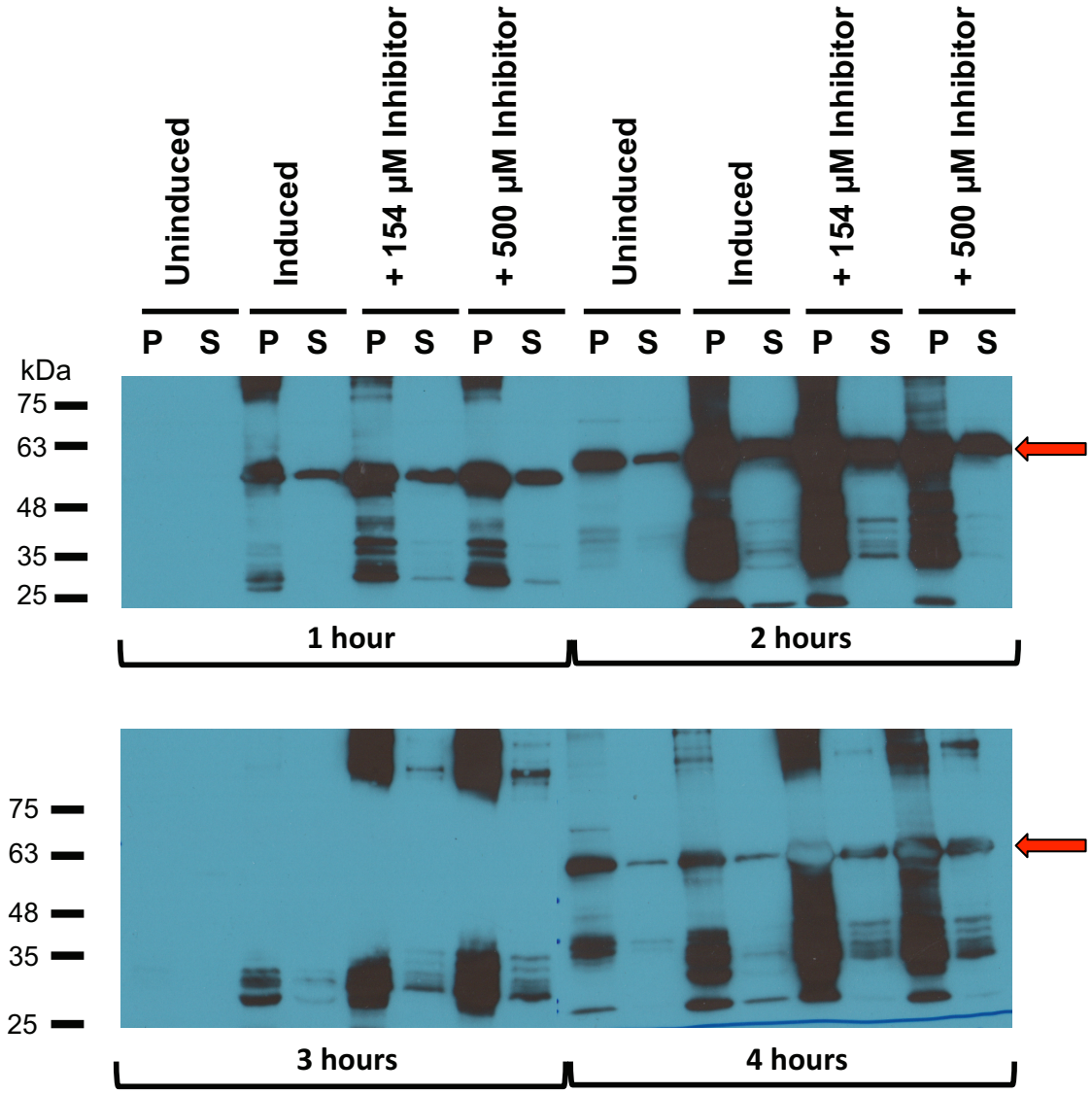

Figure 3.23 Further optimisation of bacterial VL-proCASP3 expression

Small-scale cultures of transformed bacterial cells were induced to express the tagged VL-proCASP3 protein by addition of IPTG, with or without reversible CASP3 inhibitor at two concentrations, 154 and 500µM. Expression was performed at 37°C, with expression time compared from 1-4 hours. Equal volumes of bacteria were lysed by sonication and fractions separated by centrifugation. Equivalent volumes were loaded per lane of a 12% acrylamide gel, which was later transferred to membrane for Western blotting. Protein was detected by with the CASP3 antibody. The highest levels of intact protein (red arrow) is found in the soluble fraction when VL-proCASP3 expression is allowed to proceed for two hours. Presence of the inhibitor increases protein levels. Increasing the inhibitor concentration from 154 to 500µM reduces the breakdown products due to CASP3 activation.

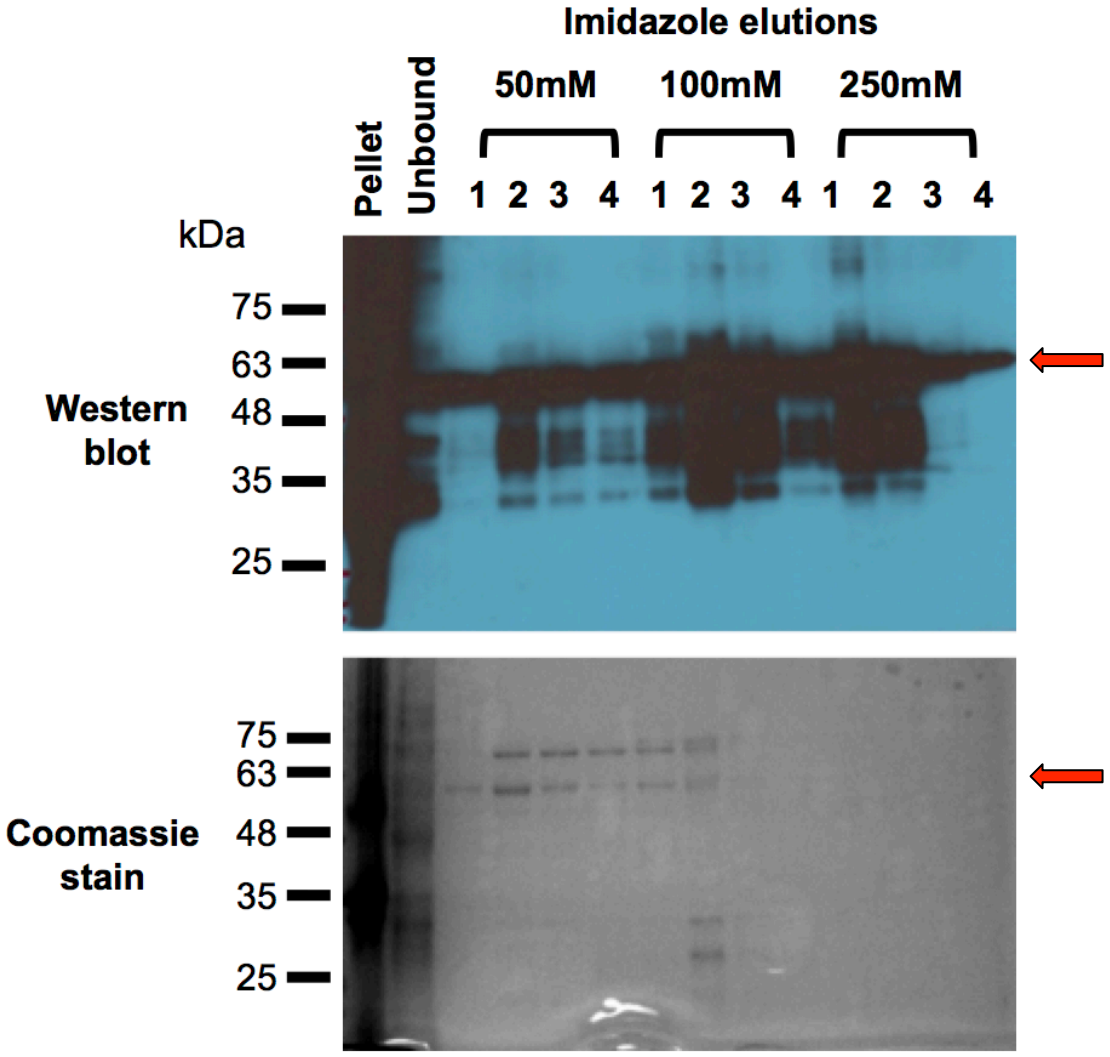

Figure 3.24 Large-scale purification of VH-proCASP3

Large-scale expression cultures (8L) of VH-proCASP3 proteins were prepared and purified by immobilised metal affinity chromatography over Ni-NTA agarose beads. Protein was eluted over rising imidazole concentrations. Equal volumes of eluate were loaded onto acrylamide gels and transferred to membrane for Western blot detection by the CASP3 antibody or stained with Coomassie stain to directly visualise the protein. Western blotting shows that Eluate 4 with 250mM imidazole elutes the most concentrated, full-length protein (red arrows), although the band cannot be visualized by Coomassie staining at eluate 4, it can be seen earlier in the purification profile.

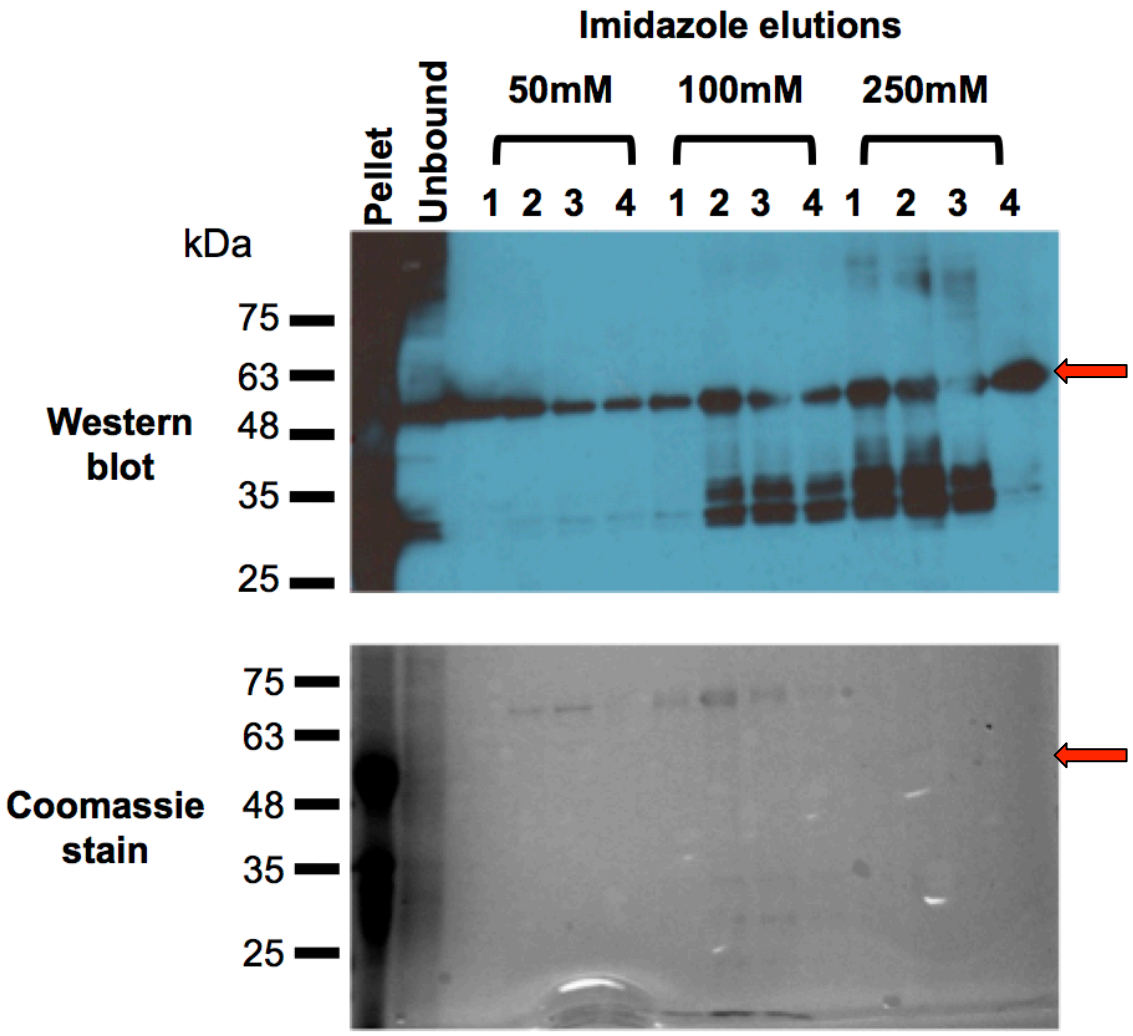

Figure 3.25 Large-scale purification of VL-proCASP3

Large-scale expression cultures (8L) of VL-proCASP3 proteins were prepared and purified by immobilised metal affinity chromatography over Ni-NTA agarose beads. Protein was eluted over rising imidazole concentrations. Equal volumes of eluate were loaded onto acrylamide gels and transferred to membrane for Western blot detection by the CASP3 antibody or stained with Coomassie stain to directly visualise the protein. Western blotting shows that Eluate 4 with 250mM imidazole elutes the most concentrated, full-length protein (red arrows), although the band cannot be visualized by Coomassie staining.

3.9 Discussion

This chapter presents the initial testing of the AIDA system in a human cancer cell line. Stable cell lines were successfully created and shown to express the VH- and/or VL-proCASP3 fusion proteins specifically upon Tet induction. Clones with the highest similarity of expression levels (relative to its own and other clone types) were carried forward for further analysis to ensure as fair a comparison as possible.

The results of the various assays employed within this chapter correlate with our hypothesised effects of each construct (represented previously in Chapter 1, Figure 1.15). When expressed alone, the VL-proCASP3 fusion (VL-Only) failed to impart an apoptotic phenotype. This is perhaps unsurprising given that the VL interaction with mutant RAS comprises of only one putative hydrogen bond from a single residue in CDR3 (Tanaka et al., 2007) when analysed as part of an scFv with VH#Y6. However, the lack of observed phenotype of the induced VL-Only clones suggests that the presence of these singly expressed proCASP3 domain is not deleterious to the cell in itself, nor is the resulting concentration gradient conferred by the membrane localisation enough to engage proximity activation. This data is in accordance with earlier findings suggesting that overexpressed proCASP3 is inefficient at self-activation (Colussi et al., 1998).

The expression of both VH-proCASP3 and VL-proCASP3 (VH+VL clones) is linked with cell death across all measurements. In addition to the morphological evidence of wide-spread cell death with the tetracycline induced VH+VL clones, the vast reduction in cell viability confirms a lowered live cell population remaining in the culture upon expression of both single domain fusion proteins. Moreover, the loss of membrane integrity, exemplified by the Annexin-V, 7-AAD stained flow cytometry experiments, is a key indicator of the dysregulation that is associated with apoptosis and other forms of cell death. The presence of active CASP3, detected by Western blot and fluorescent substrate conversion monitoring, and the successful partial

rescue of cell death phenotype by the CASP3 inhibitor, implies that the mechanism of observed phenotype is directed through activation of CASP3. Whilst it is evident form the breakdown products seen by Western blot that the fused proCASP3 moiety of the VH/VL fusion proteins undergoes proteolytic cleavage consistent with self-activation, it doesn't specify the causation of this effect. Although we hypothesise that the CASP3 activation originates from antigen-mediated association of the VH and VL-proCASP3 fusions, the data described in this chapter cannot exclude the possibility of endogenous CASP3 activation mechanisms being the initiating factor.

Lone expression of the VH-proCASP3 fusion (VH-Only) showed no obvious increase in dead or dying cells by microscopic inspection, and neither was there an appreciable difference in membrane integrity upon its expression. However, indications of CASP3 activation were found with Western blot and fluorogenic substrate data, although treatment with the inhibitor was to no perceptible consequence. It had been anticipated that VH-proCASP3 binding to cellular RAS without the VL-proCASP3 protein would convey a cytostatic effect on the cells, following previous findings that VH#Y6 retarded tumour growth *in vivo* through interference with oncogenic RAS signaling (Tanaka 2010 oncogene). The reduction in viability of the cells upon VH-proCASP3 expression implies a decrease in live cells, and this could result from either growth inhibition or cell death. As cell death was not obvious, and the morphological changes resemble known alterations from cell cycle arrest, it is likely RAS inhibition is the driving factor in the generation of these results. The low level CASP3 activation may be natural consequence of this unnatural growth arrest, or it may indicate unanticipated antigen-interaction mediated activation of the proCASP3 domains. Reports of RAS aggregates or 'nanoclusters' within the inner leaflet of the cell membrane exist (Prior et al., 2003, Plowman et al., 2005), which are postulated to provide enhanced signal transduction. This may present a means of low level proCASP3 moiety activation, through proximity of RAS-bound, VH-proCASP3 chains. However, the dimerisation 'face' of the molecule appears to

be opposite to that containing the switch regions, which is the location of VH#Y6 binding. This would, at the very least, provide a buffering distance (if not full insulation) from any RAS aggregation effect. In a similar manner, VH:VH dimerisation has been documented (Baral et al., 2012), and is plausible when viewed in context of the natural VH:VL association via hydrophobic framework interactions. This notion could explain the VH-Only effect, particularly if the VH:VH interaction is inefficient. However it would also raise the question of whether antigen dependency is fully required for the VH:VL interaction to occur.

Expression and purification of high enough levels of the VH- and VL-proCASP3 proteins was challenging. Mammalian expression systems could not produce enough protein in the scalable formats available. Fortunately, the fusion proteins seemed suited to bacterial expression, resulting in the production of larger quantities of protein than were possible in the mammalian system. However, as has been encountered by other researchers attempting to purify CASP3 (Mittl et al., 1997, Ryser et al., 1999, Fernandes-Alnemri et al., 1994), auto-activation of the proCASP3 domains is commonplace, and almost impossible to prevent. The presence of the single domain fragments may have helped to reduce this concentration effect, and that addition of the reversible inhibitor (Lee et al., 2001, Lee et al., 2000) may similarly have helped prevent activation. However, it has been demonstrated that whilst the protein yield is inefficient, purification of the full-length AIDA constructs is possible.

3.10 Conclusion

The results presented in this chapter indicate that the AIDA system can be a potential anti-tumour therapy, having now been demonstrated to work in proof-of-principle experiments against a relevant human oncogene in a human tumour cell line. Both VH-proCASP3 and VL-proCASP3 appear necessary to produce apoptosis and these data suggest that the hypothesised mode of action is correct. In addition, a

strategy of recombinant AIDA protein expression and purification has been developed. This will enable testing of an in vitro ‘cell-free’ system, should this method be required.

Chapter 4 Testing AIDA antigen dependency and efficacy in tumour models

4.1 Introduction

The creation and characterisation of the initial AIDA clones in the HT1080TetOn cell line had worked well. Generation of mutant versions of the AIDA constructs could provide additional confirmation of the method working by antigen dependency and origin of the activated CASP3. This approach should be viable as it would build on the functional methods described in Chapter 3. A schematic representation of where these mutations could be introduced is showing in Figure 4.1.

Mutations could be placed in the VH domain to reduce and ablate binding of the fragment to mutant RAS. Previous work in the laboratory had already characterised amino acid substitutions in one or two of the three CDR loops of VH#Y6, to produce mutants with altered binding capabilities (Tanaka et al., 2007). A reduced affinity mutant, herein known as dematured Y6 (VH#Y6dm for short), containing CDR1 and CDR2 substitutions resulted in a dissociation constant one thousand fold lower than the VH#Y6. A non-binding mutant, herein referred to as mutant Y6 (VH#Y6mut for short), was created with only CDR1 residue mutations. The altered VH#Y6 sequences and resulting dissociation constant magnitudes are shown in Table 4.1.

Employing a non-RAS binding VH#Y6mut would act as an antigen control, given the unavailability of a suitable RAS-free system, whilst VH#Y6dm may lessen any phenotype resulting from RAS inhibition. Similarly, catalytic residue mutations could be placed within the proCASP3 moieties to yield an inactive enzyme, upon proCASP3 element processing. Catalysis is mediated through primarily through the action of two residues, Cys163 and His121 (Nicholson, 1999). The cysteine residue forms hydrogen bonds which anchor the substrate and polarises the carbonyl bond of the recognition motif's second aspartate residue, leaving the same carbonyl bond susceptible to nucleophilic attack from the sulphur atom of Cys163 (Fuentes-Prior and Salvesen, 2004). The His residue acts to protonate the amino group of peptide

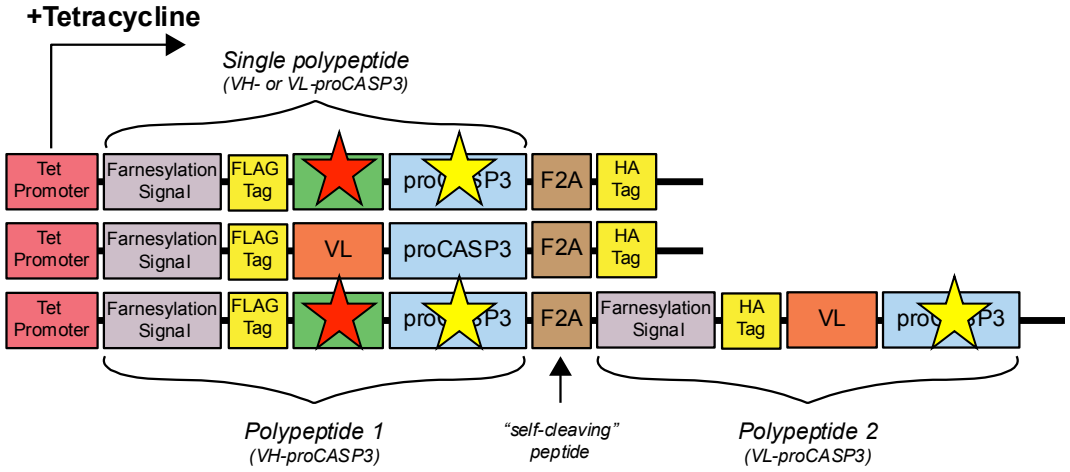

Figure 4.1 Illustration of the AIDA construct mutations

Schematic diagram of the desired mutations within the original AIDA constructs to allow determination of antigen dependency and origin of CASP3 activation. Mutations within the VH domain are indicated by a red star, whilst catalytic residue mutations within the proCASP3 domains are denoted by a yellow star. The AIDA cassettes were cloned into a Tetracycline-dependent expression plasmid, pUHD10, containing a hygromycin selectable marker. Each AIDA cassette contains an N-terminal farnesylation sequence to target both elements to the cell membrane. Single cassette vectors are FLAG-tagged for affinity recognition of the VH/VL-proCASP3 polypeptide. The viral F2A sequence follows to cleave the proteins. Vectors containing both AIDA cassettes possess a second polypeptide after the F2A sequence. This codes the VL-proCASP3 fusion which is haemagglutinin (HA)-tagged for identification. All vectors were linearised with SspI restriction endonuclease for stable transfection.

VH	RAS binding	Kd	CDR1	CDR2	CDR3
Y6	“original”	nM	GFTFSTFSMN	YISRTSKTIYYADSVKG	ARGRFFDY
Y6dm	“dematured”	μM	GFAFAAFSMN	YISRTSKTIYYADSVKG	ARGAAFDY
Y6mut	“mutant”	Not detected	GFTFSRPQMA	YISRTSKTIYYADSVKG	ARGRFFDY

Table 4.1 VH#Y6 variant sequences

The corresponding published CDR sequences of the anti-RAS VH#Y6 variants are shown, with amino acid residue substitutions highlighted in red. The CDRs corresponding to those defined by the ImMunoGeneTics (IMGT) system are underlined, and each CDR is 8 residues long. The magnitude of their respective dissociation constants, determined as scFv with VL#204, are indicated (Tanaka et al., 2007).

bond to release the second half of the substrate, and then coordinates a hydrolytic water molecule to attack the thioester bond between Cys163 and the substrate (Fuentes-Prior and Salvesen, 2004). Mutation of Cys163 to serine was demonstrated to ablate catalytic activity in AIDA (Tse and Rabbitts, 2000) and mutation of His121 has been shown to reduce caspase 1 catalysis (Wilson et al., 1994). These RAS and proCASP3 mutations would, in theory, allow discrimination between RAS inhibition and CASP3 activation effects, in addition to identifying that the observed cell death is primarily activated through the exogenous proCASP3 domains rather than activation of endogenous CASP3.

The AIDA system has so far only been assessed in cells grown in monolayer. Whilst the main focus of this thesis was to develop a method of leukaemic cancer cell killing, both RAS and LMO2 have also been implicated in solid tumours, such as glioblastoma (Kim et al., 2015), pancreatic (Nakata et al., 2009) and colorectal cancers (Bos et al., 1987). Therefore, it would be advantageous to ascertain whether the same AIDA effect could be produced within three dimensional growths to clear a solid tumour mass.

4.1.1 Aim

The aim of this chapter is to provide further confirmation of the antibody-antigen specificity and dependency for the AIDA effect using RAS affinity VH mutants, and to verify that apoptosis is specifically induced from the macrodrug VH/VL-proCASP3 elements rather than endogenous assaults by testing proCASP3 domain catalytic mutants. Moreover, this chapter will investigate AIDA in both monolayer cultures and in three-dimensional tumour assays, to ascertain suitability of the system in clearing tumour masses.

4.2 Creation of mutant vectors and stable cell line characterisation

To create the VH variant constructs, VH#Y6 was excised from the VH-Only and VH+VL AIDA vectors, and replaced with either VH#Y6dm or VH#Y6mut to create VHdm-Only, VHmut-Only, VHdm+VL and VHmut+VL plasmid constructs. To create the proCASP3 domain catalytic mutants, single and double amino acid residue mutant domains (Δ and ΔΔ respectively) were amplified and cloned into the VH-Only and VH+VL constructs to replace the wild-type proCASP3 domain. Resulting plasmids were sequenced and linearised for stable transfection into HT1080TetOn cells. Colonies were selected and propagated for assessment. Tetracycline induction of the mutant VH- and VL-proCASP3 moieties was performed and cell lysates subjected to Western blot analysis to confirm expression (Figure 4.2). Single expressing clones were obtained from VHdm-Only, VH+VLΔ and VH+VLΔΔ transfectant screening. Again, detection of FLAG-tagged protein was difficult, although detection of the correctly sized bands were identifiable with the CASP3 antibody. The HA-tag was sometimes still attached to the VH-proCASP3 chains, indicating variable efficiency of the 2A site 'cleavage'.

Morphological changes associated with the expression of the proteins were investigated (Appendix I). Expression of the VH+VL mutant clones resulted in the same altered appearance noted in the VH-Only clones (discussed in Chapter 3), compared with the original VH+VL clones that were destroyed through cell death. In particular, the VH+VL catalytic CASP3 mutant clones did not display an increase in dead cells, supporting the abrogation of the proCASP3 domain activity. The clones expressing VHdm+VL fusions possess a morphology between that of the VH Only and the uninduced sample. Similarly, VHdm-Only reaches confluence, but still has the flattened and enlarged appearance of the VH-Only clones.

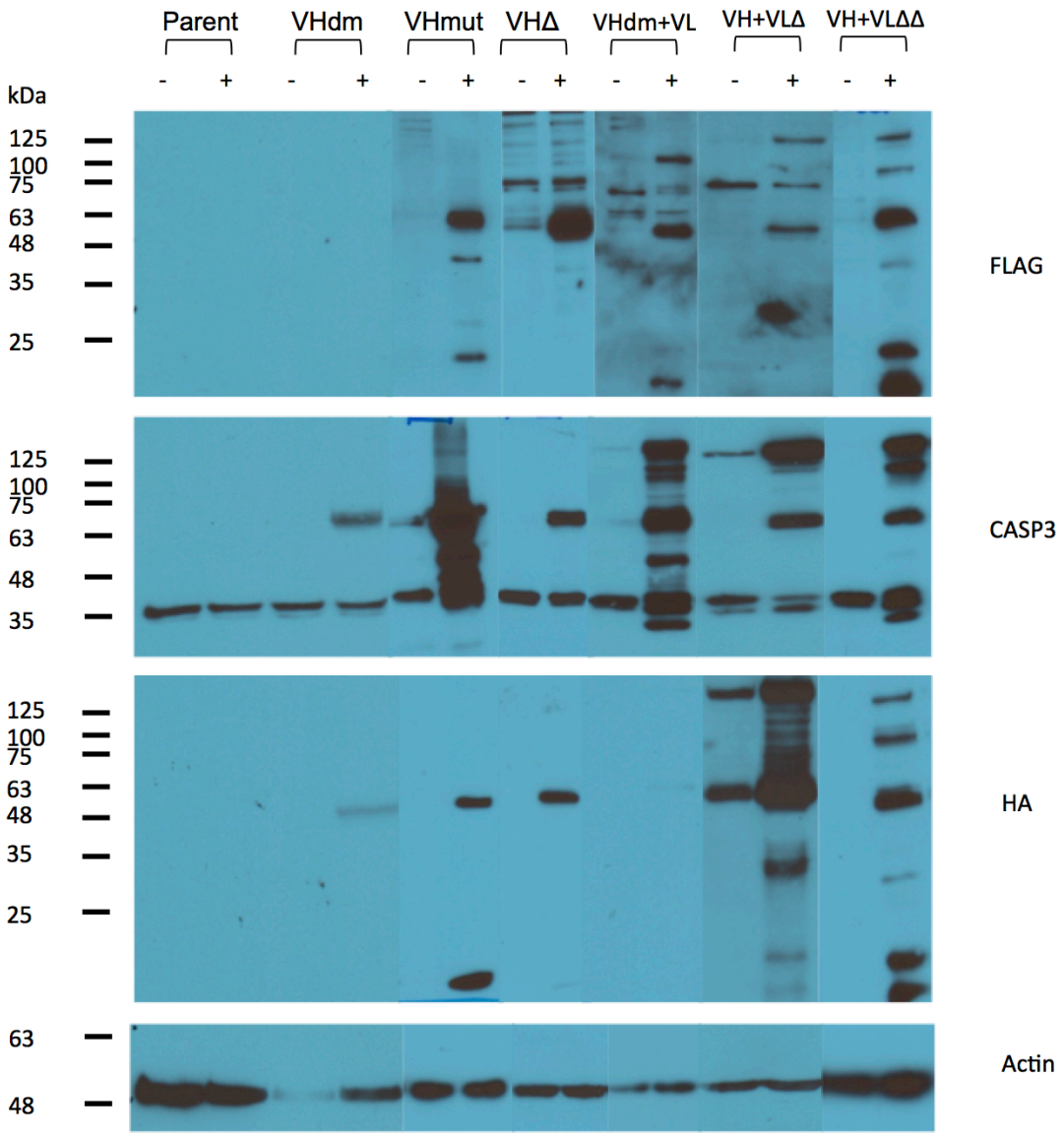

Figure 4.2 Confirmation of variant AIDA construct expression

The variant AIDA constructs were stably transfected into HT1080TetOn (Parent) cells, and tetracycline inducible expression of the fragments was assessed by Western blot after 48 hours expression. The protein concentration of each lysate was determined by BCA assay, with 10µg loaded per lane. The variant VH/VL-proCASP3 moieties were detected with antibodies specific for the FLAG tag, the HA tag and CASP3 protein. Actin levels confirmed protein loading. The FLAG tag shows stochastic detection of the AIDA fragments (approximately 50kDa), although the CASP3 antibody could confirm their expression in the absence of FLAG antibody binding. Endogenous CASP3 is also detected by the CASP3 antibody, resolving at 35kDa. The HA tag is found most strongly expressed in the VH+VL variant clones, although inefficient F2A 'cleavage' is found because VH-Only variants do show some HA tag presence.

Previous work demonstrated that maintenance of tumour growth suppression in mice was dependent on continued VH expression (Tanaka and Rabbitts, 2010a). Therefore, removal of tetracycline from the growth medium was investigated. Within two days, VH-Only and VHdm-Only clones reverted to normal morphology, although VH+VLΔ required a further 48 hours to recover. The VH+VL clones were completely dead (as shown previously in Appendix H). The Kd of the VH interaction with RAS as an scFv is lower than that of the VH alone (0.35nM vs. 6.2nM respectively) (Tanaka et al., 2007). The increased time taken for the VH+VLΔ clone to revert to their usual appearance is therefore unsurprising, as the expression of both fusion proteins would form an Fv, with a similar RAS affinity.

4.3 Apoptosis-related cell surface changes

The apoptotic profile of the clones was assessed by flow cytometry, with Annexin V protein and 7-AAD vital dye as performed in Chapter 3. The data show the VH+VL clones divides into two distinct, and almost equal, apoptotic populations of Annexin V-positive, 7-AAD negative and Annexin V/7-AAD double positive stains upon addition of tetracycline (Figure 4.3). VHdm-Only expression replicates the effect of VH-Only expression, whilst VHmut Only expression produces no meaningful increase in apoptotic populations relative to the uninduced sample of the same clone. The VHdm+VL clones experience a severely reduced apoptotic phenotype compared with the VH+VL clones. Here less than 4% of cells can be identified as in the late stages of apoptosis, and less than 15% are in the early stages.

The proCASP3 catalytic mutant clones result in a highly similar phenotype upon expression of the proteins. A large early apoptotic population (~50%) is present which mirrors that of the VH+VL clones, but with a 6 to 8 fold lower population of cells in the late phase of apoptosis. This finding parallels with the earlier observation that VH+VL binds to RAS more tightly than just VH, as mentioned in section 4.2 with the reversion to normal morphology after protein expression is stopped, and with

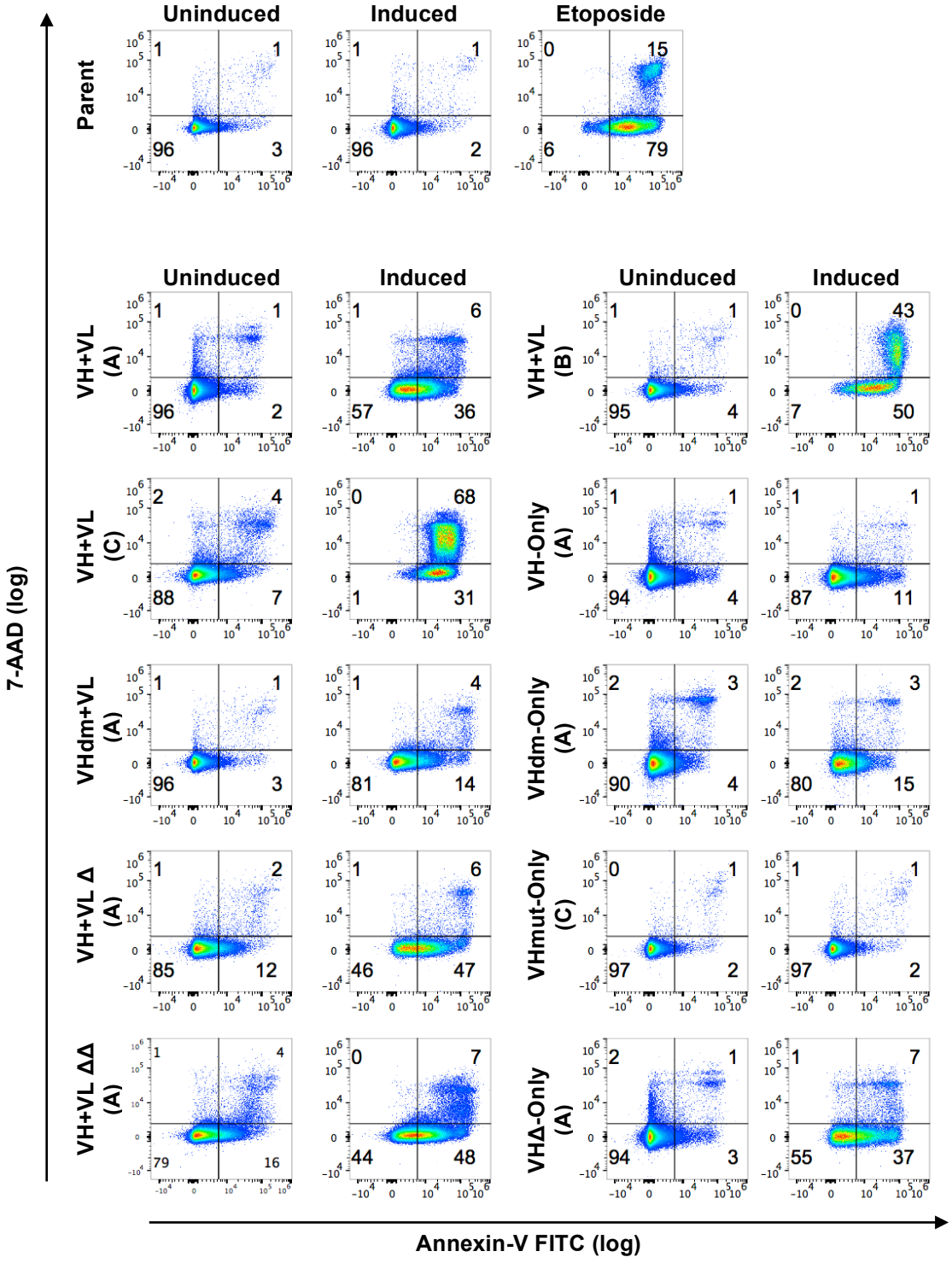

Figure 4.3 Apoptosis-associated cell surface changes

Analysis of the cell surface changes associated with the AIDA construct expression was monitored by flow cytometry. Clones were expressed for 48 hours with and without tetracycline induction (induced vs. uninduced). A positive control for apoptosis was with 8 hour etoposide treatment on the parental cell line. Triplicate samples were stained with Annexin V protein (FITC conjugated) and 7-AAD, and analysed. The plots shown here are representative. Single cells were gated according to size and granularity parameters on the parental cell line, as was the quadrant fluorescence gate. Compensation was performed with single stained colour controls. Percentage of cell population occupying the quadrants are shown. Individual clone numbers (A-C) are indicated in the panels.

the published binding kinetics of VH+VL and VH Only (Tanaka et al., 2007). The similarity of VH+VΔ/ΔΔ with VHΔ-Only is likely due to the exceptionally high expression level of VHΔ-Only increasing the perturbation of RAS inhibition (refer to Figure 4.2). The flow cytometry data discussed here are represented in full in table format (Table 4.2).

4.4 Multiparameter assessment of apoptosis

To streamline the assessment of cell viability and CASP3 activation across the mutant clones, the Promega ApoToxGlo commercial assay was used. The assay would permit multiplexed determination of the effect of mutant VH- and VL-CASP3 expression by three parameters of cell death, namely cell viability, CASP3 activation and cytotoxicity, without the variation of repeated plating for different assays. The assays were performed at 18 and 48 hours after Tet induction of the fusion proteins.

4.4.1 ApoTox Glo cell viability measurements

In constrast with the resazurin-based viability measurements performed in chapter 3, this cell viability assay employs a cell-permeable fluorogenic substrate, glycylphenylalanyl-aminofluorocoumarin (GF-AFC), which is cleaved by cellular aminopeptidases such as Cathepsin C, to release the fluorescent AFC portion of the substrate (Niles et al., 2007). Dead and dying cells lose surface membrane integrity, releasing cellular contents into the surrounding medium. These 'live cell' aminopeptidases become inactive outside of the cellular milieu, meaning that the fluorescent signal generated is proportional only to viable cells. The viability results are shown in Figure 4.4.

After 18 hours of protein expression, very little effect on cell viability was detected. By 48 hours, the assay could recapitulate the resazurin dye-based viability experiments that were performed on the original AIDA construct clones (shown in Chapter 3, Fig 3.5). Upon analysis, VH+VL clones had reduced viability to an

A

Clone Type	Growth Conditions	Replicates	% Live 7AAD- AnnV-	% Early 7AAD- AnnV+	% Late 7AAD+ AnnV+	% Necrotic 7AAD+ AnnV-
Parent	Uninduced	11	94	5	1	1
	Induced	11	94	4	1	1
	Etoposide	10	24	59	15	1
VH+VL	Uninduced	12	93	4	2	1
	Induced	12	17	40	43	1
VH-Only	Uninduced	6	89	8	2	1
	Induced	6	64	33	3	1
VHdm-Only	Uninduced	3	89	5	4	2
	Induced	3	75	20	3	2
VHmut-Only	Uninduced	6	96	2	1	1
	Induced	6	97	2	1	1
VHΔ-Only	Uninduced	6	93	5	1	1
	Induced	6	51	42	7	1
VHdm+VL	Uninduced	6	96	2	1	1
	Induced	6	84	11	3	2
VH+VL Δ	Uninduced	7	86	10	3	1
	Induced	7	51	44	5	1
VH+VL ΔΔ	Uninduced	6	85	10	3	2
	Induced	6	56	39	5	1

B

VH+VL Clone	Growth Conditions	Replicates	% Live 7AAD- AnnV-	% Early 7AAD- AnnV+	% Late 7AAD+ AnnV+	% Necrotic 7AAD+ AnnV-
A	Uninduced	3	94	1	4	1
	Induced	3	9	44	47	0
B	Uninduced	6	91	2	5	1
	Induced	6	3	61	35	1
C	Uninduced	3	95	1	2	2
	Induced	3	52	6	42	1

Table 4.2 Summarised data of apoptosis-related cell surface changes

Panel A shows the set of averaged Annexin-V, 7-AAD stained populations (from figure 4.3), indicating the number of clones and replicates tested. The apoptotic death stages are given in the column headers. Percentage values rounded to the nearest whole number tell the size of those populations within the cell sample. VH+VL are 3 clones combined in panel A, and individual results shown in panel B.

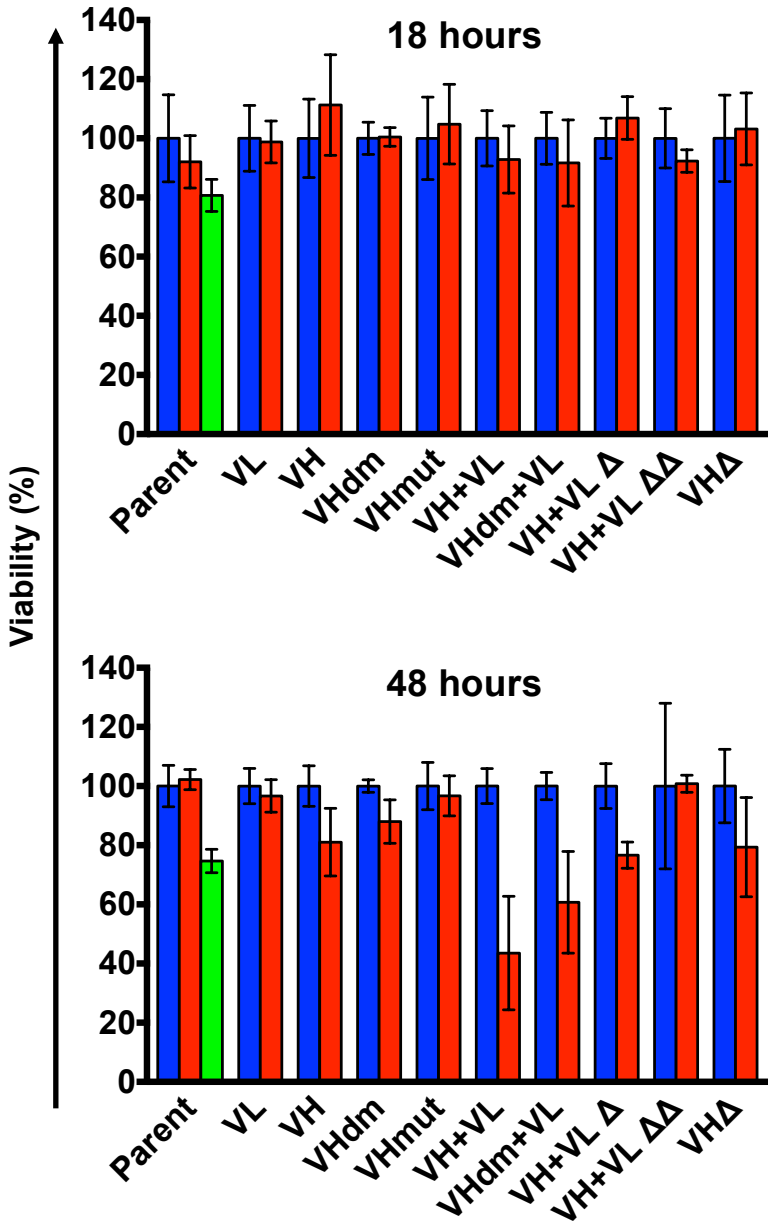

Figure 4.4 ApoToxGlo cell viability assay

Clones were plated in 96-well plates and treated with tetracycline to induce expression (red bars) or without as uninduced controls (blue bars) for 18 and 48 hours. The parental HT1080TetOn line was treated with etoposide for 8 hours as an apoptosis control (green bar), although a longer incubation may provide greater induction of apoptosis in these control samples. Clones were assayed with the Promega ApoToxGlo reagents. Cell viability was measured by the conversion of a fluorescent substrate, which was read by fluorescent plate reader. A: 18 hours, B: 48 hours. All samples were read in triplicate, with background (no cell) well readings subtracted. Fluorescence readings were converted to a percentage viability, with the uninduced samples averaged reading set to 100%, to allow comparison between clone types. Error bars show the standard deviation from the mean.

average of approximately 45%, with VHdm+VL clones having an enhanced survival at 60% that of the uninduced sample. The proCASP3 single catalytic mutant clones (VHΔ-Only and VH+VLΔ) possess viability scores highly similar to VH-Only cells, indicating the RAS inhibition effect. VHmut-Only cells were comparable to VL-Only clones, confirming abrogation of RAS inhibiton conferred by the mutations of the VH CDRs. Unexpectedly, the expression of VH+VLΔΔ had no effect on cell viability. Given the VH+VL moieties allowing reconstitution of the higher affinity Fv, a reduction in cell viability was predicted at least to the same extent as the single mutant version, based on the similar membrane integrity profiles generated by Annexin V and 7-AAD staining (Figure 4.3).

4.4.2 ApoTox Glo cytotoxicity measurements

The cytotoxicity parameter of the combined assay investigates the activity of proteases which are released into the culture medium following disruption of the cell membrane during cell death. Both apoptosis and necrosis produce alterations in membrane integrity, although activation of the executioner Caspases are required to differentiate the two process of cell death. 'Dead cell' proteases, such as tripeptidyl protease 2, retain enzymatic activity in culture medium. Therefore, cleavage of a cell impermeable, fluorogenic substrate quenched by a tripeptide leader sequence can give a proportional measure of cytosolic release due to cell death (Niles et al., 2007). The substrate used in this measure is bis-alanyl-alanyl phenylalanyl Rhodamine 110 (bis-AAF-R110). The cytotoxicity results are shown in Figure 4.5.

In contrast to the viability measurements, only the cytotoxicity measurement taken at 18 hours after induction gave positive fluorescence readings compared with the uninduced controls. The 48 hour readings showed a lower fluorescence level in the cells expressing the AIDA constructs when compared with the uninduced samples. This likely results from inactivation of the protease after an extended period within the culture medium prior to analysis, leading to anomalous results that

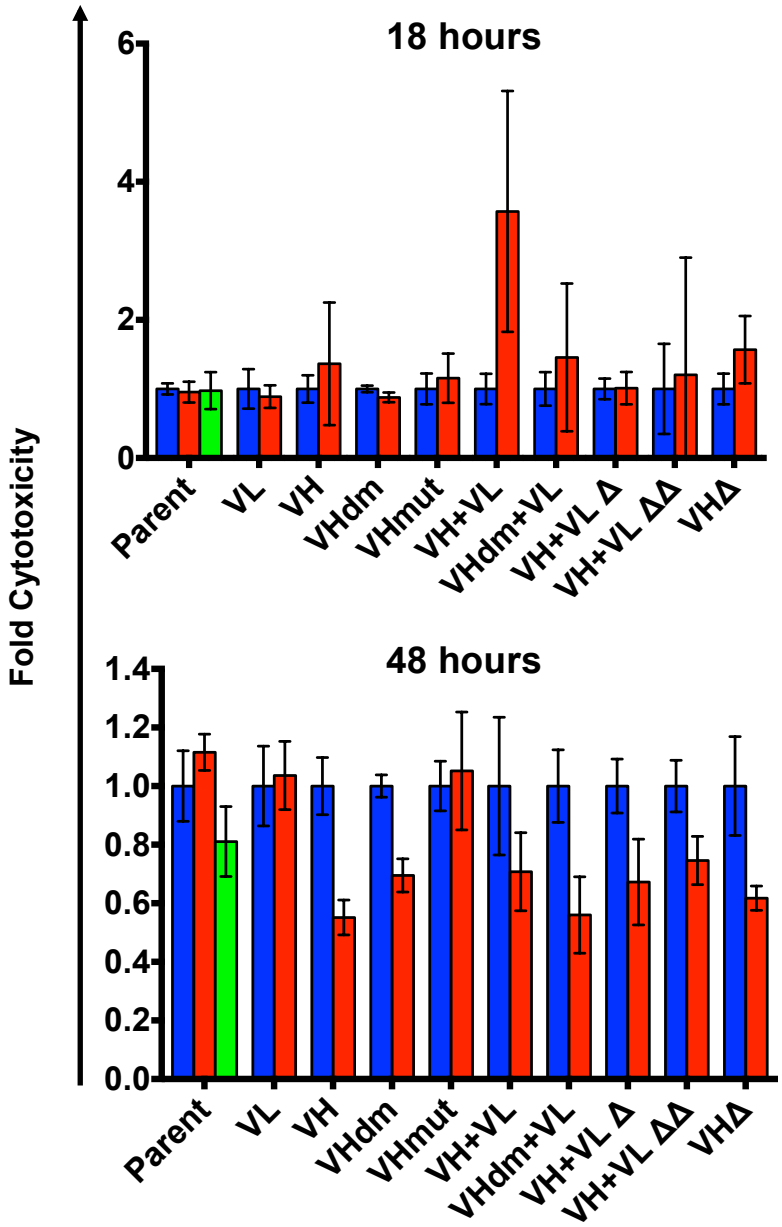

Figure 4.5 ApoToxGlo cytotoxicity assay

Clones were plated in 96-well plates and treated with tetracycline to induce expression (red bars) or without as uninduced controls (blue bars) for 18 and 48 hours. The parental HT1080TetOn line was treated with etoposide for 8 hours as an apoptosis control (green bar). Clones were assayed with the Promega ApoToxGlo reagents. Cell cytotoxicity was measured by the conversion of a fluorescent substrate, which was read by fluorescent plate reader. A: 18 hours, B: 48 hours. All samples were read in triplicate, with background (no cell) well readings subtracted. Fluorescence readings were converted to a fold cytotoxicity, with the uninduced samples averaged reading set to 1, to allow relative comparison between clone types. Although both sets of data were analysed in the same manner, the scales of both graphs differ to show the detail within the data. Error bars show the standard deviation from the mean.

necessitates optimisation of incubation time (Niles et al., 2007). However, the 18 hour time point was early enough to detect the enzyme activity in these experiments. At this measurement, induced VH+VL clones showed an average 3.5 fold increase in fluorescence over uninduced sample. A slight increase in signal, up to 1.5 times higher, was detected in the VH-Only and most of the mutant clones. This data confirms the findings of the other assays, showing cell death is only occurring with expression of original VH+VL fusion proteins, and is abrogated in the various mutant forms.

4.4.3 ApoToxGlo active CASP3 measurements

The CASP3 activation assay measures the luminescent signal generated via CASP3 cleavage of luminogenic substrate, similar in principle to the fluorogenic CASP3 substrate used in the fluorogenic substrate assay in Chapter 3. Instead, luciferin is released and converted to fluorescent form by exogenously supplied luciferase. The CASP3 activation data derived at both the 18 and 48 hour readings are virtually identical (Figure 4.6). At both timepoints, induced VH+VL clones exhibit an approximate 25 fold increase in fluorescence over their uninduced control samples. This is closely followed by VHdm+VL clones that possess a 9 fold increase upon protein expression. Minimal, low level CASP3 activation is detected in the other clones, including VL-Only, although these register at a maximum average of 1-3 times that of the uninduced controls.

4.5 Effect upon the cell cycle and DNA degradation

A hallmark of CASP3 activation is the digestion of genomic DNA at internucleosomal sites. This results from CASP3 cleavage of the inhibitor of caspase-activated DNase (ICAD), allowing the caspase-activated DNase (CAD) activity to degrade chromosomal DNA. Only CASP3 has been implicated in this cleavage (Sakahira et al., 1998), despite CASP3 and CASP7 recognising highly

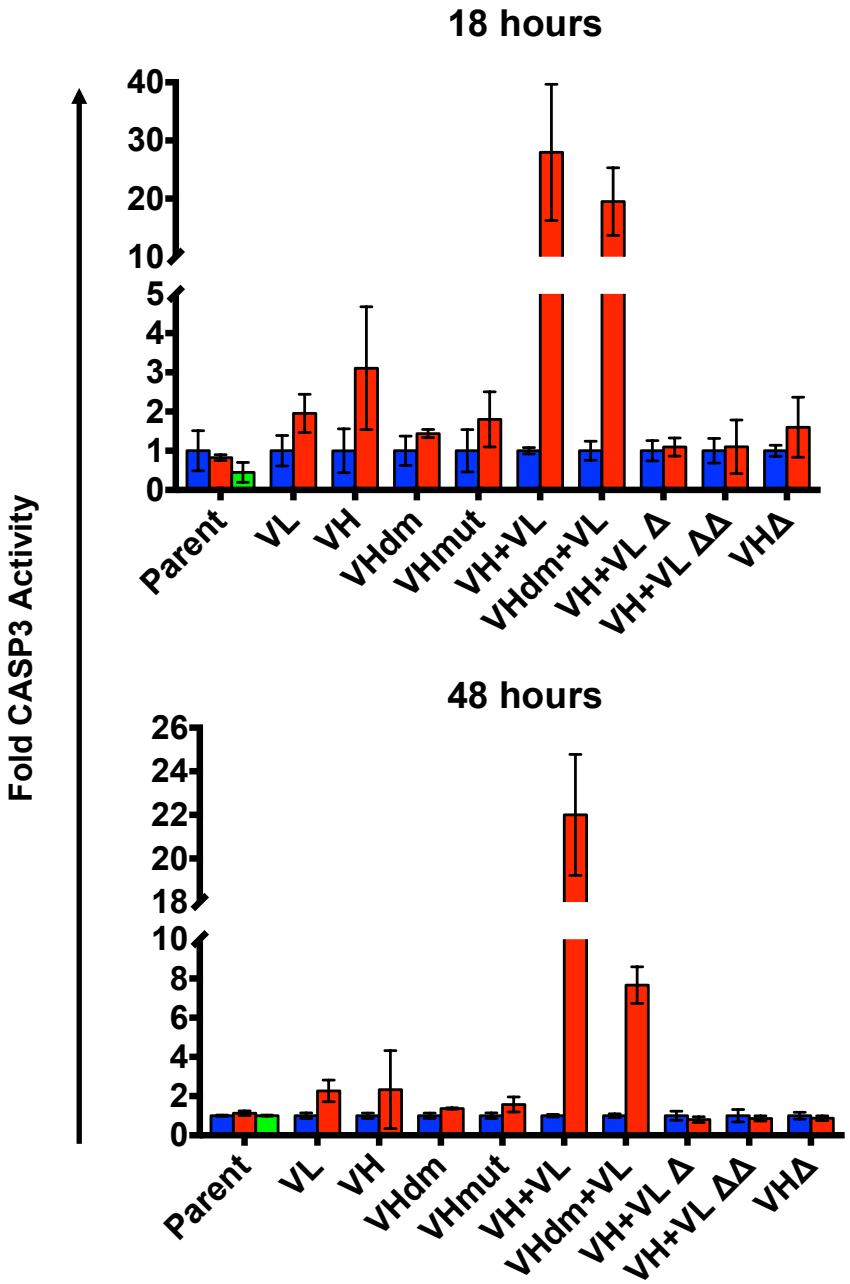

Figure 4.6 ApoToxGlo CASP3 activity assay

Clones were plated in 96-well plates and treated with tetracycline to induce expression (red bars) or without as uninduced controls (blue bars) for 18 and 48 hours. The parental HT1080TetOn line was treated with etoposide for 8 hours as an apoptosis control (green bar) although a longer incubation may provide greater induction of apoptosis in these control samples. Clones were assayed with the Promega ApoToxGlo reagents. CASP3 activity was measured by the cleavage of a luminescent substrate resulting in an increase in luminescence, which was read by a luminescence plate reader. A: 18 hours, B: 48 hours. All samples were read in triplicate, with background (no cell) well readings subtracted. Luminescence readings were converted to a fold activity, with the uninduced samples averaged reading set to 1, to allow relative comparison between clone types. Error bars show the standard deviation from the mean.

homologous and degenerate substrate peptide motifs (Fuentes-Prior and Salvesen, 2004). As such, investigation of CAD activation would specifically identify CASP3 activation and apoptosis. Cell cycle analysis by flow cytometry could provide data to indicate the occurrence of CAD-mediated DNA degradation as a sub-G1 population. This analysis could also show the effect of the VH fragments on RAS inhibition which, given the vital role of RAS in cell division (Drosten et al., 2010) it would be expected that the normal cell cycle populations would be perturbed.

The cell cycle consists of four distinct phases which are tightly controlled by the cell. The G1 phase (and G0 or quiescent cell phase) is characterised by cells containing the usual diploid (or 2N) karyotype. Cell division begins with copying chromosomal DNA, a process known as the synthesis or S phase. Finally, the cells have a full tetraploid (or 4N) genome ready for daughter cell genereation in the G2 phase, which is closely linked to the mitotic or M phase transition of full cell division whereby the cell begins to separate. These phases may be visualised by proportional differences in cell fluorescence following DNA staining with an intercalating dye. Cells with CAD-mediated DNA degradation would possess a sub-G1 phase level of fluorescence owing to loss of the usual 2N chromosome copy number.

Representative flow cytometry plots of cell cycle distributions are shown in Figure 4.7 and a breakdown of the full set of results in given in Appendix J. The Parental, VL-Only and VHmut-Only lines show no perturbation of the cell cycle upon Tet induction, which confirms previous observations of a lack of apoptotic phenotype. Dysregulation of the G1/S/G2M phase transitional peaks was discerned from the fluorescence traces in the VH-Only variant clones, with a peak in or toward S phase. This implies a synchronised halting of cell division across the induced samples relative to their uninduced controls. However, all lines expressing the original VH and VHdm exhibit a sub-G1 population of around 10 to 15% of the total cells analysed (Table 4.3) and small peaks may be seen on the plots (Figure 4.7).

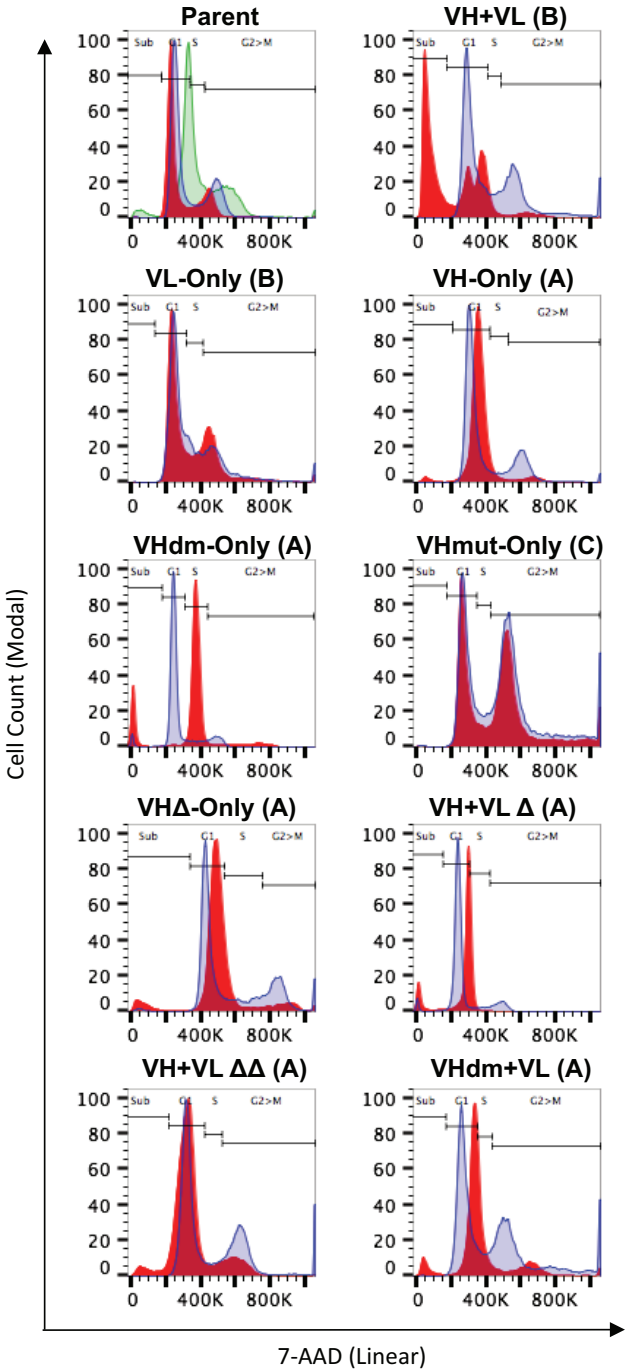

Figure 4.7 Effect of clone expression on the cell cycle

The effect of expressing the VH/VL-proCASP3 proteins and their variants on the cell cycle was assessed by flow cytometry. Cells were expressed for 48 hours (etoposide control applied for 8 hours), then fixed and permeabilised, and stained with 7-AAD. Live, single cells were gated according to their size and granularity by forward and side scatter parameters. The normal cell cycle populations (G0/G1, S and G2/M phases) were set on the uninduced Parental cell line. Data is represented as overlaid univariate intensity plots, with the cell cycle gates shown on each plot. Blue trace represents uninduced cells, whilst the red trace represents tetracycline induced cells. Green trace (in the Parental line histogram only), is the etoposide-induced apoptosis control. All plots are set to modal values to allow ratio comparison between the clone types.

The RAS inhibition effect likely acts as a cellular stress encouraging some apoptosis to occur over the uniduced populations. This is strongly contrasted by the strong peaks noticed in the VH+VL cell cycle plots, where 45% of the cells are in the sub-G1 phase. Additonally, the proportion of those in S phase are doubled, with a 5 fold reduction in the number of cells undergoing the G2/M phase transition. This indicates a high level of active CASP3 is only generated in the original VH+VL expressing cells.

4.6 Luciferase reporter confirmation of RAS-specific binding

The mutant AIDA clone data generated so far suggest that the proCASP3 activation is dependent on both VH and VL fusions binding to mutant RAS. To quantify the level of interaction, a luciferase assay was performed. This would also assess the contribution of the RAS-specific VL, and highlight if non-antigen mediated association was occurring. For this purpose the three VH#Y6 variants were cloned into the triplex luciferase vector (Tanaka and Rabbitts, 2010b), in combination with five different VL fragments. The triplex vector encodes the Renilla luciferase as well as the VP16-tagged prey and the DBD-tagged bait antibodies, from three different promoters. Expressing these cassettes from the same plasmid mitigates possible variation of plasmid uptake in co-transfection experiments. The VL fragments included the RAS-specific VL#204, a non-specific VL#I21 (Tanaka and Rabbitts, 2009) and three VL fragments selected against LMO2 (Tanaka and Rabbitts, 2009), VL#819, VL#826 and VL#827. Firefly luciferase was encoded separately on the plasmid pG5-Luc. A RAS expression vector lacking the membrane localisation domain, pPGK-His-KRAS$_{166}$G12V-Puro, was cloned as described to transiently enhance RAS levels in the HEK293T cell line. (Plasmid maps are shown in Appendix C.)

The luciferase reporter assay shows a 50 fold increase in luciferase activity in the VH+VL equivalent (VH + VL204) relative to the untransfected cells (Figure 4.8). The effect of replacing VH with VHdm results in a 15 fold luciferase activity, roughly a

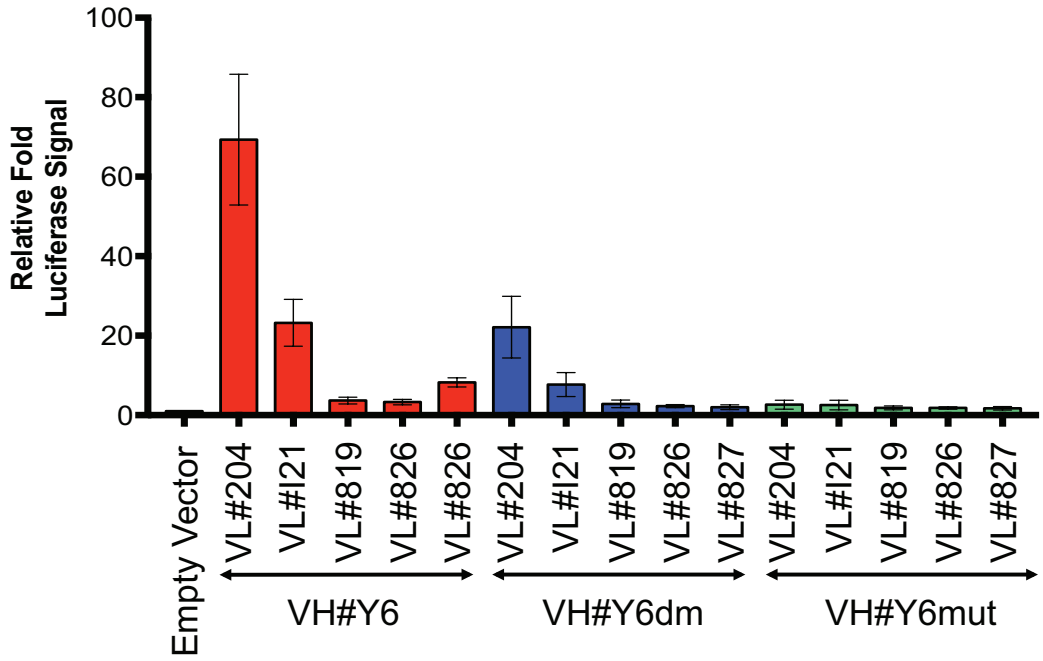

Figure 4.8 Luciferase reporter assay

VH and VL interactions were assessed by a luciferase reporter assay. HEK293T cells were transiently transfected with the triplex luciferase plasmids and the reporter and antigen plasmids, and grown for 48 hours. The luciferase assay was performed with the Dual-Glo Luciferase Assay (Promega). The empty triplex vector control is shown as a black bar. The three VH fragments were assayed in combination with five VL fragments. VH#Y6 transfections are shown as red bars, VH#Y6dm transfections are shown as blue bars, whilst VH#Y6mut transfections are shown as green bars. The corresponding VL fragments are indicated along the x axis. Error bars show the standard deviation from the mean.

two thirds less that of VH. Replacing VL204 with the non-specific VLI21 permits some expression, although this is reduced to approximately one third of the VL204 response. This pattern is conserved across both VH and VHdm combinations. The LMO2-specific VL fragments show very low luciferase levels when partnered with VH#Y6, decreasing further when expressed alongside VHdm and VHmut. (The full data set are given in Appendix K.)

The expression of the triplex vectors was confirmed by Western blot (Figure 4.9). The transient expression shows that VH and VL expression of VHmut vectors was higher than those of the original and dematured VH triplex plasmids. This supports the luciferase data (Figure 4.8) by confirming the low level of luciferase expression in these samples compared with the original VH is not due to lower VH expression. The luciferase reporter assay therefore confirms the difference in RAS binding affinity of the various VH fragments. It also suggests that AIDA operates through cooperative VH and VL binding, rather than VH aggregation. Moreover, the assay demonstrates the necessity of the antigen-specific VL fragment in the AIDA method, as non-antigen binding VLs do not appear to form non-specific framework interactions with the VH fragments.

4.7 Tumour recapitulation assays

The previous experiments have all been performed on cells grown in monolayer. To assess whether AIDA could be elicited in solid masses, tumour recapitulation assays were investigated. The experiments performed in the following sub-sections were derived from the stably transfected clones, as therapeutic vector targeting was not being tested.

4.7.1 Clonogenic assay

The clonogenic, or focus formation assay, was first described as a method to determine the reproductive capacity of irradiated adherent cells (Puck and Marcus, 1956). It has subsequently been employed to assess the effect of therapeutic agents

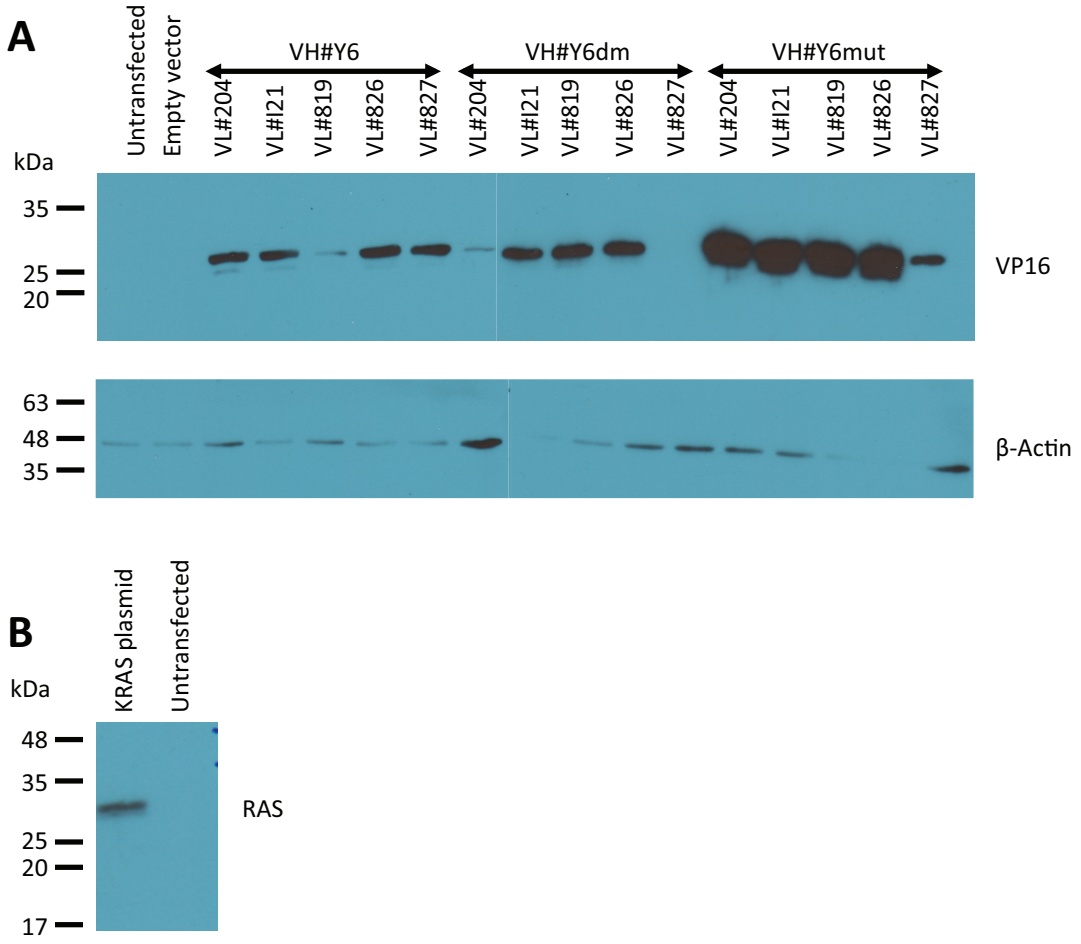

Figure 4.9 Triplex plasmid and RAS antigen expression confirmation

Protein expression from the triplex plasmids used in the luciferase reporter assay (shown in figure 4.8) was confirmed by Western blot. HEK293T cells were transiently transfected with the plasmids, and allowed to express them for 48 hours post transfection. Total protein levels were determined by BCA assay, with 10µg protein loaded per lane. A: The triplex plasmids encoding VH-VP16 and Gal4DBD-VL were assessed with anti-Gal4DBD and anti-VP16 antibodies. The VH-VP16 fusions were detected at approximately the expected size (21kDa). The Gal4DBD fusions could not be detected, although expression is apparent from the luciferase data. β-actin levels were assessed as a loading control. B: KRAS antigen plasmid protein expression was probed with Pan Ras primary antibody. The protein resolved at the expected 26kDa.

on cellular proliferative potential, and to measure the stem characteristics of progenitor populations (Franken et al., 2006). The assay measures the potential of a single cell, plated at low density, to develop into a colony despite lacking cell to cell contacts. This low density plating can affect the formation of colonies even in untreated cells (Franken et al., 2006), and different cell lines can show variation in their readiness to form such colonies (Woolston and Martin, 2011). As such, it is usual to determine the plating efficiency, or colony forming efficiency using untreated cells as a control. Colonies of cells subjected to DNA-damaging therapies are counted and compared with the plating efficiency.

The clonogenic assay was chosen to gauge whether the AIDA constructs and their derivative mutants could destroy or simply reduce the replicative potential of the tumour cells *in vitro*. Further to the evidence of RAS inhibition interfering in cell cycle progression, it was hypothesized that those cells expressing VH or VHdm would suffer reduced proliferative capacity whilst under Tet induction. As colonies are typically defined as masses comprising 50 or more cells, it was feared this cut-off limit may lead to an artificially low reporting. Therefore, the standard protocol was altered to consider masses of 10 or more cells as colonies.

As a result of reducing the colony size, the plating efficiencies of each clone at the three dilutions were upwards of 50% (Figure 4.10A), which is high compared with the usual efficiencies of 20-60% (Franken et al., 2006), although presumably due to lowering the colony cell number threshold. The surviving fraction (Figure 4.10B), or those colonies able to form despite the expression of the AIDA fusion proteins, is relative to the plating efficiency. Expression of VH Only inhibits proliferative potential by 30%, although they have not lost their ability to survive and produce progeny cells. A similar result was gained from the mutant VH+VL clones, where replacing the lower affinity VH or catalytic mutant proCASP3 domains significantly reduced proliferative potential. However, these changes were starkly contrasted by the original VH+VL expression plates, which were almost completely

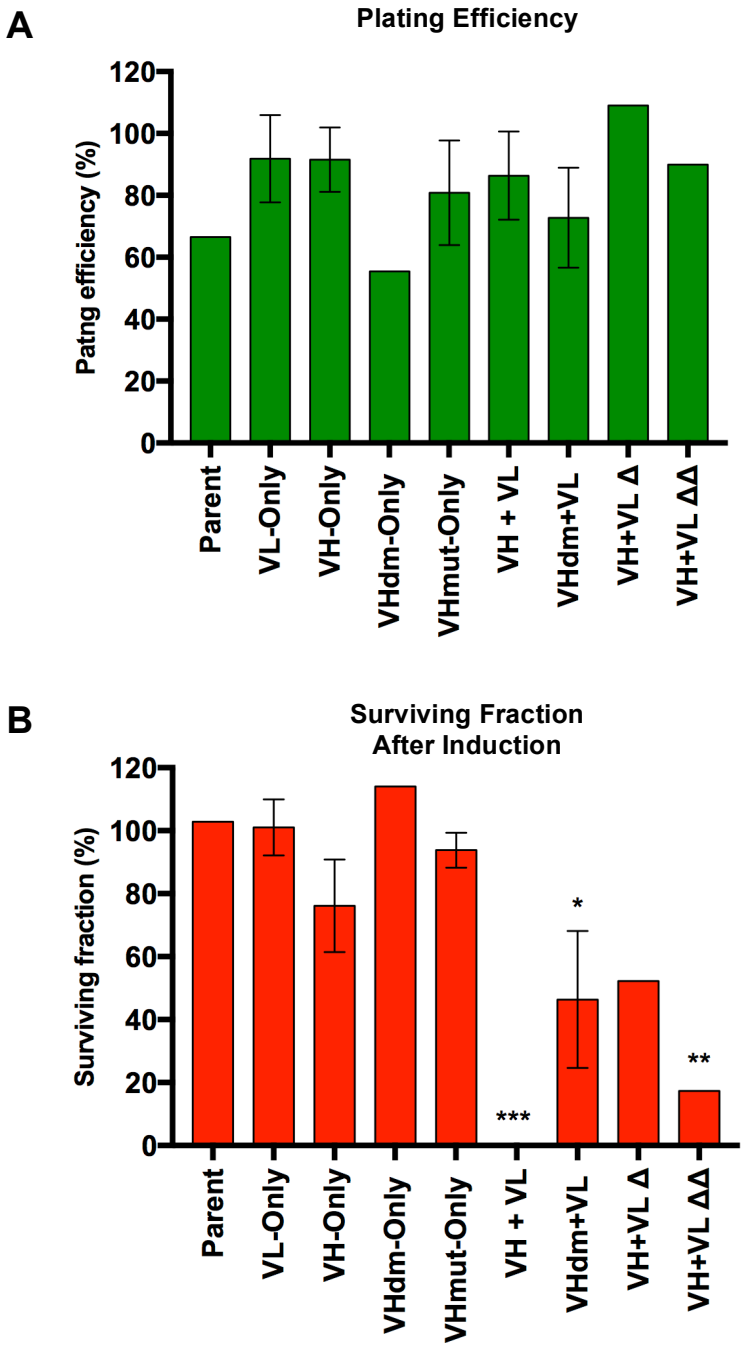

Figure 4.10 Clonogenic assay

A clonogenic assay was performed to investigate the AIDA effect in a tumour recapitulation system. Clones were plated as two sets of triplicate plates, at three different densities (20, 50 and 100 cells per 6cm dish) to allow uninduced vs. tetracycline induced comparisons. Tetracycline induction was performed for 9 days at which point plates were fixed and stained. Colonies were counted, being defined as growth patches containing greater than 10 cells. The uninduced plates acted as plating efficiency controls, whilst the tetracycline induced plates were counted to calculate the surviving fraction of colonies upon induction. A: Averaged plating efficiency of each clone type. B: Averaged surviving fraction of cells forming a colony. Statistical significance ($p \leq 0.05$) was determined with a one-way ANOVA of each clone relative to the parent line. Asterisks indicate the magnitude of the p value, * $p<0.05$, ** $p<0.01$ and *** $p<0.001$. Error bars show the standard deviation of the mean.

devoid of any remaining cells. The results of individual plating densities are shown in Figure 4.11 for each clone type. (The raw data is given in Appendix L.) This assay confirms that the only clone type to be rendered incapable of further cell division are the VH+VL clones, which cannot survive following CASP3 activation. All other VH+VL mutant clones possess replicative potential, albeit reduced, indicating that expression of the variant AIDA constructs does not cause cellular death. Instead, the data generated in this assay confirms the aforementioned results which implicate RAS inhibition as the cause of reduced proliferation and cellular stress.

4.7.2 Tumour spheroid assessment

Epithelial tumour cells can be cultured *in vitro* as rounded masses, or spheroids, to represent small cancer growths in tumourigenic assays. Analysis of anti-tumour agents on tumour spheroids is popular, owing to them being suitable for high throughput screening in multi-well plate format (Ivascu and Kubbies, 2006). The potential of the AIDA clones (mesenchymal origin) to form spheroids was investigated.

Spheroids made from the Parent line and a VH+VL clone were created as an alternative to *in vivo* models. The day after plating, once the cells had knitted into a spheroid, Tet induction was performed on half of the wells, the other half remaining uninduced as a control. Spheroids were cultured for 14 days, with images taken every 2-4 days for growth assessment, with representative images documented in Figure 4.12. Visually, the parental line spheroids grew very well in three dimensional format. After two weeks in culture the parental spheroids began to exhibit necrotic centres owing to their size (~1.5mm). Uninduced VH+VL spheroids did not grow as fast as the parental spheroids. However, Tet induced spheroids did not grow at all, and lost edge definition, appearing hazy instead.

The images allowed two dimensional area changes to be calculated using FIJI software. Graphs showing the spheroid area changes are shown in Figure 4.13A.

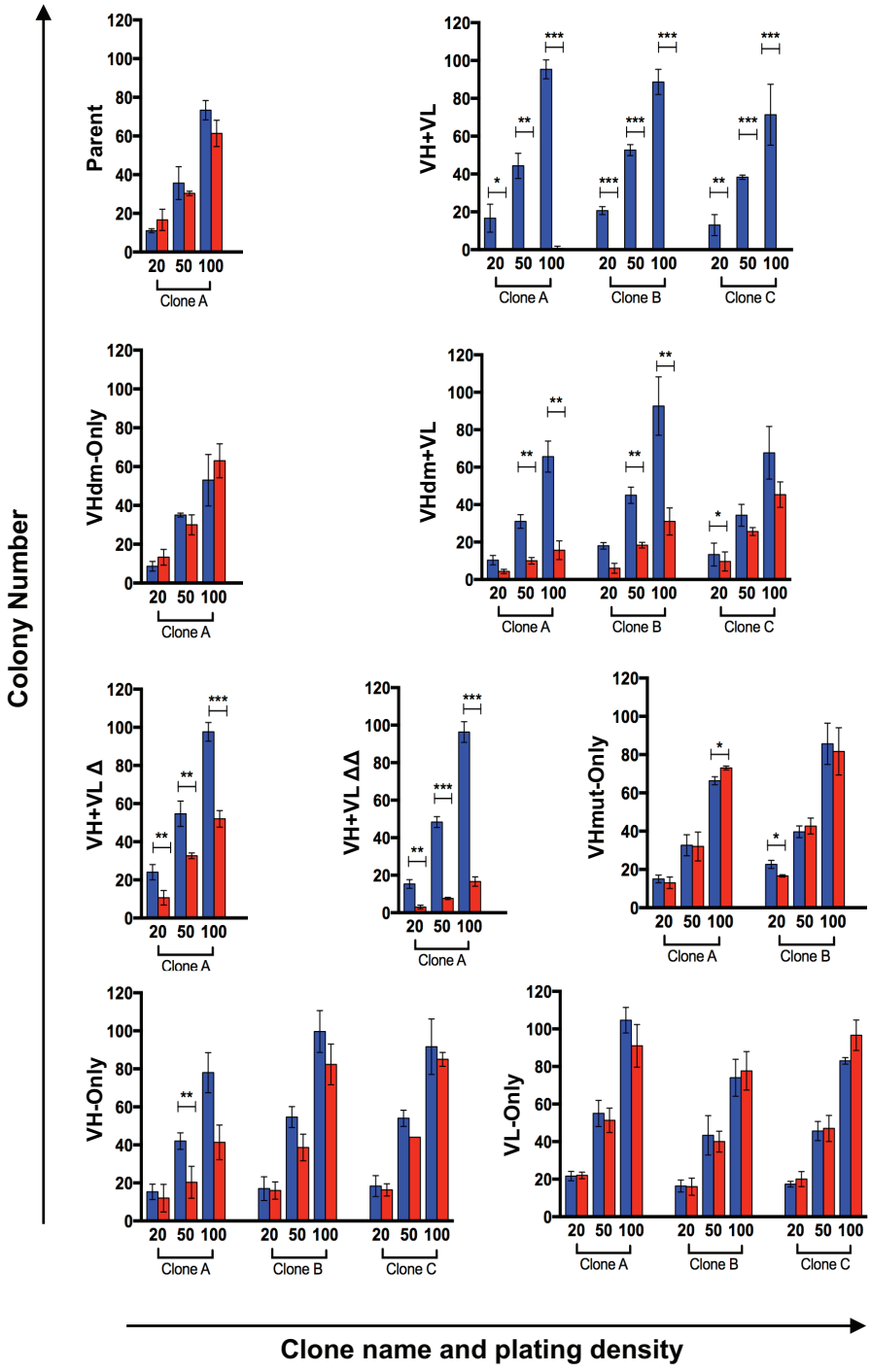

Figure 4.11 Colony number data from the clonogenic assay

The clonogenic assay data could also be represented directly as discrete colony numbers across the platings. Blue bars represent the uninduced control plates, whilst the red bars indicate the tetracycline induced plates. Each clone of the types tested are shown as separate grouped bars within the same chart. Student t tests were performed to define whether colony differences significant ($p \leq 0.05$) where * $p<0.05$, ** $p \leq 0.01$ and *** $p \leq 0.001$. Error bars show standard deviation from the mean.

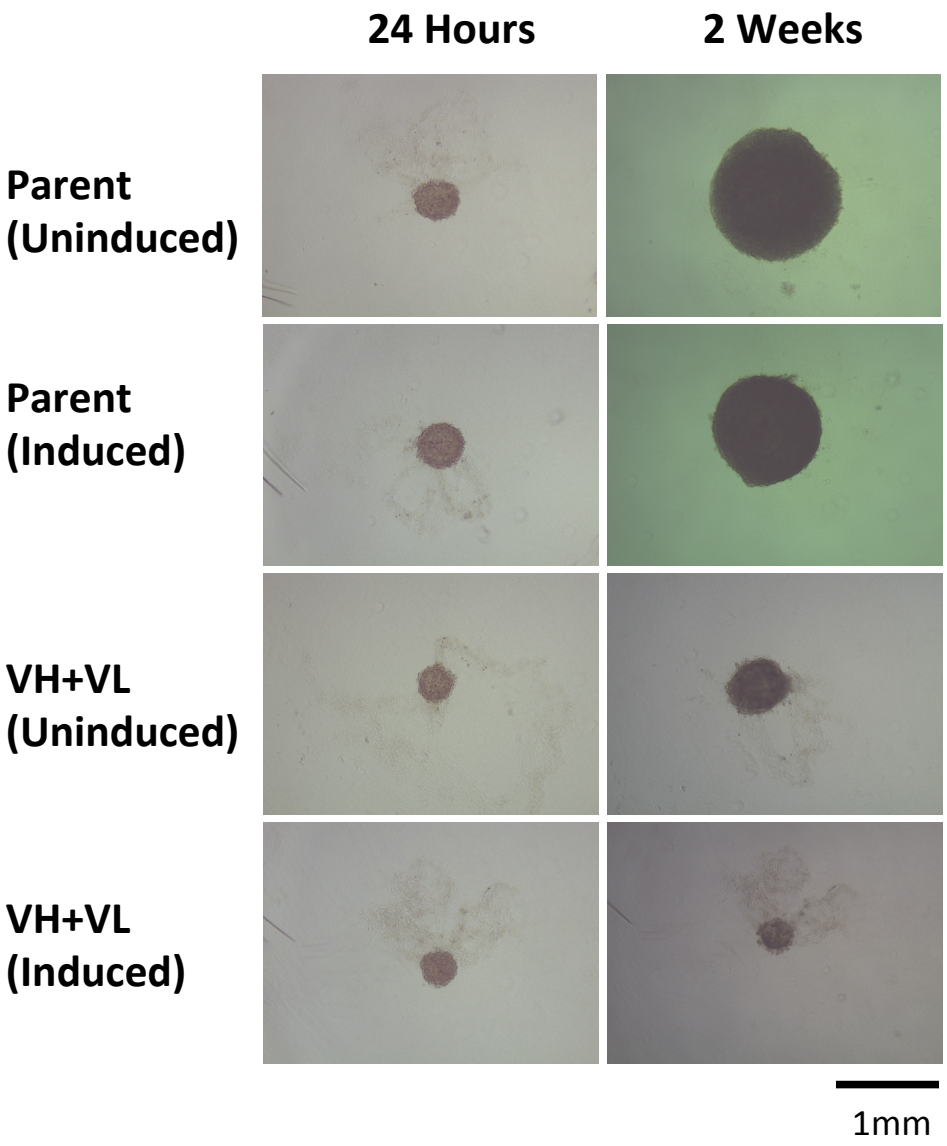

Figure 4.12 Representative tumour spheroid images

Representative spheroid images used to calculate the area changes over time. Spheroids were formed and cultured in matrigel and grown with or without tetracycline (induced vs. uninduced respectively) over two weeks. Bright field images were taken by 10x objective lens. Ablation of growth was apparent in the VH+VL (clone B) cell spheroids when expression of the AIDA fragments was induced. No effect of tetracycline on parent spheroid growth was observed.

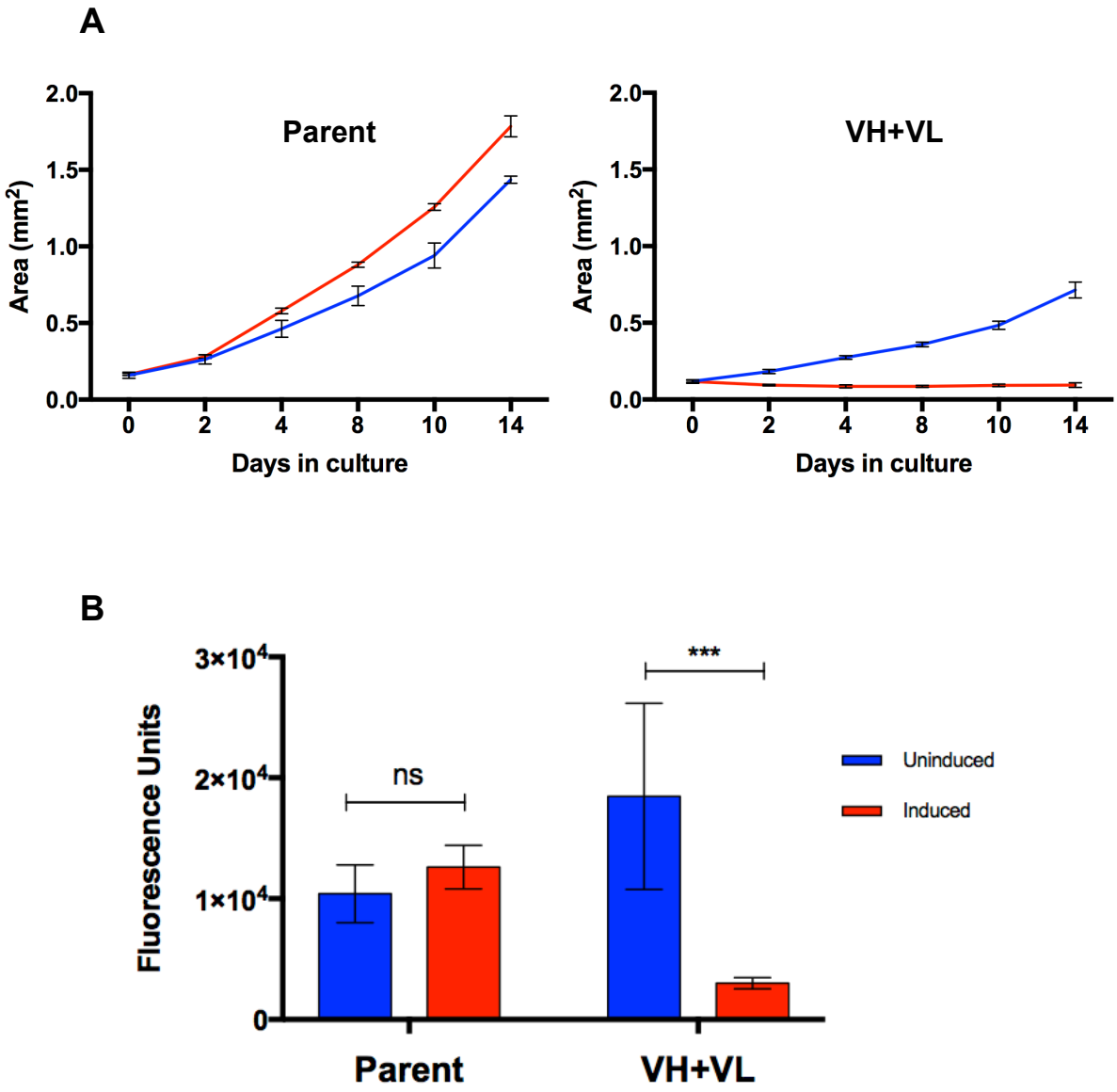

Figure 4.13 Tumour spheroids for *in vitro* tumour capitulation

Spheroids were formed in 96-well plates. Half were treated with tetracycline to induce AIDA protein expression. Spheroids were grown for two weeks. Images were taken every two to four days for calculation of area changes. A: Spheroid area changes over time. Data was compiled from four spheroids in both conditions. Blue curve represents the uninduced spheroid growth, and the red line denotes the induced. Error bars show the standard deviation from the mean. B: Spheroid viability measured by PrestoBlue reagent at the end of the growth assessment (day 14). Fluorescence readings from 12 spheroids of each condition were background subtracted from empty wells, and then averaged. Statistical significance was confirmed with an unpaired student t test, p values were determined as non significant (ns) p=0.11 for the parent line, and significant (***) for the VH+VL clone B was p=<0.001. Error bars show the standard deviation from the mean.

The parental line spheroid growth appears to plateau when the necrotic centres appear, and this was taken to be the experimental end point. The tetracycline-induced VH+VL spheroids were still present, albeit not having grown over the 14 day period. To assess whether they were alive or dead, with cellular debris retained by the matrigel layer, all spheroids had their viability assessed by PrestoBlue reagent. The induced VH+VL spheroids produced fluorescence levels only mariginally above background (Figure 4.13B), showing a lack of viability. These results show that the AIDA effect can be successfully triggered in a solid mass.

4.7.3 Preliminary *in vivo* study

A preliminary study was performed in Nude mice. Subcutaneous injection of a VH+VL cell line into was kindly performed by Dr Osama Al-Assar, former member of the Rabbitts Laboratory, WIMM, University of Oxford. Mice were monitored for tumour growth, with measurements taken every 1-2 days. Tumours only resulted in two of the mice. Once the tumours had reached 5mm in diameter, approximately 18 days after injection, one mouse was fed with Tetracycline added to their diet and drinking water, with the other as an untreated, uninduced expression control. The volume of the tumours was calculated by x and y plane diameters, and monitored over the following two weeks. The tumour growth curves are documented in Figure 4.14. The uninduced control tumour (no Tet diet) continued to grow uninhibited, until euthanasia was performed at day 11 post Tet induction as the study end-point. The tumour reached a total mass of almost $300mm^3$. The volume of the tumour developing in the mouse receiving the Tet diet remained a fairly constant size until the experiment was terminated. Post-mortem analysis of the tetracycline-induced mouse showed some inflammation surrounding the tumour. This likely contributed to the variations in tumour measurement.

For this study to have significance, a much larger cohort would be required. The apparent stochastic nature of tumour development in the mice was troublesome,

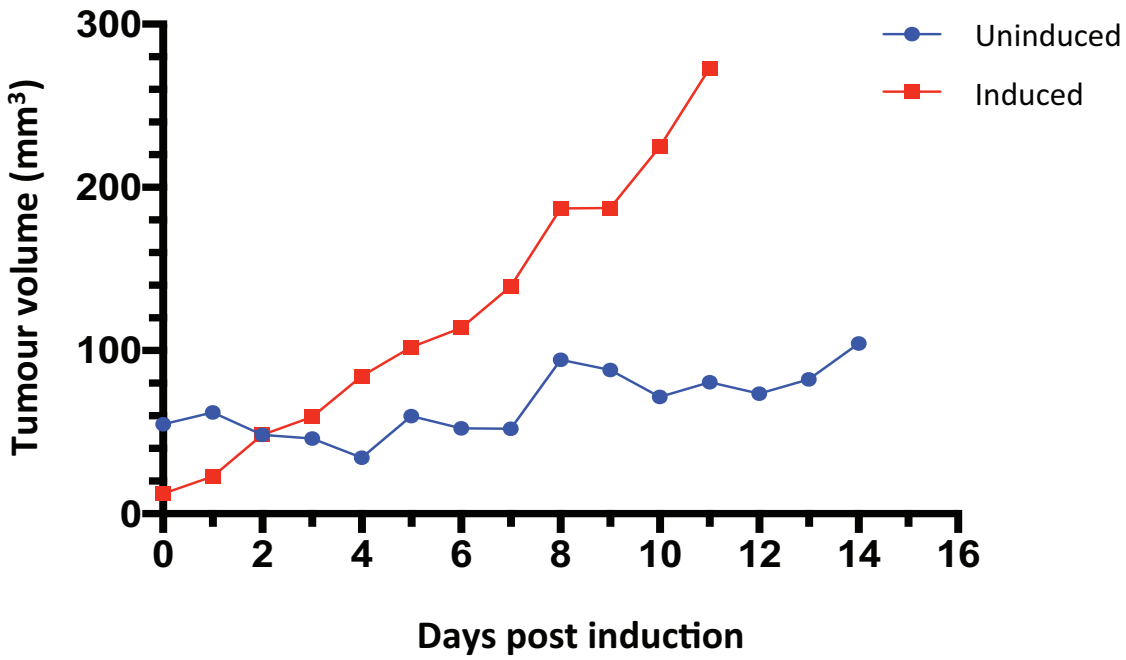

Figure 4.14 **Preliminary *in vivo* tumour growth assay**

Growth curves of subcutaneous tumour grafts of an original VH+VL clone (clone B) in two mice. Cells were allowed to graft and form tumours for 18 days, until the tumours had reached palpable size (1mm diameter). One mouse received a normal diet, whilst the other had tetracycline added to feed and drinking water. Tumour measurements were taken daily with digital calipers. Tumour growth of the animal not receiving tetracycline induction of the AIDA fragments continued until it reached 300mm^3, whereby the animal was euthanased.

and would be amplified if testing of all the mutant lines were to be investigated. Additionally this would be against the principles of the '3Rs' (reduction, refinement,replacement) in conducting animal studies.

4.8 Discussion

This chapter details the successful, further characterisation of the AIDA method with variants of the original constructs. Additional confirmation of the AIDA system mechanism was deemed necessary following the initial results, previously discussed in chapter 3. This stems from the phenotype observed when VH Only was expressed. From previous work (Tanaka and Rabbitts, 2010a) it was expected that some cytostatic effect may be encountered due to inhibition of RAS signaling. However, disproving the possibility of low level proCASP3 element activation was not possible with the three original AIDA constructs. Verification was also sought that activation of fused proCASP3 domain was the initiating factor in the observed apoptotic phenotype of the VH+VL clones.

This was achieved by exchanging VH#Y6 for a lower (VHdm) and no affinity (VHmut) versions of the same VH framework (Tanaka et al., 2007), and by introducing catalytic mutations to the proCASP3 domains (Wilson et al., 1994, Tse and Rabbitts, 2000) to inhibit their enzymatic performance upon activation. Generation of stable mutant cell lines with robust expression of the AIDA fusion proteins was achieved. The experiments described in this chapter recapitulate the data observed with the original clones, therefore comparison of the mutant clones data was feasible, and that AIDA can destroy tumours *in vitro*.

The higher affinity of the VH+VL interaction with RAS compared with VH alone was confirmed by the increased time taken for expressing cells to recover once tetracycline was removed. This tighter binding explains a greater RAS inhibition effect upon variant VH+VL clone expression, particularly those containing the proCASP3 catalytic mutations.

The CASP3 catalytic mutant clones (VH+VLΔ and VH+VLΔΔ) exhibited lowered replicative potential and inhibited cell cycle progression. However, they possessed some indication of increased incidence of apoptosis occurring, although they lacked significant CASP3 activity. The absence of high-level CASP3 activity but appearance of apoptotic populations within the catalytic mutant clones suggests that the cellular stress of RAS inhibition does promote a tendency for cellular turnover, but that the overt apoptototic phenotype observed in the original VH+VL clones initiates from the proximity-activated proCASP3 domains of the AIDA constructs. Reducing the affinity of the VH for mutant RAS imparts a partial reduction in the severity of apoptotic phenotype in the VHdm+VL clones, supporting the antigen-specificity of the AIDA system.

If aggregation of VH, either through framework interaction (Baral et al., 2012) or RAS signaling clusters (Prior et al., 2003, Plowman et al., 2005), is occurring, it doesn't activate the proCASP3 domains. The mutant (non RAS binding VH) produces no effect on the expressing across all experiments, despite high expression levels. This finding is conserved across the other VH Only mutant clones (VHmut, VHdm and VHΔ Only), and the data support the hypothesis that AIDA is antigen-binding dependent, and does not result through non-specific inter-antibody fragment contacts. Similarly, the antigen-specificity of the VL has been documented with the luciferase assay, and suggests that apoptosis occurring in the VH+VL clones was not a result of antigen-independent framework interaction. Evidence from the luciferase reporter assay showed that non-RAS specific VL fragments could not induce luciferase expression to as high a level as the RAS-specific VL#204. VL#I21 was capable of lowered, but acceptable transcriptional activity, and may therefore be suitable for AIDA if antigen-specific VL fragments could not be isolated and if apoptosis driven from the VH alone was desired.

4.9 Conclusion

This results described in this chapter successfully confirm the mechanism of the AIDA system when modeled on mutant RAS. Differences between the strong RAS inhibition effect and AIDA-mediated cell death have been investigated. The data show that the apoptotic phenotype imparted by the orginal VH+VL constructs is RAS antigen-dependent, and driven through specific, close proximity binding of both VH and VL fragments. Moreover, CASP3 activation initiates with the proCASP3 domains of the AIDA constructs, and is capable of destroying tumours *in vitro*. The AIDA system has now been demonstrated to be suitable for oncogene-targeted cancer cell death, and could be employed against other known human oncogenes. This is explored in the following chapters.

Chapter 5 Development of an *in vitro* VL screening method

5.1 Introduction

The AIDA human targeted cancer cell killing method has been validated against mutant RAS. It is envisaged that this system will be applicable to other oncogenes or fusion products implicated in human cancers. LMO2 is a T cell specific oncogene, not normally expressed in normal, healthy thymocytes (Herblot et al., 2000, Foroni et al., 1992, Kenny et al., 1998) yet expressed in up to 50% of T-ALL (Girardi et al., 2017, Ferrando and Look, 2003). As such, targeted therapies against LMO2 are clinically relevant, although none are currently available. LMO2 has no necessary role in T cells, which should preclude the occurrence of a similar growth inhibition phenotype as seen when modelled against mutant RAS, as discussed in the previous chapters. LMO2 therefore represents an ideal target molecule for the AIDA method.

Isolation of both heavy and light chain fragments can be performed by various methods, employing different techniques of reporting protein:protein interactions. Typically, two-hybrid screens, either in yeast (Tanaka et al., 2003a) or through bacteriophage display (de Wildt et al., 2000) are performed. For isolation of a co-binding VL fragment, a variation on a three-hybrid screen is required. The CatcherAb method (Tanaka and Rabbitts, 2009), a variant of yeast intracellular antibody capture (IAC) (Tanaka et al., 2003a), is one such approach and resulted in the isolation of seventeen LMO2-specific VL fragments. Of these, three VL fragments (VL#819, VL#826 and VL#827) were demonstrated to have increased luciferase reporter activity that was dependent upon co-expression with the anti-LMO2 VH, VH#576 (Tanaka and Rabbitts, 2009). It is unknown whether these pre-existing VL antibodies may be suitable for AIDA with VH#576. If they do bind closely situated epitopes to that of VH#576, it is likely some maturation experiments would be required to improve binding affinity as these antibodies were only CDR3 randomised, and mutagenesis of the other CDRs would likely improve binding affinity. In light of

these factors, a new VL screen would be performed in parallel to improve the likelihood of isolating a complementary light chain. A schematic overview is shown in Figure 5.1. The laboratory has already isolated a high-affinity VH domain fragment against LMO2 (Tanaka et al., 2011), which has been demonstrated to distort the protein structure, preventing nucleation of the LMO2-dependent transcription factor complex (Sewell et al., 2014). Although LMO2-specific light chains have been isolated (Tanaka and Rabbitts, 2009), their epitopes, and their subsequent suitability for the AIDA system, have not been fully investigated.

To increase the speed and efficiency of the protocol, a mammalian screen would be developed by adapting the CatcherAb yeast screening method (Tanaka and Rabbitts, 2009). This would also ensure correct folding and glycosylation of the antibodies for future applications, as those expressed in yeast may not accurately reflect mammalian *in vivo* protein:protein interactions (Luo et al., 1997). This screening method would employ a split fluorescent reporter protein, fused to the VH and VL fragments, generating biomolecular fluorescence complementation upon co-localisation (Hu and Kerppola, 2003). The tripartite split GFP reporter or sensor (Cabantous et al., 2013) with smaller sized GFP tags would be ideal for investigating the tri-molecular interaction of antigen, VH and VL (Figure 5.2). Reconstitution of a functional protein would also demonstrate the close proximity necessary for auto-activation of the proCASP3 domains in the AIDA system. Fluorescently labelled cells could be single cell sorted by flow cytometry, and the VL-containing plasmid amplified by PCR. Sequenced inserts could be sub-cloned back into the screening vector for CDR mutagenesis as described in the CatcherAb and IAC methods (Tanaka and Rabbitts, 2010b, Tanaka and Rabbitts, 2009), to yield a fully-matured, optimised light chain fragment.

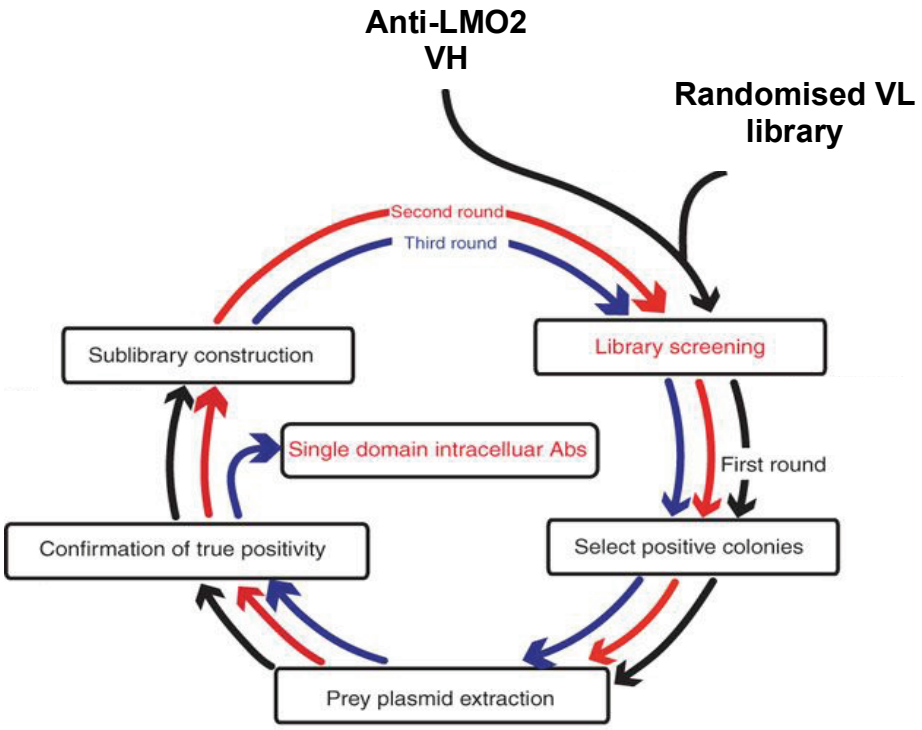

Figure 5.1 Single domain antibody library selection process

Flow chart diagram of process involved in intracellular antibody capture (IAC) technology (Tanaka and Rabbitts, 2010b) that would be combined with the screening principles outlined in the CatcherAb method (Tanaka and Rabbitts, 2009). Here up to three rounds of screening would be perfomed, with VL CDR3 randomisation screening in the first round of selection (black arrows), CDR2 selection in the second round (red arrows) and finally selection of CDR1 randomised VL antibodies in the third round (blue arrows). The anti-LMO2 VH antibody (VH#576, (Tanaka et al., 2011)) would be incorporated to aid binding of the low-affinity VL to LMO2 antigen. Reporter assessment would be through tripartite GFP reconstitution (Cabantous et al., 2013) in mammalian cells. Figure adapted and reproduced from (Tanaka and Rabbitts, 2010b) with permission from Springer Nature publishers.

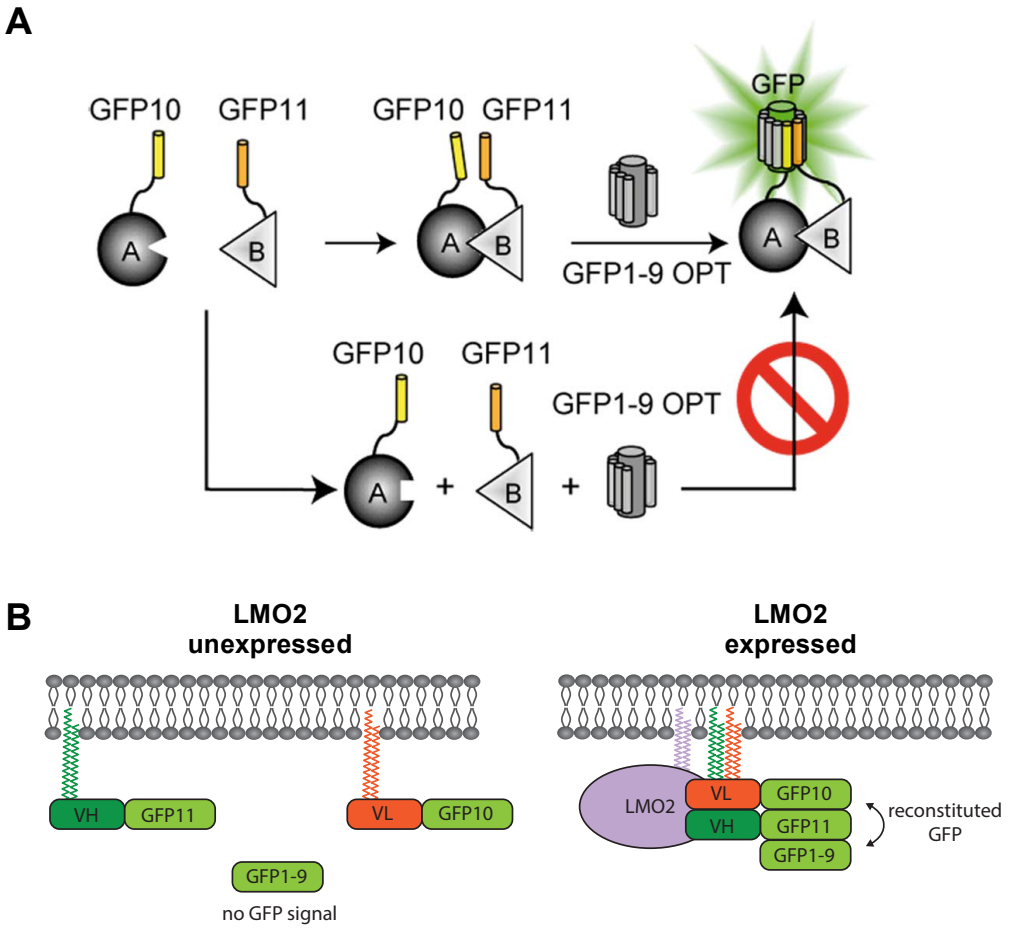

Figure 5.2 Tripartite GFP reconstitution diagram

Diagrams to show the general theory behind the tripartite reconstitution. Biomolecular fluorescence complementation (BiFC) can be generated from split fluorescent proteins refolding when tagged to two interacting bait/prey proteins. A: Cabantous *et al* (Cabantous et al., 2013) split GFP into three parts; β strand 10 (GFP10), β strand 11 (GFP11) and the rest of the molecule comprising β strands 1-9 and the helical regions (GFP1-9). The small GFP10 and GFP11 sequences were tagged to two interacting proteins, which acts to tether the proteins in proximity, allowing association with GFP1-9 to reconstitute the fluorescent signal. Without the protein interactions, GFP10 and GFP11 are unable to localise efficiently for GFP1-9 association. B: Hypothesised functioning of the tripartite GFP system for use in the anti-LMO2 VL mammalian screening method. Anti-LMO2 VH#576 and VL library members are linked to GFP11 and GFP10 respectively. GFP reconstitution should only occur if VH#576 and a VL domain interact with LMO2 at close epitopes. In the absence of LMO2, no fluorescence complementation should occur. Membrane localisation was incorporated into the VH-GFP11, VL-GFP10 and LMO2 proteins by addition of the N-termnial farnesylation sequence, as it was thought this may enhance their interaction. Note, GFP1-9 was not membrane localised to prevent a concentration gradient causing non-specific association. Figure A is reproduced from (Cabantous et al., 2013) under the creative commons licence CC BY-NC-ND 3.0.

5.1.1 Aim

The aim of this chapter was to develop the AIDA system for targeting LMO2 in LMO2-positive T-ALL. LMO2 represents a particularly advantageous antigen for this method as it is aberrantly expressed in up to 50% of T-ALL cases yet absent from most normal thymocytes. This would be achieved by screening for VL domain antibodies that bind LMO2 at close epitopic regions as the LMO2-specific VH#576. This necessitated the development of a novel mammalian VL screening method using tripartite GFP reconstitution as a reporter for the ternary complex formed by VH, VL and antigen. This screening system, and its first randomised CDR3 libraries, are now ready for screening against LMO2, and the approach would be suitable for other oncogenic targets.

5.2 Initial assessment of screening by the tripartite GFP method

For this second targeting test of AIDA, an LMO2-specific light chain fragment would be needed. The previously isolated CatcherAb anti-LMO2 VL fragments (Tanaka and Rabbitts, 2009) could be assessed for their suitability in parallel with a new VL screen. Tripartite GFP reconstitution (Cabantous et al., 2013) as a method to confirm protein:protein interaction was already being used in the laboratory. As such, three mammalian tripartite GFP expression plasmids containing i) GFP1-9 fragment, ii) N-terminal farnesylated (NF) non-specific VL#I21 linked to the GFP10 fragment and iii) NF- VH#576 linked to GFP11 fragment were obtained from Dr Ami Miller (Rabbitts Laboratory, WIMM, University of Oxford) (plasmid maps are shown in Appendix G). These plasmids had been constructed for use as controls in experiments involving different antigens. Therefore, it was necessary to provide initial confirmation that the GFP reconstitution would function with minimal background fluorescence. Following this, the plasmids would be adapted for screening purposes by excising VL#I21 and introducing a random VL library. For confirmation of the tripartite GFP reconstitution, a cell line expressing NF-LMO2 was required. A suitable

expression vector was constructed which incorporated NF-LMO2 antigen and the GFP1-9 fragment separated by an Internal Ribosome Entry Site (IRES) for dual expression of both cistrons (Appendix G). A Puromycin resistance cassette was included for antibiotic selection.

CHO cells were transiently transfected with the NF-LMO2-IRES-GFP1-9 expression plasmid, alone and with the NF-VL#I21-GFP10 and NF-VH#576-GFP11 plasmids. VL#I21 was chosen to provide an indication of background GFP reconstitution when VH#576 was paired with a non-revelant VL domain. Western blot analysis of the whole cell lysate showed robust LMO2 expression in both NF-LMO2-IRES-GFP1-9 transfections (Figure 5.3A). Two products were observed, resolving at a close molecular mass, which likely results from the readily reversible addition of the farnesyl groups to the N-terminal membrane localisation tag. An absence of LMO2 was confirmed in cells transfected with the original GFP1-9 vector alongside the NF-VL#I21-GFP10 and NF-VH#576-GFP11 plasmids.

The same transient transfections were assessed for GFP signal. No fluorescence was noted by microscope analysis or by flow cytometry upon triple transfection of NF-LMO2-IRES-GFP1-9, NF-VL#I21-GFP10 and NF-VH#576-GFP11 plasmids (Figure 5.3B). A modest background fluorescence was detected in 3% of cells following the no antigen control triple transfection (GFP1-9, NF-VL#I21-GFP10 and NF-VH#576-GFP11 plasmids). As NF-LMO2 expression had been confirmed in these cells, and a small fluorescent background was noted with the GFP1-9 plasmid, early indications were that the GFP1-9 fragment from the NF-LMO2-IRES-GFP1-9 construct was either not expressed or expressed at levels too low to detect reconstituted GFP. This could be remedied with supplementation of the original GFP1-9 vector at transfection.

Stable transfections of CHO with the NF-LMO2-IRES-GFP1-9 plasmid were screened by Western blot (Figure 5.4A). The best LMO2 expressing clone, clone 19, was expanded, and transiently transfected with the tripartite GFP plasmids

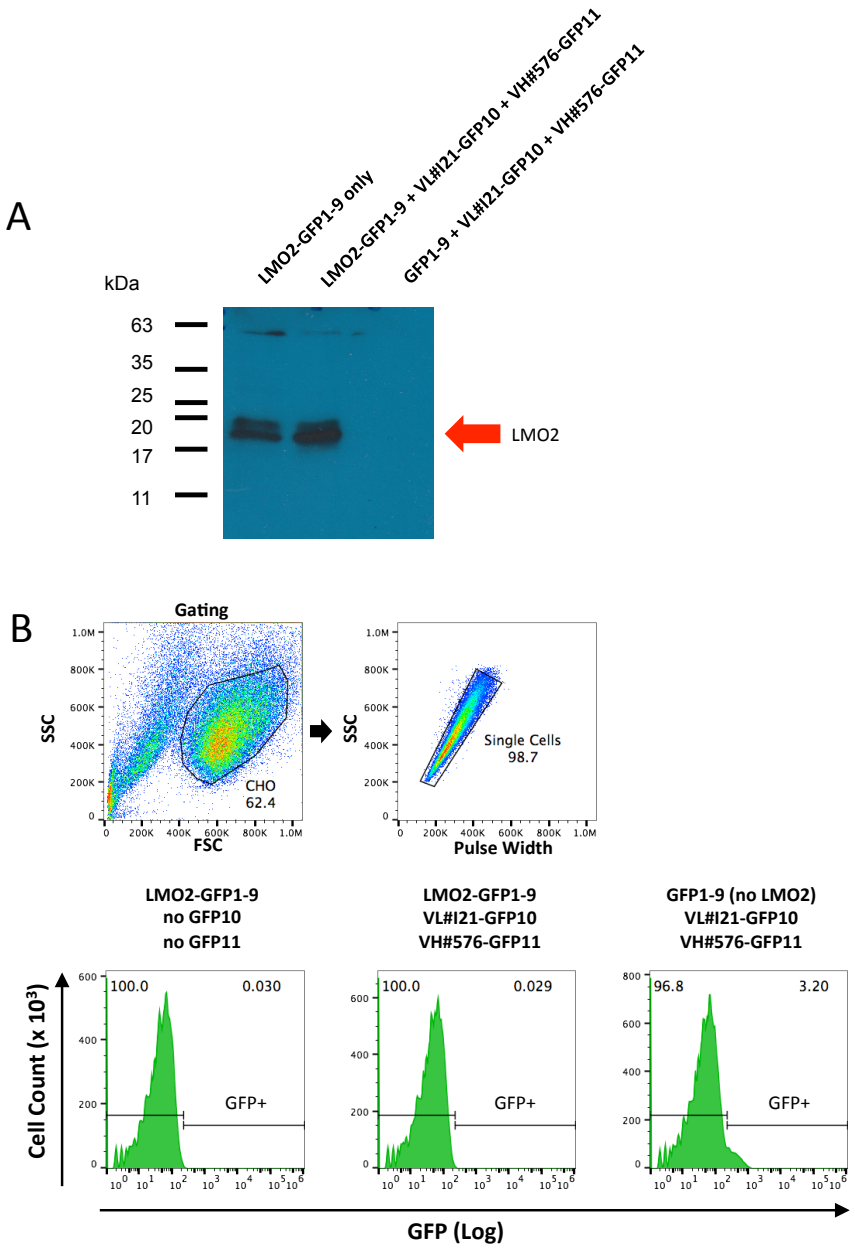

Figure 5.3 Initial test of the tripartite plasmids

CHO cells were transiently co-transfected with the tripartite GFP plasmids pEF-NFarn-VH#576-GFP11, pEF-NFarn-VL#I21-GFP10 and either pEF-NFarn-LMO2-IRES-GFP1-9 or pEF-GFP1-9. Cells were harvested 48 hour post-transfection for analysis. A: Western blot analysis of LMO2 expression of the three transient transfections. The band corresponding to LMO2 resolves at approximately 20kDa. Two bands are visible which represents the membrane localisation signal being reversibly farnesylated. B: Flow cytometry analysis for GFP reconstitution, read on the FL1 (FITC) channel. The gating strategy according to cell size and granularity (FSC vs SSC) and single cell selection (pulse width vs. SSC) is shown. Histograms showing the GFP fluorescence level show no appreciable GFP reconstitution upon transfection. Only low-level background fluorescence occurs when the GFP10 and GFP11 plasmids are expressed alongside GFP1-9 (without LMO2). However, this background fluorescence is not detectable in the transfectants with the LMO2-IRES-GFP1-9 plasmid, which may indicate low or absent GFP1-9 expression levels from this plasmid.

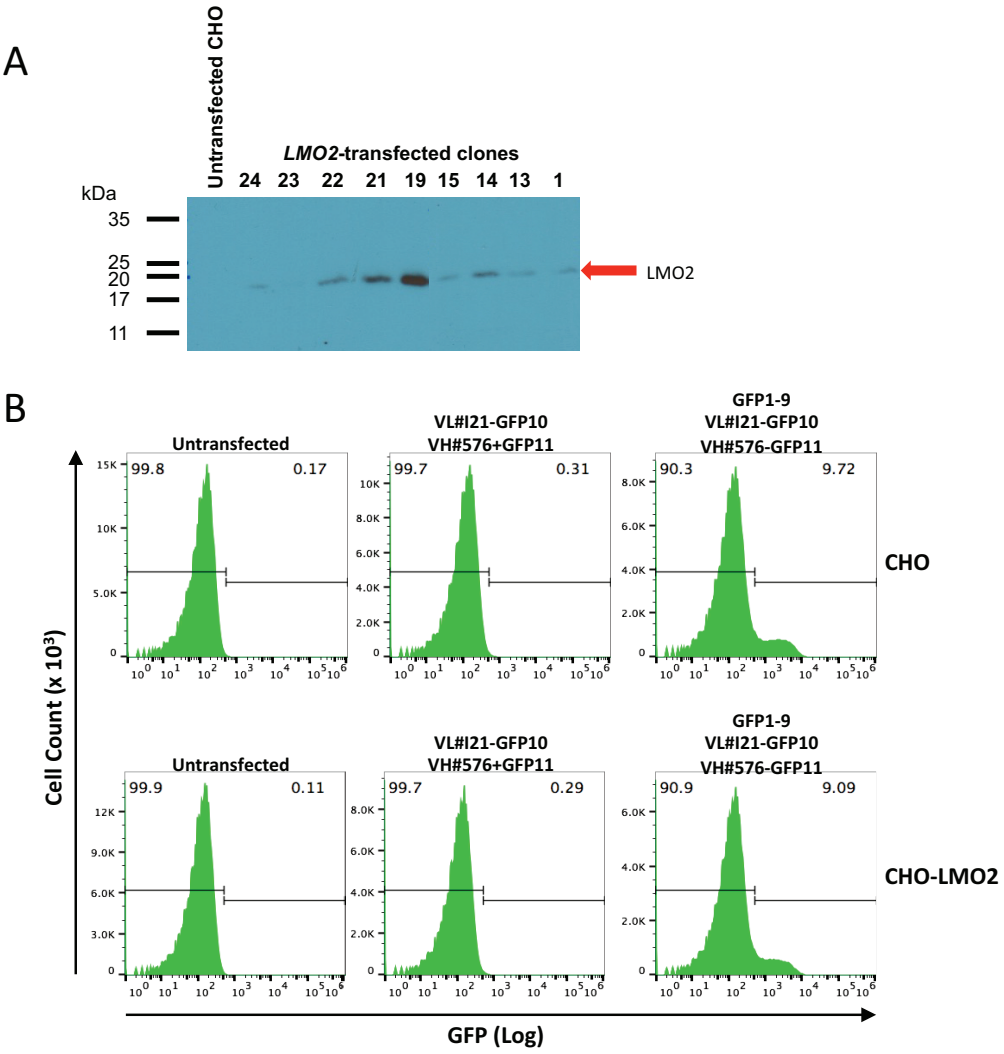

Figure 5.4 Tripartite test with stable LMO2 expression

Characterisation of GFP reconstitution when LMO2 is stably transfected and additional GFP1-9 is transiently transfected. A: Western blot confirming LMO2 expression from the NF-LMO2-IRES-GFP1-9 stably transfected clones, resolving at the expected 20kDa size. Clone 19 displays robust LMO2 expression and was carried forward for transient tripartite GFP plasmid transfection. B: Flow cytometry detection of reconstituted tripartite GFP fluorescence 48 hours after transient triple co-transfection in both parent CHO cells and in the CHO-LMO2 stable cell line (clone 19). No GFP fluorescence was detectable without supplementation of the original GFP1-9 vector. There is no difference in the level of cells containing tripartite GFP reconstitution when LMO2 antigen is expressed, showing that this level of low intensity fluorescence is background, non-specific reconstitution.

to test both GFP1-9 expression from the stable transfection and antigen dependency of any resulting GFP signal. Again, fluorescence was only evident in cells where GFP1-9 was supplied by the original GFP1-9 vector (Figure 5.4B). However, this signal was not antigen dependent as a similar sized fluorescent population (approximately 9% gated cells) was apparent in parental CHO cells lacking the NF-LMO2-IRES-GFP1-9 insertion.

5.3 Modification of the tripartite GFP vectors

The antigen-independent GFP reconstitution observed in the preliminary testing of the tripartite GFP system could be background due to chance interaction between the GFP fragments. However, the membrane localisation may have inadvertently exacerbated normal background fluorescence levels by artificially imparting a localised concentration effect, and so a second, non-farnesylated version was created for parallel investigation. Therefore, the three tripartite vectors were modified by replacing the farnesylation sequence with a small oligonucleotide stuffer fragment, and a new antigen expression vector was cloned to express non-membrane targeted LMO2 without GFP1-9. LMO2 expression was confirmed by Western blot (Figure 5.5). CHO cells were transiently co-transfected with the three tripartite GFP plasmids, with and without the non-farnesylated LMO2 vector to test for antigen-dependency. GFP reconstitution was also investigated by transfection of HEK293T cells, in case cell transfection efficiencies made a difference.

Flow cytometric analysis of GFP signal in each transfection showed no antigen-dependent increase in fluorescence above the 4% of transfected CHO with background interaction (Figure 5.5). By contrast, the HEK293T transfections resulted in a 3% increase in fluorescent cells above background when LMO2 was expressed. Although a minimal increase was noted, this may be due to VL#I21 lacking antigen specificity and thus showing this assay to have a low background of antigen independent GFP reconstitution. Moreover, the result was generated from a four

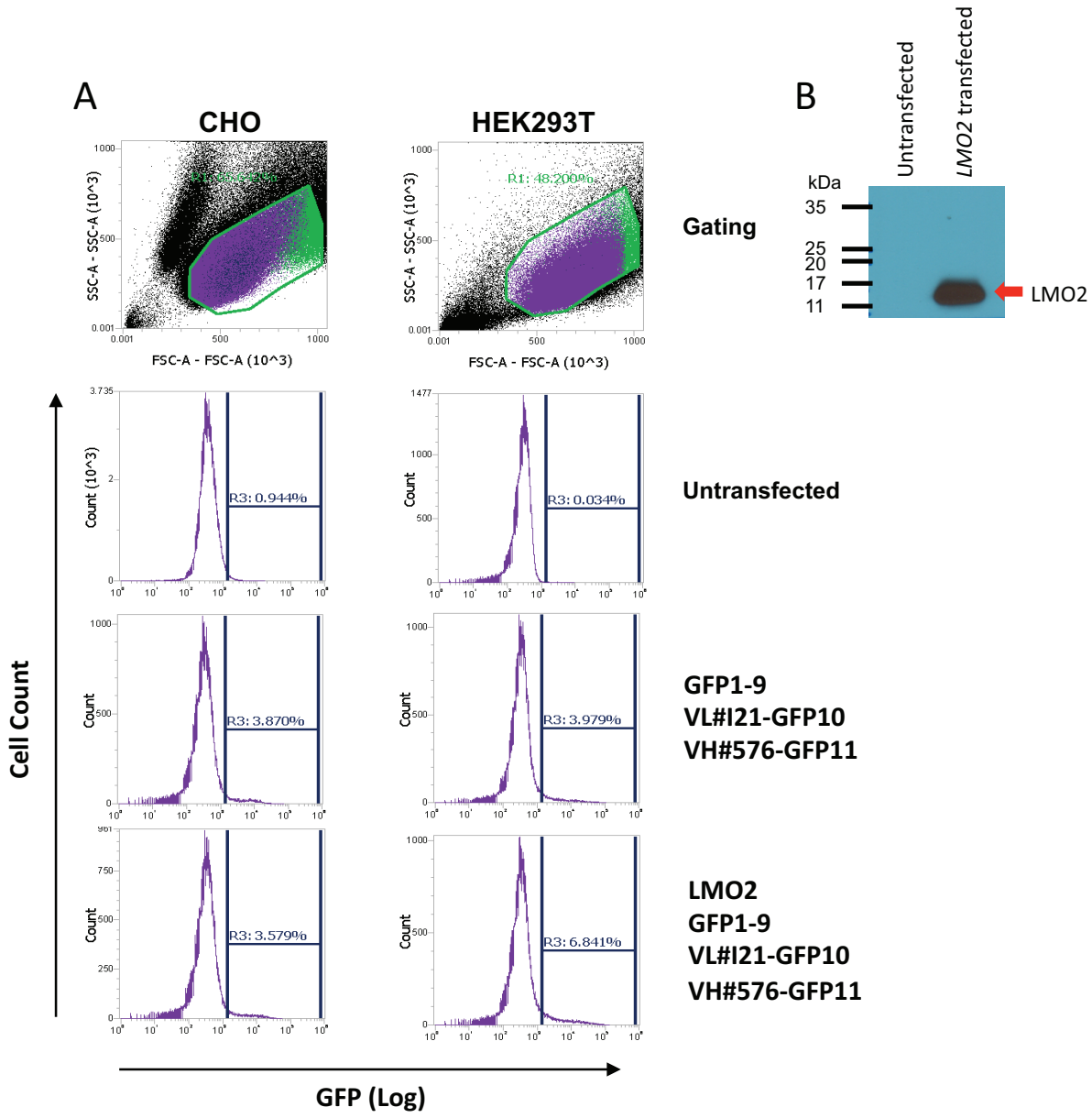

Figure 5.5 Comparison of GFP reconstitution in different cell lines

CHO and HEK293T cells were transiently co-transfected with the non-N-terminally farnesylated tripartite GFP plasmids alongside the pEF-LMO2-Puro vector, and analysed 48 hours post transfection. A: Flow cytometry detection of reconstituted tripartite GFP fluorescence following transfection with the non-farnesylated constructs. There is no difference in the level of CHO cells containing tripartite GFP reconstitution when LMO2 antigen is expressed. A slight increase is seen above background level of GFP positive HEK293T cells when the non-farnesylated LMO2 is co-transfected. B: Western blot confirmation of LMO2 expression from the non-N-terminal farnesylated LMO2 vector, lacking the GFP1-9 fragment, in CHO cells. LMO2 is expressed and resolves at the expected size of 18kDa.

plasmid co-transfection compared with a three plasmid co-transfection. This may have altered the stoichiometry of plasmids successfully taken up by the cells. Therefore addition of a non-relevant antigen control may result in a lower background population, thus effectively increasing the proportion of cells showing antigen-dependent GFP signal.

5.4 Expansion of the tripartite GFP screening test

Investigation of tripartite GFP reconstitution as a reporter for mammalian VL library screen binding molecules had relied upon an association of the anti-LMO2 VH (VH#576) with the 'common', non-specific light chain VL#I21 following kinetic measurements performed with scFv. The efficiency with which VH#576 can reconstitute an LMO2-dependent Fv with singly expressed VL#I21 or VL#826 is unknown, although the scFv kinetics may provide some insight. When bound to LMO2, the VH#576-VL#I21 scFv has a dissociation constant (Kd) of 94nM (Tanaka and Rabbitts, 2009). It is assumed that in this example, the affinity for LMO2 derives solely from the VH, as when partnered with an LMO2-specific VL, VL#826, the scFv possessed a higher affinity, with a Kd of 4.3nM (Tanaka and Rabbitts, 2009).

However, it has been shown that the creation of an anti-RAS scFv with the RAS-specific VL#204 increases the affinity of VH#Y6 for mutant RAS almost 18-fold, with a Kd lowered from 6.2nM as a single domain to 0.35nM as part of the scFv (Tanaka et al., 2007). Indeed, the data generated during this thesis (Chapters 3 and 4) shows that singly expressed anti-RAS VH and VL can re-associate in an antigen-dependent manner, presumably forming an Fv.

For a complete picture of how the single domains interact within the tripartite GFP assay, combinations of different VH and VL with both antigens were performed. To achieve this, additional GFP10 and GFP11 plasmids were cloned to allow combined transfection of VL#I21, #204, #819, #826 or #827 with either VH#576, #Y6 or variants #Y6dm and #Y6mut. The $KRAS_{166}$(G12V) mammalian expression

plasmid used in the luciferase assay from Chapter 4 was employed to express the opposite antigen. Expression of the plasmids was confirmed by Western blot (Figure 5.6). The VH-GFP11 plasmids express uniformly although the VL plasmids produce two additional larger bands, appearing at varying intensities across the samples above the observed, expected band. The absence of these products in the untransfected control and VH-GFP11 samples implies that these extra bands are not simply non-specific primary or secondary antibody binding. It is possible that there could be some element of stop codon readthrough occurring (Dabrowski et al., 2015, Loughran et al., 2014), although the vector backbones of the VH-GFP11 and VL-GFP10 plasmids are identical.

Transiently transfected samples were analysed for GFP reconstitution by flow cytometry (Figure 5.7). (The full set of data is represented in Appendix M). When the combined data is represented graphically (Figure 5.8), it is clear that LMO2-dependency of VH#576 and the VL fragments is minimal. The greatest LMO2-specific dependency occurs when paired with VL#I21, which sees the proportion of GFP positive cells increase by approximately 6% compared with the RAS antigen. Interestingly, when VH#576 is combined with the LMO2-specific light chain VL#826 (Tanaka and Rabbitts, 2009), the tripartite GFP reconstitution is approximately half as efficient than with VL#I21, despite very similar Western blot expression profiles of the two samples as shown in Figure 5.6. This is in stark contrast with the reported scFv dissociation constant affinity measurements (Tanaka and Rabbitts, 2009). Moreover, combining VH#576 with the anti-RAS VL#204 results in the highest proportion of GFP positive cells (average 18%), although again the antigen specificity is low.

The anti-RAS VH#Y6 was included as a positive control and to validate the assay as a potential screening system. Signal generation was expected in the samples transfected with LMO2 antigen, because HEK293T cells will express

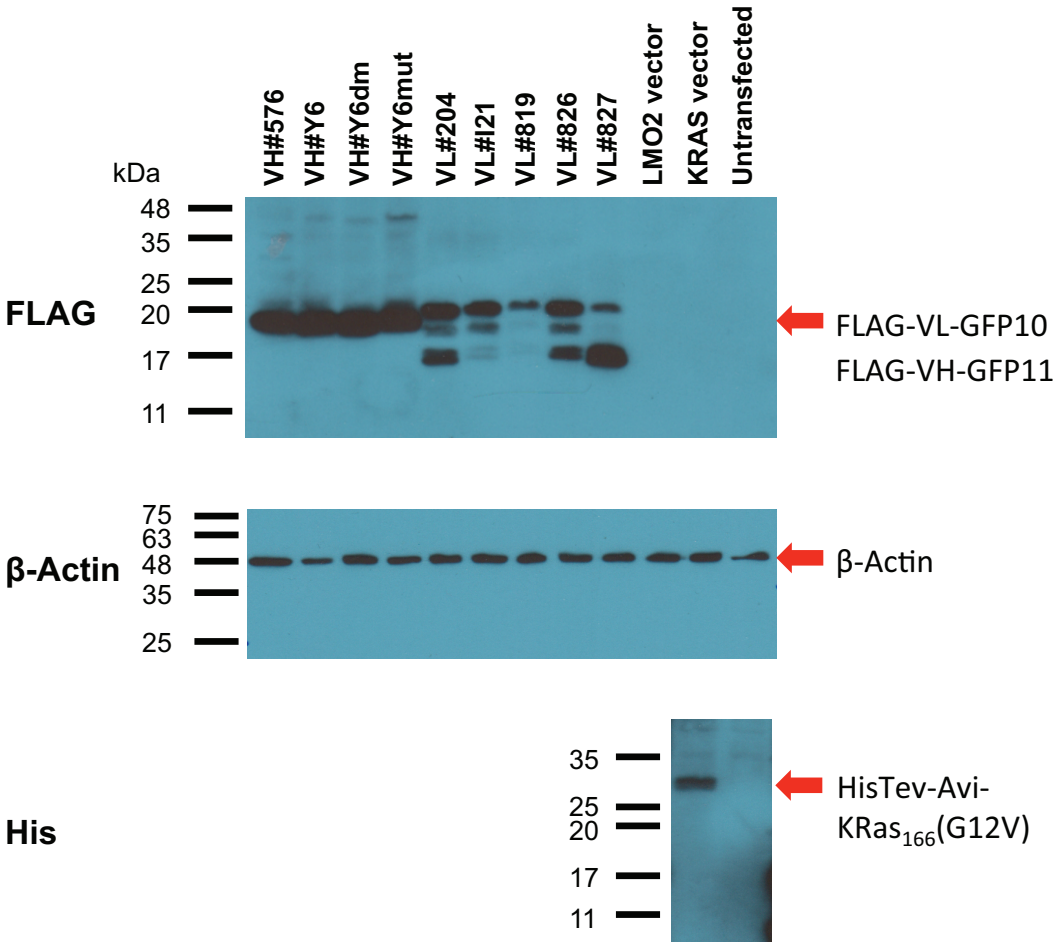

Figure 5.6 Confirmation of tripartite plasmid VH and VL expression

Western blot confirmation of variant VH and VL tripartite GFP plasmid expression in transiently transfected HEK293T cells. After 48 hours post transfection, cells were lysed and total protein levels were quantified by BCA assay. An equal loading (4.4µg) of total protein was applied per lane on 15% acrylamide gels. A: FLAG-tag detection of the VH-GFP11 and VL-GFP10, expected at approximately 19-20kDa. Multiple products are detected in the VL-GFP10 transfection samples. B: Equal protein loading was confirmed by β-actin levels. C: Expression of the KRas166(G12V) antigen plasmid pPGK-HisTev-Avi-KRAS166(G12V)-Puro was also confirmed, resolving at the approximately at the expected size of 26kDa.

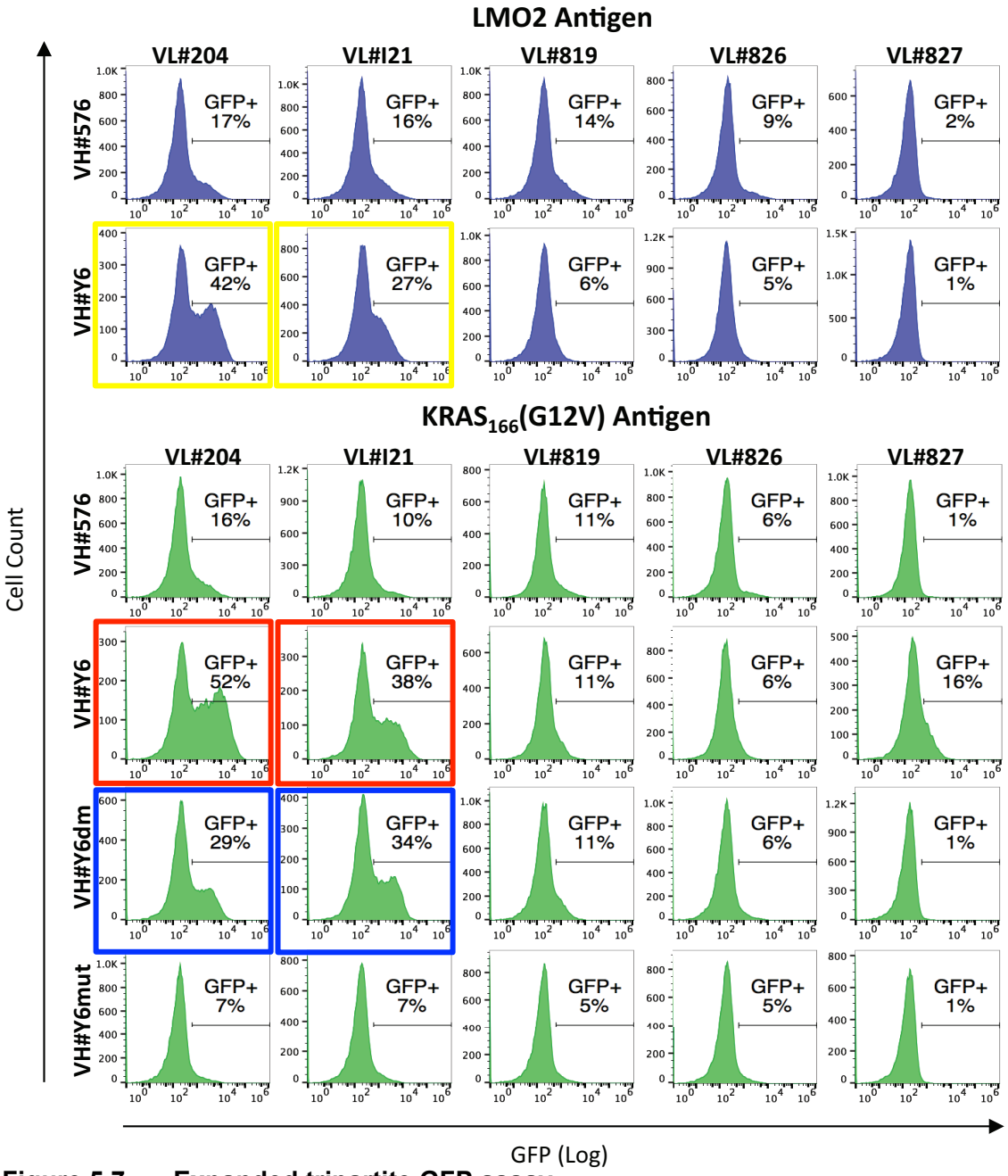

Figure 5.7 Expanded tripartite GFP assay

Following initial testing, the tripartite GFP reconstitution assay was expanded to include both LMO2 and mutant KRAS antigens, as RAS could act as a control with the characterized VH#Y6 and VL#204 pair. The CatcherAb isolated anti-LMO2 VLs (#819, #826 and #827) were included to check if these bound in proximity. HEK293T cells were transiently co-transfected with VL-GFP10 and VH-GFP11 combinations alongside LMO2 and $KRAS_{166}$(G12V) antigens. Transfections were performed in duplicate and analysed after 48 hours. GFP fluorescence was analysed by flow cytometry and is represented by univariate intensity plots (blue traces denote LMO2 antigen, green traces denote KRAS antigen). Untransfected cells were used to gate the cells according to size, and to set the baseline GFP level. The percentage of cells in the GFP positive gate were analysed. The anti-LMO2 VLs do not show an enhanced GFP level when assayed against LMO2 antigen ,and act as a negative control in the RAS antigen transfections. In the RAS antigen assays, GFP reconstitution is observed when the anti-RAS high affinity VH#Y6 and lower affinity VH#Y6dm are coexpressed with the anti-RAS VL#204, and to a lesser extent with VL#I21 (plots highlighted with red (VH#Y6) and blue (VH#Y6dm) boxes respectively). GFP reconstitution is also observed in the LMO2 antigen assay when VH#Y6 is coexpressed with either VL#204 or VL#I21 (yellow boxes) due to the presence of endogenous, cellular RAS.

endogenous RAS for normal cellular signal transduction. This proved correct, but exogenous RAS-dependent increases in the number of fluorescent cells were obvious (Figures 5.7 and 5.8). Unsurprisingly, the highest GFP positive population (50% of gated cells) occurs when VH#Y6 is partnered with the RAS-specific VL#204. This VH and VL combination also produces the brightest population (Figure 5.7), reflecting the pair's affinity and specificity for GTP-bound RAS. When VH#Y6 is paired with VL#I21, the exogenously supplied antigen-dependent increase in fluorescent cells is largest, although the discrete values are around 10% lower than seen with VL#204. However, the VH#Y6-VL#I2I interaction with exogenous RAS mirrors that of VH#Y6-VL#204 with exogenous LMO2 (i.e. 'without' RAS). This supports the driving member of the binding reaction being the VH, and that the fold of VL#I21 is unique in permitting generalised Fv formation compared with the LMO2-specific VL fragments.

The same assay also explored the effect of the VH#Y6 variants on the reconstitution of tripartite GFP with mutant RAS antigen (Figure 5.8B). A clear decrease in the proportion of fluorescent cells correlates with the lowering or ablating VH affinity, and to a lesser extent VL affinity, for mutant RAS. For example, exchanging VH#Y6 for #Y6dm results in a decrease in GFP positive cells from 50% to 30%, whilst a reduction to 5% is evident upon supplying #Y6mut. Similarly, replacing VL#204 with the anti-LMO2 VL fragments produces around 80% less cells with reconstituted GFP.

5.5 Preparation of CDR3 randomised VL libraries

To allow screening of both membrane localised and non-localised antibody-antigen interactions, two randomised VL (CDR3) libraries were cloned for testing in the tripartite GFP screening method for isolating antigen-specific VL fragments complementary to anti-LMO2 VH#576. The first library (Library 1) incorporated the N-terminal farnesylation sequence upstream of the VL fragment, the second library

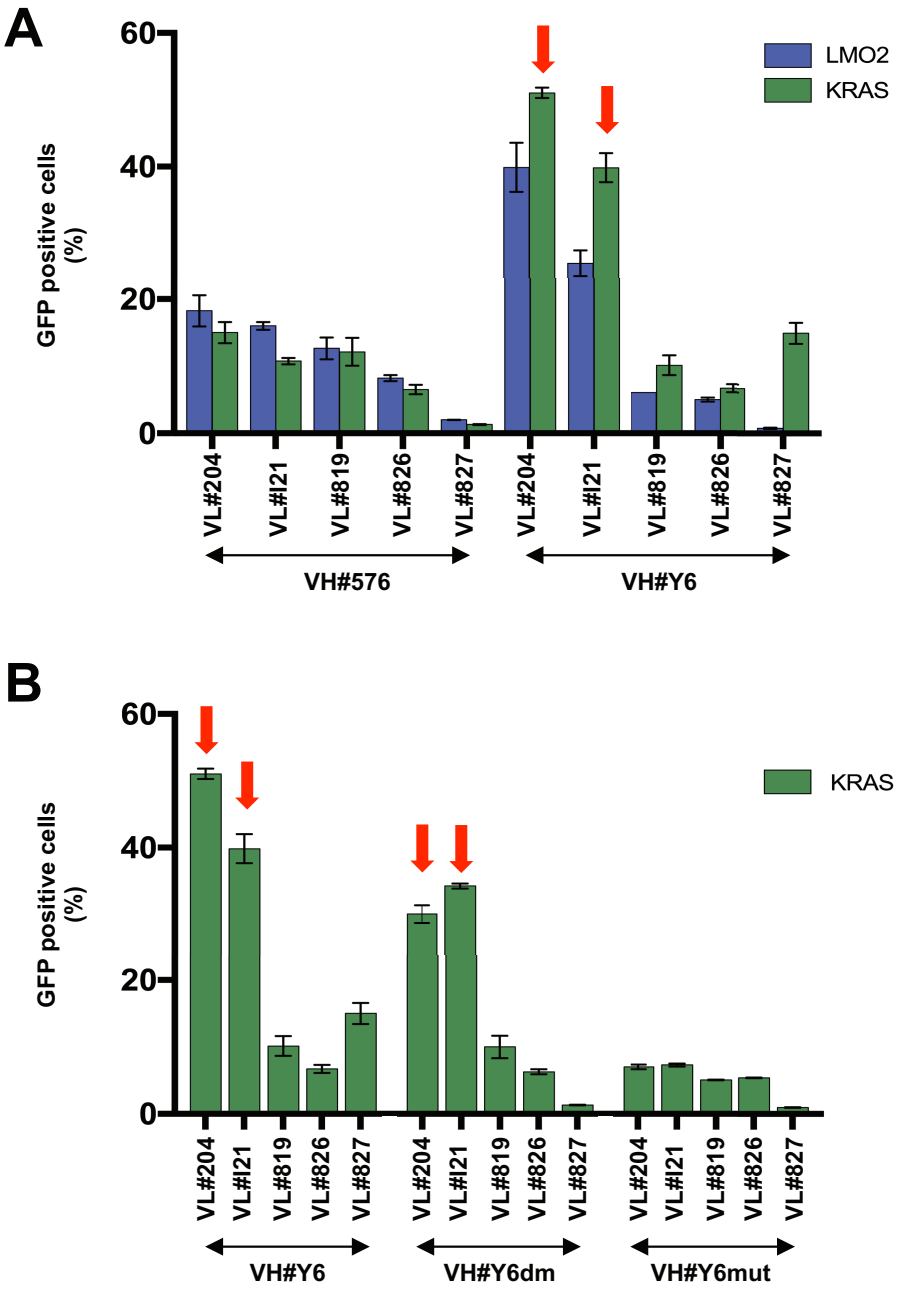

Figure 5.8 Graphical representation of the tripartite GFP assay

The expanded tripartite GFP reconstitution assay results are represented as bar charts to aid comparison between transfections. A: Bar chart detailing the effect of both LMO2 (blue) and mutant KRAS (green) antigens and different VL-GFP10 fragments on the generation of GFP positive cells transfected with either VH#576-GFP11 or VH#Y6-GFP11. None of the VH#576 and VL fragments produce strong GFP fluorescence. A substantial increase in GFP signal is only detected when the anti-RAS VH is paired with VL#204 and VL#l21 (highlighted by red arrows). N.B. increased GFP signal is seen in the samples transfected with LMO2 due to the presence of endogenous RAS in the cells. B: Bar chart showing the effect of combining the VH#Y6 variant fragments and VL variants (cotransfected with RAS antigen) upon the proportion of GFP positive transiently transfected cells. The proportion of GFP positive cells decreases and virtually ablates across VH#Y6 reduced affinity variants. The highest fluorescence reconstitution (highlighted by red arrows) occurs with the RAS-specific VL#204, and to a lesser extent with the non-relevant VL#l21.

(Library 2) was cloned without.

Library 1 randomisation was performed by PCR mutagenesis of VL#I21 with oligonucleotide primers containing random nucleotides within the non-conserved region of the VL CDR3 sequence. The amplified VL sequences were then cloned into the screening vector, and assessed for CDR3 randomisation by sequencing, following a small-scale transformation of the plasmid ligation into chemical competent DH5α E.coli. Twelve colonies were picked and sent for sequencing. One clone failed to generate a sequencing read and was discarded. The other eleven clones returned with a fully randomised CDR3 amino acid sequence in the non-conserved residues (i.e. X residues in the amino acid sequence QQXXXXPXT), when compared with the template, VL#I21 (Figure 5.9). The original VL#I21 sequence was not detected in the clones tested. Interestingly, two of the clones possessed residue mutations in either CDR2 or in the areas of the framework due to PCR error. The large-scale library transformation was performed by electroporation into commercially sourced electro-competent DH10β E.coli. A small aliquot of the transformation was reserved for efficiency plating, where ten-fold serial dilutions were plated onto small dishes. The library size was then calculated from the resulting colony numbers. The library size was estimated to be approximately 10^5 random sequences, and colonies on the screening plates were harvested for plasmid purification.

Library 2 was constructed with VL#204 as the VL template for construction of the second randomised library. VL#204 and VL#I21 have almost identical framework sequences but with different CDR sequences. However, VL#204 had resulted in slightly higher levels of GFP positive cells when paired with VH#576 in the tripartite assay and therefore may aid in isolation of an anti-LMO2 VL fragment, complementary to VH#576. The randomisation of the ligation was confirmed with a small-scale transformation, as was done previously for Library 1. The nineteen clones sequenced showed successful CDR3 randomisation (Figure 5.9). However,

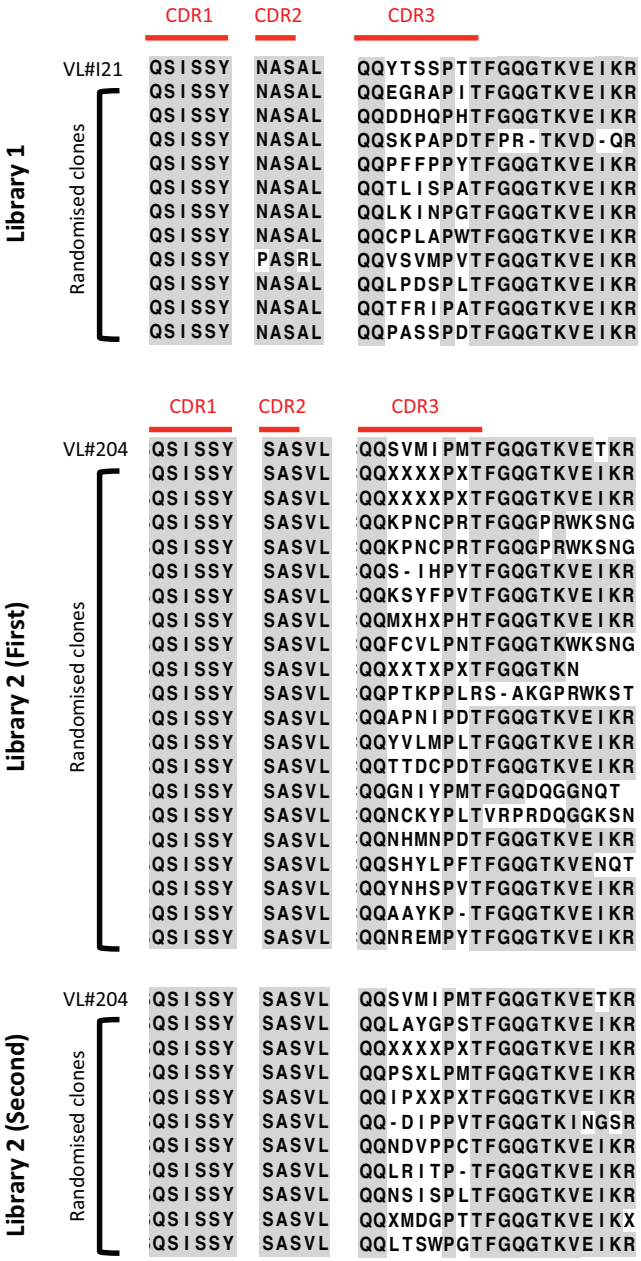

Figure 5.9 CDR3 randomised VL libraries

Clones from the two CDR3 randomised VL libraries were sequenced and translated. Amino acid Clustal alignments show matched (grey) and mismatched (white) residues. . CDR regions are highlighted (red boxes). 'X' denotes unidentifiable bases due to multiple traces within the sequencing read. Missing residues and translational stop codons are indicated by a line. Library 1 was PCR randomised from a VL#I21 template, whilst Library 2 was based on VL#204. Library 2 was prepared twice owing to a large number of PCR mutations leading to frameshifts in the GFP10 region. First set of clones sequenced were successfully randomised in CDR3, although approximately half possessed frameshift mutations. The second set preparation was similarly successfully mutated within CDR3, with only one clone containing a frameshift PCR error and two clones incorporating a stop codon. Occasional C-terminal framework mutations are observed.

some clones appeared to contain a second sequence trace at CDR3 indicating a mixed colony had been prepared. These cases resulted in a translated sequence with 'X' residues. Moreover, approximately half of the clones had introduced small PCR errors leading to frameshift mutations toward the 3' end of the VL sequence and therefore a missense translation of the GFP10 fragment. This would prevent tripartite screening of almost 50% of the VL fragments generated, and so a second round of preparation was performed. A further set of colonies sequenced for the generation Library 2 where CDR3 randomisation had been efficient (Figure 5.9), although once again some clones displayed a second sequencing trace indicating a mixed plasmid preparation. However, one of the ten clones was a re-ligated vector (without insertion of a VL fragment). Two clones had incorporated a translation stop codon, although one of these clones also contained a similar frameshift PCR error as some of the first set has possessed. Upon electroporation, the library size was calculated to be approximately $3.5x10^4$ transformants. Based on the sequencing data, approximately $2.5x10^4$ would be randomised and not incorporating a translational stop codon or frameshift mutation.

5.6 Discussion

This chapter presents the development of a novel, but as yet unproven, method of mammalian screening for the isolation of a single domain VL fragment specific for another T-ALL oncogene, LMO2. Use of the tripartite GFP fragments (Cabantous et al., 2013) as a monitor of VH and VL proximity interactions represents a fast and simple method for screening new complementary single domain fragments, particularly when compared with the more usual yeast screening methods (Tanaka et al., 2003a, Tanaka and Rabbitts, 2010b, Tanaka and Rabbitts, 2009) or indeed bacteriophage protein interaction protocols (de Wildt et al., 2000). The GFP reconstitution also appears to be capable of reflecting the binding affinities of the resulting Fv, as greater fluorescence intensity was generated with the high affinity

VH#Y6 and VL#204 combination compared to that of VH#576 with the same VL. However, the method may benefit from stable transfection of the antigen, GFP1-9 and VH-GFP11 plasmids so only one vector is transiently transfected. This may ensure a more equal and improved plasmid uptake, which may possibly increase the observed GFP intensity.

Importantly, the tripartite GFP assay has shown that the interaction between VH#Y6 and VL#204 is antigen dependent, as decreasing GFP signal is observed when the lower affinity VH variants and non-relevant VL fragments are substituted. This recapitulates the findings in seen in Chapter 4 in the luciferase assay data. Furthermore, increasing the cellular concentration of RAS generates a higher, more intense fluorescence, indicating antigen dependency of VH and VL interaction mediated GFP reconstitution and, by default, the AIDA effect.

Although the first round of randomised VL-GFP10 libraries have been created, the time constraints of this thesis unfortunately prevented the screening from being performed. However, the downstream process would involve fluorescence activated single cell sorting of cells with a fluorescence intensity or 'brightness' over a threshold, determined by the control light chain fragment, which in this case would be VL#I21. Cell lysis, PCR amplification, and sequencing of the isolated VLs would provide the CDR3 randomised sequences to reclone and mature further with CDR1 and 2 randomisations, until a fully matured VL is obtained.

5.7 Conclusion

The methods developed in this chapter provide a framework around which the efficacy of AIDA against two common oncogenes implicated in human T-ALL may be tested. The preliminary suitability of a novel, mammalian complementary VL screening method has been established, and the associated first round CDR3 randomised libraries have been generated. These are now ready for subsequent screening by the tripartite GFP assay that has been developed within this chapter.

Chapter 6 Development of a method for testing AIDA in T-ALL

6.1 Introduction

Demonstration of AIDA in leukaemic cells would be advantageous for pre-clinical testing. This would be achieved by sequential analysis in human T cell lines, murine leukaemia resulting from *LMO2* expression (Ruggero et al., 2016), and primary human T-ALL samples. However, primary tumour lymphocytes require the thymic environment to propagate and differentiate correctly (Petrie, 2002, Miller, 2002). As a result they are usually propagated *in vivo*. This would not be suitable to study the AIDA effect in detail given the fast progression of AIDA observed against mutant RAS in the cancer cell line. An *in vitro* method of tumour cell growth and proliferation would be therefore be valuable for assessing AIDA in T-ALL.

In vitro T cell culture experiments are generally performed to investigate the differentiation process of normal thymocytes. Protocols for this already existed within the laboratory (Dr Katia Ruggero, former member of the Rabbitts laboratory, WIMM, University of Oxford) and so these conditions were adopted for testing tumour maintenance and propagation. It was not known whether these conditions would be suitable for maintaining the tumour phenotype without differentiation, and so phenotypic changes would need to be assessed.

A thymocyte co-culture method on an OP9 murine bone marrow stromal cell layer expressing the Notch ligand Delta-like 1 (DL1) (OP9-DL1 cells) has been used to support differentiation of embryonic and haematopoietic stem cells into mature T cells (Schmitt and Zuniga-Pflucker, 2002). Activation of Notch signalling specifies T cell differentiation over B cell commitment in early progenitors (Han et al., 2002, Wilson et al., 2001), even in extra-thymic locations (Pui et al., 1999), and promotes proliferation and maturation (Sambandam et al., 2005, Taghon et al., 2006). Supplementation of growth medium with interleukin 2 (IL-2) and 7 (IL-7) should stimulate T cell differentiation as DN thymocytes and double positive cells undergoing positive thymic selection show expression of CD25 or IL2RA (Hanke et

al., 1994) and IL7RA (Munitic et al., 2004). IL-2 has been demonstrated to stimulate T cell propagation (Bamford et al., 1994) and may support CD4-postive T cell maturation (Sakaguchi, 2000). IL-7 is expressed by the thymic stroma, is essential for normal thymic cellularity (von Freeden-Jeffry et al., 1995) and may promote TCRB chain rearrangement by induction of RAG expression (Laouar et al., 2004).

A variety of synthetic media have been developed for use with serum to support general and haematopoietic cell culture. Minimal Essential Medium (MEM) alpha formulation supports a wide range of cell types and has been shown to most appropriate for the culture of the OP9-DL1 cells during HSC co-culture (Schmitt and Zuniga-Pflucker, 2002). Iscove's Modified Dulbecco's Medium (IMDM) is a highly enriched medium that has been used for T cell and lymphoid differentiation studies (Veldhoen et al., 2009, Cavazzana-Calvo et al., 1996) as is well-suited to maintaining rapidly dividing cultures at high denisties. The use of Roswell Park Memorial Institute (RPMI) formulation 1640 (RPMI-1640) medium was included for testing as it was originally developed for the culture of lymphocytes and leukaemic T cell lines (Moore et al., 1966, Moore et al., 1967) and therefore may be advantageous for tumour culture.

T cells are difficult to transfect by regular methods such as lipid particles or electroporation (Chang et al., 2017). The multiple transfection steps performed in the creation of the HT1080-based clones would therefore not be suitable given the low efficiency of T cell transfection. Lentiviral transduction systems (Zufferey et al., 1998), are widely used gene transfer methods with broad-range envelope proteins incorporated for a wider host range. Cloning of a 'TetOn' lentiviral expression vector would be required to recapitulate the temporally-controlled AIDA experiments in the leukaemic cell lines and tumour samples.

6.1.1 Aim

The aim of this chapter was to develop the AIDA system further, toward LMO2 as the oncogenic antigen. This would validate the method against another antigens, enhancing the applicability of AIDA as a potential anti-cancer therapy. This necessitated simultaneous development of *ex vivo* lymphocyte culture and conceptualising a unique gene transfer vector to incorporate our gene inserts and allow monitoring of AIDA in real time. This has been achieved, and the system is now ready for deployment against LMO2 and other oncogenic targets.

6.2 Culture of *Lmo2*-driven mouse T cell tumours

Tumourigenic T cells from the *Lck-Lmo2* transgenic mouse model of LMO2-mediated T-ALL (Ruggero et al., 2016) were propagated in immunodeficient, non-obese diabetic (NOD) SCID gamma (NSG) mice. Spleens were harvested approximately three weeks post-transplant and the *Lck-Lmo2* cells derived from this experiment were demonstrated to be of the DN1/DN2 stage transition (Figure 6.1). It is more common for these *Lck-Lmo2* tumours to be of the DN2/DN3 stage transition (Ruggero et al., 2016), although owing to the heterogeneity of tumours, differentiation blocks at others stages have been noted.

Ex vivo culture was tested with *Lck-Lmo2* cells plated at two densities (10^6 and 10^7 cells/ml) with and without an OP9-DL1 stromal layer, in the three types of basal medium (RPMI, IMDM and MEM) supplemented with serum and containing IL2 and IL7 (detailed in Chapter 2, section 2.2.4). The tumour cells were cultured for one week, at which time cell counts were performed (Table 6.1). The only condition to have generated an increase in cell numbers was that containing IMDM-based medium with an OP9-DL1 cell layer, giving rise to a modest doubling of total cell number when plated at a initial density of 10^6 cells/ml. The effect of the OP9-DL1 cells was evident across all three media tested, with more *Lck-Lmo2* cells remaining in those wells with the stromal layer. The cells were assessed for cell marker

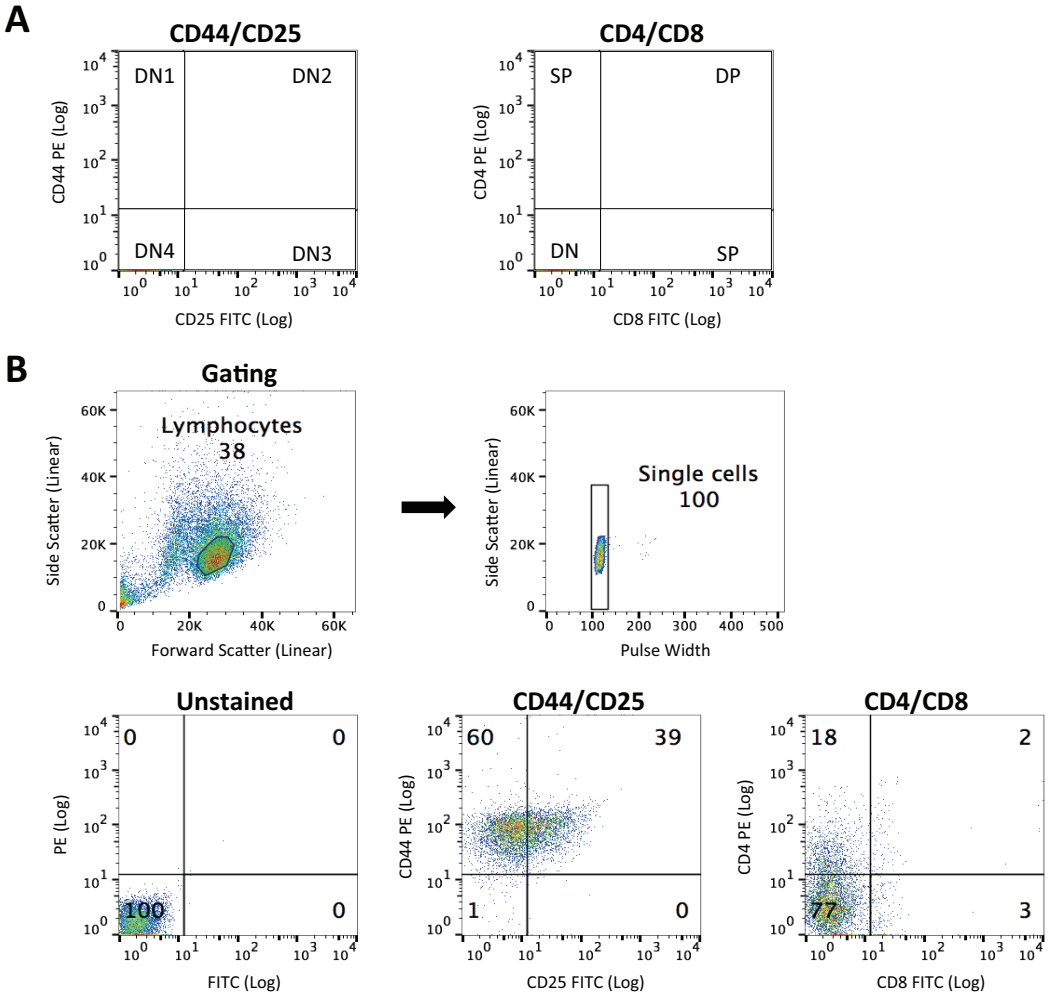

Figure 6.1 Transplanted *Lck-Lmo2* T cell tumour phenotype

Flow cytometry analysis of tertiary transplanted *Lck-Lmo2* T cell tumour, isolated from NSG mouse spleens. A: Example population gates for the two CD marker sets. CD44/CD25 identify immature T cells which occupy the CD4 and CD8 double negative (DN) subtypes. CD4/CD8 profiling indicates T cell maturation, from the DN stage to double positive (DP) and finally maturing to single positive (SP) CD4 or CD8 marker T cells. B: Lymphocytes were gated according to size and granularity by forward and side scatter characteristics, then single cells gated according to pulse width. Following single colour fluorescence compensation, quadrant gates were set relative to the unstained control sample. T cell markers were analysed in pairs; CD44 with CD25 to examine the double negative (DN) populations, and CD4 with CD8 to analyse mature, double and single positive (DP and SP respectively). This mouse T cell tumour identifies as DN1/DN2 transition, with minimal CD4 expression.

Base Medium	OP9-DL1 Layer	Plating (Day 1)	Count (Day 8)
RPMI	-	1×10^6	1.1×10^5
RPMI	-	1×10^7	1.8×10^6
RPMI	+	1×10^6	6.5×10^5
RPMI	+	1×10^7	8.7×10^5
IMDM	-	1×10^6	1.5×10^4
IMDM	-	1×10^7	7.7×10^5
IMDM	+	1×10^6	2.1×10^6
IMDM	+	1×10^7	1.8×10^6
MEM	-	1×10^6	1.6×10^5
MEM	-	1×10^7	1.5×10^6
MEM	+	1×10^6	3.7×10^5
MEM	+	1×10^7	6.8×10^5

Table 6.1 Cultured *Lck-Lmo2* tumour cell counts

Cell count data of initial test of *In vitro* cultured *Lck-Lmo2* tumour cells. Cells were plated (day 1) at either 10^6 and 10^7 cells in a total volume of 1ml. Cultures were grown in three types of medium, with and without an OP9-DL1 stromal cell layer (denoted as +/- respectively). Cell counts were performed one week later (day 8). Only one condition (10^6 cells in IMDM medium with an OP9-DL1 layer, pink highlight) resulted in an increase in cell number. Note: lots of dead cells were evident in the cultures at day 8 but were not counted. Growth condition key: RPMI, *Roswell Park Memorial Institute 1640 medium*, IMDM, *Iscove's Modified Dulbecco's Medium*, MEM, *Minimal Essential Medium*. The full media compositions, including additives, are described in Chapter 2, section 2.2.4.

expression at the end of the experiment, with antibody pairs CD44/CD25 (Figure 6.2) and CD4/CD8 (Figure 6.3) to define their differentiation status. Again, the IMDM base with the OP9-DL1 cell layer was phenotypically closest to the starting population (Figure 6.1). A starting density of 10^6 cells/ml was best for the maintenance of the CD44/CD25 profile, which seemed to lose CD25 expression across all 10^7 platings without the OP9-DL1 layer. Of note, no expansion in CD4/CD8 stained populations was evident indicating that the tumour cells were not differentiating.

A second culture test was performed again over two cell densities (this time 10^5 and 10^6 cells/ml owing to the negative effect seen at 10^7 cells/ml) and a growth curve was determined to interrogate cellular proliferation over the course of the week. The medium was the IMDM-based medium with an OP9-DL1 layer. The counts showed an increase in cell number, with final counts at day 8 between 3 and four times higher than the starting density (Figure 6.4). The 10^5 plating density displayed typical sigmoidal growth kinetics, reaching what appeared to be the plateau phase at day 7 and 8, although this is to be expected due to an increase in apoptosis in cells maintained at high density. The 10^6 plating showed a similar profile, although they reached their highest density (4-fold increase) by day 5, with a slight crisis after day 6 resulting in a 1.5 fold decrease in cell number, although cell proliferation subsequently resumed.

Flow cytometric profiling was performed as before, alongside isotype control antibodies to document no cross-reactivity of the antibody with cellular Fc receptors (Figure 6.5). Very little difference in antibody staining was observed, except for a slight decrease of approximately 1 log in PE (CD44) intensity.

The *ex vivo* culture of *Lck-Lmo2* tumour cells were viable over the course of the week long experiment, with no critical perturbation of T cell differentiation encountered. Either density of 10^5 or 10^6 cells/ml would be suitable for *ex vivo* culture,

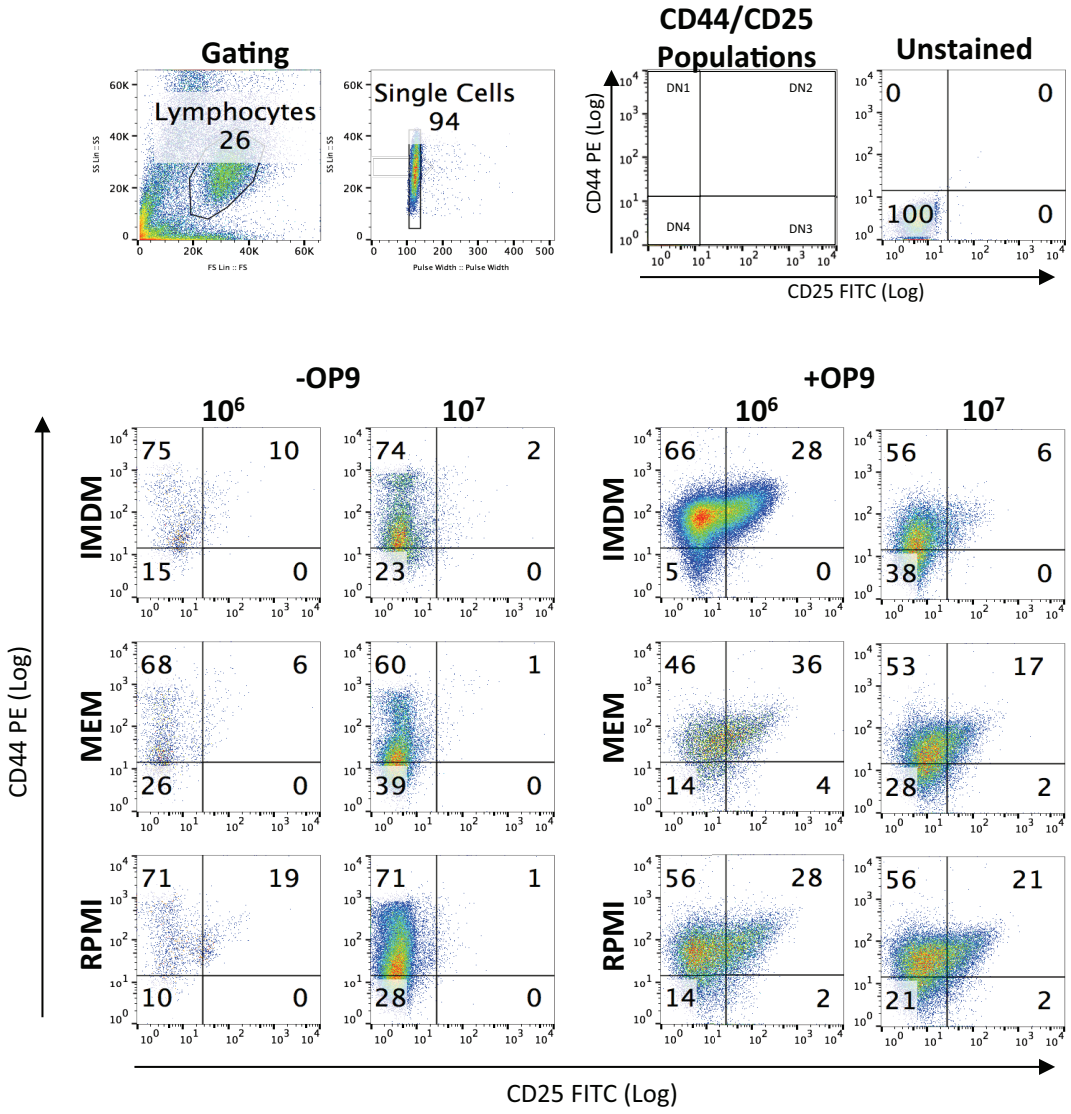

Figure 6.2 Cultured *Lck-Lmo2* cell differentiation analysis: CD44/CD25

Flow cytometry analysis of CD44 and CD25 cell surface marker expression of *in vitro* cultured *Lck-Lmo2* tumourigenic T cells. T cell differentiation progresses through stages defined by cell surface marker expression. CD4 and CD8 double negative (or DN) cells are the early T cell progenitors within the thymus, and can be further subdivided into four DN stages according to their differential CD44 and CD25 expression patterns (see example plot, third plot from left on top row). Lymphocytes cultured in the different media were examined by with CD44 and CD25 antibodies to ascertain whether culture conditions had impacted their differentiation status. Cells were grown in 24-well plates, and one well each condition was taken directly for analysis without cell counting to reduce loss of cells, as numbers were low. Lymphocytes were gated according to size and granularity by forward and side scatter characteristics, and single cells ensured by gating according to pulse width. Following single colour fluorescence compensation, quadrant gates were set relative to the unstained control sample. Antibodies raised against CD44(PE) and CD25(FITC) were used to examine changes within the double negative (DN) populations as a result of the culture conditions. The mouse T cell tumour identified as DN1/DN2 transition previously. Without the OP9-DL1 stromal layer both cell densities lose CD25 expression, whilst presence a layer at the lower cell density maintains the cell surface phenotype.

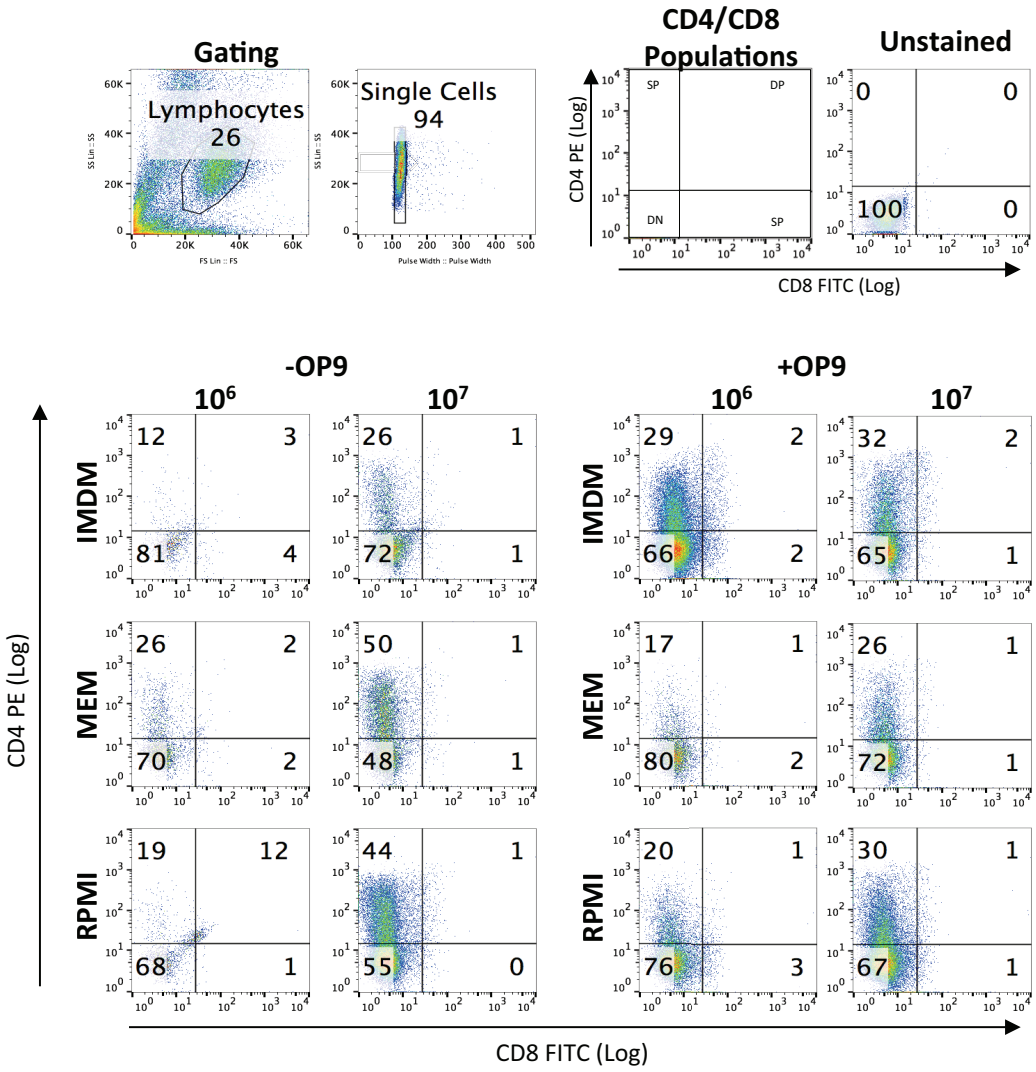

Figure 6.3 Cultured *Lck-Lmo2* cell differentiation analysis: CD4/CD8

Flow cytometry analysis of CD4 and CD8 cell surface marker expression of *in vitro* cultured *Lck-Lmo2* tumourigenic T cells. Lymphocytes were gated according to size and granularity by forward and side scatter characteristics, and single cells ensured by gating according to pulse width. Following single colour fluorescence compensation, quadrant gates were set relative to the unstained control sample. Antibodies raised against CD4(PE) and CD8(FITC) were used to examine changes within the double and single positive populations (DP and SP respectively, as indicated in the example plot, upper panel) as a result of the culture conditions. The mouse T cell tumour identified as possessing some low CD4 expression previously. No expansion into the CD8 positive population is evident, indicating no maturation or differentiation of the tumour results from the culture conditions.

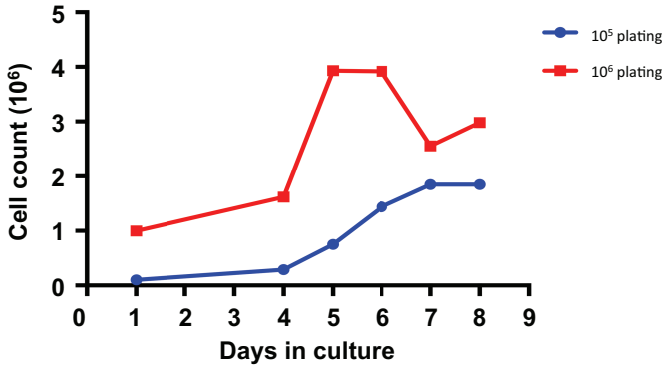

Figure 6.4 Cell counts of expanded *Lck-Lmo2* culture

Line graph representation of the cell count data of expanded test of *in vitro* cultured *Lck-Lmo2* tumour cells. Cells were plated (day 1) at 10^5 and 10^6 cells in a total volume of 1ml. Cells were grown in the IMDM base medium, containing serum and the interleukin additives with an OP9-DL1 layer as these conditions gave the best growth result in the initial in vitro growth assay. Cell counts were performed daily for one week, with cells carried forward for differentiation analysis (see figure 6.5). The 10^5 plating curve (blue line) shows sigmoidal growth tendencies before reaching stationary phase at day 7-8. The 10^6 (red line) plating cell counts show a similar curve although they reach plateau at day 5-6 and a small crisis, after which cell number is reduced before new growth recommences. Data refers to single well cell counts, without replicates due to the limited availability of reagents. Repeated counts would be advantageous to confirm this result.

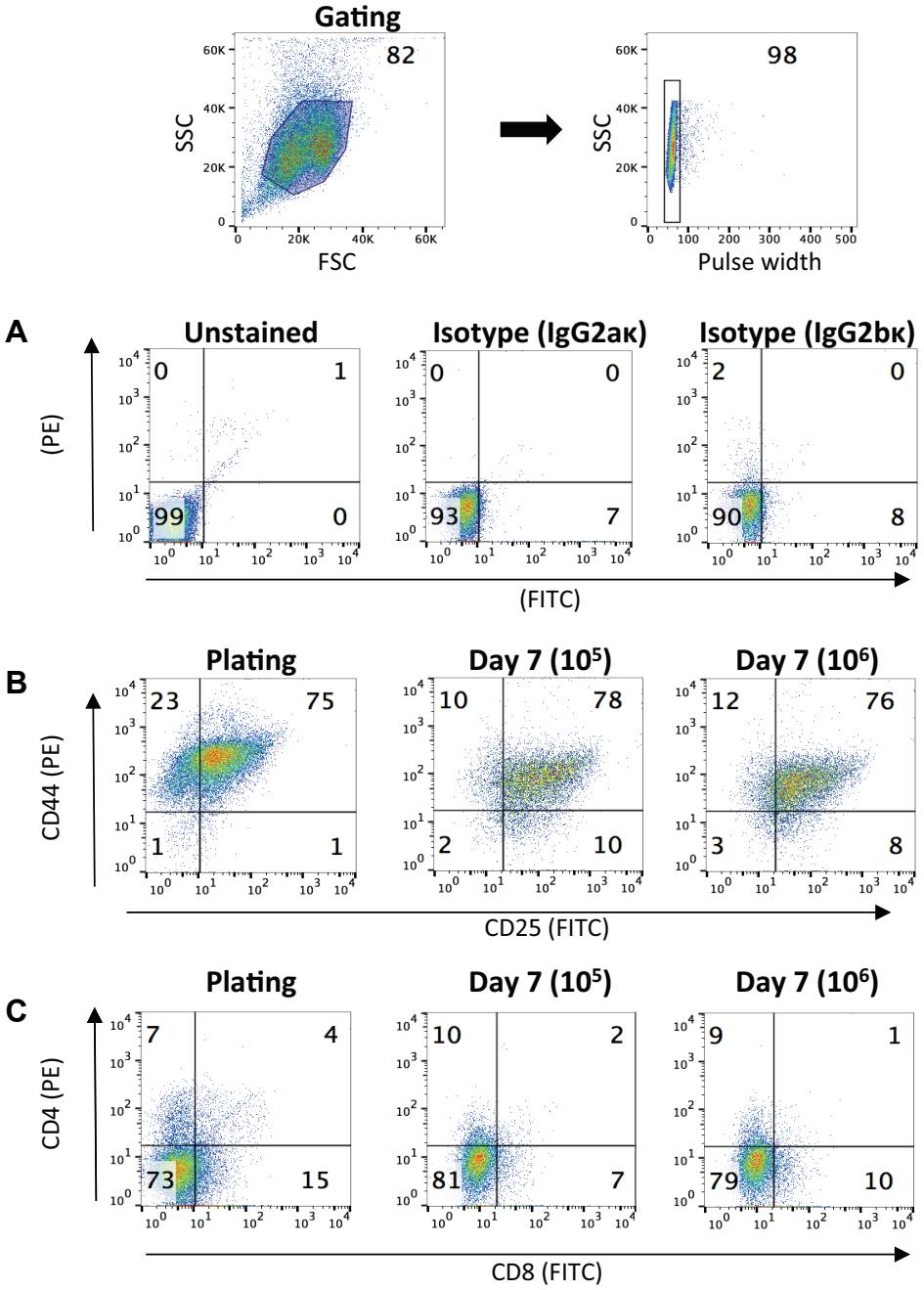

Figure 6.5 Expanded *Lck-Lmo2* culture differentiation analysis

Flow cytometry analysis of cell surface marker expression of the expanded *in vitro Lck-Lmo2* cell culture at plating and at day 7. Following cell counts (data shown in figure 6.4) lymphocytes were gated according to size and granularity by forward and side scatter characteristics, and single cells gated according to pulse width. A: Following single colour fluorescence compensation, quadrant gates were set relative to the unstained control sample and antibody isotype controls were negative for non-specific binding. B&C: Antibodies raised against CD44 or CD4 (both PE conjugated) and CD25 or CD8 (both FITC conjugated) were used in pairs to examine changes within the immature double negative (DN) T cells (B: CD44 and CD25 pair) and the mature double and single positive (DP and SP respectively) populations (C: CD4 and CD8 pair) as a result of the culture conditions. Minimal marker expression is observed, although the CD44 PE intensity measures one log lower. Some decreased CD4 fluorescence is also observed, but no evidence of tumour cell maturation is apparent.

although 10^6 cells would need passaging more frequently to maintain growth and avoid crisis.

6.3 Propagation of T-ALL leukaemic samples *in vivo*

A small panel of paediatric T-ALL tumour samples expressing LMO2 and possessing the activating t(11;14)(p13;q11) translocation were obtained from Dr Victoria Weston (formerly of the University of Birmingham, U.K.) and Dr Cristina Meccuci (Dept. of Medicine, University of Perugia, Italy). These samples were passaged through NSG mice to make laboratory stocks for later use, with the help and guidance of Dr Osama Al-Assar (former member of the Rabbitts Laboratory, WIMM, University of Oxford). The cells were initially passaged through mice before testing *in vitro* growth conditions to ensure that the samples were not lost whilst attempting to optimise conditions. Engraftment of the human T-ALLs was monitored by the ratio of human to mouse CD45 positive (CD45+) cells in the peripheral blood.

CD45 (also known as Protein tyrosine phosphatase, receptor type C, PTPRC) is a pan-leukocyte marker. Although functionally identical, mice possess one of two distinct allotypes, CD45.1 (Ly-5.1) or CD45.2 (Ly-5.2). Allogeneic CD45 mouse strains are widely used in transplant studies to discriminate between host and donor material (Spangrude et al., 1988). NSG mice are regarded as possessing the CD45.1 allotype (Naramura et al., 2010).

The T-ALL xenografts were monitored by fortnightly blood samples. The proportion of human to mouse CD45+ cells was determined by flow cytometry (Figure 6.6), using two different antibodies that are specific for differences between the human and mouse CD45 protein, with non-transplanted NSG mice as a control. Within two weeks of transplant, mice injected with the MB sample had a high peripheral blood level of 75-80% human CD45+ cells. Although the animals did not display any overt signs of ill health, they were humanely sacrificed. Post mortem examination revealed a slightly enlarged spleen, in comparison to normal NSG mice

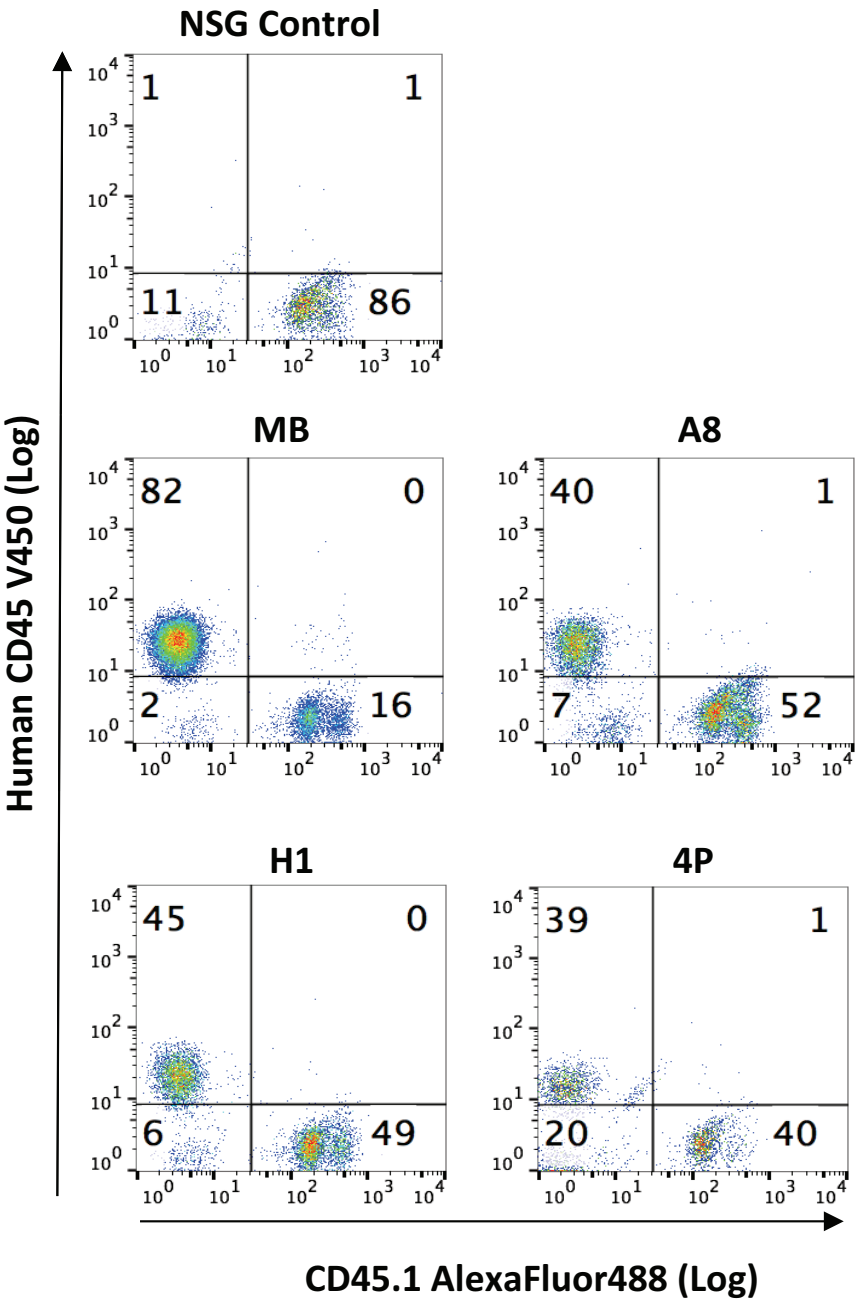

Figure 6.6 Propagation of T-ALL samples

Engraftment of T-ALL samples in NSG mice was monitored by flow cytometric analysis of the appearance of human CD45-positive cells in the peripheral blood. Viable T-ALL cells obtained from four paediatric T-ALL patients (named as MB, A8, H1 and 4P) were injected into NSG mice and allowed to propagate over an 8 week period, monitored by blood sampling every two weeks. Lymphocytes were prepared from blood samples and gated according to their size and granularity by forward and side scatter characteristics, and single cells ensured by gating according to pulse width. Following single colour fluorescence compensation, quadrant gates were set relative to the unstained control sample. The plots above represent the blood samplings taken closest to euthanasia. Each T-ALL sample engrafted and propagated successfully.

but not in relation to fully immune-competent strains. Some evidence of thymic enlargement was visible although cell counts were low. Blood sampling was repeated over the next 6-8 weeks until all four T-ALL xenograft experiments had been harvested. Owing to Home Office regulations, blood sampling could not be performed more regularly than bi-monthly collections, therefore the final three sets were sacrificed according to judgment of animal welfare. The harvested tissues were processed into single cell preparations and frozen form later use. Post mortem cell counts are detailed in Table 6.2.

6.4 Trial *ex vivo* culture of T-ALL samples

The OP9-DL1 co-culture system had shown to permit the growth of a short-term culture of murine leukaemic T cells. Although the stromal layer and ectopically expressed *Dl1* is of mouse origin (Schmitt and Zuniga-Pflucker, 2002), this co-culture system has been used with human haematopoietic cells (La Motte-Mohs et al., 2005, Martin et al., 2008). Therefore, *ex vivo* culture and propagation of the T-ALL samples was investigated, according to the method defined with the *Lck-Lmo2* mouse tumour cells.

Two initial plating densities per T-ALL sample were seeded as before at 10^6 spleen cells/ml. Cell counts were measured every 3-4 days, and cells reseeded back at their original plating density. Cultures were maintained for 22 days. Cell counts are represented graphically in Figure 6.7. Both H1 and 4P explants grow well in extended culture, although by the sixth passage (day 22) the cells appear to be experiencing a reduction in proliferative potential as less cells repopulate per passage. By contrast, MB and A8 explants fail to thrive, despite showing the strongest engraftment in the mice.

Flow cytometric profiling of H1 (Figure 6.8) and 4P (Figure 6.9) cultures show a sustained cell surface marker phenotype of the CD44/CD25 and CD4/CD8 differentiation markers at plating and at day 8. However, the T-ALL explants appear

hT-ALL	Spleen $x10^8$	Bone Marrow $x10^7$	Thymus $x10^6$
MB	1.4	0.1	0.3
	1.9	0.6	2.0
A8	1.4	1.6	Not found
	1.1	1.8	Not found
H1	2.8	0.6	Not found
	2.3	0.9	Not found
4P	1.8	1.5	Not found
	2.0	2.7	3.0

Table 6.2 T-ALL transplant post-mortem cell counts

Table shows the cell counts of xenografted hT-ALL cells taken from haematopoietic tissues at mouse post-mortem. NSG recipient mice (two per hT-ALL transplant) were monitored regularly for hT-ALL cell appearance in the peripheral blood. Upon critical level being reached or signs of ill health, mice were sacrificed and single cell preparations were made from the spleen, bone marrow or thymus (if present). Cell counts of the haematopoietic tissues at post-mortem harvest are indicated. Samples were then frozen for future experimental use.

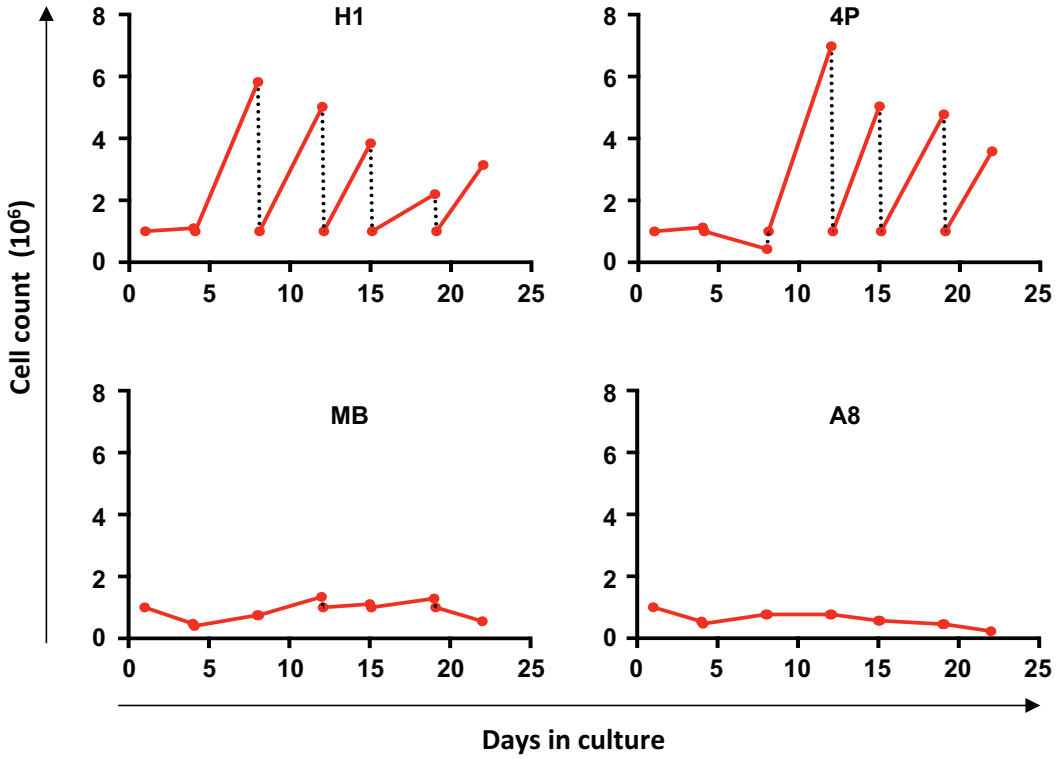

Figure 6.7 ***Ex vivo*** **cultured T-ALL growth curves**

Graphical representation of cell counts of *ex vivo* cultured hT-ALL cells. Cells were grown from an initial plating density of 10^6 cells in 1ml of the IMDM-base medium on an OP9-DL1 stromal cell layer (as determined form the *Lck-Lmo2* culture test). Samples were counted every 3-4 days, over a 22 day period. At each count, cells were replated in fresh growth medium according to their starting density. H1 and 4P leukaemic cells adapted to the *ex vivo* growth conditions after 4-8 days, with subsequent robust propagation. Evidence of reduced proliferative potential was observed toward the end of the experiment, as cells failed to expand as strongly as at the beginning. MB and A8 cells failed to thrive, with cell densities remaining static over the course of the experiment. Red solid line represents the growth between plating and cell counting, the black dotted line (where visible) shows the replating of the cells back to the initial starting density.

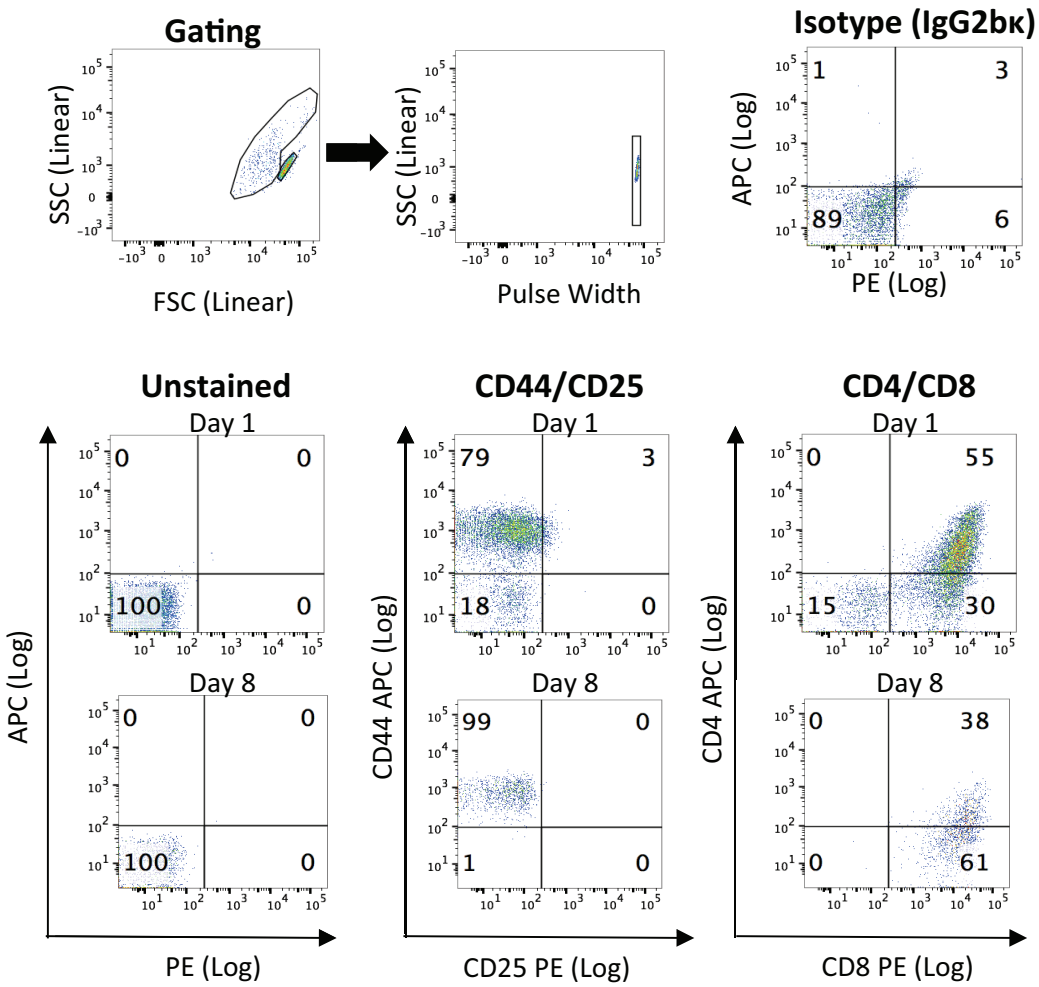

Figure 6.8 H1 sample differentiation analysis

Flow cytometry analysis of cell surface marker expression of the *ex vivo* expanded H1 T-ALL cell cultures at plating and at day 8 to determine whether in vitro differentiation had occurred (as was performed with the *Lck-Lmo2* mouse tumour culture). Lymphocytes were gated according to size and granularity by forward and side scatter characteristics, and single cells ensured by gating according to pulse width. Following single colour fluorescence compensation, quadrant gates were set relative to the unstained control sample. Antibodies raised against CD44/CD4(APC) and CD25/CD8(PE) were used in pairs to examine changes within the immature double negative (DN) T cells and the mature double and single positive (DP and SP respectively) populations as a result of the culture conditions. The culture conditions do not appear to affect surface marker expression, as minimal differences in antibody binding are observed. Antibody isotype controls were negative for non-specific binding.

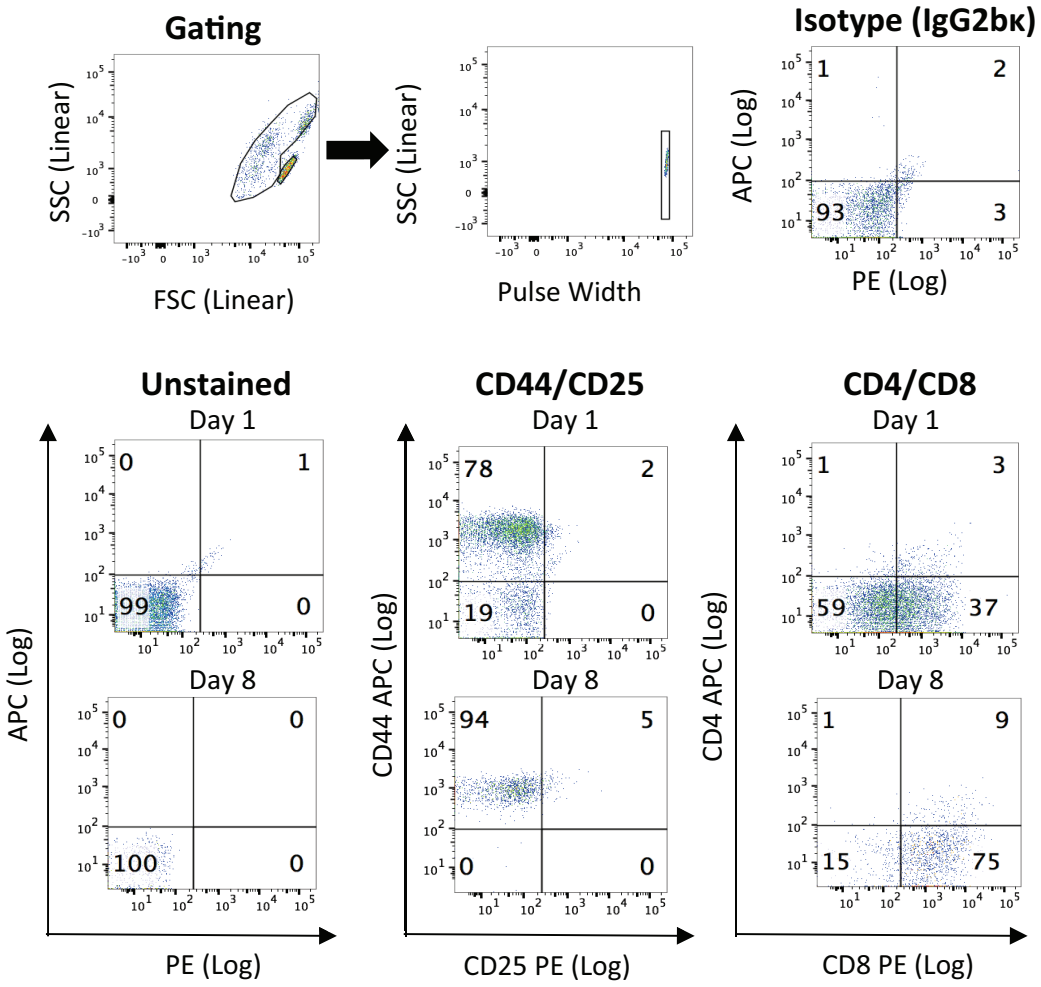

Figure 6.9 4P sample differentiation analysis

Flow cytometry analysis of cell surface marker expression of the *ex vivo* expanded 4P T-ALL cell cultures at plating and at day 8 to determine whether in vitro differentiation had occurred (as was performed with the *Lck-Lmo2* mouse tumour culture). Lymphocytes were gated according to size and granularity by forward and side scatter characteristics, and single cells ensured by gating according to pulse width. Following single colour fluorescence compensation, quadrant gates were set relative to the unstained control sample. Antibodies raised against CD44/CD4(APC) and CD25/CD8(PE) were used in pairs to examine changes within the immature double negative (DN) T cells and the mature double and single positive (DP and SP respectively) populations as a result of the culture conditions. The culture conditions do not appear to affect surface marker expression, as minimal differences in antibody binding are observed. Antibody isotype controls were negative for non-specific binding.

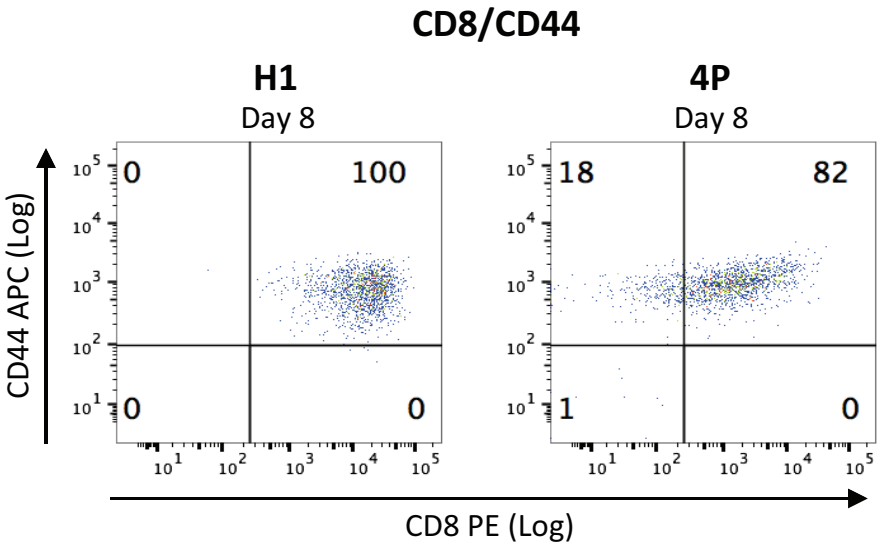

Figure 6.10 CD8/CD44 analysis of *ex vivo* cultured T-ALL samples

Flow cytometry analysis of CD44 and CD8 cell surface marker expression of the *ex vivo* expanded H1 and 4P T-ALL cell cultures at day 8. Lymphocytes were gated according to size and granularity by forward and side scatter characteristics, and single cells ensured by gating according to pulse width (shown in fig 6.8 and 6.9). Following single colour fluorescence compensation, quadrant gates were set relative to the unstained control sample. Antibodies raised against CD44(APC) and CD8(PE) were used to identify that these human leukaemia samples co-express both CD44 and CD8.

to co-express CD44 alongside CD8 and/or CD4. Indeed, this was confirmed by flow cytometry with CD44/CD8 double staining (Figure 6.10).

6.5 Lentiviral vector cloning

The *ex vivo* experiments successfully showed that short-term cultures of both mouse and primary human tumour samples was possible. For these to have practical use, the next stage was to design and test transduction of a lentiviral expression vector, where the virus could later be modified to incorporate the AIDA domain antibody-proCASP3 fusions. Temporal control of the VH/VL-proCASP3 fusions would be necessary, and because the TetOn expression system had worked well for the purposes of the anti-RAS AIDA assessment (chapters 3-5), a similar approach was investigated for T cell transduction. Creation of the HT1080-based clones had involved two transfection steps; TetOn plasmid transfection for constitutive expression of the TetOn (rtTA) protein, and AIDA plasmid transfection. Moreover each transfection had necessitated antibiotic selection of transfectants. To expedite the T cell transduction process a commercial vector, pLVX-TetOne (Clontech), encoding the rtTA in reverse orientation to the transgene insertion site was obtained. The anti-LMO2 VH#576 was cloned into the vector, with downstream fluorescent reporter protein, yellow fluorescent protein (YFP), incorporated instead of a resistance marker. (The lentiviral vector maps are shown in Appendix F.)

Tetracycline-specific induction of YFP expression was assessed by flow cytometry. Transiently transfected HEK293T cells with the pLVX-TetOne-VH#576-YFP vector were grown in both normal and certified tetracycline-free serum (Figure 6.11). Transfected cells with tetracycline induction of the VH#576-YFP cassette showed a peak fluorescence approximately 2-3 log brighter than the untransfected cells. Some tetracycline independent YFP expression was evident at 1-2 log lower than the induced fluorescence peak. No difference in Tet-independent YFP expression was observed between the two serums.

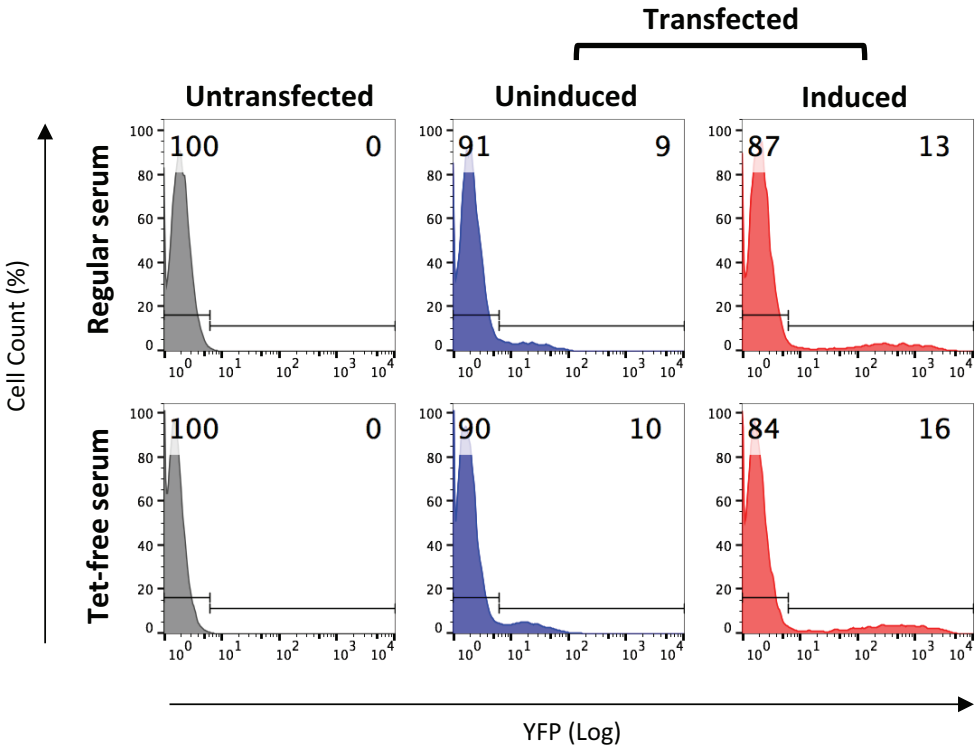

Figure 6.11 Lentiviral construct expression test

Initial testing of the cloned commercial lentiviral vector, pLVX-TetOne in the HEK293T cell line. Plasmid was transiently transfected into cells using Lipofectamine 2000 (Invitrogen), with and without the addition of 1µg/ml Tetracycline to induce expression of the YFP moiety. Univariate intensity plots show the detection of YFP fluorescence by flow cytometry 48 hours after transfection. The YFP gates were set on the untransfected samples, where no effect of Tetracycline addition is noted. Although the efficiency of transfection is low, the transfected samples express high levels of YFP upon tetracycline induction, evidenced by the fluorescence intensity occurring at 2-3 log higher compared to the untransfected cells. However, some uninduced leaky expression is evident, with peak fluorescence around one log higher than background levels.

The vector was further altered to incorporate a second fluorescent reporter, the red mRuby2 protein (Kredel et al., 2009), after the rtTA protein following a viral 2A peptide to enable simplified monitoring of transduction efficiency. Additionally, the YFP moiety was tagged with five affinity tags (FLAG, HA, V5, Myc and His tags) to allow titration of antibody fragment and fluorescent protein expression by Western blot at a later stage. Once constructed, the vector was again tested for expression by transient transfection of HEK293T cells (Figure 6.12). The effect of fixation on fluorescence quenching was also investigated, to ensure compliance with local safety guidelines was appropriate to study of these reagents. The previous YFP-only vector and an empty mRuby2-only vector were transfected in parallel as colour controls. Both mRuby2-containing vectors displayed Tet-independent, constitutive reporter expression, with transfection efficiencies between 40-55% of total cells. The leaky, Tet-independent YFP expression is noticeable, although the gating shows the fluorescence intensities above 3 log are increased by 35% of the gated population with tetracycline induction. The vector containing both the constitutive reporter and the Tet-induced expression reporter show a clear double positive fluorescence profile. Moreover, co-expression of both reporters was only visible by microscopy upon Tet-induction, whilst mRuby2 expression was confirmed as constitutive (Figure 6.13).

6.6 Lentivirus transduction efficiency testing

Recombinant virus-like particles were packaged and the transducing particle concentration was determined by spinoculation of a titration of an increasing virus preparation volume into HEK293T cells, from 0.1-20µl. Uninfected cells were used as an mRuby2 negative control, allowing the negative get to be set. An increasing proportion of mRuby2 fluorescence was discernible across the rising titration (Figure 6.14), with approximately 90% of cells expressing mRuby2 from the empty vector at the highest titre assessed (20µl neat virus preparation). By contrast, the vector containing the VH#576-tag-YFP cassette showed a significantly lower transduction

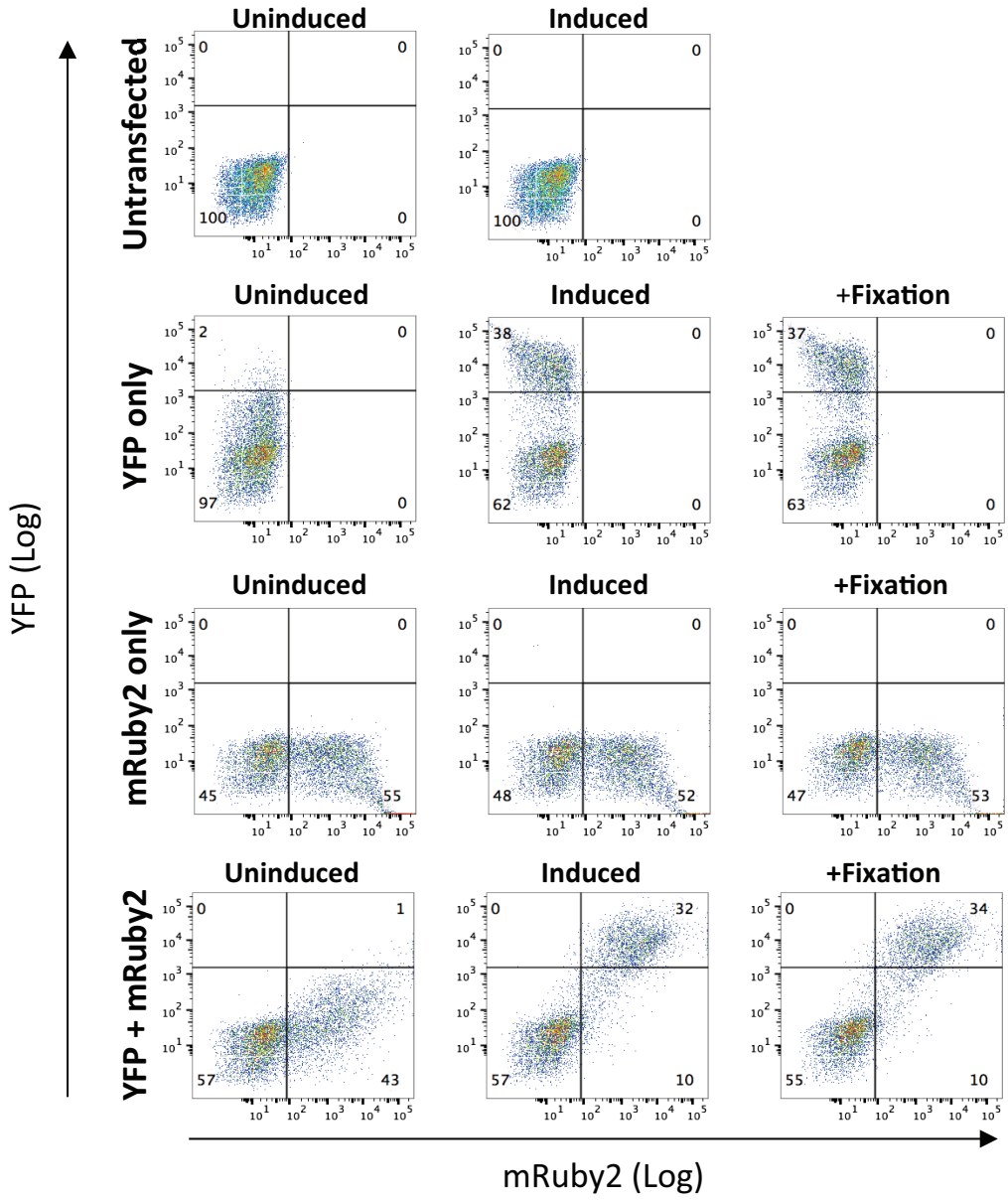

Figure 6.12 mRuby2 lentiviral vector expression test

Initial testing of the cloned commercial lentiviral vector (pLVX-TetOne) modified to express constitutive mRuby2 reporter protein and the inducible YFP cassette. Plasmids were transiently transfected into HEK293T cells, with (induced) and without (uninduced) the addition of 1µg/ml Tetracycline for YFP expression. Analysis of reporter expression was performed 48 hours after transfection. Single reporter versions of the construct were transfected as colour controls, and used to define quadrant gate settings. The lentiviral vector showed constitutive mRuby2 expression and Tetracycline-inducible YFP expression with double fluorescence positive cell population clearly visible. The effect of paraformaldehyde fixation (+Fixation) was tested and found to have no effect on fluorescence quenching.

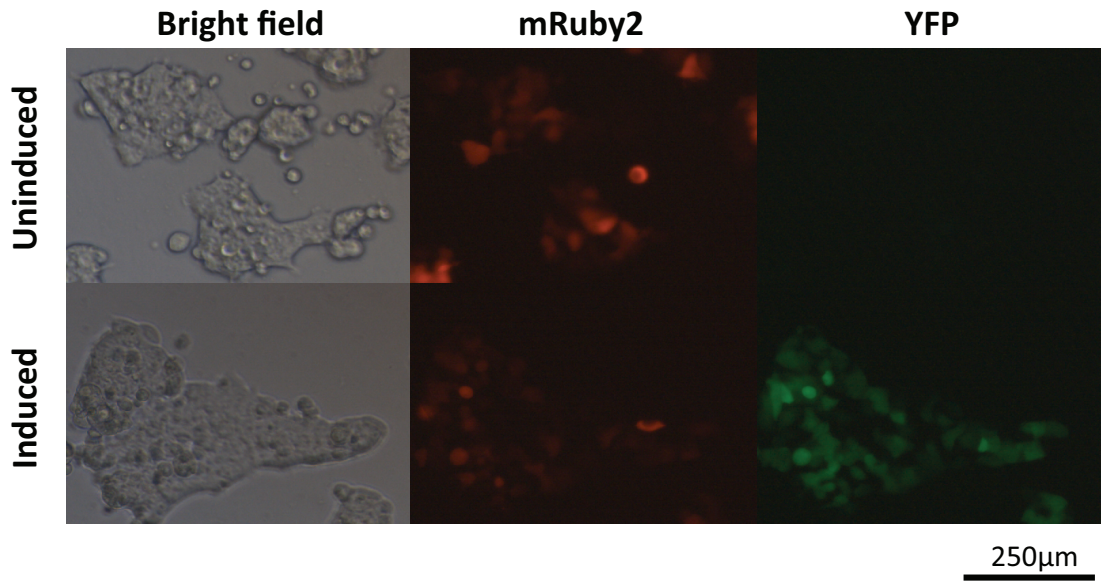

Figure 6.13 Fluorescent images of lentiviral reporter expression

Fluorescence microscope images of the cloned commercial lentiviral vector, pLVX-TetOne, modified to express constitutive mRuby2 reporter protein and the inducible YFP cassette. Plasmids were transiently transfected into HEK293T cells, with (induced) and without (uninduced) the addition of 1µg/ml Tetracycline for YFP expression. Analysis of reporter expression was performed 48 hours after transfection, by visualising cells for mRuby2 expression (td-tomato filter, 546/22nm excitation, 590/23nm emission) and for YFP expression (YFP filter, 500/20nm excitation, 535/30nm emission). The vector showed constitutive mRuby2 expression and Tet-inducible YFP expression. YFP was not visible without Tet induction.

efficiency at the same volume of preparation, with only 35% of cells mRuby2 positive, indicating differences in viral titres of the two plasmid preparations. Fluorescence levels were background corrected and converted to a virus concentration of Transducing Units (TU) per ml. The averaged readings across the titres tested show a linear correlation. This was used to calculate the volume of virus preparation required for a multiplicity of infection (MOI) of 5 particles per cell.

The infection potential of the recombinant viruses were tested on Jurkat, KOPT-K1 and MOLT4 T cell lines. These cell lines were transduced according to the same protocol, at an MOI of 5. Cells positive for mRuby2 expression were bulk sorted by flow cytometry (Figure 6.15). Despite correcting for virus concentration, cell line differences in transduction efficiency were noticeable; Jurkat were most readily transduced, with over twice the number of mRuby2 positive cells resulting from infection with the empty vector virus compared with the vector containing the VH#576-tag-YFP cassette. A similar transduction ratio was observed between the two viral vectors when assessed in MOLT4 and KOPT-K1 cells, albeit at a lower efficiencies.

Fluorescence sorted cells corresponding to negative and positive mRuby2 populations were cultured for expansion. The expanded sorted cell populations were assessed for continued mRuby2 expression at five to eight weeks post transduction (Figure 6.16). Fluorescence was maintained in the Jurkat positive-sorted samples, with both viral vectors showing a peak fluorescence intensity around 2 logs higher than that of the negative-sorted samples. Some mRuby2 expression persisted in the KOPT-K1 positive-sorted sample, although no expression above that of the negative-sorted samples was detected when analysing the MOLT4 populations, despite both sorted fractions possessing some fluorescence compared with the untransduced control. The flow cytometry data was confirmed by RT-PCR of mRuby2 cDNA (Figure 6.17). Interestingly, the negative-sorted populations of each cell line were

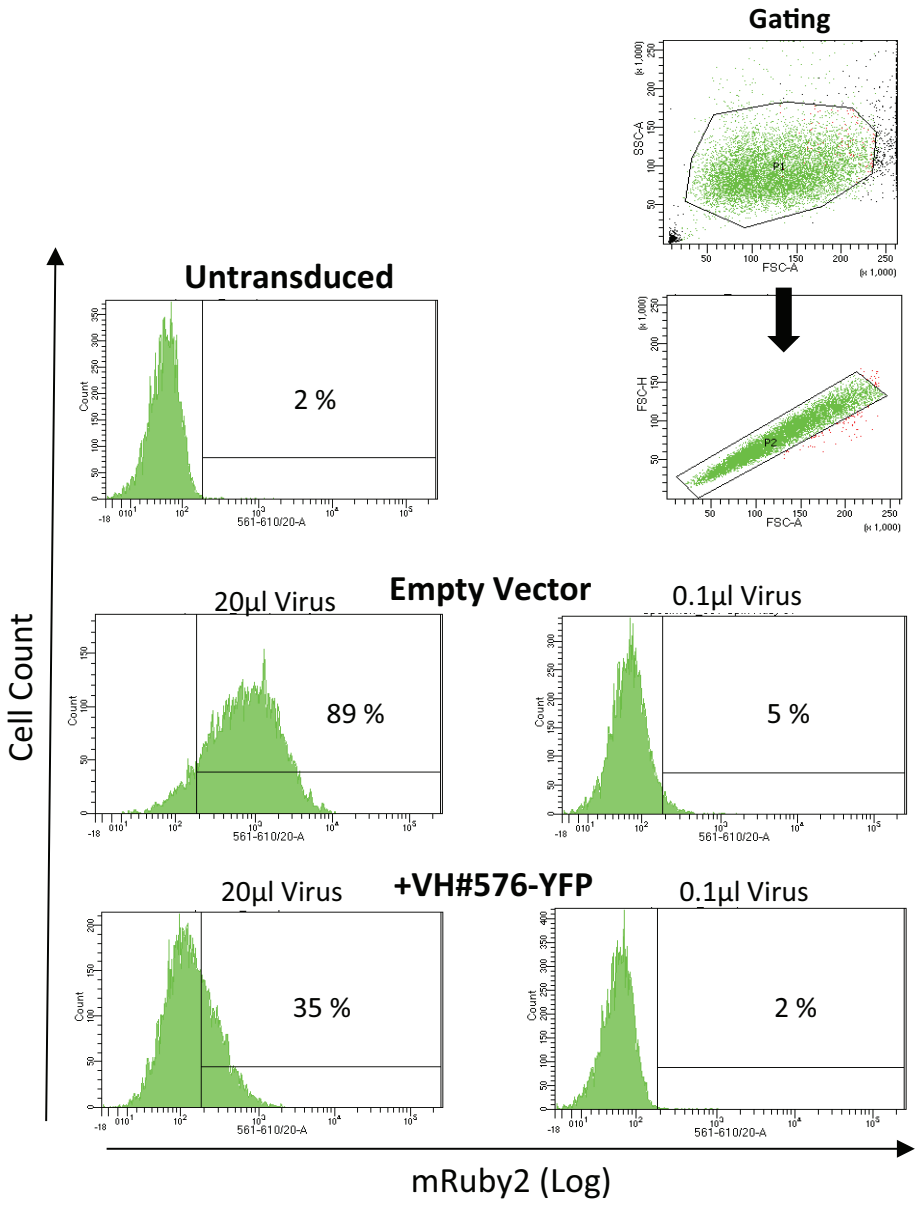

Figure 6.14 Titration of lentivirus-like particles into HEK293T cells

Lentivirus preparations of pLVX-TetOne-Ruby (empty vector) and pLVX-TetOne-Ruby-FLAG-VH#576-P2A-YFP (+VH#576-YFP) were tested for transducibility and calculation of viral concentration by titration of transduction into HEK293T cells. Volumes of neat virus ranging from 0.1 to 20µl were used to infect cells (the 20µl and 0.1µl transductions are shown). After 48 hours, transduction efficiency was monitored by flow cytometry for mRuby2 fluorescence. The proportion of fluorescent cells resulting at each titre was used to calculate the number of viral transducing units (TU). The empty vector has a concentration of 1.7 x 10^8 TU/ml, whilst that of the +VH#576-YFP vector was calculated to be 1.1 x10^7 TU/ml. A higher fluorescence intensity was observed with the empty virus preparation than with the +VH#576-YFP preparation at comparable virus volumes, indicating a more concentrated viral preparation.

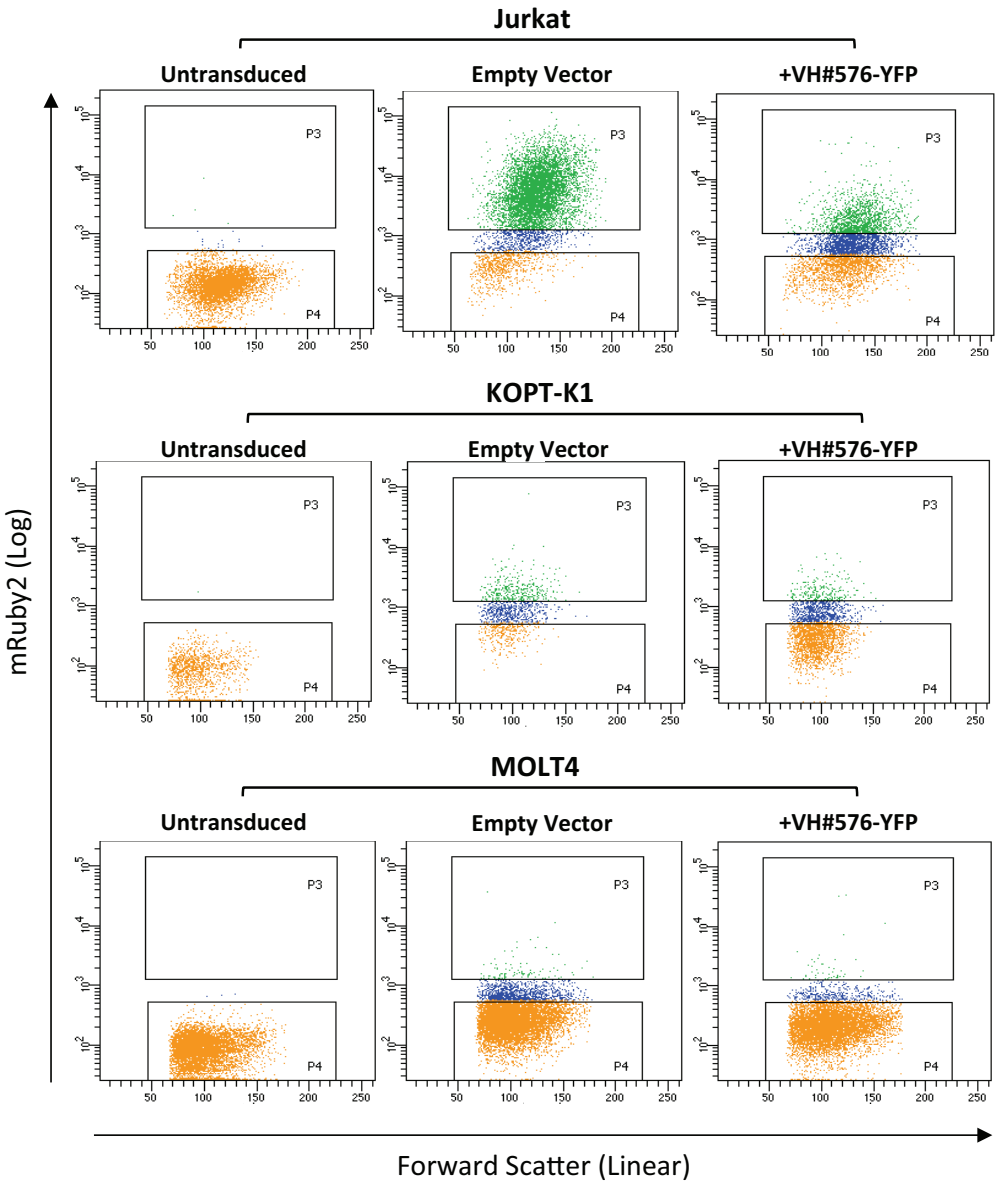

Figure 6.15 Lentiviral transduction of T cell lines

Packaged lentivirus preparations of pLVX-TetOne-Ruby (empty vector) and pLVX-TetOne-Ruby-FLAG-VH#576-P2A-YFP (+VH#576-YFP) used to transduce T cell lines at a multiplicity of infection (MOI) of 5 particle per cell. Cells expressing mRuby2 were bulk sorted by flow cytometry 48 hours after transduction (shown as a green highlighted dot plot in the 'P3' upper box gate). Cells negative for mRuby2 expression (lower box gate, orange dot plots) were also bulk sorted. The efficiency of transduction was monitored by flow cytometry for mRuby2 fluorescence. A higher fluorescence intensity indicated a greater transduction efficiency with the empty virus preparation than with the +VH#576-YFP preparation despite titration of the virus concentration. Similarly, the different cell lines possessed different level of transducibility, with Jurkat having the highest proportion of mRuby2 positve cells, and MOLT4 transductions the lowest number of transductants.

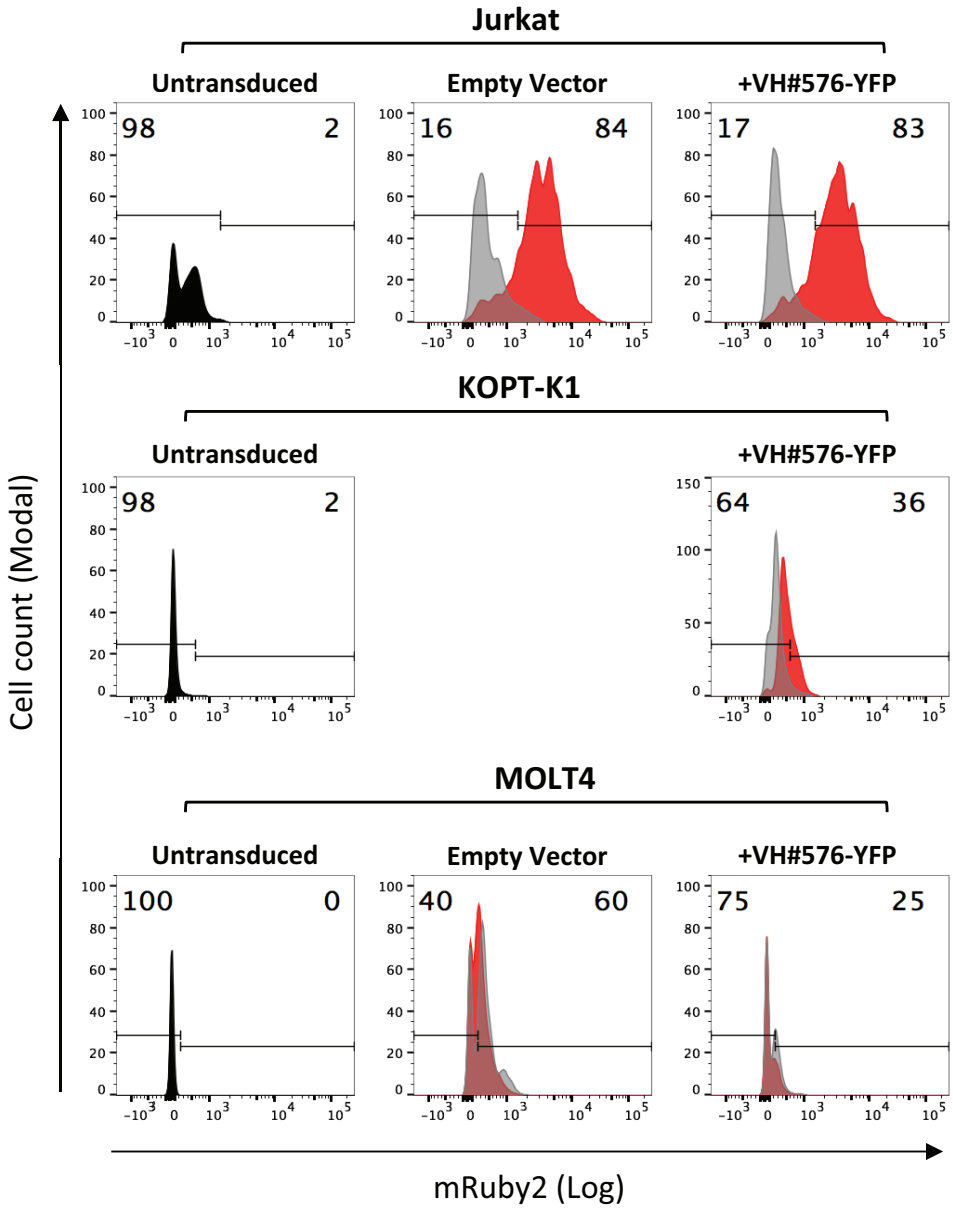

Figure 6.16 Assessment of long-term mRuby2 expression

The lentiviral transduced T cell lines that were sorted by flow cytometry (see figure 6.15) were assessed for continued constitutive mRuby2 expression. The bulk sorted mRuby2-positive and negative samples were expanded over four weeks and then examined for the reporter. Overlaid univariate intensity plots represent the intensity of the fluorescence detected, with red traces denoting the positive sorted cells, and grey traces the negative sorted samples. The black single traces show the untransduced control sample used for applying the mRuby2 gate. Jurkat cells showed prolonged constitutive reporter expression. The KOPT-K1 cells transduced with the empty vector virus could not be maintained. Some mRuby2 expression was noted in the MOLT4 negative sorted sample, to a level equivalent with the positive sorted cells.

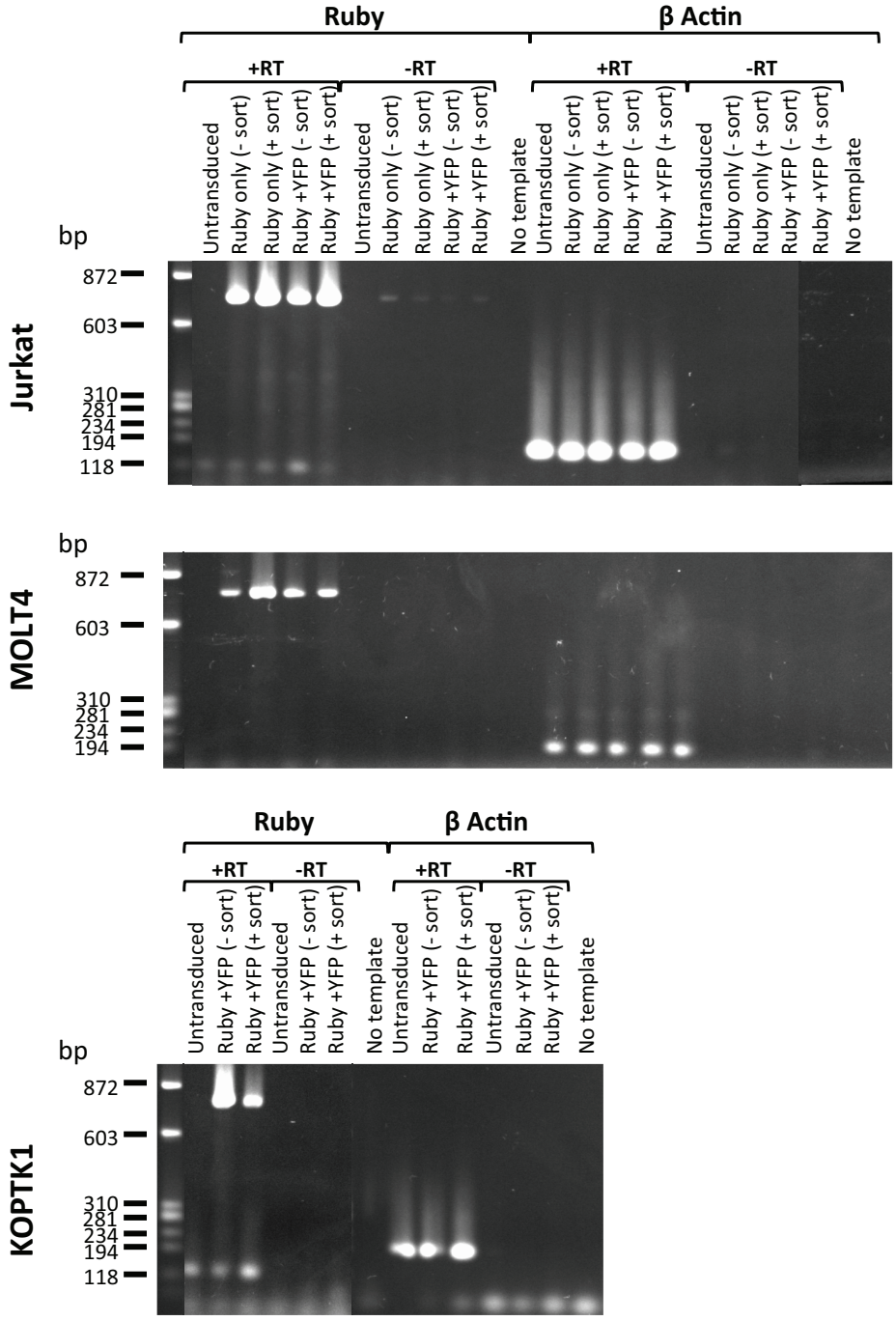

Figure 6.17 RT-PCR confirmation of mRuby2 expression

RT-PCR confirmation of mRuby2 expression in the lentivirus transduced sorted cell samples (positive and negative) was performed following the fluorescence signals seen in fig 6.16. RNA from the Jurkat, KOPT-K1 and MOLT4 samples was extracted and converted to cDNA by reverse transcription (+RT). No reverse transcription (-RT) control samples were produced for all samples. The cDNA sets were PCR amplified with mRuby2 and β-actin primer pairs, and the product visualized on a 1.5% TBE gel. The expected product sizes were 700bp (mRuby2) and 200bp (actin cDNA, 300bp for genomic DNA). Expression of the mRuby2 reporter is strong across all samples, including the transduced, fluorescent negative sorted samples. The no reverse transcriptase (-RT) controls are clear, except form some slight genomic DNA contamination in the Jurkat mRuby2 amplification and the MOLT4 actin amplifications. Amplification of β-Actin as a control amplicon is present at the expected across all +RT samples.

positive for the mRuby2 PCR product indicating mRNA expression in these cells but with YFP expression below the fluorescence threshold.

6.7 Discussion

This chapter presents the development of a strategy to test the AIDA system further. This has involved setting up a suitable system for the in vitro culture of leukaemic T cells, and a method for introducing the AIDA constructs into T cell tumours and cell lines.

Tumour cell lines have proved to be extremely useful and convenient disease models in the search for anti-cancer agents (Goodspeed et al., 2016). However, debate continues as to how accurately the common cell lines represent clinical disease (Gillet et al., 2011). Despite their transformed status, mouse and patient T cell tumours require factors derived from a host organism to propagate successfully although this may be overcome with careful medium selection. Transplantation can be a stochastic procedure, certainly with regard to the incubation period, and performing experiments in statistically significant numbers can be a challenge, particularly when trying to keep replicates to a minimum for ethical and welfare concerns. Typically, *in vitro* T cell growth experiments are performed with normal thymic progenitors, to delineate the differentiation process. Differentiation of tumourigenic T cells is not desirable in this culture setting, as the model should replicate the initial disease as faithfully as possible. The approach undertaken in this chapter was therefore to investigate if tumourigenic T cells, derived from both a mouse model of *Lmo2*-induced leukaemia and clinical patient samples, could be maintained without significant perturbation of their differentiation status. The use of the OP9-DL1 co-culture system alongside the enriched IMDM medium containing IL-2 and IL-7 supported both tumour types.

It was interesting to note that in this study the mouse tumour identified as being at the DN1/DN2 stage transition. This is unusual, as most *Lck-Lmo2* tumours

have been defined at the DN2/DN3 stage transition (Ruggero et al., 2016). This reflects the heterogeneity of the tumours, and highlights their mimicking human disease patterns. During assessment of the T-ALL samples, it was found that both H1 and 4P co-expressed CD44 and CD8 (Figure 6.10). Initially this seemed at odds with the normal T cell maturation process, which progresses through the DN stages where CD44 expression becomes down regulated, and culminates in expression of either CD4 or CD8 on the mature T cell surface. However, there are reports of CD44-expressing CD8-positive memory cells and CD4-positive helper cells being a regular biological phenomenon (Baaten et al., 2010a), with CD44 possibly aiding evasion of apoptosis through sequestration of FAS ligand (Baaten et al., 2010b). Indeed, normal expression profiles do not necessarily apply to transformed cells, and therefore this may simply be an artefact of their abnormal status.

Transfection of T cells is challenging. Viral transduction by lentivirus-like particles allow transduction of genetic material into dividing and quiescent cells. Moreover, nuclear targeting and host genome integration of the virus ensures long-term expression of the transgene cassette. Therapeutic lentivirus preparations are applied *ex vivo* for haematopoietic lineage gene correction, as exemplified by the X-SCID gene therapy trials (Hacein-Bey-Abina et al., 2002), which highlights the suitability of these viral particles for use as efficient transgene delivery mechanisms to blood cell malignancies. The project necessitated temporal control over AIDA protein expression, which required use of the 'TetOn' system (Gossen et al., 1995). Because of the difficulty in T cell transfection, a virus particle encoding both the AIDA constructs and the tetracycline reverse transactivator protein was sourced. Addition of a constitutively expressed fluorescent reporter was added as a transduction control (mRuby2). This allowed monitoring of plasmid uptake and expression prior to induction of the tetracycline-responsive cassette. For subsequent testing of AIDA in T cell leukaemis, this will be invaluable. The virus was successful in transducing T cell lines, although the efficiency varied. Moreover, although slight leakiness was

detected, tetracycline-dependent high-level expression of the YFP reporter was observed. Long-term expression of the mRuby2 reporter was also apparent, detectable by RT-PCR after 5-8 weeks of culture, even in apparently mRuby2-negative cells. As transduction was only investigated at an MOI of 5, increasing the viral titre applied to the cells may overcome this and should be investigated by further optimisation.

The results outlined in this chapter indicate that a simple culture method of these tumours is possible, certainly for one week, with continued growth potential remaining for up to three weeks. Furthermore, the T cell differentiation markers investigated continued to be expressed, with minimal phenotypic alterations observed. It also allows monitoring of the AIDA effect in real-time, which would not be possible in an *in vivo* model system. Furthermore, the 'TetOn' lentivirus construct which incorporates two fluorescence reporter proteins, has shown efficacy in preliminary testing. The culture and transduction mechanisms discussed in this chapter therefore represent a facile approach for subsequent testing of AIDA in T-ALL.

6.8 Conclusion

The methods developed in this chapter provide a framework around which the efficacy of AIDA against two common oncogenes implicated in human T-ALL may be tested. Sustained *in vitro* culture of human-derived tumour samples has been demonstrated, and a temporally-controlled lentiviral expression vector has been designed that, with subsequent modification and optimisation, will likely permit expression of the AIDA constructs in the tumour samples.

Chapter 7 General discussion and future work

7.1 General Discussion

This thesis details the successful implementation of a novel method of cancer cell killing, targeted toward a specific oncogenic protein in a human tumour cell line. The work herein builds upon the first description of this method (Tse and Rabbitts, 2000), where AIDA was executed in the CHO cell line against the bacterial protein β-Galactosidase as the antigen, with proCASP3-linked scFv raised against it. The work detailed in this thesis now shows the suitability of the AIDA system against a relevant human oncogene, in this case mutant RAS, in a human cancer cell line possessing the NRAS Q61K mutation. Moreover, this adaptation of the AIDA system employs two separate VH and VL single domain antibodies, both of which specifically bind to mutant RAS protein at close epitopic regions. This close binding of both VH and VL likely recapitulates the fold of the scFv the fragments derive from, permitting antigen binding dependent, proximity-induced auto-activation of their fused proCASP3 chains. Moreover, we show direct evidence of apoptosis occurring from this system, which initiates from the antigen-bound VH- and VL-proCASP3 fusion proteins.

This thesis also introduces a novel method for isolating complementary VL fragments in mammalian cells for translation of the AIDA system toward other clinically relevant human oncogenes, with a focus on LMO2 in T-ALL. Furthermore, a strategy for testing of AIDA in primary human tumour samples has been proposed.

7.1.1 The AIDA System targeting mutant RAS

The data derived from the VL Only and non-binding VH (VHmut) clone expression demonstrate that the presence of the proCASP3 fusion proteins are not deleterious to the cell per se, despite the localised concentration imparted by the membrane targeting. This reiterates previous studies, which show cellular overexpression of CASP3 produces no effect unless it becomes activated (MacCorkle et al., 1998, Yamabe et al., 1999).

The potency with which VH#Y6 inhibits RAS signalling made assessment of the higher affinity VH-proCASP3 element challenging to confirm. Alongside the previous *in vivo* findings showing that VH#Y6 causes reduced tumour growth and prevents mutant RAS induced tumour formation (Tanaka et al., 2007, Tanaka and Rabbitts, 2010a), the data presented in this thesis confirms the cytostatic effect of VH#Y6. Meaningful evidence of apoptosis resulting from VH#Y6 binding (without VL#204 binding) was not found, despite having the apoptotic pro-enzyme attached. Moreover, cessation of VH-proCASP3 expression reverts the cells to normal growth patterns. This reflects earlier assertions that malignant growth can be prevented by RAS inhibition, but that it is not sufficient to destroy the tumour (Tanaka and Rabbitts, 2010a).

Overt apoptosis was only apparent in the VH+VL clones, indicating that the hypothesised requirement of both VH-proCASP3 and VH-proCASP3 for cancer cell destruction was correct. Owing to the normal scFv structure having a stabilising interaction between the exposed hydrophobic regions of the VH and VL domains (Worn and Pluckthun, 1998, Rothlisberger et al., 2005), and the Fab VH:VL interaction comprising mostly framework β-strand interaction with some CDR residue interactions (Chothia et al., 1985), the possibility of antigen independent VH:VL interaction was investigated. The inability of RAS-less cells to grow in culture (Drosten et al., 2010) without compensation from mutant downstream effectors necessitated the use of reduced and no affinity mutants to act as ‘no antigen’ equivalent controls. These controls verified antigen binding as an obligatory step in single domain AIDA. Furthermore, the absence of apoptosis deriving from expression of the VH+VL catalytic CASP3 mutant proteins demonstrates the observed cell death is not initiated as bystander effect of RAS inhibition.

With up to 20% of T-ALL cases possessing NRAS or KRAS mutations (Girardi et al., 2017, Neri et al., 1988, Browett and Norton, 1989), mutant RAS represents an important clinical target for T-ALL therapies. The anti-RAS AIDA that

has been developed in this thesis is therefore a promising and relevant potential therapy for mutant RAS-bearing T-ALL, particularly given the current lack of targeted small molecule drug therapies. The challenge encountered with this system was the anti-RAS antibodies recognising wildtype, active (GTP-bound) RAS in addition to the constitutively GTP-bound mutant forms. This could be overcome by screening for further single domain antibodies in the search for mutation-specific binders, although these have so far proved elusive, and may be impossible to isolate. However, the anti-RAS VH and VL pair demonstrates such high efficacy that their use would be preferred. In this case, targeting specific tumour cell delivery would be an alternative to preventing widespread RAS inhibition by the AIDA system (discussed further in section 7.1.5). Moreover, as RAS mutations exist in up to 30% of all human cancers, AIDA could be an applicable approach to treat a range of malignancies. However, as this preliminary work has only been shown in one cell line, further testing of the AIDA system across a panel of mutant RAS positive cancer cell lines would be required to understand whether this is feasible.

7.1.2 Developing AIDA against LMO2

LMO2 is also a T-ALL oncogene, whose aberrant expression is implicated in approximately 50% of cases. Despite its oncogenicity being well documented (Hacein-Bey-Abina et al., 2003b, Hacein-Bey-Abina et al., 2003a, Hacein-Bey-Abina et al., 2008, Fisch et al., 1992, Larson et al., 1994), there are currently no approved LMO2-specific anti-cancer therapies. LMO2 is therefore another candidate oncogene for the development of novel, targeted T-ALL therapies. As LMO2 is not normally expressed in T cells (Foroni et al., 1992, Neale et al., 1995, Kenny et al., 1998), except for some low expression in early DN1 thymic progenitors (Herblot et al., 2000), it represents an excellent target for oncogene-activated tumour cell killing by AIDA and would obviate the difficulties encountered in the RAS AIDA model. The anti-mutant RAS AIDA has acted as a paradigm of a potential anti-LMO2 T cell

leukaemia killing method. With successful deployment of AIDA against mutant RAS, the translation of the method toward LMO2 began. This was a multi-faceted approach, involving the generation of methods for T cell modelling and isolation of an LMO2-specific VL fragment.

Testing of anti-LMO2 AIDA as an T-ALL therapy would be advantageous if performed in cellular models closely resembling the clinical disease. Growth of mouse model tumours or clinically derived primary tumour samples *in vitro* presents an opportunity for reproducible and fast high throughput analysis. Furthermore, *ex vivo* tumour growth would allow real-time analysis of AIDA, rather than only endpoint studies. Several methods of *in vitro* tumour growth exist. Thymic organoid cultures provide a short-term culture method (Nitta et al., 2013), but require a high-level of technical skill as well as animal involvement. Novel cancer cell lines may be established from these primary tumours to obviate the need for *in vivo* studies, although this reintroduces the debate as to whether the procedure and continued propagation has altered the cell genotype and phenotype. However, this argument also applies to xenograft experiments where changes to the heterogeneity of the original tumours may be introduced (Wilding and Bodmer, 2014) and so a compromise would be the determination of appropriate culture conditions to favour short-term tumour culture. Specialised culture conditions are common in the study of thymocyte development (Zuniga-Pflucker, 2004), but not with regard to leukaemic cell growth for therapeutic testing. In this thesis, successful short-term (three week) co-culture of the mouse tumour and half of the human leukaemias with stromal OP9-DL1 cells was achieved, with no detected deviation from their normal phenotype.

In addition, a system was initiated for introduction of the AIDA fusion proteins in a temporally-controlled manner. Thymocytes are typically difficult to transfect, although replication incompetent lentivirus-like particles are capable of transducing dividing and quiescent cells (Zufferey et al., 1998) for stable integration of the vector into the host cell genome. Development of a lentiviral expression vector with

temporal control and dual fluorescence reporter monitoring has been achieved, with transduction efficacy demonstrated in the T cell lines. However, reporter expression was stochastic across those samples infected with the recombinant virus, although mRNA was detectable. Further studies with increasing MOIs may circumvent this. For future application, it may be advantageous to consider commercial electroporation methods that have been developed for T cell transduction (Chang et al., 2017, Chicaybam et al., 2013).

Furthermore, a novel method for screening and isolating a VL fragment with a complimentary epitope to the anti-LMO2 VH#576 has been conceptualised, with initial findings suggestive of it being a suitable approach although this remains to be proven with further experimental work. The tripartite GFP reconstitution screening method reproduced the binding affinities of the VH and VL pairs tested. The fluorescence intensity resulting from true binding interactions may be enhanced by co-expression of an anti-GFP camelid VH domain (V_HH) (Koraichi et al., 2018). This V_HH (Kirchhofer et al., 2010), which alters the GFP absorption spectra, may also act to stabilise the reconstituted GFP, and therefore increase sensitivity of the intracellular antibody screening method. Similarly, recently published work has used split luciferase reconstitution linked to antibodies and DARPins for immunoassay applications, requiring two molecules to bind the antigen to detect proteins at very low (picogram) quantities (Dixon et al., 2017), supporting the applicability of the tripartite GFP screening method developed within this thesis.

These methods provide a framework system for both continuation of the search for LMO2-specific fragments and induction of AIDA in the treatment of leukaemia.

7.1.3 AIDA against other oncogenic targets

It is possible that AIDA may have wide-reaching applicability with respect to other tumour types and their oncogenes. Oncogenic fusion proteins represent an

alternative target protein for AIDA, whereby two single domain antibodies spanning the fusion junction could be used. The chimaeric fusion proteins resulting from chromosomal translocations would never be encountered within a normal cell and thus would be excellent targets for the AIDA system. Examples of blood cancer fusions include the Philadelphia chromosome translocation t(9;22)(q34;q11) producing the BCR-ABL fusion in chronic myeloid leukaemia (CML) (Rowley, 1973, Nowell and Hungerford, 1960, de Klein et al., 1982, Heisterkamp et al., 1983, Heisterkamp et al., 1982). The ABL domain imparts aberrant tyrosine kinase activity, which has been successfully treated with tyrosine kinase inhibitors. However, therapeutic resistance has emerged (O'Hare et al., 2007), providing a rationale for additional targeted therapies. MLL translocations at 11q23 are found in ALL and AML, which links the methyltransferase activity of MLL to transcriptional activation domains of fusion partner such as AF4, AF9 and ENL. These translocations are found in up to 50% of infant ALL and 10% of paediatric and adult AML cases (Liu et al., 2009). Methyltransferase inhibitors are widely used but suffer with low stability in the blood and high toxicity (Pechalrieu et al., 2017). Non-haematopoietically restricted translocations include those involving another tyrosine kinase, ALK. EML4-ALK fusions have been detected in non-small cell lung cancers (Soda et al., 2007) whilst NPM-ALK fusions are found in non-Hodgkin lymphoma (Morris et al., 1994). Kinase inhibitors are employed as treatments but resistance mutations occur as seen with BCR-ABL (Rothenstein and Chooback, 2018). Therefore, the use of AIDA within drug-resistant tumours could be advantageous, particularly those possessing an oncogenic fusion protein, subject to isolation of appropriate single domain antibodies. Moreover, upon advances in targeted tumour cell delivery, AIDA could offer advantages over the systemic toxicity generated by these inhibitors.

7.1.4 Potential Improvements to AIDA

Reflection on the work detailed in this thesis has identified some key areas which may lead to improvements with the AIDA system. The RAS inhibition effect was caused by the VH preventing active RAS signalling. This implies that future AIDA target antigens may benefit from VH and VL fragments binding to epitopes that are not critical for protein function. Of course, in the context of aberrantly expressed oncogenic proteins, such as LMO2, this would be less important. But for mutated, ubiquitously expressed proteins such as the RAS family, it remains a potential development.

The anti-RAS VH#Y6 has a very high affinity for RAS. This means that an efficient Fv formation at the antigenic determinant site was possible. If VH fragments with lower affinity are developed, the use of a second VH in place of the VL fragment may be worthwhile, for an scFv-like fold. Whilst VH:VH interaction is rare, and may not strictly be required if binding of both VH fragments was non-competitive, VH dimerisation could be selected for with particular residue changes (Baral et al., 2012). Alternatively, two camelid V_HH antibodies, which do not self-aggregate due to their natural monomeric state, may impart the advantage of possessing longer CDR3 loops for antigen cleft penetration, although this same CDR region is implicated in maintaining their structure and so full CDR3 randomisation may be detrimental (Barthelemy et al., 2008). Although this would not abide by the principle of a VH and VL antibody fragment, it would still require formation of a ternary complex, and may hold the advantage of expediting fragment isolation if only antigen-specific VH fragments were necessary.

Modulation of the catalytic activity of CASP3 may be another area of improvement to the system. Combinatorial VH:VL pairs with lower target affinities than that of the anti-RAS pair may benefit from a more efficient enzymatic function, achieved by altering protein solvation (Maciag et al., 2016). Conversely, CASP3 moieties with reduced catalytic potential may improve the safety profile of the AIDA

system, and may also be useful in the purification of the AIDA fusion proteins for *in vitro* testing. However, the efficiency with which AIDA initiates is unknown, and may depend upon the individual characteristics of the single domain fragments. For this, a cell-free assay using recombinant proteins could provide stoichiometric determination of the VH/VL-proCASP3 concentrations required and corresponding catalytic activities generated. Evidence for the literature suggests that isolation of inactive proCASP3 zymogen is difficult (Mittl et al., 1997, Ryser et al., 1999, Fernandes-Alnemri et al., 1994). In this study, there was some success in purifying full-length VH/VL-proCASP3 proteins, possibly due to the presence of the antibody domains acting as a solubility tag. However, the process was largely inefficient, certainly when compared with the RAS purification. This method could be revisited with the reduced catalytic CASP3 (Maciag et al., 2016). Alternatively, some insight may be gained through transfection of defined quantities of *in vitro* transcribed mRNA (IVT-mRNA) (Sahin et al., 2014) or with viral transduction at low MOI.

7.1.5 AIDA as a clinical therapy

The major barrier to therapies like AIDA is their delivery and uptake by the tumour cells over their normal, healthy counterparts. The direct targeting of AIDA to tumour cells was not part of the work presented in this thesis. Instead the aim was to develop the technology. However, this is a very important aspect for the future viability of the technology, and it is therefore discussed below. This problem also hinders the application of all intracellular and gene replacement therapies. As such, the goal of many research laboratories worldwide is to develop efficient and safe modalities for these types of therapies to achieve mainstream clinical use.

The work presented in this thesis was directed toward developing a novel treatment of T-ALL. Both oncogene targets investigated have been implicated in T-ALL, but also in other cancers. Oncogenic mutations in the RAS family of small GTPases are particularly commonplace, having been found in up to 30% of all

malignancies. These include other blood cancers, such as myeloid leukaemias and multiple myeloma (Reuter et al., 2000), but also solid tumours, including colorectal and pancreatic cancers (Prior et al., 2012, Bos et al., 1987, Nakata et al., 2009). Leukaemia is typically easier to access, certainly from a cell targeting viewpoint,as they tend not to form masses. Solid tumour penetration is more difficult to achieve, although the tumour blood vessel network provides an access point for intravenously delivered therapeutics. However, tumour neovascularisation can produce abnormal vessels (Vaupel et al., 1989), and penetration from the blood vessel network through to the inner tumour mass may be challenging (Jain, 1990), with increasing size of therapeutic particle reducing the efficiency of tumour permeation (Dreher et al., 2006) although large molecules including therapeutic monoclonal antibodies can penetrate tumour masses. However, additional considerations include the efficiency with which the AIDA transfer vectors are taken up by the cell, and the efficiency with which the AIDA proteins are actively expressed.

AIDA would require only transient expression of the VH- and VL-proCASP3 proteins for induction of antigen-dependent apoptosis. Therefore, long-term gene expression that is only viable through stable integration of the therapeutic agent is not required. This obviates the need for use of genome integrating vectors, such as the lentivirus-like particles, which are often transduced *ex vivo* to the target cells in clinical use. This enhances the safety aspect of AIDA therapy considerably, given the occurrence of leukaemia following retroviral gene therapy in the X-SCID trials (Hacein-Bey-Abina et al., 2008).

Viral delivery methods resulting in episomal maintenance of the therapeutic genetic material include adenovirus and adeno-associated virus (AAV) based particles (Lee et al., 2017). These vectors have a safe history of use and, like the lentiviral vectors, are non-replicative, meaning spread of therapeutic virus beyond first infection is impossible. Use of naturally occurring serotypes not prevalent in the population lessens attenuating host immune reponses and side-effects, although

repeat administration of the same virus may lead to an inflammatory response. The viruses can infect a wide range of cell and tissue types, although certain virus serotypes have enhanced tropism toward particular locations, with capsid engineering being employed to direct cell-specific targeting (Kotterman and Schaffer, 2014). Redirection of tissue tropism is often investigated by directed evolution of the capsid proteins whereby regions of a coat protein are randomised and selected for *in vitro* (Perabo et al., 2003). An alternative development is the use of affinity molecules grafted into the capsid structure. DARPins (Munch et al., 2013) and scFv (Hedley et al., 2006) have been incorporated into projected domains on the coat proteins of AAV and Adenovirus respectively, which do not interfere with normal capsid assembly. This could therefore be expanded to include single domain antibodies, which are of a similar size to DARPins. However, the identification of target-specific cell surface molecules to assist in virus entry would be vital in achieving cell tropism. A method developed within the laboratory of combining subtractive RNA sequencing data with predicted cell surface protein expression has identified cancer cell line-specific molecules that could act as therapeutic targets (Town et al., 2016). Moreover, a more accessible approach could be to compare the expression profiles of cell lines. These methods could therefore be widely employed to discover other tumour-specific membrane proteins to aid the development of targeted viral delivery systems.

An interesting development on simply using a virus as a method of introducing the nucleic acid encoding the AIDA constructs would be to use AIDA as part of an ‘armed’ oncolytic virus (Seymour and Fisher, 2016). Oncolytic viruses were first created to provide a method of tumour killing as part of the natural lytic phase of the viral life cycle (Bischoff et al., 1996) although recently the idea that the lysis of cancer cells primes the immune system to ‘see’ the tumour, almost as type of vaccination following the release of tumour cell contents into the tissue environment (Seymour and Fisher, 2016). These viruses possess deletion of key genes, meaning that virus replication is conditional on certain cancer-causing mutations such as p53

inactivation. This conditional replication would therefore permit localised spread of the therapeutic virus within tumours, sparing normal tissue. Despite being well-tolerated clinical trials, the oncolytic viruses are less potent than desired (Bauzon and Hermiston, 2012, Parato et al., 2005). The concept of 'armed' oncolytic viruses was to therefore raise their efficiency of cancer cell destruction. Typically this involves addition of a passenger gene to elicit additional effect, either directly inhibitory to the tumour (such as a pro-drug converting enzyme) or allowing enhancement of the immune system by expressing cytokines (Seymour and Fisher, 2016). Addition of the AIDA constructs to these viruses would form a complementary system of in-tumour virus spread, forgoing the need for multiple rounds of dosing, whilst potentiating cell death and immune cell detection of the tumour following the induction of apoptosis by AIDA or by the lytic phase of the viral life cycle.

Non-viral delivery methods are gaining momentum, with liposomes and nanoparticles showing improvements in cell targeting by incorporation of antibody-based or other affinity molecules into their structure (Hill et al., 2016). These particles would be particularly well suited to delivering *in vitro* transcribed mRNA as the therapeutic genetic material, with efficient encapsulation techniques (Sahin et al., 2014). Unfortunately, they are currently inefficient at endosomal release of their cargo, for which viral particles have evolved pH-dependent structural changes to disrupt the vesicle, although on-going improvements to these methods will no doubt ensure their future in clinical gene delivery (Stewart et al., 2016).

7.2 Conclusion

In conclusion, the AIDA technology described in this thesis offers a potential method of targeted cancer killing therapy. This system has been modelled on the successful destruction of tumour cells possessing RAS mutations, with a view to providing a targeted therapy for drug-resistant, LMO2-positive T-ALL. The work herein provides a strong basis for further development of LMO2-specific AIDA in T cell leukaemia. It

is envisaged that AIDA could be widely applicable to a range of tumour types subject to the identification of tumour-specific intracellular antigens. Upon advances in gene delivery systems, AIDA could be a rational approach to the elimination of human cancers, reducing the reliance on the current chemotherapeutic and radiotherapeutic treatment regimens.

References

ADAMS, G. P., SCHIER, R., MCCALL, A. M., SIMMONS, H. H., HORAK, E. M., ALPAUGH, R. K., MARKS, J. D. & WEINER, L. M. 2001. High affinity restricts the localization and tumor penetration of single-chain fv antibody molecules. *Cancer Res,* 61**,** 4750-5.

ADAMS, J. M. & CORY, S. 1991. Transgenic models of tumor development. *Science,* 254**,** 1161-7.

ADJEI, A. A. 2001. Blocking oncogenic Ras signaling for cancer therapy. *J Natl Cancer Inst,* 93**,** 1062-74.

AGULNICK, A. D., TAIRA, M., BREEN, J. J., TANAKA, T., DAWID, I. B. & WESTPHAL, H. 1996. Interactions of the LIM-domain-binding factor Ldb1 with LIM homeodomain proteins. *Nature,* 384**,** 270-2.

AKASHI, K., HE, X., CHEN, J., IWASAKI, H., NIU, C., STEENHARD, B., ZHANG, J., HAUG, J. & LI, L. 2003. Transcriptional accessibility for genes of multiple tissues and hematopoietic lineages is hierarchically controlled during early hematopoiesis. *Blood,* 101**,** 383-9.

ALLART-VORELLI, P., PORRO, B., BAGUET, F., MICHEL, A. & COUSSON-GELIE, F. 2015. Haematological cancer and quality of life: a systematic literature review. *Blood Cancer J,* 5**,** e305.

ALMASBAK, H., AARVAK, T. & VEMURI, M. C. 2016. CAR T Cell Therapy: A Game Changer in Cancer Treatment. *J Immunol Res,* 2016**,** 5474602.

AMYLON, M. D., SHUSTER, J., PULLEN, J., BERARD, C., LINK, M. P., WHARAM, M., KATZ, J., YU, A., LAVER, J., RAVINDRANATH, Y., KURTZBERG, J., DESAI, S., CAMITTA, B. & MURPHY, S. B. 1999. Intensive high-dose asparaginase consolidation improves survival for pediatric patients with T cell acute lymphoblastic leukemia and advanced stage lymphoblastic lymphoma: a Pediatric Oncology Group study. *Leukemia,* 13**,** 335-42.

APPERT, A., NAM, C. H., LOBATO, N., PRIEGO, E., MIGUEL, R. N., BLUNDELL, T., DRYNAN, L., SEWELL, H., TANAKA, T. & RABBITTS, T. 2009. Targeting LMO2 with a peptide aptamer establishes a necessary function in overt T-cell neoplasia. *Cancer Res,* 69**,** 4784-90.

ARBER, D. A., ORAZI, A., HASSERJIAN, R., THIELE, J., BOROWITZ, M. J., LE BEAU, M. M., BLOOMFIELD, C. D., CAZZOLA, M. & VARDIMAN, J. W. 2016. The 2016 revision to the World Health Organization classification of myeloid neoplasms and acute leukemia. *Blood,* 127**,** 2391-405.

ARCHER, V. E., BRETON, J., SANCHEZ-GARCIA, I., OSADA, H., FORSTER, A., THOMSON, A. J. & RABBITTS, T. H. 1994. Cysteine-rich LIM domains of LIM-homeodomain and LIM-only proteins contain zinc but not iron. *Proc Natl Acad Sci U S A,* 91**,** 316-20.

BAATEN, B. J., LI, C. R. & BRADLEY, L. M. 2010a. Multifaceted regulation of T cells by CD44. *Commun Integr Biol,* 3**,** 508-12.

BAATEN, B. J., LI, C. R., DEIRO, M. F., LIN, M. M., LINTON, P. J. & BRADLEY, L. M. 2010b. CD44 regulates survival and memory development in Th1 cells. *Immunity,* 32**,** 104-15.

BAER, R. 1993. TAL1, TAL2 and LYL1: a family of basic helix-loop-helix proteins implicated in T cell acute leukaemia. *Semin Cancer Biol,* 4**,** 341-7.

BAMFORD, R. N., GRANT, A. J., BURTON, J. D., PETERS, C., KURYS, G., GOLDMAN, C. K., BRENNAN, J., ROESSLER, E. & WALDMANN, T. A. 1994. The interleukin (IL) 2 receptor beta chain is shared by IL-2 and a cytokine, provisionally designated IL-T, that stimulates T-cell proliferation and the induction of lymphokine-activated killer cells. *Proc Natl Acad Sci U S A,* 91**,** 4940-4.

BARAL, T. N., CHAO, S. Y., LI, S., TANHA, J., ARBABI-GHAHROUDI, M., ZHANG, J. & WANG, S. 2012. Crystal structure of a human single domain antibody dimer formed through V(H)-V(H) non-covalent interactions. *PLoS One,* 7**,** e30149.

BARTHELEMY, P. A., RAAB, H., APPLETON, B. A., BOND, C. J., WU, P., WIESMANN, C. & SIDHU, S. S. 2008. Comprehensive analysis of the factors contributing to the stability and solubility of autonomous human VH domains. *J Biol Chem,* 283**,** 3639-54.

BAUZON, M. & HERMISTON, T. W. 2012. Oncolytic viruses: the power of directed evolution. *Adv Virol,* 2012**,** 586389.

BEGLEY, C. G., APLAN, P. D., DENNING, S. M., HAYNES, B. F., WALDMANN, T. A. & KIRSCH, I. R. 1989. The gene SCL is expressed during early hematopoiesis and encodes a differentiation-related DNA-binding motif. *Proc Natl Acad Sci U S A,* 86**,** 10128-32.

BENEDICT, W. F., WEISSMAN, B. E., MARK, C. & STANBRIDGE, E. J. 1984. Tumorigenicity of human HT1080 fibrosarcoma X normal fibroblast hybrids: chromosome dosage dependency. *Cancer Res,* 44**,** 3471-9.

BERNDT, N., HAMILTON, A. D. & SEBTI, S. M. 2011. Targeting protein prenylation for cancer therapy. *Nat Rev Cancer,* 11**,** 775-91.

BISCHOFF, J. R., KIRN, D. H., WILLIAMS, A., HEISE, C., HORN, S., MUNA, M., NG, L., NYE, J. A., SAMPSON-JOHANNES, A., FATTAEY, A. & MCCORMICK, F. 1996. An adenovirus mutant that replicates selectively in p53-deficient human tumor cells. *Science,* 274**,** 373-6.

BOEHM, T., FORONI, L., KANEKO, Y., PERUTZ, M. F. & RABBITTS, T. H. 1991a. The rhombotin family of cysteine-rich LIM-domain oncogenes: distinct members are involved in T-cell translocations to human chromosomes 11p15 and 11p13. *Proc Natl Acad Sci U S A,* 88**,** 4367-71.

BOEHM, T., GREENBERG, J. M., BULUWELA, L., LAVENIR, I., FORSTER, A. & RABBITTS, T. H. 1990. An unusual structure of a putative T cell oncogene which allows production of similar proteins from distinct mRNAs. *EMBO J,* 9**,** 857-68.

BOEHM, T., SPILLANTINI, M. G., SOFRONIEW, M. V., SURANI, M. A. & RABBITTS, T. H. 1991b. Developmentally regulated and tissue specific expression of mRNAs encoding the two alternative forms of the LIM domain oncogene rhombotin: evidence for thymus expression. *Oncogene,* 6**,** 695-703.

BORIACK-SJODIN, P. A., MARGARIT, S. M., BAR-SAGI, D. & KURIYAN, J. 1998. The structural basis of the activation of Ras by Sos. *Nature,* 394**,** 337-43.

BOROSS, P. & LEUSEN, J. H. 2012. Mechanisms of action of CD20 antibodies. *Am J Cancer Res,* 2**,** 676-90.

BOS, J. L., FEARON, E. R., HAMILTON, S. R., VERLAAN-DE VRIES, M., VAN BOOM, J. H., VAN DER EB, A. J. & VOGELSTEIN, B. 1987. Prevalence of ras gene mutations in human colorectal cancers. *Nature,* 327**,** 293-7.

BOSE, K. & CLARK, A. C. 2001. Dimeric procaspase-3 unfolds via a four-state equilibrium process. *Biochemistry,* 40**,** 14236-42.

BOURNE, H. R., SANDERS, D. A. & MCCORMICK, F. 1990. The GTPase superfamily: a conserved switch for diverse cell functions. *Nature,* 348**,** 125-32.

BROWETT, P. J. & NORTON, J. D. 1989. Analysis of ras gene mutations and methylation state in human leukemias. *Oncogene,* 4**,** 1029-36.

BROWN, J. M. & ATTARDI, L. D. 2005. The role of apoptosis in cancer development and treatment response. *Nat Rev Cancer,* 5**,** 231-7.

BUCKLEY, C. D., PILLING, D., HENRIQUEZ, N. V., PARSONAGE, G., THRELFALL, K., SCHEEL-TOELLNER, D., SIMMONS, D. L., AKBAR, A. N., LORD, J. M. & SALMON, M. 1999. RGD peptides induce apoptosis by direct caspase-3 activation. *Nature,* 397**,** 534-9.

CABANTOUS, S., NGUYEN, H. B., PEDELACQ, J. D., KORAICHI, F., CHAUDHARY, A., GANGULY, K., LOCKARD, M. A., FAVRE, G., TERWILLIGER, T. C. & WALDO, G. S. 2013. A new protein-protein interaction sensor based on tripartite split-GFP association. *Sci Rep,* 3**,** 2854.

CAVAZZANA-CALVO, M., HACEIN-BEY, S., DE SAINT BASILE, G., DE COENE, C., SELZ, F., LE DEIST, F. & FISCHER, A. 1996. Role of interleukin-2 (IL-2), IL-7, and IL-15 in natural killer cell differentiation from cord blood hematopoietic progenitor cells and from gamma c transduced severe combined immunodeficiency X1 bone marrow cells. *Blood,* 88**,** 3901-9.

CHAMBERS, J. & RABBITTS, T. H. 2015. LMO2 at 25 years: a paradigm of chromosomal translocation proteins. *Open Biol,* 5**,** 150062.

CHANG, S., ANDRONIKOU, N. & DU JEU, X. D. 2017. Optimization of Gene Editing in Human Primary T Cells with Neon (R) Transfection System. *Journal of Immunology,* 198.

CHELUR, D. S. & CHALFIE, M. 2007. Targeted cell killing by reconstituted caspases. *Proc Natl Acad Sci U S A,* 104**,** 2283-8.

CHEN, S., NAGEL, S., SCHNEIDER, B., KAUFMANN, M., MEYER, C., ZABORSKI, M., KEES, U. R., DREXLER, H. G. & MACLEOD, R. A. 2011. Novel non-TCR chromosome translocations t(3;11)(q25;p13) and t(X;11)(q25;p13) activating LMO2 by juxtaposition with MBNL1 and STAG2. *Leukemia,* 25**,** 1632-5.

CHICAYBAM, L., SODRE, A. L., CURZIO, B. A. & BONAMINO, M. H. 2013. An efficient low cost method for gene transfer to T lymphocytes. *PLoS One,* 8**,** e60298.

CHOTHIA, C., NOVOTNY, J., BRUCCOLERI, R. & KARPLUS, M. 1985. Domain association in immunoglobulin molecules. The packing of variable domains. *J Mol Biol,* 186**,** 651-63.

CHUNG, C. T. & MILLER, R. H. 1988. A rapid and convenient method for the preparation and storage of competent bacterial cells. *Nucleic Acids Res,* 16**,** 3580.

CLEVELAND, S. M., SMITH, S., TRIPATHI, R., MATHIAS, E. M., GOODINGS, C., ELLIOTT, N., PENG, D., EL-RIFAI, W., YI, D., CHEN, X., LI, L., MULLIGHAN, C., DOWNING, J. R., LOVE, P. & DAVE, U. P. 2013. Lmo2 induces hematopoietic stem cell-like features in T-cell progenitor cells prior to leukemia. *Stem Cells,* 31**,** 882-94.

COLUSSI, P. A., HARVEY, N. L., SHEARWIN-WHYATT, L. M. & KUMAR, S. 1998. Conversion of procaspase-3 to an autoactivating caspase by fusion to the caspase-2 prodomain. *J Biol Chem,* 273**,** 26566-70.

COMA, S., ALLARD-RATICK, M., AKINO, T., VAN MEETEREN, L. A., MAMMOTO, A. & KLAGSBRUN, M. 2013. GATA2 and Lmo2 control angiogenesis and lymphangiogenesis via direct transcriptional regulation of neuropilin-2. *Angiogenesis,* 16**,** 939-52.

COOPER, D. M. 2012. The balance between life and death: Defining a role for apoptosis in aging. *J Clin Exp Pathol***,** 001.

COUSTAN-SMITH, E., SANDLUND, J. T., PERKINS, S. L., CHEN, H., CHANG, M., ABROMOWITCH, M. & CAMPANA, D. 2009. Minimal disseminated disease in childhood T-cell lymphoblastic lymphoma: a report from the children's oncology group. *J Clin Oncol,* 27**,** 3533-9.

COX, A. D., FESIK, S. W., KIMMELMAN, A. C., LUO, J. & DER, C. J. 2014. Drugging the undruggable RAS: Mission possible? *Nat Rev Drug Discov,* 13**,** 828-51.

CREAGH, E. M., CONROY, H. & MARTIN, S. J. 2003. Caspase-activation pathways in apoptosis and immunity. *Immunol Rev,* 193**,** 10-21.

CRIST, W. M., SHUSTER, J. J., FALLETTA, J., PULLEN, D. J., BERARD, C. W., VIETTI, T. J., ALVARADO, C. S., ROPER, M. A., PRASTHOFER, E. & GROSSI, C. E. 1988. Clinical features and outcome in childhood T-cell leukemia-lymphoma according to stage of thymocyte differentiation: a Pediatric Oncology Group Study. *Blood,* 72**,** 1891-7.

CUBEDO, E., GENTLES, A. J., HUANG, C., NATKUNAM, Y., BHATT, S., LU, X., JIANG, X., ROMERO-CAMARERO, I., FREUD, A., ZHAO, S., BACCHI, C. E., MARTINEZ-CLIMENT, J. A., SANCHEZ-GARCIA, I., MELNICK, A. & LOSSOS, I. S. 2012. Identification of LMO2 transcriptome and interactome in diffuse large B-cell lymphoma. *Blood,* 119**,** 5478-91.

CULLY, M., YOU, H., LEVINE, A. J. & MAK, T. W. 2006. Beyond PTEN mutations: the PI3K pathway as an integrator of multiple inputs during tumorigenesis. *Nat Rev Cancer,* 6**,** 184-92.

DABROWSKI, M., BUKOWY-BIERYLLO, Z. & ZIETKIEWICZ, E. 2015. Translational readthrough potential of natural termination codons in eucaryotes--The impact of RNA sequence. *RNA Biol,* 12**,** 950-8.

DAVE, U. P., AKAGI, K., TRIPATHI, R., CLEVELAND, S. M., THOMPSON, M. A., YI, M., STEPHENS, R., DOWNING, J. R., JENKINS, N. A. & COPELAND, N. G. 2009. Murine leukemias with retroviral insertions at Lmo2 are predictive of the leukemias induced in SCID-X1 patients following retroviral gene therapy. *PLoS Genet,* 5**,** e1000491.

DAVIES, J. & RIECHMANN, L. 1994. 'Camelising' human antibody fragments: NMR studies on VH domains. *FEBS Lett,* 339**,** 285-90.

DE KLEIN, A., VAN KESSEL, A. G., GROSVELD, G., BARTRAM, C. R., HAGEMEIJER, A., BOOTSMA, D., SPURR, N. K., HEISTERKAMP, N., GROFFEN, J. & STEPHENSON, J. R. 1982. A cellular oncogene is translocated to the Philadelphia chromosome in chronic myelocytic leukaemia. *Nature,* 300**,** 765-7.

DE WILDT, R. M., MUNDY, C. R., GORICK, B. D. & TOMLINSON, I. M. 2000. Antibody arrays for high-throughput screening of antibody-antigen interactions. *Nat Biotechnol,* 18**,** 989-94.

DEANE, J. E., SUM, E., MACKAY, J. P., LINDEMAN, G. J., VISVADER, J. E. & MATTHEWS, J. M. 2001. Design, production and characterization of FLIN2 and FLIN4: the engineering of intramolecular ldb1:LMO complexes. *Protein Eng,* 14**,** 493-9.

DER, C. J., KRONTIRIS, T. G. & COOPER, G. M. 1982. Transforming genes of human bladder and lung carcinoma cell lines are homologous to the ras genes of Harvey and Kirsten sarcoma viruses. *Proc Natl Acad Sci U S A,* 79**,** 3637-40.

DIXON, A. S., KIM, S. J., BAUMGARTNER, B. K., KRIPPNER, S. & OWEN, S. C. 2017. A Tri-part Protein Complementation System Using Antibody-Small Peptide Fusions Enables Homogeneous Immunoassays. *Sci Rep,* 7**,** 8186.

DORES, G. M., DEVESA, S. S., CURTIS, R. E., LINET, M. S. & MORTON, L. M. 2012. Acute leukemia incidence and patient survival among children and adults in the United States, 2001-2007. *Blood,* 119**,** 34-43.

DOWNWARD, J. 2003. Targeting RAS signalling pathways in cancer therapy. *Nat Rev Cancer,* 3**,** 11-22.

DREHER, M. R., LIU, W., MICHELICH, C. R., DEWHIRST, M. W., YUAN, F. & CHILKOTI, A. 2006. Tumor vascular permeability, accumulation, and penetration of macromolecular drug carriers. *J Natl Cancer Inst,* 98**,** 335-44.

DROSTEN, M., DHAWAHIR, A., SUM, E. Y., UROSEVIC, J., LECHUGA, C. G., ESTEBAN, L. M., CASTELLANO, E., GUERRA, C., SANTOS, E. & BARBACID, M. 2010. Genetic analysis of Ras signalling pathways in cell proliferation, migration and survival. *EMBO J,* 29**,** 1091-104.

EHRENMANN, F., GIUDICELLI, V., DUROUX, P. & LEFRANC, M. P. 2011. IMGT/Collier de Perles: IMGT standardized representation of domains (IG, TR, and IgSF variable and constant domains, MH and MhSF groove domains). *Cold Spring Harb Protoc,* 2011**,** 726-36.

EL OMARI, K., HOOSDALLY, S. J., TULADHAR, K., KARIA, D., HALL-PONSELE, E., PLATONOVA, O., VYAS, P., PATIENT, R., PORCHER, C. & MANCINI, E. J. 2013. Structural basis for LMO2-driven recruitment of the SCL:E47bHLH heterodimer to hematopoietic-specific transcriptional targets. *Cell Rep,* 4**,** 135-47.

EL OMARI, K., HOOSDALLY, S. J., TULADHAR, K., KARIA, D., VYAS, P., PATIENT, R., PORCHER, C. & MANCINI, E. J. 2011. Structure of the leukemia oncogene LMO2: implications for the assembly of a hematopoietic transcription factor complex. *Blood,* 117**,** 2146-56.

ELMORE, S. 2007. Apoptosis: a review of programmed cell death. *Toxicol Pathol,* 35**,** 495-516.

ENGELMAN, J. A., CHEN, L., TAN, X., CROSBY, K., GUIMARAES, A. R., UPADHYAY, R., MAIRA, M., MCNAMARA, K., PERERA, S. A., SONG, Y., CHIRIEAC, L. R., KAUR, R., LIGHTBOWN, A., SIMENDINGER, J., LI, T., PADERA, R. F., GARCIA-ECHEVERRIA, C., WEISSLEDER, R., MAHMOOD, U., CANTLEY, L. C. & WONG, K. K. 2008. Effective use of PI3K and MEK inhibitors to treat mutant Kras G12D and PIK3CA H1047R murine lung cancers. *Nat Med,* 14**,** 1351-6.

EVANS, T., REITMAN, M. & FELSENFELD, G. 1988. An erythrocyte-specific DNA-binding factor recognizes a regulatory sequence common to all chicken globin genes. *Proc Natl Acad Sci U S A,* 85**,** 5976-80.

FAN, L., FREEMAN, K. W., KHAN, T., PHAM, E. & SPENCER, D. M. 1999. Improved artificial death switches based on caspases and FADD. *Hum Gene Ther,* 10**,** 2273-85.

FERNANDES-ALNEMRI, T., LITWACK, G. & ALNEMRI, E. S. 1994. CPP32, a novel human apoptotic protein with homology to Caenorhabditis elegans cell death protein Ced-3 and mammalian interleukin-1 beta-converting enzyme. *J Biol Chem,* 269**,** 30761-4.

FERRANDO, A. A. & LOOK, A. T. 2003. Gene expression profiling in T-cell acute lymphoblastic leukemia. *Semin Hematol,* 40**,** 274-80.

FERRANDO, A. A., NEUBERG, D. S., STAUNTON, J., LOH, M. L., HUARD, C., RAIMONDI, S. C., BEHM, F. G., PUI, C. H., DOWNING, J. R., GILLILAND, D. G., LANDER, E. S., GOLUB, T. R. & LOOK, A. T. 2002. Gene expression signatures define novel oncogenic pathways in T cell acute lymphoblastic leukemia. *Cancer Cell,* 1**,** 75-87.

FINGER, L. R., KAGAN, J., CHRISTOPHER, G., KURTZBERG, J., HERSHFIELD, M. S., NOWELL, P. C. & CROCE, C. M. 1989. Involvement of the TCL5 gene on human

chromosome 1 in T-cell leukemia and melanoma. *Proc Natl Acad Sci U S A,* 86**,** 5039-43.
FIORUCCI, G. & HALL, A. 1988. All three human ras genes are expressed in a wide range of tissues. *Biochim Biophys Acta,* 950**,** 81-3.
FISCH, P., BOEHM, T., LAVENIR, I., LARSON, T., ARNO, J., FORSTER, A. & RABBITTS, T. H. 1992. T-cell acute lymphoblastic lymphoma induced in transgenic mice by the RBTN1 and RBTN2 LIM-domain genes. *Oncogene,* 7**,** 2389-97.
FORBES, S., CLEMENTS, J., DAWSON, E., BAMFORD, S., WEBB, T., DOGAN, A., FLANAGAN, A., TEAGUE, J., WOOSTER, R., FUTREAL, P. A. & STRATTON, M. R. 2006. Cosmic 2005. *Br J Cancer,* 94**,** 318-22.
FORONI, L., BOEHM, T., WHITE, L., FORSTER, A., SHERRINGTON, P., LIAO, X. B., BRANNAN, C. I., JENKINS, N. A., COPELAND, N. G. & RABBITTS, T. H. 1992. The rhombotin gene family encode related LIM-domain proteins whose differing expression suggests multiple roles in mouse development. *J Mol Biol,* 226**,** 747-61.
FOSTER, S. D., ORAM, S. H., WILSON, N. K. & GOTTGENS, B. 2009. From genes to cells to tissues--modelling the haematopoietic system. *Mol Biosyst,* 5**,** 1413-20.
FRANKEN, N. A., RODERMOND, H. M., STAP, J., HAVEMAN, J. & VAN BREE, C. 2006. Clonogenic assay of cells in vitro. *Nat Protoc,* 1**,** 2315-9.
FREYD, G., KIM, S. K. & HORVITZ, H. R. 1990. Novel cysteine-rich motif and homeodomain in the product of the Caenorhabditis elegans cell lineage gene lin-11. *Nature,* 344**,** 876-9.
FUENTES-PRIOR, P. & SALVESEN, G. S. 2004. The protein structures that shape caspase activity, specificity, activation and inhibition. *Biochem J,* 384**,** 201-32.
FUJITA, J., YOSHIDA, O., YUASA, Y., RHIM, J. S., HATANAKA, M. & AARONSON, S. A. 1984. Ha-ras oncogenes are activated by somatic alterations in human urinary tract tumours. *Nature,* 309**,** 464-6.
GARCIA, I. S., KANEKO, Y., GONZALEZ-SARMIENTO, R., CAMPBELL, K., WHITE, L., BOEHM, T. & RABBITTS, T. H. 1991. A study of chromosome 11p13 translocations involving TCR beta and TCR delta in human T cell leukaemia. *Oncogene,* 6**,** 577-82.
GILL, G. N. 1995. The enigma of LIM domains. *Structure,* 3**,** 1285-9.
GILLET, J. P., CALCAGNO, A. M., VARMA, S., MARINO, M., GREEN, L. J., VORA, M. I., PATEL, C., ORINA, J. N., ELISEEVA, T. A., SINGAL, V., PADMANABHAN, R., DAVIDSON, B., GANAPATHI, R., SOOD, A. K., RUEDA, B. R., AMBUDKAR, S. V. & GOTTESMAN, M. M. 2011. Redefining the relevance of established cancer cell lines to the study of mechanisms of clinical anti-cancer drug resistance. *Proc Natl Acad Sci U S A,* 108**,** 18708-13.
GIRARDI, T., VICENTE, C., COOLS, J. & DE KEERSMAECKER, K. 2017. The genetics and molecular biology of T-ALL. *Blood,* 129**,** 1113-1123.
GOODSPEED, A., HEISER, L. M., GRAY, J. W. & COSTELLO, J. C. 2016. Tumor-Derived Cell Lines as Molecular Models of Cancer Pharmacogenomics. *Mol Cancer Res,* 14**,** 3-13.
GOSSEN, M., FREUNDLIEB, S., BENDER, G., MULLER, G., HILLEN, W. & BUJARD, H. 1995. Transcriptional activation by tetracyclines in mammalian cells. *Science,* 268**,** 1766-9.
GRATZINGER, D., ZHAO, S., WEST, R., ROUSE, R. V., VOGEL, H., GIL, E. C., LEVY, R., LOSSOS, I. S. & NATKUNAM, Y. 2009. The transcription factor LMO2 is a robust marker of vascular endothelium and vascular neoplasms and selected other entities. *Am J Clin Pathol,* 131**,** 264-78.
GRUTZ, G. G., BUCHER, K., LAVENIR, I., LARSON, T., LARSON, R. & RABBITTS, T. H. 1998. The oncogenic T cell LIM-protein Lmo2 forms part of a DNA-binding complex specifically in immature T cells. *EMBO J,* 17**,** 4594-605.
GUPTA, S., RAMJAUN, A. R., HAIKO, P., WANG, Y., WARNE, P. H., NICKE, B., NYE, E., STAMP, G., ALITALO, K. & DOWNWARD, J. 2007. Binding of ras to phosphoinositide 3-kinase p110alpha is required for ras-driven tumorigenesis in mice. *Cell,* 129**,** 957-68.
HACEIN-BEY-ABINA, S., GARRIGUE, A., WANG, G. P., SOULIER, J., LIM, A., MORILLON, E., CLAPPIER, E., CACCAVELLI, L., DELABESSE, E., BELDJORD, K., ASNAFI, V., MACINTYRE, E., DAL CORTIVO, L., RADFORD, I., BROUSSE, N., SIGAUX, F., MOSHOUS, D., HAUER, J., BORKHARDT, A., BELOHRADSKY, B. H., WINTERGERST, U., VELEZ, M. C., LEIVA, L., SORENSEN, R., WULFFRAAT, N.,

BLANCHE, S., BUSHMAN, F. D., FISCHER, A. & CAVAZZANA-CALVO, M. 2008. Insertional oncogenesis in 4 patients after retrovirus-mediated gene therapy of SCID-X1. *J Clin Invest,* 118**,** 3132-42.

HACEIN-BEY-ABINA, S., LE DEIST, F., CARLIER, F., BOUNEAUD, C., HUE, C., DE VILLARTAY, J. P., THRASHER, A. J., WULFFRAAT, N., SORENSEN, R., DUPUIS-GIROD, S., FISCHER, A., DAVIES, E. G., KUIS, W., LEIVA, L. & CAVAZZANA-CALVO, M. 2002. Sustained correction of X-linked severe combined immunodeficiency by ex vivo gene therapy. *N Engl J Med,* 346**,** 1185-93.

HACEIN-BEY-ABINA, S., VON KALLE, C., SCHMIDT, M., LE DEIST, F., WULFFRAAT, N., MCINTYRE, E., RADFORD, I., VILLEVAL, J. L., FRASER, C. C., CAVAZZANA-CALVO, M. & FISCHER, A. 2003a. A serious adverse event after successful gene therapy for X-linked severe combined immunodeficiency. *N Engl J Med,* 348**,** 255-6.

HACEIN-BEY-ABINA, S., VON KALLE, C., SCHMIDT, M., MCCORMACK, M. P., WULFFRAAT, N., LEBOULCH, P., LIM, A., OSBORNE, C. S., PAWLIUK, R., MORILLON, E., SORENSEN, R., FORSTER, A., FRASER, P., COHEN, J. I., DE SAINT BASILE, G., ALEXANDER, I., WINTERGERST, U., FREBOURG, T., AURIAS, A., STOPPA-LYONNET, D., ROMANA, S., RADFORD-WEISS, I., GROSS, F., VALENSI, F., DELABESSE, E., MACINTYRE, E., SIGAUX, F., SOULIER, J., LEIVA, L. E., WISSLER, M., PRINZ, C., RABBITTS, T. H., LE DEIST, F., FISCHER, A. & CAVAZZANA-CALVO, M. 2003b. LMO2-associated clonal T cell proliferation in two patients after gene therapy for SCID-X1. *Science,* 302**,** 415-9.

HALL, A., MARSHALL, C. J., SPURR, N. K. & WEISS, R. A. 1983. Identification of transforming gene in two human sarcoma cell lines as a new member of the ras gene family located on chromosome 1. *Nature,* 303**,** 396-400.

HAMERS-CASTERMAN, C., ATARHOUCH, T., MUYLDERMANS, S., ROBINSON, G., HAMERS, C., SONGA, E. B., BENDAHMAN, N. & HAMERS, R. 1993. Naturally occurring antibodies devoid of light chains. *Nature,* 363**,** 446-8.

HAMERSCHLAK, N. 2008. Leukemia: genetics and prognostic factors. *J Pediatr (Rio J),* 84**,** S52-7.

HAMMOND, S. M., CRABLE, S. C. & ANDERSON, K. P. 2005. Negative regulatory elements are present in the human LMO2 oncogene and may contribute to its expression in leukemia. *Leuk Res,* 29**,** 89-97.

HAN, C., LIU, H., LIU, J., YIN, K., XIE, Y., SHEN, X., WANG, Y., YUAN, J., QIANG, B., LIU, Y. J. & PENG, X. 2005. Human Bex2 interacts with LMO2 and regulates the transcriptional activity of a novel DNA-binding complex. *Nucleic Acids Res,* 33**,** 6555-65.

HAN, H., TANIGAKI, K., YAMAMOTO, N., KURODA, K., YOSHIMOTO, M., NAKAHATA, T., IKUTA, K. & HONJO, T. 2002. Inducible gene knockout of transcription factor recombination signal binding protein-J reveals its essential role in T versus B lineage decision. *Int Immunol,* 14**,** 637-45.

HANAHAN, D. & WEINBERG, R. A. 2011. Hallmarks of cancer: the next generation. *Cell,* 144**,** 646-74.

HANCOCK, J. F., CADWALLADER, K. & MARSHALL, C. J. 1991. Methylation and proteolysis are essential for efficient membrane binding of prenylated p21K-ras(B). *EMBO J,* 10**,** 641-6.

HANCOCK, J. F., MAGEE, A. I., CHILDS, J. E. & MARSHALL, C. J. 1989. All ras proteins are polyisoprenylated but only some are palmitoylated. *Cell,* 57**,** 1167-77.

HANKE, T., MITNACHT, R., BOYD, R. & HUNIG, T. 1994. Induction of interleukin 2 receptor beta chain expression by self-recognition in the thymus. *J Exp Med,* 180**,** 1629-36.

HASEGAWA, J., KAMADA, S., KAMIIKE, W., SHIMIZU, S., IMAZU, T., MATSUDA, H. & TSUJIMOTO, Y. 1996. Involvement of CPP32/Yama(-like) proteases in Fas-mediated apoptosis. *Cancer Res,* 56**,** 1713-8.

HEDLEY, S. J., AUF DER MAUR, A., HOHN, S., ESCHER, D., BARBERIS, A., GLASGOW, J. N., DOUGLAS, J. T., KOROKHOV, N. & CURIEL, D. T. 2006. An adenovirus vector with a chimeric fiber incorporating stabilized single chain antibody achieves targeted gene delivery. *Gene Ther,* 13**,** 88-94.

HEISTERKAMP, N., GROFFEN, J., STEPHENSON, J. R., SPURR, N. K., GOODFELLOW, P. N., SOLOMON, E., CARRITT, B. & BODMER, W. F. 1982. Chromosomal localization of human cellular homologues of two viral oncogenes. *Nature,* 299**,** 747-9.

HEISTERKAMP, N., STEPHENSON, J. R., GROFFEN, J., HANSEN, P. F., DE KLEIN, A., BARTRAM, C. R. & GROSVELD, G. 1983. Localization of the c-ab1 oncogene adjacent to a translocation break point in chronic myelocytic leukaemia. *Nature,* 306**,** 239-42.

HERBLOT, S., STEFF, A. M., HUGO, P., APLAN, P. D. & HOANG, T. 2000. SCL and LMO1 alter thymocyte differentiation: inhibition of E2A-HEB function and pre-T alpha chain expression. *Nat Immunol,* 1**,** 138-44.

HERRMANN, C., BLOCK, C., GEISEN, C., HAAS, K., WEBER, C., WINDE, G., MOROY, T. & MULLER, O. 1998. Sulindac sulfide inhibits Ras signaling. *Oncogene,* 17**,** 1769-76.

HILL, A. B., CHEN, M., CHEN, C. K., PFEIFER, B. A. & JONES, C. H. 2016. Overcoming Gene-Delivery Hurdles: Physiological Considerations for Nonviral Vectors. *Trends Biotechnol,* 34**,** 91-105.

HINKS, G. L., SHAH, B., FRENCH, S. J., CAMPOS, L. S., STALEY, K., HUGHES, J. & SOFRONIEW, M. V. 1997. Expression of LIM protein genes Lmo1, Lmo2, and Lmo3 in adult mouse hippocampus and other forebrain regions: differential regulation by seizure activity. *J Neurosci,* 17**,** 5549-59.

HO, I. C., VORHEES, P., MARIN, N., OAKLEY, B. K., TSAI, S. F., ORKIN, S. H. & LEIDEN, J. M. 1991. Human GATA-3: a lineage-restricted transcription factor that regulates the expression of the T cell receptor alpha gene. *EMBO J,* 10**,** 1187-92.

HOBBS, G. A., DER, C. J. & ROSSMAN, K. L. 2016. RAS isoforms and mutations in cancer at a glance. *J Cell Sci,* 129**,** 1287-92.

HOLLIGER, P. & HUDSON, P. J. 2005. Engineered antibody fragments and the rise of single domains. *Nat Biotechnol,* 23**,** 1126-36.

HOWE, S. J., MANSOUR, M. R., SCHWARZWAELDER, K., BARTHOLOMAE, C., HUBANK, M., KEMPSKI, H., BRUGMAN, M. H., PIKE-OVERZET, K., CHATTERS, S. J., DE RIDDER, D., GILMOUR, K. C., ADAMS, S., THORNHILL, S. I., PARSLEY, K. L., STAAL, F. J., GALE, R. E., LINCH, D. C., BAYFORD, J., BROWN, L., QUAYE, M., KINNON, C., ANCLIFF, P., WEBB, D. K., SCHMIDT, M., VON KALLE, C., GASPAR, H. B. & THRASHER, A. J. 2008. Insertional mutagenesis combined with acquired somatic mutations causes leukemogenesis following gene therapy of SCID-X1 patients. *J Clin Invest,* 118**,** 3143-50.

HSU, H. L., CHENG, J. T., CHEN, Q. & BAER, R. 1991. Enhancer-binding activity of the tal-1 oncoprotein in association with the E47/E12 helix-loop-helix proteins. *Mol Cell Biol,* 11**,** 3037-42.

HSU, H. L., WADMAN, I. & BAER, R. 1994. Formation of in vivo complexes between the TAL1 and E2A polypeptides of leukemic T cells. *Proc Natl Acad Sci U S A,* 91**,** 3181-5.

HU, C. D. & KERPPOLA, T. K. 2003. Simultaneous visualization of multiple protein interactions in living cells using multicolor fluorescence complementation analysis. *Nat Biotechnol,* 21**,** 539-45.

HUSSACK, G. & TANHA, J. 2010. Toxin-specific antibodies for the treatment of Clostridium difficile: current status and future perspectives. *Toxins (Basel),* 2**,** 998-1018.

IRANI, V., GUY, A. J., ANDREW, D., BEESON, J. G., RAMSLAND, P. A. & RICHARDS, J. S. 2015. Molecular properties of human IgG subclasses and their implications for designing therapeutic monoclonal antibodies against infectious diseases. *Mol Immunol,* 67**,** 171-82.

IVASCU, A. & KUBBIES, M. 2006. Rapid generation of single-tumor spheroids for high-throughput cell function and toxicity analysis. *J Biomol Screen,* 11**,** 922-32.

JAIN, R. K. 1990. Vascular and interstitial barriers to delivery of therapeutic agents in tumors. *Cancer Metastasis Rev,* 9**,** 253-66.

JAMES, G., GOLDSTEIN, J. L. & BROWN, M. S. 1996. Resistance of K-RasBV12 proteins to farnesyltransferase inhibitors in Rat1 cells. *Proc Natl Acad Sci U S A,* 93**,** 4454-8.

JAMES, G. L., BROWN, M. S., COBB, M. H. & GOLDSTEIN, J. L. 1994. Benzodiazepine peptidomimetic BZA-5B interrupts the MAP kinase activation pathway in H-Ras-transformed Rat-1 cells, but not in untransformed cells. *J Biol Chem,* 269**,** 27705-14.

JEVREMOVIC, D., RODEN, A. C., KETTERLING, R. P., KURTIN, P. J. & MCPHAIL, E. D. 2016. LMO2 Is a Specific Marker of T-Lymphoblastic Leukemia/Lymphoma. *Am J Clin Pathol,* 145**,** 180-90.

JURATA, L. W., KENNY, D. A. & GILL, G. N. 1996. Nuclear LIM interactor, a rhombotin and LIM homeodomain interacting protein, is expressed early in neuronal development. *Proc Natl Acad Sci U S A,* 93**,** 11693-8.

KAAS, Q., EHRENMANN, F. & LEFRANC, M. P. 2007. IG, TR and IgSF, MHC and MhcSF: what do we learn from the IMGT Colliers de Perles? *Brief Funct Genomic Proteomic,* 6**,** 253-64.

KANG, H. J., LEE, Y. M., JEONG, Y. J., PARK, K., JANG, M., PARK, S. G., BAE, K. H., KIM, M. & CHUNG, S. J. 2008. Large-scale preparation of active caspase-3 in E. coli by designing its thrombin-activatable precursors. *BMC Biotechnol,* 8**,** 92.

KARLSSON, O., THOR, S., NORBERG, T., OHLSSON, H. & EDLUND, T. 1990. Insulin gene enhancer binding protein Isl-1 is a member of a novel class of proteins containing both a homeo- and a Cys-His domain. *Nature,* 344**,** 879-82.

KARNOUB, A. E. & WEINBERG, R. A. 2008. Ras oncogenes: split personalities. *Nat Rev Mol Cell Biol,* 9**,** 517-31.

KELLEY, G. G., REKS, S. E., ONDRAKO, J. M. & SMRCKA, A. V. 2001. Phospholipase C(epsilon): a novel Ras effector. *EMBO J,* 20**,** 743-54.

KENNY, D. A., JURATA, L. W., SAGA, Y. & GILL, G. N. 1998. Identification and characterization of LMO4, an LMO gene with a novel pattern of expression during embryogenesis. *Proc Natl Acad Sci U S A,* 95**,** 11257-62.

KERR, J. F., WYLLIE, A. H. & CURRIE, A. R. 1972. Apoptosis: a basic biological phenomenon with wide-ranging implications in tissue kinetics. *Br J Cancer,* 26**,** 239-57.

KHWAJA, A., BJORKHOLM, M., GALE, R. E., LEVINE, R. L., JORDAN, C. T., EHNINGER, G., BLOOMFIELD, C. D., ESTEY, E., BURNETT, A., CORNELISSEN, J. J., SCHEINBERG, D. A., BOUSCARY, D. & LINCH, D. C. 2016. Acute myeloid leukaemia. *Nat Rev Dis Primers,* 2**,** 16010.

KIKUCHI, A., DEMO, S. D., YE, Z. H., CHEN, Y. W. & WILLIAMS, L. T. 1994. ralGDS family members interact with the effector loop of ras p21. *Mol Cell Biol,* 14**,** 7483-91.

KIM, S. H., KIM, E. J., HITOMI, M., OH, S. Y., JIN, X., JEON, H. M., BECK, S., JIN, X., KIM, J. K., PARK, C. G., CHANG, S. Y., YIN, J., KIM, T., JEON, Y. J., SONG, J., LIM, Y. C., LATHIA, J. D., NAKANO, I. & KIM, H. 2015. The LIM-only transcription factor LMO2 determines tumorigenic and angiogenic traits in glioma stem cells. *Cell Death Differ,* 22**,** 1517-25.

KIPPS, T. J., STEVENSON, F. K., WU, C. J., CROCE, C. M., PACKHAM, G., WIERDA, W. G., O'BRIEN, S., GRIBBEN, J. & RAI, K. 2017. Chronic lymphocytic leukaemia. *Nat Rev Dis Primers,* 3**,** 17008.

KIRCHHOFER, A., HELMA, J., SCHMIDTHALS, K., FRAUER, C., CUI, S., KARCHER, A., PELLIS, M., MUYLDERMANS, S., CASAS-DELUCCHI, C. S., CARDOSO, M. C., LEONHARDT, H., HOPFNER, K. P. & ROTHBAUER, U. 2010. Modulation of protein properties in living cells using nanobodies. *Nat Struct Mol Biol,* 17**,** 133-8.

KO, L. J. & ENGEL, J. D. 1993. DNA-binding specificities of the GATA transcription factor family. *Mol Cell Biol,* 13**,** 4011-22.

KOPETZ, S., DESAI, J., CHAN, E., HECHT, J. R., O'DWYER, P. J., MARU, D., MORRIS, V., JANKU, F., DASARI, A., CHUNG, W., ISSA, J. P., GIBBS, P., JAMES, B., POWIS, G., NOLOP, K. B., BHATTACHARYA, S. & SALTZ, L. 2015. Phase II Pilot Study of Vemurafenib in Patients With Metastatic BRAF-Mutated Colorectal Cancer. *J Clin Oncol,* 33**,** 4032-8.

KORAICHI, F., GENCE, R., BOUCHENOT, C., GROSJEAN, S., LAJOIE-MAZENC, I., FAVRE, G. & CABANTOUS, S. 2018. High-content tripartite split-GFP cell-based assays to screen for modulators of small GTPase activation. *J Cell Sci,* 131.

KOTTERMAN, M. A. & SCHAFFER, D. V. 2014. Engineering adeno-associated viruses for clinical gene therapy. *Nat Rev Genet,* 15**,** 445-51.

KREDEL, S., OSWALD, F., NIENHAUS, K., DEUSCHLE, K., ROCKER, C., WOLFF, M., HEILKER, R., NIENHAUS, G. U. & WIEDENMANN, J. 2009. mRuby, a bright monomeric red fluorescent protein for labeling of subcellular structures. *PLoS One,* 4**,** e4391.

KRIVEGA, I., DALE, R. K. & DEAN, A. 2014. Role of LDB1 in the transition from chromatin looping to transcription activation. *Genes Dev,* 28**,** 1278-90.

LA MOTTE-MOHS, R. N., HERER, E. & ZUNIGA-PFLUCKER, J. C. 2005. Induction of T-cell development from human cord blood hematopoietic stem cells by Delta-like 1 in vitro. *Blood,* 105**,** 1431-9.
LACAUD, G., KELLER, G. & KOUSKOFF, V. 2004. Tracking mesoderm formation and specification to the hemangioblast in vitro. *Trends Cardiovasc Med,* 14**,** 314-7.
LAOUAR, Y., CRISPE, I. N. & FLAVELL, R. A. 2004. Overexpression of IL-7R alpha provides a competitive advantage during early T-cell development. *Blood,* 103**,** 1985-94.
LARSON, R. C., FISCH, P., LARSON, T. A., LAVENIR, I., LANGFORD, T., KING, G. & RABBITTS, T. H. 1994. T cell tumours of disparate phenotype in mice transgenic for Rbtn-2. *Oncogene,* 9**,** 3675-81.
LARSON, R. C., LAVENIR, I., LARSON, T. A., BAER, R., WARREN, A. J., WADMAN, I., NOTTAGE, K. & RABBITTS, T. H. 1996. Protein dimerization between Lmo2 (Rbtn2) and Tal1 alters thymocyte development and potentiates T cell tumorigenesis in transgenic mice. *EMBO J,* 15**,** 1021-7.
LARSON, R. C., OSADA, H., LARSON, T. A., LAVENIR, I. & RABBITTS, T. H. 1995. The oncogenic LIM protein Rbtn2 causes thymic developmental aberrations that precede malignancy in transgenic mice. *Oncogene,* 11**,** 853-62.
LEE, C. S., BISHOP, E. S., ZHANG, R., YU, X., FARINA, E. M., YAN, S., ZHAO, C., ZHENG, Z., SHU, Y., WU, X., LEI, J., LI, Y., ZHANG, W., YANG, C., WU, K., WU, Y., HO, S., ATHIVIRAHAM, A., LEE, M. J., WOLF, J. M., REID, R. R. & HE, T. C. 2017. Adenovirus-Mediated Gene Delivery: Potential Applications for Gene and Cell-Based Therapies in the New Era of Personalized Medicine. *Genes Dis,* 4**,** 43-63.
LEE, D., LONG, S. A., ADAMS, J. L., CHAN, G., VAIDYA, K. S., FRANCIS, T. A., KIKLY, K., WINKLER, J. D., SUNG, C. M., DEBOUCK, C., RICHARDSON, S., LEVY, M. A., DEWOLF, W. E., JR., KELLER, P. M., TOMASZEK, T., HEAD, M. S., RYAN, M. D., HALTIWANGER, R. C., LIANG, P. H., JANSON, C. A., MCDEVITT, P. J., JOHANSON, K., CONCHA, N. O., CHAN, W., ABDEL-MEGUID, S. S., BADGER, A. M., LARK, M. W., NADEAU, D. P., SUVA, L. J., GOWEN, M. & NUTTALL, M. E. 2000. Potent and selective nonpeptide inhibitors of caspases 3 and 7 inhibit apoptosis and maintain cell functionality. *J Biol Chem,* 275**,** 16007-14.
LEE, D., LONG, S. A., MURRAY, J. H., ADAMS, J. L., NUTTALL, M. E., NADEAU, D. P., KIKLY, K., WINKLER, J. D., SUNG, C. M., RYAN, M. D., LEVY, M. A., KELLER, P. M. & DEWOLF, W. E., JR. 2001. Potent and selective nonpeptide inhibitors of caspases 3 and 7. *J Med Chem,* 44**,** 2015-26.
LEFRANC, M. P. & RABBITTS, T. H. 1985. Two tandemly organized human genes encoding the T-cell gamma constant-region sequences show multiple rearrangement in different T-cell types. *Nature,* 316**,** 464-6.
LENTJES, M. H., NIESSEN, H. E., AKIYAMA, Y., DE BRUINE, A. P., MELOTTE, V. & VAN ENGELAND, M. 2016. The emerging role of GATA transcription factors in development and disease. *Expert Rev Mol Med,* 18**,** e3.
LIU, H., CHENG, E. H. & HSIEH, J. J. 2009. MLL fusions: pathways to leukemia. *Cancer Biol Ther,* 8**,** 1204-11.
LIU, L., DUDLER, T. & GELB, M. H. 1996. Purification of a protein palmitoyltransferase that acts on H-Ras protein and on a C-terminal N-Ras peptide. *J Biol Chem,* 271**,** 23269-76.
LOBELL, R. B., OMER, C. A., ABRAMS, M. T., BHIMNATHWALA, H. G., BRUCKER, M. J., BUSER, C. A., DAVIDE, J. P., DESOLMS, S. J., DINSMORE, C. J., ELLIS-HUTCHINGS, M. S., KRAL, A. M., LIU, D., LUMMA, W. C., MACHOTKA, S. V., RANDS, E., WILLIAMS, T. M., GRAHAM, S. L., HARTMAN, G. D., OLIFF, A. I., HEIMBROOK, D. C. & KOHL, N. E. 2001. Evaluation of farnesyl:protein transferase and geranylgeranyl:protein transferase inhibitor combinations in preclinical models. *Cancer Res,* 61**,** 8758-68.
LOSSOS, I. S., CZERWINSKI, D. K., ALIZADEH, A. A., WECHSER, M. A., TIBSHIRANI, R., BOTSTEIN, D. & LEVY, R. 2004. Prediction of survival in diffuse large-B-cell lymphoma based on the expression of six genes. *N Engl J Med,* 350**,** 1828-37.
LOUGHRAN, G., CHOU, M. Y., IVANOV, I. P., JUNGREIS, I., KELLIS, M., KIRAN, A. M., BARANOV, P. V. & ATKINS, J. F. 2014. Evidence of efficient stop codon readthrough in four mammalian genes. *Nucleic Acids Res,* 42**,** 8928-38.
LUO, Y., BATALAO, A., ZHOU, H. & ZHU, L. 1997. Mammalian two-hybrid system: a complementary approach to the yeast two-hybrid system. *Biotechniques,* 22**,** 350-2.

MACCORKLE, R. A., FREEMAN, K. W. & SPENCER, D. M. 1998. Synthetic activation of caspases: artificial death switches. *Proc Natl Acad Sci U S A,* 95**,** 3655-60.
MACIAG, J. J., MACKENZIE, S. H., TUCKER, M. B., SCHIPPER, J. L., SWARTZ, P. & CLARK, A. C. 2016. Tunable allosteric library of caspase-3 identifies coupling between conserved water molecules and conformational selection. *Proc Natl Acad Sci U S A,* 113**,** E6080-E6088.
MANAIA, A., LEMARCHANDEL, V., KLAINE, M., MAX-AUDIT, I., ROMEO, P., DIETERLEN-LIEVRE, F. & GODIN, I. 2000. Lmo2 and GATA-3 associated expression in intraembryonic hemogenic sites. *Development,* 127**,** 643-53.
MARINE, J. & WINOTO, A. 1991. The human enhancer-binding protein Gata3 binds to several T-cell receptor regulatory elements. *Proc Natl Acad Sci U S A,* 88**,** 7284-8.
MARKS, D. I., PAIETTA, E. M., MOORMAN, A. V., RICHARDS, S. M., BUCK, G., DEWALD, G., FERRANDO, A., FIELDING, A. K., GOLDSTONE, A. H., KETTERLING, R. P., LITZOW, M. R., LUGER, S. M., MCMILLAN, A. K., MANSOUR, M. R., ROWE, J. M., TALLMAN, M. S. & LAZARUS, H. M. 2009. T-cell acute lymphoblastic leukemia in adults: clinical features, immunophenotype, cytogenetics, and outcome from the large randomized prospective trial (UKALL XII/ECOG 2993). *Blood,* 114**,** 5136-45.
MARKS, D. I. & ROWNTREE, C. 2017. Management of adults with T-cell lymphoblastic leukemia. *Blood,* 129**,** 1134-1142.
MARTIN, C. H., WOLL, P. S., NI, Z., ZUNIGA-PFLUCKER, J. C. & KAUFMAN, D. S. 2008. Differences in lymphocyte developmental potential between human embryonic stem cell and umbilical cord blood-derived hematopoietic progenitor cells. *Blood,* 112**,** 2730-7.
MATTHEWS, J. M., LESTER, K., JOSEPH, S. & CURTIS, D. J. 2013. LIM-domain-only proteins in cancer. *Nat Rev Cancer,* 13**,** 111-22.
MATTHEWS, J. M. & VISVADER, J. E. 2003. LIM-domain-binding protein 1: a multifunctional cofactor that interacts with diverse proteins. *EMBO Rep,* 4**,** 1132-7.
MATTHEWS, J. M., VISVADER, J. E. & MACKAY, J. P. 2001. 1H, 15N and 13C assignments of FLIN2, an intramolecular LMO2:ldb1 complex. *J Biomol NMR,* 21**,** 385-6.
MCCORMACK, M. P., FORSTER, A., DRYNAN, L., PANNELL, R. & RABBITTS, T. H. 2003. The LMO2 T-cell oncogene is activated via chromosomal translocations or retroviral insertion during gene therapy but has no mandatory role in normal T-cell development. *Mol Cell Biol,* 23**,** 9003-13.
MCCORMACK, M. P. & RABBITTS, T. H. 2004. Activation of the T-cell oncogene LMO2 after gene therapy for X-linked severe combined immunodeficiency. *N Engl J Med,* 350**,** 913-22.
MCCORMACK, M. P., SHIELDS, B. J., JACKSON, J. T., NASA, C., SHI, W., SLATER, N. J., TREMBLAY, C. S., RABBITTS, T. H. & CURTIS, D. J. 2013. Requirement for Lyl1 in a model of Lmo2-driven early T-cell precursor ALL. *Blood,* 122**,** 2093-103.
MCCORMACK, M. P., YOUNG, L. F., VASUDEVAN, S., DE GRAAF, C. A., CODRINGTON, R., RABBITTS, T. H., JANE, S. M. & CURTIS, D. J. 2010. The Lmo2 oncogene initiates leukemia in mice by inducing thymocyte self-renewal. *Science,* 327**,** 879-83.
MEERGANS, T., HILDEBRANDT, A. K., HORAK, D., HAENISCH, C. & WENDEL, A. 2000. The short prodomain influences caspase-3 activation in HeLa cells. *Biochem J,* 349**,** 135-40.
MILBURN, M. V., TONG, L., DEVOS, A. M., BRUNGER, A., YAMAIZUMI, Z., NISHIMURA, S. & KIM, S. H. 1990. Molecular switch for signal transduction: structural differences between active and inactive forms of protooncogenic ras proteins. *Science,* 247**,** 939-45.
MILLER, J. F. 2002. The discovery of thymus function and of thymus-derived lymphocytes. *Immunol Rev,* 185**,** 7-14.
MITTL, P. R., DI MARCO, S., KREBS, J. F., BAI, X., KARANEWSKY, D. S., PRIESTLE, J. P., TOMASELLI, K. J. & GRUTTER, M. G. 1997. Structure of recombinant human CPP32 in complex with the tetrapeptide acetyl-Asp-Val-Ala-Asp fluoromethyl ketone. *J Biol Chem,* 272**,** 6539-47.
MOORE, G. E., GERNER, R. E. & FRANKLIN, H. A. 1967. Culture of normal human leukocytes. *JAMA,* 199**,** 519-24.
MOORE, G. E., ITO, E., ULRICH, K. & SANDBERG, A. A. 1966. Culture of human leukemia cells. *Cancer,* 19**,** 713-23.

MORRIS, S. W., KIRSTEIN, M. N., VALENTINE, M. B., DITTMER, K. G., SHAPIRO, D. N., SALTMAN, D. L. & LOOK, A. T. 1994. Fusion of a kinase gene, ALK, to a nucleolar protein gene, NPM, in non-Hodgkin's lymphoma. *Science,* 263**,** 1281-4.

MUNCH, R. C., JANICKI, H., VOLKER, I., RASBACH, A., HALLEK, M., BUNING, H. & BUCHHOLZ, C. J. 2013. Displaying high-affinity ligands on adeno-associated viral vectors enables tumor cell-specific and safe gene transfer. *Mol Ther,* 21**,** 109-18.

MUNITIC, I., WILLIAMS, J. A., YANG, Y., DONG, B., LUCAS, P. J., EL KASSAR, N., GRESS, R. E. & ASHWELL, J. D. 2004. Dynamic regulation of IL-7 receptor expression is required for normal thymopoiesis. *Blood,* 104**,** 4165-72.

MUZIO, M., STOCKWELL, B. R., STENNICKE, H. R., SALVESEN, G. S. & DIXIT, V. M. 1998. An induced proximity model for caspase-8 activation. *J Biol Chem,* 273**,** 2926-30.

NAKATA, K., OHUCHIDA, K., NAGAI, E., HAYASHI, A., MIYASAKA, Y., KAYASHIMA, T., YU, J., AISHIMA, S., ODA, Y., MIZUMOTO, K., TANAKA, M. & TSUNEYOSHI, M. 2009. LMO2 is a novel predictive marker for a better prognosis in pancreatic cancer. *Neoplasia,* 11**,** 712-9.

NAM, C. H., LOBATO, M. N., APPERT, A., DRYNAN, L. F., TANAKA, T. & RABBITTS, T. H. 2008. An antibody inhibitor of the LMO2-protein complex blocks its normal and tumorigenic functions. *Oncogene,* 27**,** 4962-8.

NARAMURA, M., NANDWANI, N., GU, H., BAND, V. & BAND, H. 2010. Rapidly fatal myeloproliferative disorders in mice with deletion of Casitas B-cell lymphoma (Cbl) and Cbl-b in hematopoietic stem cells. *Proc Natl Acad Sci U S A,* 107**,** 16274-9.

NATKUNAM, Y., FARINHA, P., HSI, E. D., HANS, C. P., TIBSHIRANI, R., SEHN, L. H., CONNORS, J. M., GRATZINGER, D., ROSADO, M., ZHAO, S., POHLMAN, B., WONGCHAOWART, N., BAST, M., AVIGDOR, A., SCHIBY, G., NAGLER, A., BYRNE, G. E., LEVY, R., GASCOYNE, R. D. & LOSSOS, I. S. 2008. LMO2 protein expression predicts survival in patients with diffuse large B-cell lymphoma treated with anthracycline-based chemotherapy with and without rituximab. *J Clin Oncol,* 26**,** 447-54.

NATKUNAM, Y., ZHAO, S., MASON, D. Y., CHEN, J., TAIDI, B., JONES, M., HAMMER, A. S., HAMILTON DUTOIT, S., LOSSOS, I. S. & LEVY, R. 2007. The oncoprotein LMO2 is expressed in normal germinal-center B cells and in human B-cell lymphomas. *Blood,* 109**,** 1636-42.

NEALE, G. A., MAO, S., PARHAM, D. M., MURTI, K. G. & GOORHA, R. M. 1995. Expression of the proto-oncogene rhombotin-2 is identical to the acute phase response protein metallothionein, suggesting multiple functions. *Cell Growth Differ,* 6**,** 587-96.

NERI, A., KNOWLES, D. M., GRECO, A., MCCORMICK, F. & DALLA-FAVERA, R. 1988. Analysis of RAS oncogene mutations in human lymphoid malignancies. *Proc Natl Acad Sci U S A,* 85**,** 9268-72.

NICHOLSON, D. W. 1999. Caspase structure, proteolytic substrates, and function during apoptotic cell death. *Cell Death Differ,* 6**,** 1028-42.

NILES, A. L., MORAVEC, R. A., ERIC HESSELBERTH, P., SCURRIA, M. A., DAILY, W. J. & RISS, T. L. 2007. A homogeneous assay to measure live and dead cells in the same sample by detecting different protease markers. *Anal Biochem,* 366**,** 197-206.

NITTA, T., OHIGASHI, I. & TAKAHAMA, Y. 2013. The development of T lymphocytes in fetal thymus organ culture. *Methods Mol Biol,* 946**,** 85-102.

NOWELL, P. C. & HUNGERFORD, D. A. 1960. Chromosome studies on normal and leukemic human leukocytes. *J Natl Cancer Inst,* 25**,** 85-109.

NUTTALL, S. D., KRISHNAN, U. V., HATTARKI, M., DE GORI, R., IRVING, R. A. & HUDSON, P. J. 2001. Isolation of the new antigen receptor from wobbegong sharks, and use as a scaffold for the display of protein loop libraries. *Mol Immunol,* 38**,** 313-26.

O'HARE, T., EIDE, C. A. & DEININGER, M. W. 2007. Bcr-Abl kinase domain mutations, drug resistance, and the road to a cure for chronic myeloid leukemia. *Blood,* 110**,** 2242-9.

O'SULLIVAN, B., BRIERLEY, J., BYRD, D., BOSMAN, F., KEHOE, S., KOSSARY, C., PINEROS, M., VAN EYCKEN, E., WEIR, H. K. & GOSPODAROWICZ, M. 2017. The TNM classification of malignant tumours-towards common understanding and reasonable expectations. *Lancet Oncol,* 18**,** 849-851.

ONO, Y., FUKUHARA, N. & YOSHIE, O. 1997. Transcriptional activity of TAL1 in T cell acute lymphoblastic leukemia (T-ALL) requires RBTN1 or -2 and induces TALLA1, a highly specific tumor marker of T-ALL. *J Biol Chem,* 272**,** 4576-81.

ONO, Y., FUKUHARA, N. & YOSHIE, O. 1998. TAL1 and LIM-only proteins synergistically induce retinaldehyde dehydrogenase 2 expression in T-cell acute lymphoblastic leukemia by acting as cofactors for GATA3. *Mol Cell Biol,* 18**,** 6939-50.

ORAM, S. H., THOMS, J. A., PRIDANS, C., JANES, M. E., KINSTON, S. J., ANAND, S., LANDRY, J. R., LOCK, R. B., JAYARAMAN, P. S., HUNTLY, B. J., PIMANDA, J. E. & GOTTGENS, B. 2010. A previously unrecognized promoter of LMO2 forms part of a transcriptional regulatory circuit mediating LMO2 expression in a subset of T-acute lymphoblastic leukaemia patients. *Oncogene,* 29**,** 5796-808.

ORKIN, S. H. 1992. GATA-binding transcription factors in hematopoietic cells. *Blood,* 80**,** 575-81.

OSADA, H., GRUTZ, G., AXELSON, H., FORSTER, A. & RABBITTS, T. H. 1995. Association of erythroid transcription factors: complexes involving the LIM protein RBTN2 and the zinc-finger protein GATA1. *Proc Natl Acad Sci U S A,* 92**,** 9585-9.

OSHIMA, K., KHIABANIAN, H., DA SILVA-ALMEIDA, A. C., TZONEVA, G., ABATE, F., AMBESI-IMPIOMBATO, A., SANCHEZ-MARTIN, M., CARPENTER, Z., PENSON, A., PEREZ-GARCIA, A., ECKERT, C., NICOLAS, C., BALBIN, M., SULIS, M. L., KATO, M., KOH, K., PAGANIN, M., BASSO, G., GASTIER-FOSTER, J. M., DEVIDAS, M., LOH, M. L., KIRSCHNER-SCHWABE, R., PALOMERO, T., RABADAN, R. & FERRANDO, A. A. 2016. Mutational landscape, clonal evolution patterns, and role of RAS mutations in relapsed acute lymphoblastic leukemia. *Proc Natl Acad Sci U S A,* 113**,** 11306-11311.

PARATO, K. A., SENGER, D., FORSYTH, P. A. & BELL, J. C. 2005. Recent progress in the battle between oncolytic viruses and tumours. *Nat Rev Cancer,* 5**,** 965-76.

PECHALRIEU, D., ETIEVANT, C. & ARIMONDO, P. B. 2017. DNA methyltransferase inhibitors in cancer: From pharmacology to translational studies. *Biochem Pharmacol,* 129**,** 1-13.

PELLS, S., DIVJAK, M., ROMANOWSKI, P., IMPEY, H., HAWKINS, N. J., CLARKE, A. R., HOOPER, M. L. & WILLIAMSON, D. J. 1997. Developmentally-regulated expression of murine K-ras isoforms. *Oncogene,* 15**,** 1781-6.

PERABO, L., BUNING, H., KOFLER, D. M., RIED, M. U., GIROD, A., WENDTNER, C. M., ENSSLE, J. & HALLEK, M. 2003. In vitro selection of viral vectors with modified tropism: the adeno-associated virus display. *Mol Ther,* 8**,** 151-7.

PEREZ-ALVARADO, G. C., KOSA, J. L., LOUIS, H. A., BECKERLE, M. C., WINGE, D. R. & SUMMERS, M. F. 1996. Structure of the cysteine-rich intestinal protein, CRIP. *J Mol Biol,* 257**,** 153-74.

PERI, F., AIROLDI, C., COLOMBO, S., MARTEGANI, E., VAN NEUREN, A. S., STEIN, M., MARINZI, C. & NICOTRA, F. 2005. Design, synthesis and biological evaluation of sugar-derived Ras inhibitors. *Chembiochem,* 6**,** 1839-48.

PETRIE, H. T. 2002. Role of thymic organ structure and stromal composition in steady-state postnatal T-cell production. *Immunol Rev,* 189**,** 8-19.

PEVNY, L., SIMON, M. C., ROBERTSON, E., KLEIN, W. H., TSAI, S. F., D'AGATI, V., ORKIN, S. H. & COSTANTINI, F. 1991. Erythroid differentiation in chimaeric mice blocked by a targeted mutation in the gene for transcription factor GATA-1. *Nature,* 349**,** 257-60.

PLASSCHAERT, S. L., KAMPS, W. A., VELLENGA, E., DE VRIES, E. G. & DE BONT, E. S. 2004. Prognosis in childhood and adult acute lymphoblastic leukaemia: a question of maturation? *Cancer Treat Rev,* 30**,** 37-51.

PLOWMAN, S. J., MUNCKE, C., PARTON, R. G. & HANCOCK, J. F. 2005. H-ras, K-ras, and inner plasma membrane raft proteins operate in nanoclusters with differential dependence on the actin cytoskeleton. *Proc Natl Acad Sci U S A,* 102**,** 15500-5.

POP, C., CHEN, Y. R., SMITH, B., BOSE, K., BOBAY, B., TRIPATHY, A., FRANZEN, S. & CLARK, A. C. 2001. Removal of the pro-domain does not affect the conformation of the procaspase-3 dimer. *Biochemistry,* 40**,** 14224-35.

PRIOR, I. A., LEWIS, P. D. & MATTOS, C. 2012. A comprehensive survey of Ras mutations in cancer. *Cancer Res,* 72**,** 2457-67.

PRIOR, I. A., MUNCKE, C., PARTON, R. G. & HANCOCK, J. F. 2003. Direct visualization of Ras proteins in spatially distinct cell surface microdomains. *J Cell Biol,* 160**,** 165-70.

PUCK, T. T. & MARCUS, P. I. 1956. Action of x-rays on mammalian cells. *J Exp Med,* 103**,** 653-66.

PUI, C. H., RELLING, M. V. & DOWNING, J. R. 2004. Acute lymphoblastic leukemia. *N Engl J Med,* 350**,** 1535-48.

PUI, J. C., ALLMAN, D., XU, L., DEROCCO, S., KARNELL, F. G., BAKKOUR, S., LEE, J. Y., KADESCH, T., HARDY, R. R., ASTER, J. C. & PEAR, W. S. 1999. Notch1 expression in early lymphopoiesis influences B versus T lineage determination. *Immunity,* 11**,** 299-308.

QUEVEDO, C. E., CRUZ-MIGONI, A., BERY, N., MILLER, A., TANAKA, T., PETCH, D., BATAILLE, C. J. R., LEE, L. Y. W., FALLON, P. S., TULMIN, H., EHEBAUER, M. T., FERNANDEZ-FUENTES, N., RUSSELL, A. J., CARR, S. B., PHILLIPS, S. E. V. & RABBITTS, T. H. 2018. Small molecule inhibitors of RAS-effector protein interactions derived using an intracellular antibody fragment. *Nat Commun,* 9**,** 3169.

RABBITTS, T. H. 1991. Translocations, master genes, and differences between the origins of acute and chronic leukemias. *Cell,* 67**,** 641-4.

RABBITTS, T. H., LEFRANC, M. P., STINSON, M. A., SIMS, J. E., SCHRODER, J., STEINMETZ, M., SPURR, N. L., SOLOMON, E. & GOODFELLOW, P. N. 1985. The chromosomal location of T-cell receptor genes and a T cell rearranging gene: possible correlation with specific translocations in human T cell leukaemia. *EMBO J,* 4**,** 1461-5.

RAHMAN, S., MAGNUSSEN, M., LEON, T. E., FARAH, N., LI, Z., ABRAHAM, B. J., ALAPI, K. Z., MITCHELL, R. J., NAUGHTON, T., FIELDING, A. K., PIZZEY, A., BUSTRAAN, S., ALLEN, C., POPA, T., PIKE-OVERZET, K., GARCIA-PEREZ, L., GALE, R. E., LINCH, D. C., STAAL, F. J. T., YOUNG, R. A., LOOK, A. T. & MANSOUR, M. R. 2017. Activation of the LMO2 oncogene through a somatically acquired neomorphic promoter in T-cell acute lymphoblastic leukemia. *Blood,* 129**,** 3221-3226.

REUTER, C. W., MORGAN, M. A. & BERGMANN, L. 2000. Targeting the Ras signaling pathway: a rational, mechanism-based treatment for hematologic malignancies? *Blood,* 96**,** 1655-69.

ROBB, L., LYONS, I., LI, R., HARTLEY, L., KONTGEN, F., HARVEY, R. P., METCALF, D. & BEGLEY, C. G. 1995. Absence of yolk sac hematopoiesis from mice with a targeted disruption of the scl gene. *Proc Natl Acad Sci U S A,* 92**,** 7075-9.

ROTHENSTEIN, J. M. & CHOOBACK, N. 2018. ALK inhibitors, resistance development, clinical trials. *Curr Oncol,* 25**,** S59-S67.

ROTHLISBERGER, D., HONEGGER, A. & PLUCKTHUN, A. 2005. Domain interactions in the Fab fragment: a comparative evaluation of the single-chain Fv and Fab format engineered with variable domains of different stability. *J Mol Biol,* 347**,** 773-89.

ROUX, K. H., GREENBERG, A. S., GREENE, L., STRELETS, L., AVILA, D., MCKINNEY, E. C. & FLAJNIK, M. F. 1998. Structural analysis of the nurse shark (new) antigen receptor (NAR): molecular convergence of NAR and unusual mammalian immunoglobulins. *Proc Natl Acad Sci U S A,* 95**,** 11804-9.

ROWLEY, J. D. 1973. Letter: A new consistent chromosomal abnormality in chronic myelogenous leukaemia identified by quinacrine fluorescence and Giemsa staining. *Nature,* 243**,** 290-3.

ROY, S., BAYLY, C. I., GAREAU, Y., HOUTZAGER, V. M., KARGMAN, S., KEEN, S. L., ROWLAND, K., SEIDEN, I. M., THORNBERRY, N. A. & NICHOLSON, D. W. 2001. Maintenance of caspase-3 proenzyme dormancy by an intrinsic "safety catch" regulatory tripeptide. *Proc Natl Acad Sci U S A,* 98**,** 6132-7.

ROYER-POKORA, B., LOOS, U. & LUDWIG, W. D. 1991. TTG-2, a new gene encoding a cysteine-rich protein with the LIM motif, is overexpressed in acute T-cell leukaemia with the t(11;14)(p13;q11). *Oncogene,* 6**,** 1887-93.

ROYER-POKORA, B., ROGERS, M., ZHU, T. H., SCHNEIDER, S., LOOS, U. & BOLITZ, U. 1995. The TTG-2/RBTN2 T cell oncogene encodes two alternative transcripts from two promoters: the distal promoter is removed by most 11p13 translocations in acute T cell leukaemia's (T-ALL). *Oncogene,* 10**,** 1353-60.

RUGGERO, K., AL-ASSAR, O., CHAMBERS, J. S., CODRINGTON, R., BREND, T. & RABBITTS, T. H. 2016. LMO2 and IL2RG synergize in thymocytes to mimic the evolution of SCID-X1 gene therapy-associated T-cell leukaemia. *Leukemia,* 30**,** 1959-62.

RUIZ, M. & LEFRANC, M. P. 2002. IMGT gene identification and Colliers de Perles of human immunoglobulins with known 3D structures. *Immunogenetics,* 53**,** 857-83.

RYSER, S., VIAL, E., MAGNENAT, E., SCHLEGEL, W. & MAUNDRELL, K. 1999. Reconstitution of caspase-mediated cell-death signalling in Schizosaccharomyces pombe. *Curr Genet,* 36**,** 21-8.
SADLER, I., CRAWFORD, A. W., MICHELSEN, J. W. & BECKERLE, M. C. 1992. Zyxin and cCRP: two interactive LIM domain proteins associated with the cytoskeleton. *J Cell Biol,* 119**,** 1573-87.
SAHIN, U., KARIKO, K. & TURECI, O. 2014. mRNA-based therapeutics--developing a new class of drugs. *Nat Rev Drug Discov,* 13**,** 759-80.
SAKAGUCHI, S. 2000. Regulatory T cells: key controllers of immunologic self-tolerance. *Cell,* 101**,** 455-8.
SAKAHIRA, H., ENARI, M. & NAGATA, S. 1998. Cleavage of CAD inhibitor in CAD activation and DNA degradation during apoptosis. *Nature,* 391**,** 96-9.
SAMBANDAM, A., MAILLARD, I., ZEDIAK, V. P., XU, L., GERSTEIN, R. M., ASTER, J. C., PEAR, W. S. & BHANDOOLA, A. 2005. Notch signaling controls the generation and differentiation of early T lineage progenitors. *Nat Immunol,* 6**,** 663-70.
SCHEFFZEK, K., AHMADIAN, M. R., KABSCH, W., WIESMULLER, L., LAUTWEIN, A., SCHMITZ, F. & WITTINGHOFER, A. 1997. The Ras-RasGAP complex: structural basis for GTPase activation and its loss in oncogenic Ras mutants. *Science,* 277**,** 333-8.
SCHINDELIN, J., ARGANDA-CARRERAS, I., FRISE, E., KAYNIG, V., LONGAIR, M., PIETZSCH, T., PREIBISCH, S., RUEDEN, C., SAALFELD, S., SCHMID, B., TINEVEZ, J. Y., WHITE, D. J., HARTENSTEIN, V., ELICEIRI, K., TOMANCAK, P. & CARDONA, A. 2012. Fiji: an open-source platform for biological-image analysis. *Nat Methods,* 9**,** 676-82.
SCHMEICHEL, K. L. & BECKERLE, M. C. 1997. Molecular dissection of a LIM domain. *Mol Biol Cell,* 8**,** 219-30.
SCHMITT, T. M. & ZUNIGA-PFLUCKER, J. C. 2002. Induction of T cell development from hematopoietic progenitor cells by delta-like-1 in vitro. *Immunity,* 17**,** 749-56.
SCHNEIDER, N. R., CARROLL, A. J., SHUSTER, J. J., PULLEN, D. J., LINK, M. P., BOROWITZ, M. J., CAMITTA, B. M., KATZ, J. A. & AMYLON, M. D. 2000. New recurring cytogenetic abnormalities and association of blast cell karyotypes with prognosis in childhood T-cell acute lymphoblastic leukemia: a pediatric oncology group report of 343 cases. *Blood,* 96**,** 2543-9.
SCHROEDER, H. W., JR. & CAVACINI, L. 2010. Structure and function of immunoglobulins. *J Allergy Clin Immunol,* 125**,** S41-52.
SELA-CULANG, I., KUNIK, V. & OFRAN, Y. 2013. The structural basis of antibody-antigen recognition. *Front Immunol,* 4**,** 302.
SEWELL, H., TANAKA, T., EL OMARI, K., MANCINI, E. J., CRUZ, A., FERNANDEZ-FUENTES, N., CHAMBERS, J. & RABBITTS, T. H. 2014. Conformational flexibility of the oncogenic protein LMO2 primes the formation of the multi-protein transcription complex. *Sci Rep,* 4**,** 3643.
SEYMOUR, L. W. & FISHER, K. D. 2016. Oncolytic viruses: finally delivering. *Br J Cancer,* 114**,** 357-61.
SHARIAT, S. F., DESAI, S., SONG, W., KHAN, T., ZHAO, J., NGUYEN, C., FOSTER, B. A., GREENBERG, N., SPENCER, D. M. & SLAWIN, K. M. 2001. Adenovirus-mediated transfer of inducible caspases: a novel "death switch" gene therapeutic approach to prostate cancer. *Cancer Res,* 61**,** 2562-71.
SHI, Y. 2002. Mechanisms of caspase activation and inhibition during apoptosis. *Mol Cell,* 9**,** 459-70.
SHIH, C., PADHY, L. C., MURRAY, M. & WEINBERG, R. A. 1981. Transforming genes of carcinomas and neuroblastomas introduced into mouse fibroblasts. *Nature,* 290**,** 261-4.
SHIMIZU, K., GOLDFARB, M., PERUCHO, M. & WIGLER, M. 1983. Isolation and preliminary characterization of the transforming gene of a human neuroblastoma cell line. *Proc Natl Acad Sci U S A,* 80**,** 383-7.
SHIN, S. M., CHOI, D. K., JUNG, K., BAE, J., KIM, J. S., PARK, S. W., SONG, K. H. & KIM, Y. S. 2017. Antibody targeting intracellular oncogenic Ras mutants exerts anti-tumour effects after systemic administration. *Nat Commun,* 8**,** 15090.
SHIVDASANI, R. A., MAYER, E. L. & ORKIN, S. H. 1995. Absence of blood formation in mice lacking the T-cell leukaemia oncoprotein tal-1/SCL. *Nature,* 373**,** 432-4.

SIMANSHU, D. K., NISSLEY, D. V. & MCCORMICK, F. 2017. RAS Proteins and Their Regulators in Human Disease. *Cell,* 170**,** 17-33.
SIMON, M. C. 1995. Gotta have GATA. *Nat Genet,* 11**,** 9-11.
SIMON, M. C., PEVNY, L., WILES, M. V., KELLER, G., COSTANTINI, F. & ORKIN, S. H. 1992. Rescue of erythroid development in gene targeted GATA-1- mouse embryonic stem cells. *Nat Genet,* 1**,** 92-8.
SODA, M., CHOI, Y. L., ENOMOTO, M., TAKADA, S., YAMASHITA, Y., ISHIKAWA, S., FUJIWARA, S., WATANABE, H., KURASHINA, K., HATANAKA, H., BANDO, M., OHNO, S., ISHIKAWA, Y., ABURATANI, H., NIKI, T., SOHARA, Y., SUGIYAMA, Y. & MANO, H. 2007. Identification of the transforming EML4-ALK fusion gene in non-small-cell lung cancer. *Nature,* 448**,** 561-6.
SPANGRUDE, G. J., HEIMFELD, S. & WEISSMAN, I. L. 1988. Purification and characterization of mouse hematopoietic stem cells. *Science,* 241**,** 58-62.
SPENCER, D. M., BELSHAW, P. J., CHEN, L., HO, S. N., RANDAZZO, F., CRABTREE, G. R. & SCHREIBER, S. L. 1996. Functional analysis of Fas signaling in vivo using synthetic inducers of dimerization. *Curr Biol,* 6**,** 839-47.
STENNICKE, H. R., JURGENSMEIER, J. M., SHIN, H., DEVERAUX, Q., WOLF, B. B., YANG, X., ZHOU, Q., ELLERBY, H. M., ELLERBY, L. M., BREDESEN, D., GREEN, D. R., REED, J. C., FROELICH, C. J. & SALVESEN, G. S. 1998. Pro-caspase-3 is a major physiologic target of caspase-8. *J Biol Chem,* 273**,** 27084-90.
STENNICKE, H. R. & SALVESEN, G. S. 1997. Biochemical characteristics of caspases-3, -6, -7, and -8. *J Biol Chem,* 272**,** 25719-23.
STERN, M. & HERRMANN, R. 2005. Overview of monoclonal antibodies in cancer therapy: present and promise. *Crit Rev Oncol Hematol,* 54**,** 11-29.
STEWART, M. P., SHAREI, A., DING, X., SAHAY, G., LANGER, R. & JENSEN, K. F. 2016. In vitro and ex vivo strategies for intracellular delivery. *Nature,* 538**,** 183-192.
SUN, J., BOTTOMLEY, S. P., KUMAR, S. & BIRD, P. I. 1997. Recombinant caspase-3 expressed in Pichia pastoris is fully activated and kinetically indistinguishable from the native enzyme. *Biochem Biophys Res Commun,* 238**,** 920-4.
TAGHON, T., YUI, M. A., PANT, R., DIAMOND, R. A. & ROTHENBERG, E. V. 2006. Developmental and molecular characterization of emerging beta- and gammadelta-selected pre-T cells in the adult mouse thymus. *Immunity,* 24**,** 53-64.
TANAKA, T., CHUNG, G. T., FORSTER, A., LOBATO, M. N. & RABBITTS, T. H. 2003a. De novo production of diverse intracellular antibody libraries. *Nucleic Acids Res,* 31**,** e23.
TANAKA, T., LOBATO, M. N. & RABBITTS, T. H. 2003b. Single domain intracellular antibodies: a minimal fragment for direct in vivo selection of antigen-specific intrabodies. *J Mol Biol,* 331**,** 1109-20.
TANAKA, T. & RABBITTS, T. H. 2003. Intrabodies based on intracellular capture frameworks that bind the RAS protein with high affinity and impair oncogenic transformation. *EMBO J,* 22**,** 1025-35.
TANAKA, T. & RABBITTS, T. H. 2008a. Functional intracellular antibody fragments do not require invariant intra-domain disulfide bonds. *J Mol Biol,* 376**,** 749-57.
TANAKA, T. & RABBITTS, T. H. 2008b. Interfering with protein-protein interactions: potential for cancer therapy. *Cell Cycle,* 7**,** 1569-74.
TANAKA, T. & RABBITTS, T. H. 2009. Selection of complementary single-variable domains for building monoclonal antibodies to native proteins. *Nucleic Acids Res,* 37**,** e41.
TANAKA, T. & RABBITTS, T. H. 2010a. Interfering with RAS-effector protein interactions prevent RAS-dependent tumour initiation and causes stop-start control of cancer growth. *Oncogene,* 29**,** 6064-70.
TANAKA, T. & RABBITTS, T. H. 2010b. Protocol for the selection of single-domain antibody fragments by third generation intracellular antibody capture. *Nat Protoc,* 5**,** 67-92.
TANAKA, T., SEWELL, H., WATERS, S., PHILLIPS, S. E. & RABBITTS, T. H. 2011. Single domain intracellular antibodies from diverse libraries: emphasizing dual functions of LMO2 protein interactions using a single VH domain. *J Biol Chem,* 286**,** 3707-16.
TANAKA, T., WILLIAMS, R. L. & RABBITTS, T. H. 2007. Tumour prevention by a single antibody domain targeting the interaction of signal transduction proteins with RAS. *EMBO J,* 26**,** 3250-9.
TAVERAS, A. G., REMISZEWSKI, S. W., DOLL, R. J., CESARZ, D., HUANG, E. C., KIRSCHMEIER, P., PRAMANIK, B. N., SNOW, M. E., WANG, Y. S., DEL ROSARIO, J. D., VIBULBHAN, B., BAUER, B. B., BROWN, J. E., CARR, D., CATINO, J.,

EVANS, C. A., GIRIJAVALLABHAN, V., HEIMARK, L., JAMES, L., LIBERLES, S., NASH, C., PERKINS, L., SENIOR, M. M., TSARBOPOULOS, A., WEBBER, S. E. & ET AL. 1997. Ras oncoprotein inhibitors: the discovery of potent, ras nucleotide exchange inhibitors and the structural determination of a drug-protein complex. *Bioorg Med Chem,* 5**,** 125-33.

TAYLOR, R. C., CULLEN, S. P. & MARTIN, S. J. 2008. Apoptosis: controlled demolition at the cellular level. *Nat Rev Mol Cell Biol,* 9**,** 231-41.

TERWILLIGER, T. & ABDUL-HAY, M. 2017. Acute lymphoblastic leukemia: a comprehensive review and 2017 update. *Blood Cancer J,* 7**,** e577.

TOMLINSON, I., SASIENI, P. & BODMER, W. 2002. How many mutations in a cancer? *Am J Pathol,* 160**,** 755-8.

TOWN, J., PAIS, H., HARRISON, S., STEAD, L. F., BATAILLE, C., BUNJOBPOL, W., ZHANG, J. & RABBITTS, T. H. 2016. Exploring the surfaceome of Ewing sarcoma identifies a new and unique therapeutic target. *Proc Natl Acad Sci U S A,* 113**,** 3603-8.

TRAIL, P. A., WILLNER, D., LASCH, S. J., HENDERSON, A. J., HOFSTEAD, S., CASAZZA, A. M., FIRESTONE, R. A., HELLSTROM, I. & HELLSTROM, K. E. 1993. Cure of xenografted human carcinomas by BR96-doxorubicin immunoconjugates. *Science,* 261**,** 212-5.

TSAI, F. Y., KELLER, G., KUO, F. C., WEISS, M., CHEN, J., ROSENBLATT, M., ALT, F. W. & ORKIN, S. H. 1994. An early haematopoietic defect in mice lacking the transcription factor GATA-2. *Nature,* 371**,** 221-6.

TSE, E. & RABBITTS, T. H. 2000. Intracellular antibody-caspase-mediated cell killing: an approach for application in cancer therapy. *Proc Natl Acad Sci U S A,* 97**,** 12266-71.

VALGE-ARCHER, V. E., OSADA, H., WARREN, A. J., FORSTER, A., LI, J., BAER, R. & RABBITTS, T. H. 1994. The LIM protein RBTN2 and the basic helix-loop-helix protein TAL1 are present in a complex in erythroid cells. *Proc Natl Acad Sci U S A,* 91**,** 8617-21.

VAN VLIERBERGHE, P. & FERRANDO, A. 2012. The molecular basis of T cell acute lymphoblastic leukemia. *J Clin Invest,* 122**,** 3398-406.

VAUPEL, P., KALLINOWSKI, F. & OKUNIEFF, P. 1989. Blood flow, oxygen and nutrient supply, and metabolic microenvironment of human tumors: a review. *Cancer Res,* 49**,** 6449-65.

VELDHOEN, M., HIROTA, K., CHRISTENSEN, J., O'GARRA, A. & STOCKINGER, B. 2009. Natural agonists for aryl hydrocarbon receptor in culture medium are essential for optimal differentiation of Th17 T cells. *J Exp Med,* 206**,** 43-9.

VETTER, I. R. & WITTINGHOFER, A. 2001. The guanine nucleotide-binding switch in three dimensions. *Science,* 294**,** 1299-304.

VINCI, M., GOWAN, S., BOXALL, F., PATTERSON, L., ZIMMERMANN, M., COURT, W., LOMAS, C., MENDIOLA, M., HARDISSON, D. & ECCLES, S. A. 2012. Advances in establishment and analysis of three-dimensional tumor spheroid-based functional assays for target validation and drug evaluation. *BMC Biol,* 10**,** 29.

VISVADER, J. E., MAO, X., FUJIWARA, Y., HAHM, K. & ORKIN, S. H. 1997. The LIM-domain binding protein Ldb1 and its partner LMO2 act as negative regulators of erythroid differentiation. *Proc Natl Acad Sci U S A,* 94**,** 13707-12.

VISVANATHAN, K. V., POCOCK, R. D. & SUMMERHAYES, I. C. 1988. Preferential and novel activation of H-ras in human bladder carcinomas. *Oncogene Res,* 3**,** 77-86.

VITELLI, L., CONDORELLI, G., LULLI, V., HOANG, T., LUCHETTI, L., CROCE, C. M. & PESCHLE, C. 2000. A pentamer transcriptional complex including tal-1 and retinoblastoma protein downmodulates c-kit expression in normal erythroblasts. *Mol Cell Biol,* 20**,** 5330-42.

VON FREEDEN-JEFFRY, U., VIEIRA, P., LUCIAN, L. A., MCNEIL, T., BURDACH, S. E. & MURRAY, R. 1995. Lymphopenia in interleukin (IL)-7 gene-deleted mice identifies IL-7 as a nonredundant cytokine. *J Exp Med,* 181**,** 1519-26.

WADMAN, I., LI, J., BASH, R. O., FORSTER, A., OSADA, H., RABBITTS, T. H. & BAER, R. 1994. Specific in vivo association between the bHLH and LIM proteins implicated in human T cell leukemia. *EMBO J,* 13**,** 4831-9.

WADMAN, I. A., OSADA, H., GRUTZ, G. G., AGULNICK, A. D., WESTPHAL, H., FORSTER, A. & RABBITTS, T. H. 1997. The LIM-only protein Lmo2 is a bridging molecule

assembling an erythroid, DNA-binding complex which includes the TAL1, E47, GATA-1 and Ldb1/NLI proteins. *EMBO J,* 16**,** 3145-57.
WALL, L., DEBOER, E. & GROSVELD, F. 1988. The human beta-globin gene 3' enhancer contains multiple binding sites for an erythroid-specific protein. *Genes Dev,* 2**,** 1089-100.
WARD, E. S., GUSSOW, D., GRIFFITHS, A. D., JONES, P. T. & WINTER, G. 1989. Binding activities of a repertoire of single immunoglobulin variable domains secreted from Escherichia coli. *Nature,* 341**,** 544-6.
WARREN, A. J., COLLEDGE, W. H., CARLTON, M. B., EVANS, M. J., SMITH, A. J. & RABBITTS, T. H. 1994. The oncogenic cysteine-rich LIM domain protein rbtn2 is essential for erythroid development. *Cell,* 78**,** 45-57.
WAY, J. C. & CHALFIE, M. 1988. mec-3, a homeobox-containing gene that specifies differentiation of the touch receptor neurons in C. elegans. *Cell,* 54**,** 5-16.
WEINSTEIN, I. B. 2002. Cancer. Addiction to oncogenes--the Achilles heal of cancer. *Science,* 297**,** 63-4.
WHYTE, D. B., KIRSCHMEIER, P., HOCKENBERRY, T. N., NUNEZ-OLIVA, I., JAMES, L., CATINO, J. J., BISHOP, W. R. & PAI, J. K. 1997. K- and N-Ras are geranylgeranylated in cells treated with farnesyl protein transferase inhibitors. *J Biol Chem,* 272**,** 14459-64.
WILDING, J. L. & BODMER, W. F. 2014. Cancer cell lines for drug discovery and development. *Cancer Res,* 74**,** 2377-84.
WILSON, A., MACDONALD, H. R. & RADTKE, F. 2001. Notch 1-deficient common lymphoid precursors adopt a B cell fate in the thymus. *J Exp Med,* 194**,** 1003-12.
WILSON, K. P., BLACK, J. A., THOMSON, J. A., KIM, E. E., GRIFFITH, J. P., NAVIA, M. A., MURCKO, M. A., CHAMBERS, S. P., ALDAPE, R. A., RAYBUCK, S. A. & ET AL. 1994. Structure and mechanism of interleukin-1 beta converting enzyme. *Nature,* 370**,** 270-5.
WOOLSTON, C. & MARTIN, S. 2011. Analysis of tumor and endothelial cell viability and survival using sulforhodamine B and clonogenic assays. *Methods Mol Biol,* 740**,** 45-56.
WORLD HEALTH ORGANIZATION. 2015. *Cancer* [Online]. Available: http://www.who.int/cancer/en/ [Accessed 17th July 2018].
WORN, A. & PLUCKTHUN, A. 1998. Mutual stabilization of VL and VH in single-chain antibody fragments, investigated with mutants engineered for stability. *Biochemistry,* 37**,** 13120-7.
WU, A. M. & YAZAKI, P. J. 2000. Designer genes: recombinant antibody fragments for biological imaging. *Q J Nucl Med,* 44**,** 268-83.
WU, L., XU, Y., WANG, Q., RUAN, C., DREXLER, H. G., WU, D., MACLEOD, R. A. & CHEN, S. 2015. High frequency of cryptic chromosomal rearrangements involving the LMO2 gene in T-cell acute lymphoblastic leukemia. *Haematologica,* 100**,** e233-6.
YAMABE, K., SHIMIZU, S., ITO, T., YOSHIOKA, Y., NOMURA, M., NARITA, M., SAITO, I., KANEGAE, Y. & MATSUDA, H. 1999. Cancer gene therapy using a pro-apoptotic gene, caspase-3. *Gene Ther,* 6**,** 1952-9.
YAMADA, Y., PANNELL, R., FORSTER, A. & RABBITTS, T. H. 2000. The oncogenic LIM-only transcription factor Lmo2 regulates angiogenesis but not vasculogenesis in mice. *Proc Natl Acad Sci U S A,* 97**,** 320-4.
YAMADA, Y., PANNELL, R., FORSTER, A. & RABBITTS, T. H. 2002. The LIM-domain protein Lmo2 is a key regulator of tumour angiogenesis: a new anti-angiogenesis drug target. *Oncogene,* 21**,** 1309-15.
YAMADA, Y., WARREN, A. J., DOBSON, C., FORSTER, A., PANNELL, R. & RABBITTS, T. H. 1998. The T cell leukemia LIM protein Lmo2 is necessary for adult mouse hematopoiesis. *Proc Natl Acad Sci U S A,* 95**,** 3890-5.
YAMAGUCHI, H. & MIYAZAKI, M. 2014. Refolding techniques for recovering biologically active recombinant proteins from inclusion bodies. *Biomolecules,* 4**,** 235-51.
ZHANG, J., DING, L., HOLMFELDT, L., WU, G., HEATLEY, S. L., PAYNE-TURNER, D., EASTON, J., CHEN, X., WANG, J., RUSCH, M., LU, C., CHEN, S. C., WEI, L., COLLINS-UNDERWOOD, J. R., MA, J., ROBERTS, K. G., POUNDS, S. B., ULYANOV, A., BECKSFORT, J., GUPTA, P., HUETHER, R., KRIWACKI, R. W., PARKER, M., MCGOLDRICK, D. J., ZHAO, D., ALFORD, D., ESPY, S., BOBBA, K. C., SONG, G., PEI, D., CHENG, C., ROBERTS, S., BARBATO, M. I., CAMPANA, D.,

COUSTAN-SMITH, E., SHURTLEFF, S. A., RAIMONDI, S. C., KLEPPE, M., COOLS, J., SHIMANO, K. A., HERMISTON, M. L., DOULATOV, S., EPPERT, K., LAURENTI, E., NOTTA, F., DICK, J. E., BASSO, G., HUNGER, S. P., LOH, M. L., DEVIDAS, M., WOOD, B., WINTER, S., DUNSMORE, K. P., FULTON, R. S., FULTON, L. L., HONG, X., HARRIS, C. C., DOOLING, D. J., OCHOA, K., JOHNSON, K. J., OBENAUER, J. C., EVANS, W. E., PUI, C. H., NAEVE, C. W., LEY, T. J., MARDIS, E. R., WILSON, R. K., DOWNING, J. R. & MULLIGHAN, C. G. 2012. The genetic basis of early T-cell precursor acute lymphoblastic leukaemia. *Nature,* 481**,** 157-63.

ZHANG, N., HARTIG, H., DZHAGALOV, I., DRAPER, D. & HE, Y. W. 2005. The role of apoptosis in the development and function of T lymphocytes. *Cell Res,* 15**,** 749-69.

ZHANG, Y., GAO, S., XIA, J. & LIU, F. 2018. Hematopoietic Hierarchy - An Updated Roadmap. *Trends Cell Biol*.

ZUFFEREY, R., DULL, T., MANDEL, R. J., BUKOVSKY, A., QUIROZ, D., NALDINI, L. & TRONO, D. 1998. Self-inactivating lentivirus vector for safe and efficient in vivo gene delivery. *J Virol,* 72**,** 9873-80.

ZUNIGA-PFLUCKER, J. C. 2004. T-cell development made simple. *Nat Rev Immunol,* 4**,** 67-72.

Appendix A

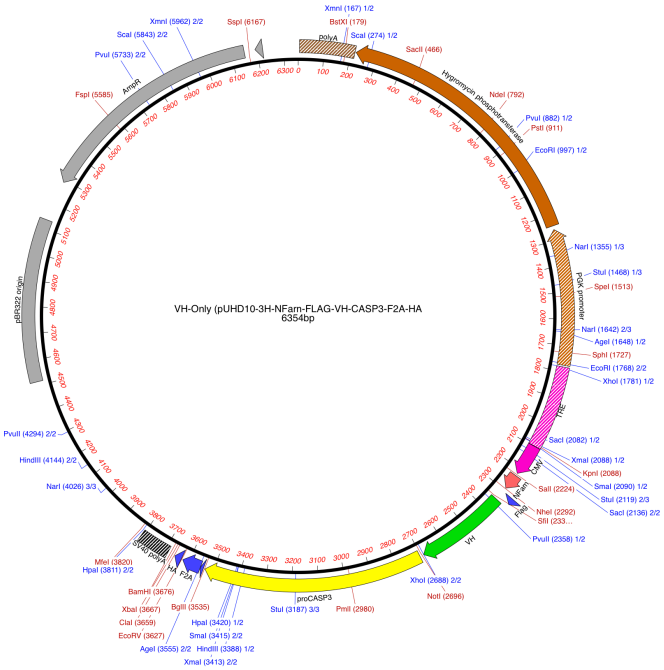

VH-Only AIDA construct: VH fragment replaced as necessary with variants. CASP3 moieties repaced with single (Δ) and double (ΔΔ) mutants as required.

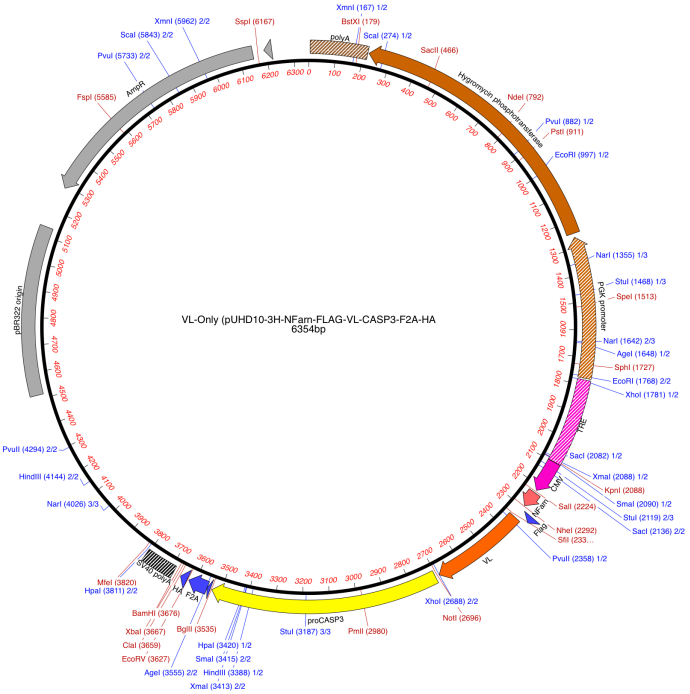

VL-Only AIDA construct.

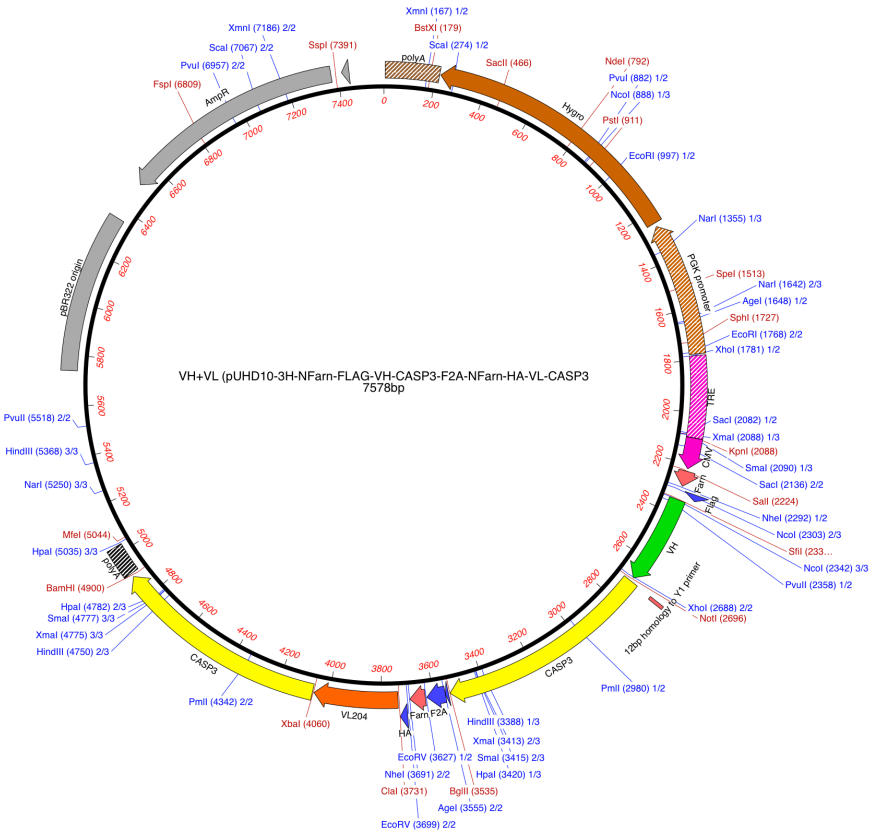

VH+VL AIDA construct: VH fragment replaced as necessary with variants. CASP3 moieties repaced with single (Δ) and double (ΔΔ) mutants as required.

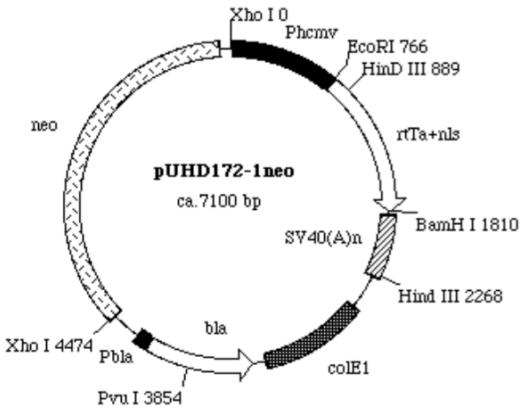

pUHD172-1Neo (TetOn coding the rtTA) had been used to create HT1080TetOn cells Reference: GOSSEN, M., FREUNDLIEB, S., BENDER, G., MULLER, G., HILLEN, W. & BUJARD, H. 1995. Transcriptional activation by tetracyclines in mammalian cells. *Science,* 268**,** 1766-9.

Cloning NFarn to single vectors and first half of VH+VL vector, via SalI/XhoI:
pUHD10 N-Fn F SalI:
5'-GAACTGGTCGACATGCTGTGCTGTATGAGAAGAA-3'
pUHD10 N-Fn R XhoI:
5'-CAGTCTCGAG*GCTAGC*TGGATCTTTTGGTCCTCATCATTC-3'

Cloning NFarn to second half of VH+VL vector, via EcoRV and orientated via NheI:
VL region of double plasmid Forward:
GAACTGGATATCATGCTGTGCTGTATGAGAAGAA
VL region of double plasmid Reverse:
CAGTGATATCGCTAGCGATCTTTTGGTCCTCATCATTC

Cloning of VH#Y6 variants:
Subcloned via SfiI/NotI from laboratory plasmids pGC-IRES-GFP-1755-3019-1, published in TANAKA, T., WILLIAMS, R. L. & RABBITTS, T. H. 2007. Tumour prevention by a single antibody domain targeting the interaction of signal transduction proteins with RAS. *EMBO J,* 26**,** 3250-9. and from plasmid 1374.2 (unpublished, also made by Dr Tomoyuki Tanaka and Prof. T.H. Rabbitts).

Cloning of single CASP3 catalytic mutants:
Template used from TSE, E. & RABBITTS, T. H. 2000. Intracellular antibody-caspase-mediated cell killing: an approach for application in cancer therapy. *Proc Natl Acad Sci U S A,* 97**,** 12266-71.

CASP3 (First moiety) via BglII.NotI
NotI-CASP3-F 5'-ATTATAGCGGCCGCAATGGAGAACACTGAAAACTC-3'
BglII-CASP3-R 5'-GTACAGAGATCCTCAGTGATAAAAATAGAGTTCTTTTG-3

CASP3 (Second moiety) via XbaI/BamHI
XbaI-CASP3-F 5'-AGCCTGTCTAGAATGGAGAACACTGAAAACTC-3'
BamHI-CASP3-R 5'-TACTGAGGATCCTCAGTGATAAAAATAGAGTTCTTTTG-3'

Cloning of double CASP3 catalytic mutant:
for inverse PCR of C163S CP3 mutant vector to incorporate His121 to Gly mutation. PCR in two sets for assembly

CP3_H121G_F 5'-GCTTCTGAGCGGTGGTGAAGAAGG-3'
CP3_H121G_R 5'-CCTTCTTCACCACCGCTCAGAAGC-3'

Pairs for single vectors and first half of VH+VL vector:
Y6-3'-Fwd 5'-GAACAGCCTGAGAGCCGAGG-3'
CP3_H121G_R 5'-CCTTCTTCACCACCGCTCAGAAGC-3'

CP3_H121G_F 5'-GCTTCTGAGCGGTGGTGAAGAAGG-3'
F2A-3'-Rev 5'-CGAGTCCAACCCTGGCCC-3'

Pairs for second half of VH+VL vector:
VL204-3'-Fwd 5'-CACCATCAGCAGTCTGCAACC-3'
CP3_H121G_R 5'-CCTTCTTCACCACCGCTCAGAAGC-3'

CP3_H121G_F 5'-GCTTCTGAGCGGTGGTGAAGAAGG-3'
SV40pA-Rev 5'-CCACAACTAGAATGCAGTGAA-3'

Appendix B

RT-PCR Primers for RAS mutation analysis

All 5'-3'. HindIII site on forward primer, BamHI on reverse primer (both underlined) for cloning into pBluescript SKII+. (Primers designed by Dr Ami Miller, Rabbitts laboratory, WIMM, University of Oxford). Clones sequenced with T7 promoter primer 5'- TAA TAC GAC TCA CTA TAG GG-3' (Source Bioscience, Nottingham, UK).

KRAS_F: TAAGCAAAGCTTATGACTGAATATAAACTTGTGGTAG
KRAS_R: TGCTTAGGATCCTTACATTATAATGCATTTTTTAATTTTC

NRAS_F: TAAGCAAAGCTTATGACTGAGTACAAACTGGTGGTGG
NRAS_R: TGCTTAGGATCCTTACATCACCACACATGGCAATCC

HRAS_F: TAAGCAAAGCTTATGACGGAATATAAGCTGGTGGTG
HRAS_R: TGCTTAGGATCCTCAGGAGAGCACACACTTGC

Appendix C

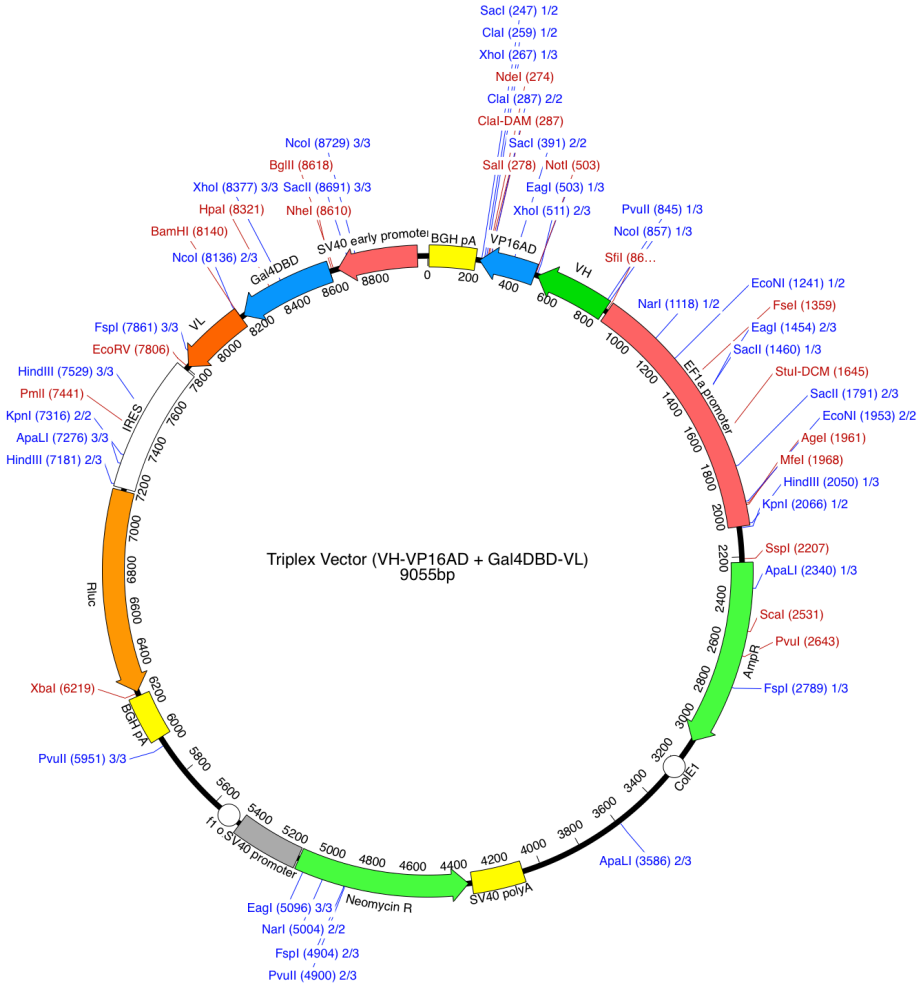

Triplex vector plasmid map, containing various VH and VL single domain fragments

VH Cloning:
SfiI VH Common Fwd
5'-TATAGGCCCAGCCGGCCATGGCCGAGGTGCAGCTGTTGG-3'
NotI VH Common Rev
5'-TACAGCGGCCGCGCTCGAGACGGTGACCAGGGTTCCCTG-3'

Digested and cloned into Triplex vector via SfiI/NotI double digest.

VL Cloning:
BamHI VL Common Fwd
5'-CTAGGGATCCATATGGACATCCAGATGACCCAG-3'
EcoRV VL Common Fwd
5'-CTAAGATATCTTACCGTTTGATTTCCACCTTGG-3'

Digested and cloned into Triplex vector via BamHI/EcoRV double digest

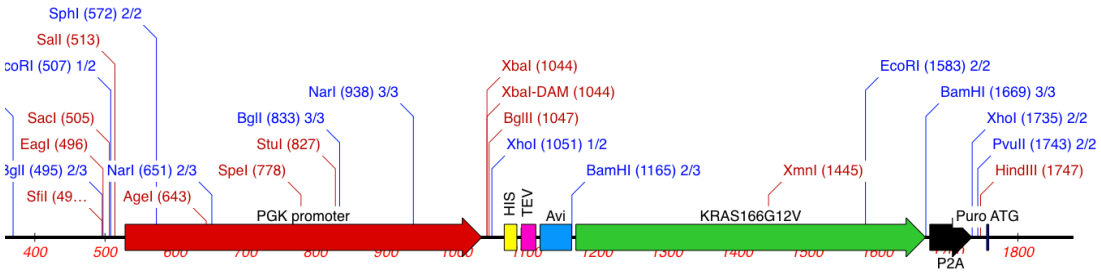

pPGK-HisTev-Avi-KRAS166(G12V)-P2A-Puro (KRAS antigen plasmid)

Fwd 5'-ATTCGATATCGCCGCCACCATGGGACATCACCATCACCATCAC-3'
Rev 5'-AGAAGATATCCTAATGTTTTCGAATTTCTCG-3'

Appendix D

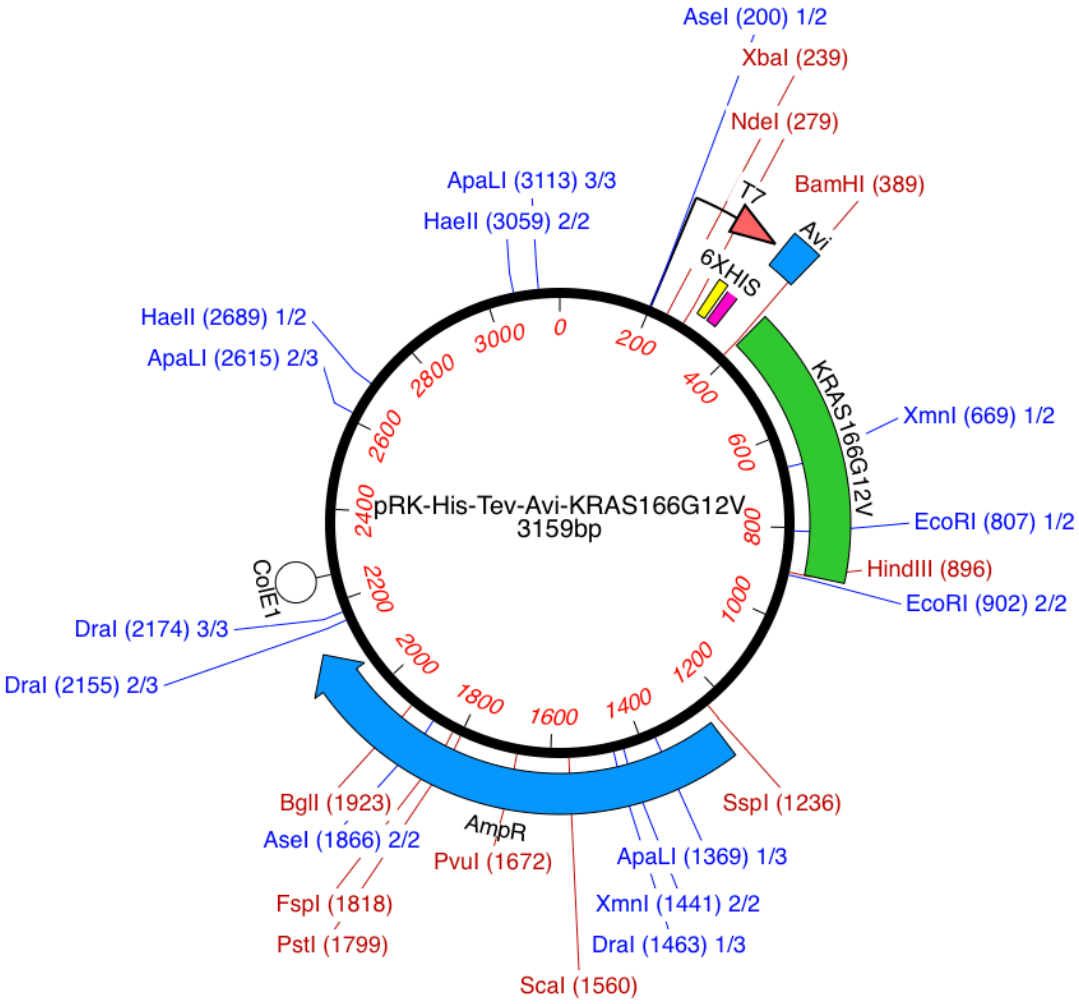

pRK-HisTev-Avi-KRAS166G12V plasmid map
(Made by and obtained from by Dr Ami Miller, Rabbitts laboratory, WIMM, University of Oxford).

pRK-HisTev-Avi-VH/VL-proCASP3 cloning

Stuffer Oligos

Oligos annealed and cloned into pRK-HisTev-Avi (with KRas excised) via BamHI/HindIII. VH/VL-proCASP3 inserts were cloned via SfiI/BglII. Restriction sites underlined.

BamHI SfiI BglII HindIII
5'-TTACGGATCCAAGGCCCAGCCGGCCCTGCAGAGATCTTAAAAGCTTACTA-3'

3'-AATGCCTAGGTTCCGGGTCGGCCGGGACGTCTCTAGAATTTTCGAATGAT-5'

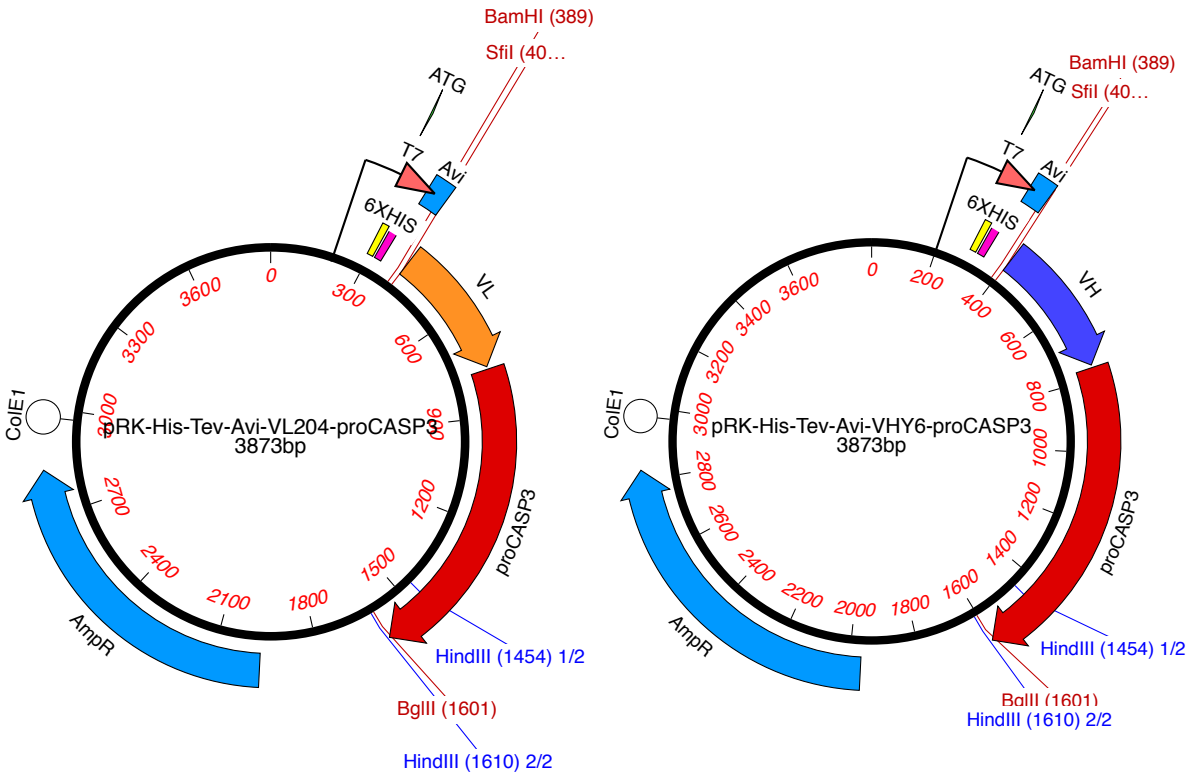

Appendix E

Reversible CASP3 inhibitor production protocol and NMR trace:

(Method written by Dr Carole Bataille, Rabbitts laboratory, Dept. of Chemistry, University of Oxford)

All solvents and reagents were used as supplied (analytical or HPLC grade) without prior purification. Water was purified by an Elix® UV-10 system. *In vacuo* refers to the use of a rotary evaporator attached to a diaphragm pump. Thin layer chromatography was performed on aluminium plates coated with 60 F254 silica. Plates were visualised using UV light (254 nm) or 1% aq. $KMnO_4$. Flash column chromatography was performed on Kieselgel 60M silica in a glass column. NMR spectra were recorded on Bruker Avance spectrometers (AVII400) in the deuterated solvent stated. The field was locked by external referencing to the relevant deuteron resonance. Chemical shifts (δ) are reported in parts per million (ppm) referenced to the solvent peak. ^1H spectra reported to two decimal places, and coupling constants (*J*) are quoted in Hz (reported to one decimal place). The multiplicity of each signal is indicated by: s (singlet); br s (broad singlet); d (doublet); t (triplet); dd (doublet of doublets); or m (multiplet). Low-resolution mass spectra were recorded on an Agilent 6120 spectrometer from solutions of MeOH; m/z values are reported in Daltons.

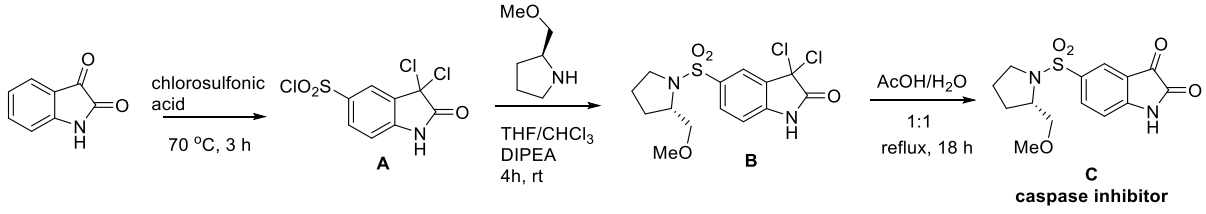

Chlorosulfonic acid (20.0 mL, 340 mmol) was added dropwise with a dropping funnel, to ice-cold isatin (10.0 g, 68.0 mmol). The resulting solution was heated to 70 C for 3h, cooled to room temperature and poured carefully in ice (200 g). After the ice melted, the aqueous phase was extracted with CH_2Cl_2 (5 x 150 mL). The organic phase was dried (Na_2SO_4), filtered and concentrated *in vacuo* to afford the desired product **A** as a bright yellow solid (11.2 g, 55%). To a solution of compound A (4.72 g, 15.8 mmol) in $CHCl_3$/THF (100 mL, 1:1) was added sequentially (*S*)-2-methoxymethylpyrrolidine (2 g, 17.4 mmol) and *N*,*N*-diisopropylethylamine (4.10 mL, 23.7 mmol). The mixture was stirred for 1 h, concentrated *in vacuo* and the resulting brown oil used directly in the next step. Compound **B** was dissolved in AcOH/water (60 mL, 1:1) and the resulting solution heated to 90 C for 18 h.The mixture was cooled down before careful addition of $NaHCO_3$ (45.0 g). The aqueous phase was extracted with EtOAc (3 x 70 mL), the combined organic phase washed with water, dried (Na_2SO_4), filtered and concentrated *in vacuo*. Purification of the crude residue on silica gel (acetone/pentane, 1:4) afforded the desired compound **C** as a yellow solid (4.23 g, 84% over two steps).

^{1}H NMR (400 MHz, $CDCl_3$) δ = 6.54 (1H, br s), 8.1 (2H, ddd, *J* 8.8, 3.4, 1.8 Hz), 7.11 (1H, d, *J* 8.8 Hz), 3.78-3.72 (1H, m), 3.51 (1H, dd, *J* 9.4, 3.9 Hz), 3.48-3.41 (1H, m), 3.40 (1H, dd, *J* 9.4, 1.8 Hz), 3.37 (3H, s), 3.19-3.12 (1H, m), 1.97-1.88 (2H, m), 1.74-1.66 (2H, m). LRMS (ESI$^-$) 323.1 $(M-H)^-$.

^{1}H NMR

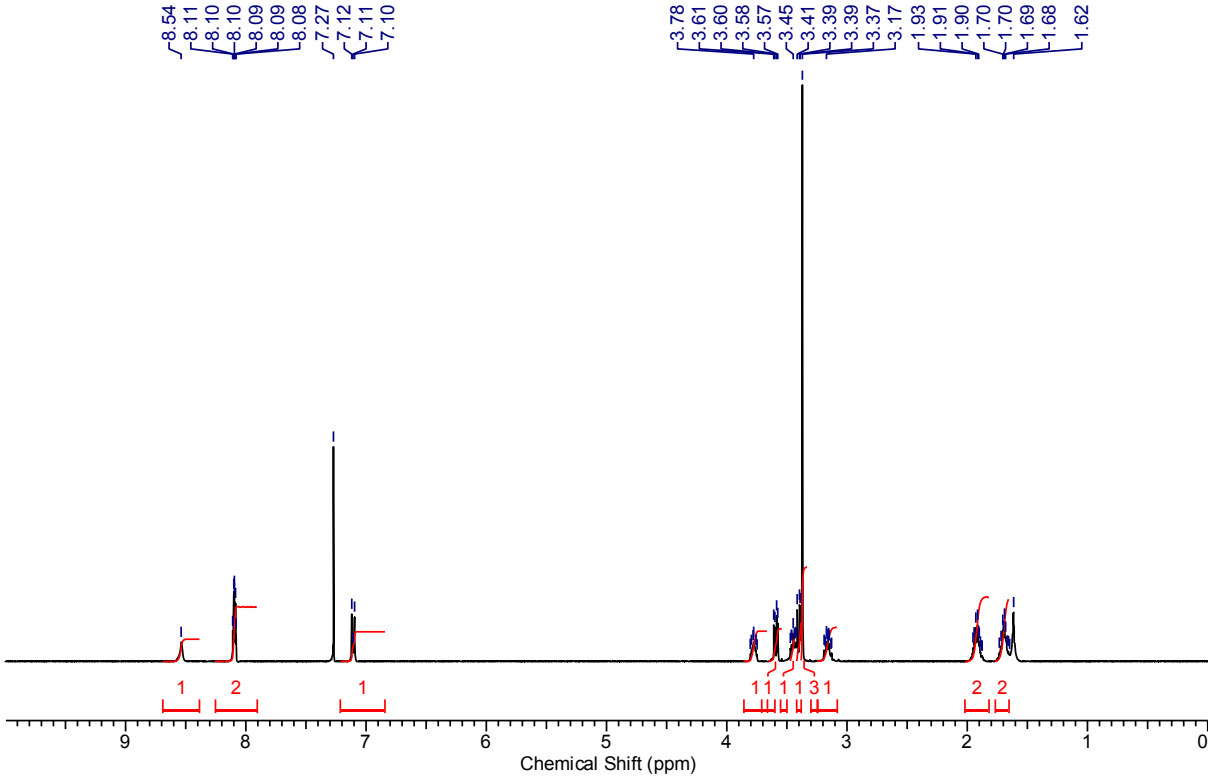

References:

LEE, D., LONG, S. A., ADAMS, J. L., CHAN, G., VAIDYA, K. S., FRANCIS, T. A., KIKLY, K., WINKLER, J. D., SUNG, C. M., DEBOUCK, C., RICHARDSON, S., LEVY, M. A., DEWOLF, W. E., JR., KELLER, P. M., TOMASZEK, T., HEAD, M. S., RYAN, M. D., HALTIWANGER, R. C., LIANG, P. H., JANSON, C. A., MCDEVITT, P. J., JOHANSON, K., CONCHA, N. O., CHAN, W., ABDEL-MEGUID, S. S., BADGER, A. M., LARK, M. W., NADEAU, D. P., SUVA, L. J., GOWEN, M. & NUTTALL, M. E. 2000. Potent and selective nonpeptide inhibitors of caspases 3 and 7 inhibit apoptosis and maintain cell functionality. *J Biol Chem,* 275**,** 16007-14.

LEE, D., LONG, S. A., MURRAY, J. H., ADAMS, J. L., NUTTALL, M. E., NADEAU, D. P., KIKLY, K., WINKLER, J. D., SUNG, C. M., RYAN, M. D., LEVY, M. A., KELLER, P. M. & DEWOLF, W. E., JR. 2001. Potent and selective nonpeptide inhibitors of caspases 3 and 7. *J Med Chem,* 44**,** 2015-26.

Appendix F

Primers for cloning mRuby2 into pLVX-TetOne (Clontech)

Primers used clone mRuby2 into pLVX-TetOne with P2A separation via PCR assembly.

Sma_Pst_P2A _F:	5'-TA*CCCGGGCTGCAGGGAGCTACTAACTTCAGCC* SmaI PstI P2A annealing
(mRuby)P2A_R:	5'-*TTAGACACCAT*AGGTCCAGGGTTCTCCTCC-3' Ruby o/hang P2A annealing
(P2A)mRuby_F:	5'-*ACCCTGGACCT*ATGGTGTCTAAGGGCGAAG-3' P2A o/hang mRuby2 annealing
S_mRuby2_R:	5'-TACCCGGGTTACTTGTACAGCTCGTCCATC-3' SmaI Stop mRuby2 annealing

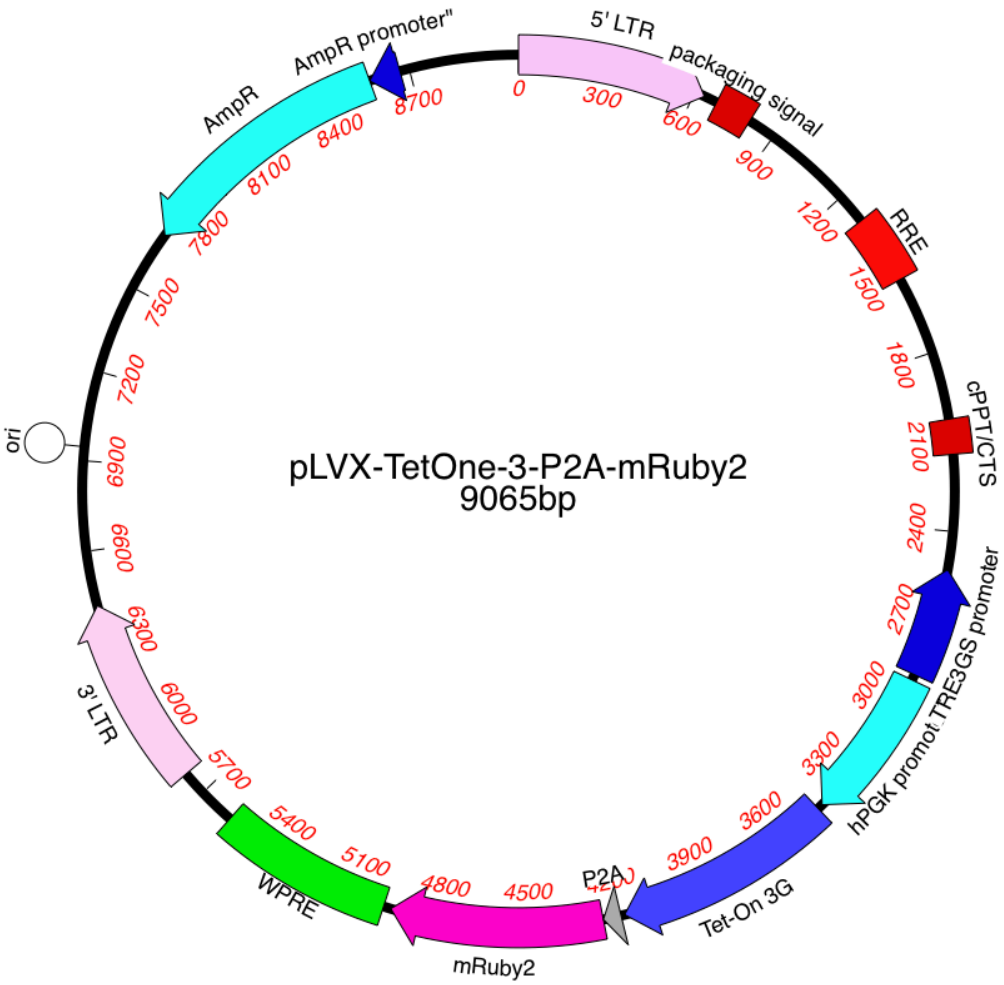

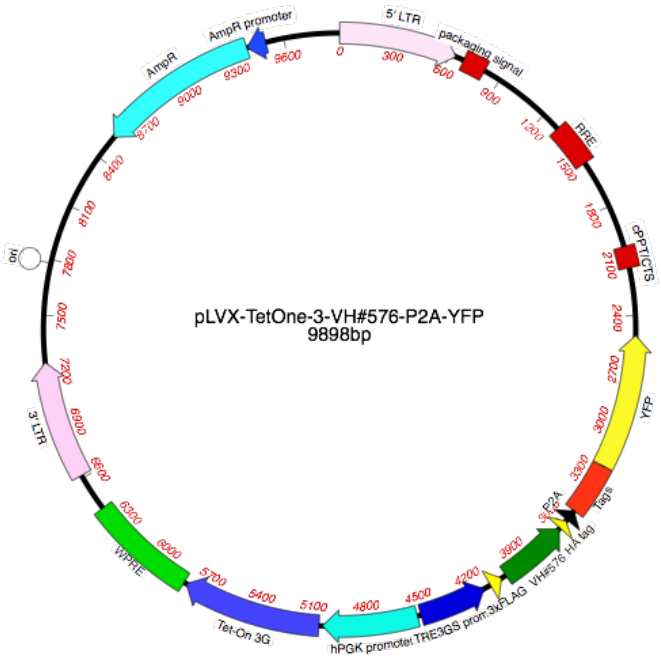

VH#576-P2A-YFP cloned into pLVX-TetOne (Clontech)

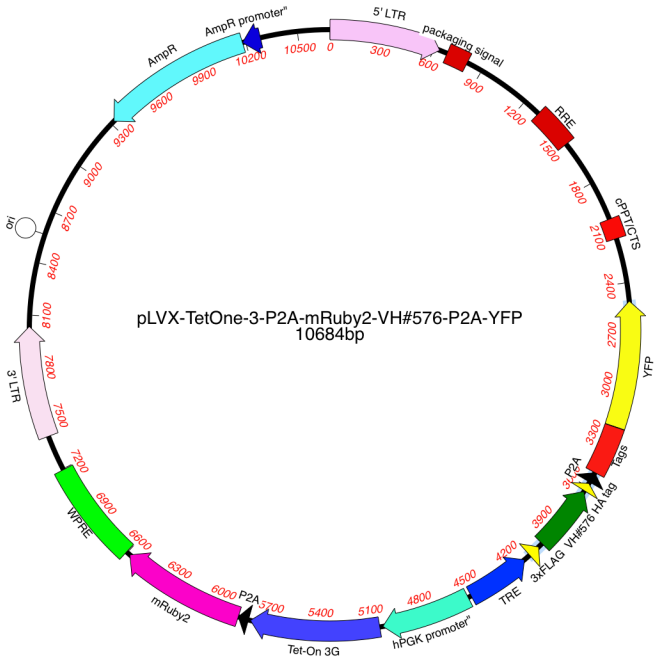

mRuby2-VH#576-P2A-YFP cloned into pLVX-TetOne (Clontech)

Appendix G

Tripartite GFP plasmids

Original plasmids containing VH#576 and VL#I21 targeted with the N-terminal farnesylation (NFarn) sequence were made by and obtained from by Dr Ami Miller, Rabbitts laboratory, WIMM, University of Oxford. Plasmids were modified during this thesis to remove the NFarn sequence and replace the VH and VL moieties with the variant antibodies.

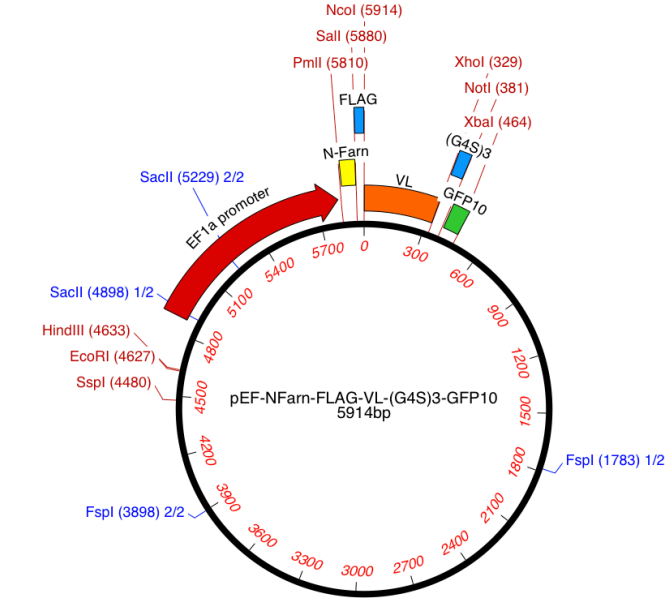

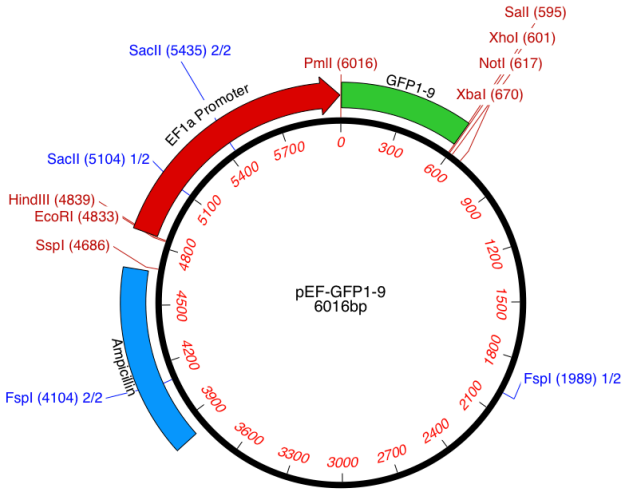

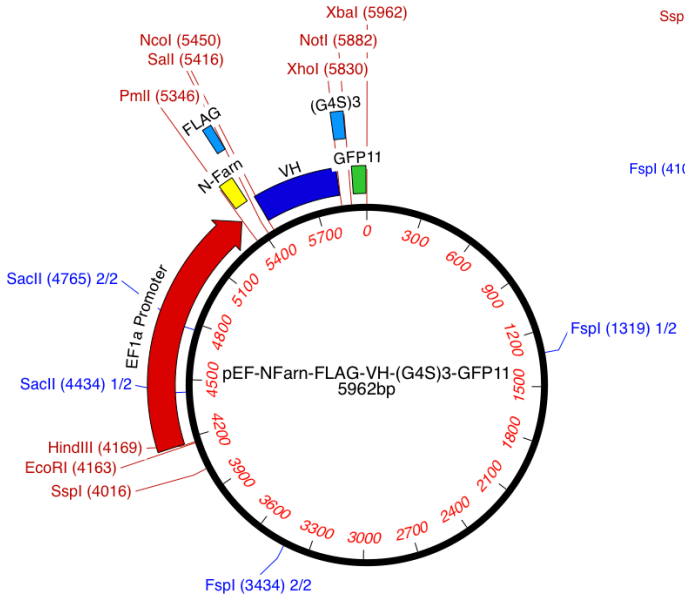

NFarn removal stuffer fragment:

PmlI SalI
Stuffer Fwd 5'-CAATCACGTGGGATCCATCGATGTCGACGCTA-3'

Stuffer Rev 5'- GTTAGTGCACCCTAGGTAGCTACAGCTGCGAT -3'

Cloning VH variants to GFP11 vector via NcoI/XhoI:

NcoI VH Common Fwd
5'-AGGCCCATGGCCGAGGTGCAGCTGTTGG-3'
XhoI VH Common Rev
5'-CGCCCTCGAGAGAACTAACGGTGACCAGGGTTC-3'

Cloning VL variants to GFP10 vector via NcoI/XhoI:

NcoI VL Common Fwd
5'-CAGGCCCATGGACATCCAGATGACCCAG-3'
XhoI VL Common Rev
5'-CGCCCTCGAGCCGTTTGATTTCCACCTTGG-3'

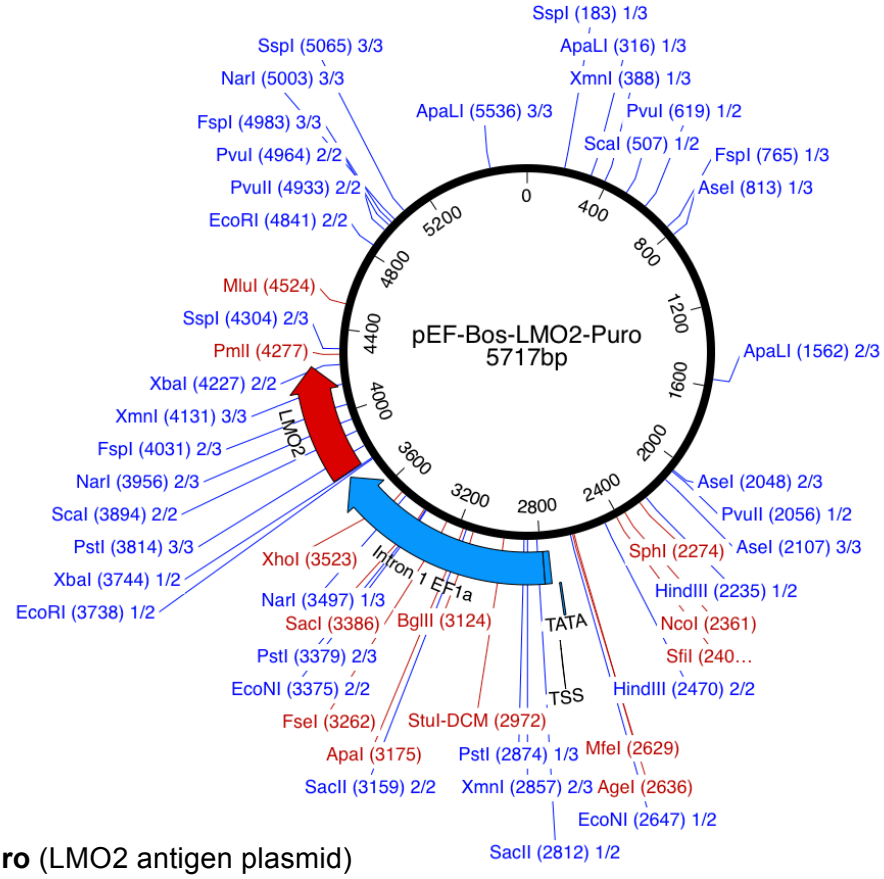

pEF-Bos-LMO2-Puro (LMO2 antigen plasmid)
Mouse *Lmo2*, subcloned via [NcoI] into pEF-Bos-Puro [BamHI].

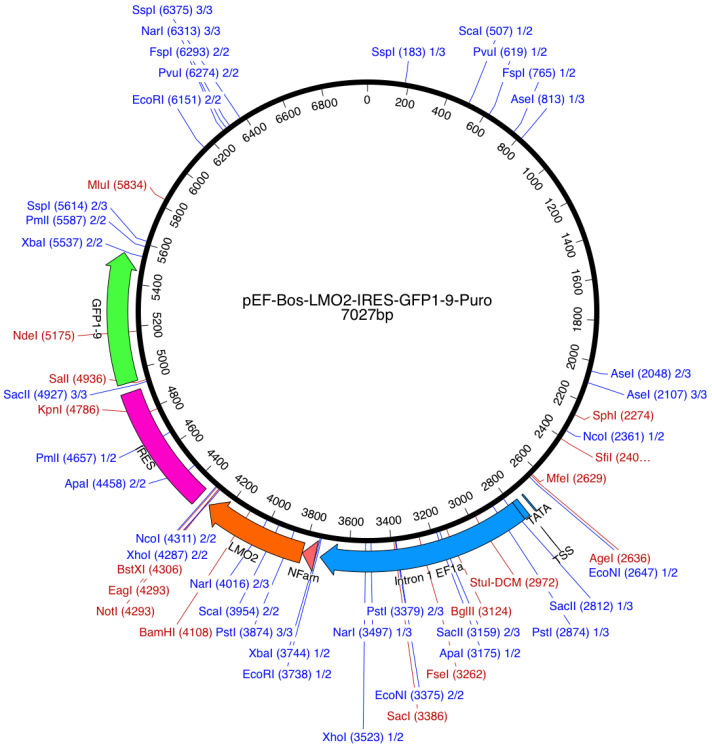

pEF-Bos-NFarn-LMO2-IRES-GFP1-9 map and construction

(Combined antigen and GFP1-9 plasmid)

PCR amplify 1) Kozak-NFarn and 2) LMO2-Ile-STOP then assemble

RV-Koz-NF Fwd 5'-GGATCGATATCGCCGCCACCATGGGAATGCTGTGCTGTATGAG
LMO2-NF Rev 5'-CCTTTCGATGGCCGAGGCCATGATCTTTTGGTCCTCATC-3'

NF-LMO2 Fwd 5'-GATGAGGACCAAAAGATCATGGCCTCGGCCATCGAAAGG-3'
LMO2-Ile-stp-RI Rev 5'-TAATCGAATTCTTAGATGATCCCATTGATCTTGGTCC-3'

Digest EcoRV and EcoRI, clone to same sites pIRES-neo2 (Clontech)Remove Neo cassette via SmaI [blunt cutter] & XhoI – this also removes the polyA. Clone in GFP1-9 via PmlI [blunt cutter] & XhoI (already contains stop codon but will not have a polyA until in the final BOS-Puro vector).

Excise whole cassette via EcoRV [blunt cutter] and [XhoI], clone into pEF-BOS-Puro via [BamHI]. Screen for orientation.

CDR randomised library degenerate primers:

XhoI-VLI21 Rev: 5'-ACTCTCGAGCCGTTTGATTTCCAC-3'
(common reverse primer for use in assembly PCR)

CDR1:
rdmVLCDR1Rev:
5'CCTGGTTTCTGCTGATACCAMNNTAAMNNGCTGCTAATMNNCTGACTTGCCCGGCAAGTGATG-3'

VLCDR1 Fwd: 5'-TGGTATCAGCAGAAACCAGG-3'

CDR2:
rdmVLCDR2 Rev:
5'AACCTTGATGGGACCCCACTMNNMNNMNNGGATGCATTATAGATCAGGAGCTTAGGGG-3'

VLCDR2 Fwd: 5'-AGTGGGGTCCCATCAAGGTTCAG-3'

CDR3:
XhoI rdmVLCDR3 Rev:
5'AGCctcgagCCGTTTGATTTCCACCTTGGTCCCTTGGCCGAACGTMNNAGGMNNMNNMNNMNNCTGTTGACAGTAGTAAGTTGC-3'

use with:
NcoI VL Common Fwd 5'-CAGGCCCATGGACATCCAGATGACCCAG-3'

Clone fragments via NoI/XhoI into GFP10 vector.

Appendix H

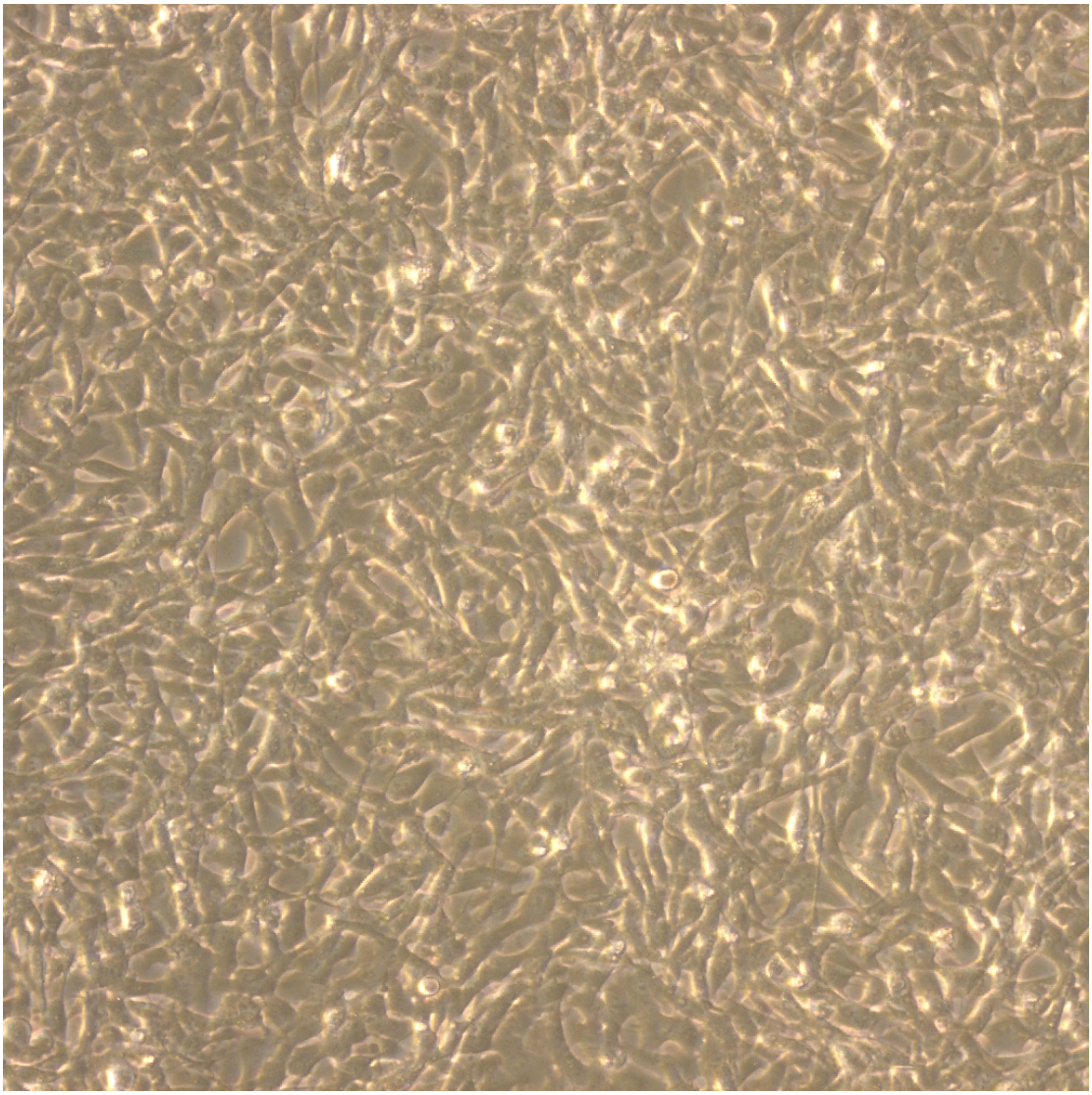

Parent cell morphology upon tetracycline induction

Images taken of the Parent clone after 72 hours tetracycline induction of expression. Images were taken with a 10x Objective lens.

Parental cells are of normal HT1080 appearance.

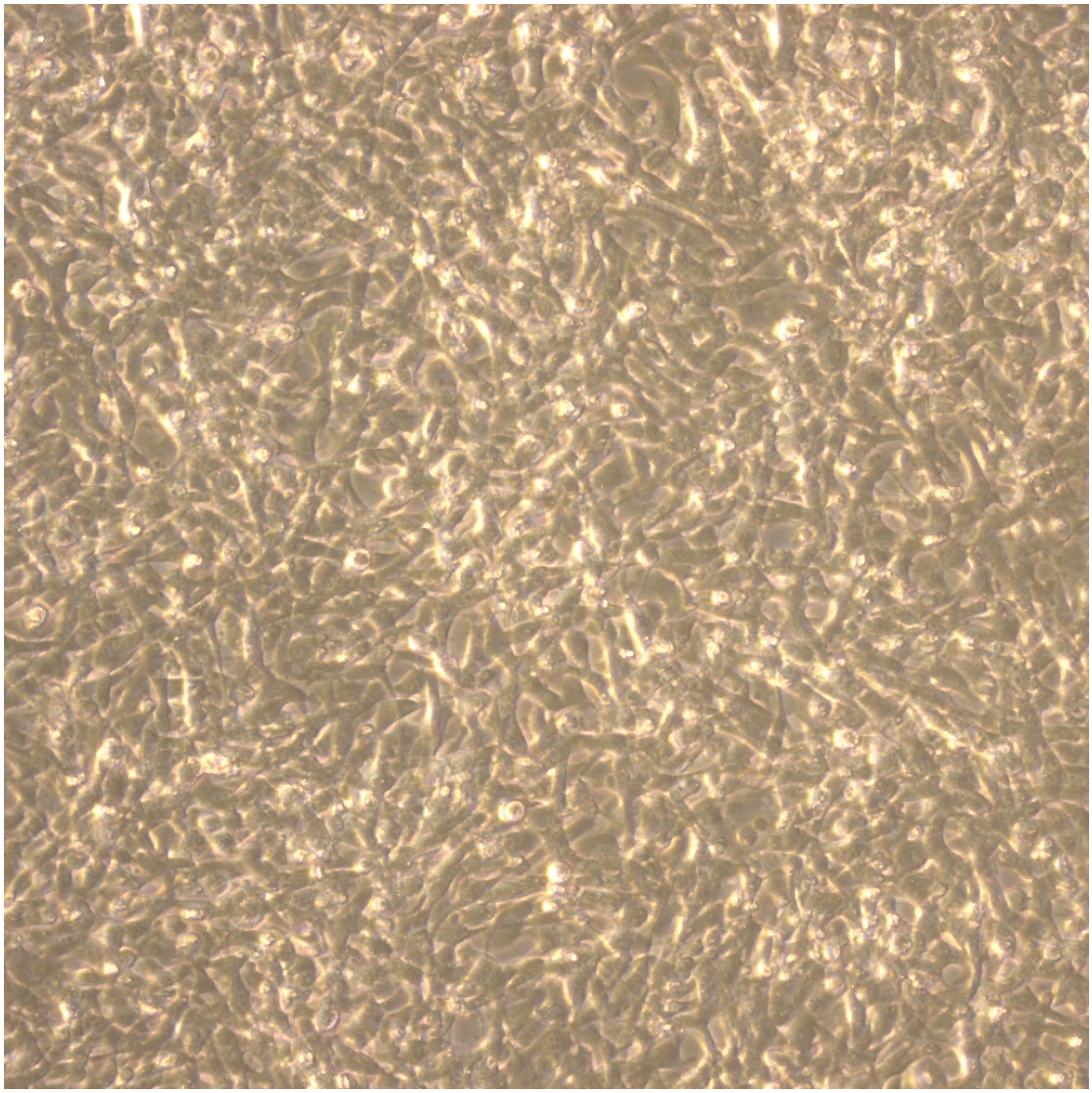

VL-Only cell morphology upon tetracycline induction

Images taken of the VL-Only clone B after 72 hours tetracycline induction of expression. Images were taken with a 10x Objective lens.

Cells appear normal.

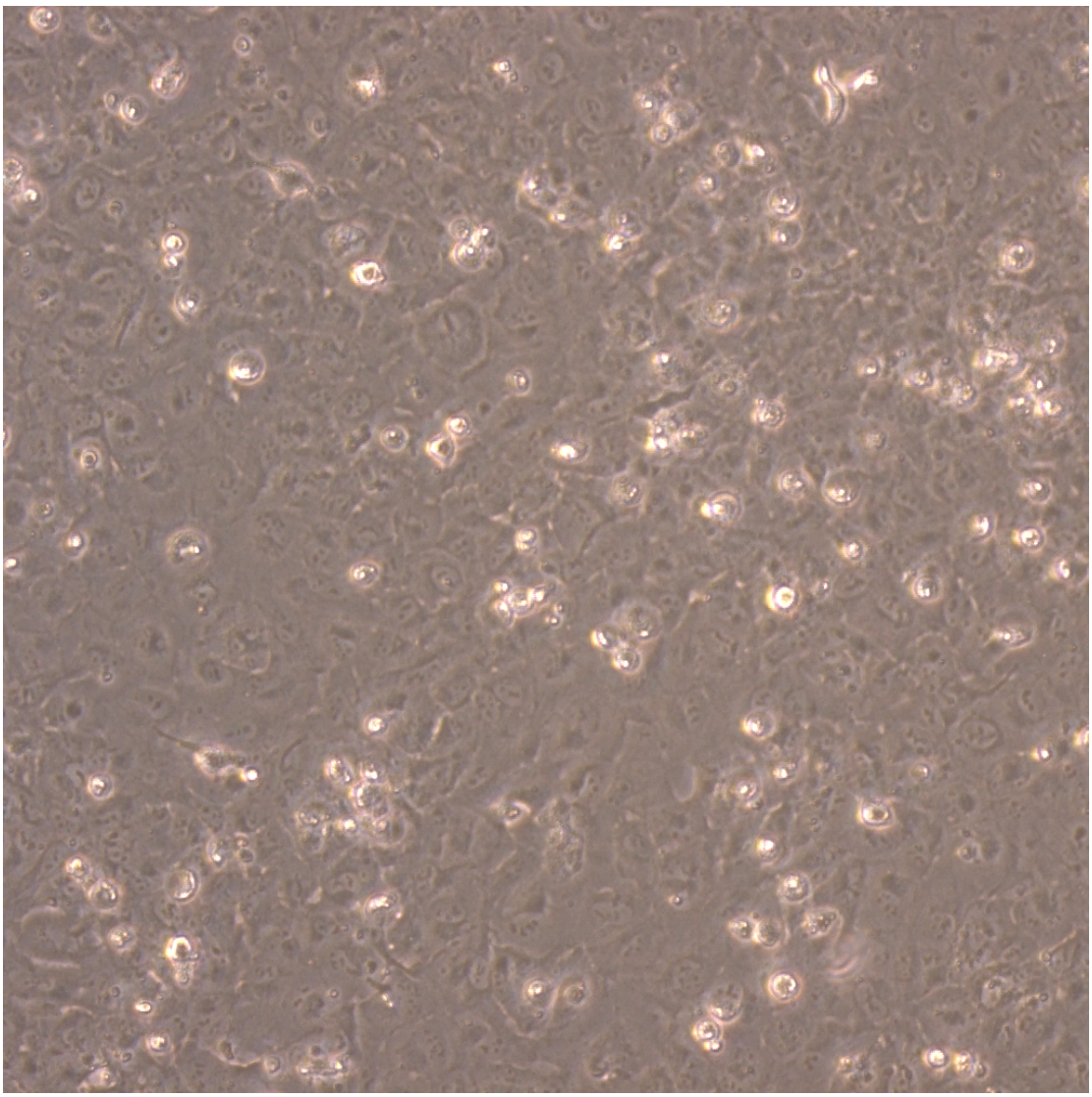

VH-Only cell morphology upon tetracycline induction

Images taken of VH-Only clone C after 72 hours tetracycline induction of expression. Images were taken with a 10x Objective lens.

Cells appear enlarged and flattened, without distinct membrane definition.

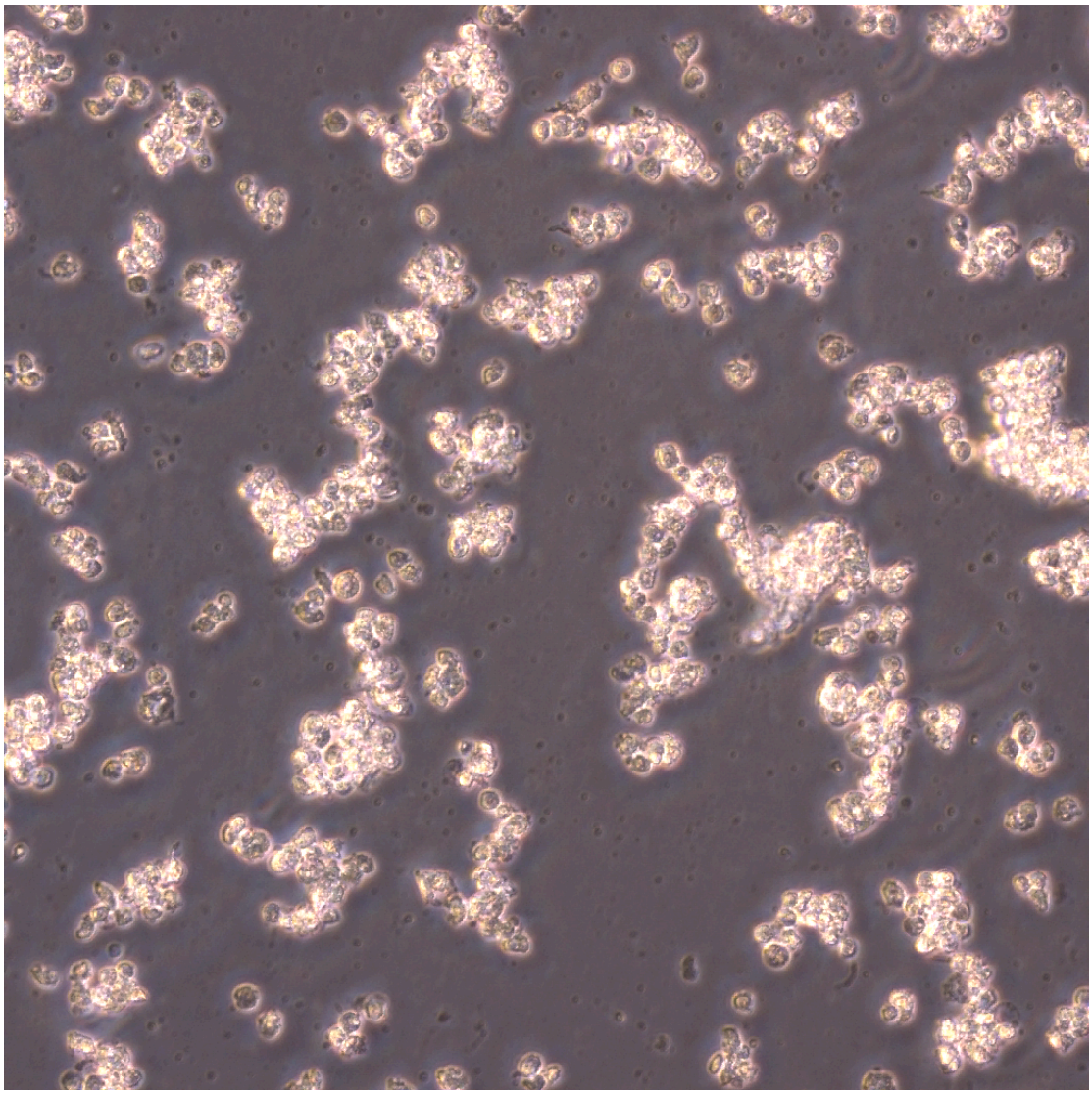

VH+VL cell morphology upon tetracycline induction

Images taken of VH+VL clone C after 72 hours tetracycline induction of expression. Images were taken with a 10x Objective lens.

All cells are dead and detached from the culture vessel.

Appendix I

Assessment of morphological changes upon AIDA construct expression

The effects of Tet-induced VH/VL-proCASP3 variant was assessed by examining changes in the morphology of expressing cells. Light microscope images were taken after 48 hours of expression at 10x magnification. Uninduced samples are shown form comparison (continued on next page). None show an obvious death effect as seen with VH+VL (Appendix H).

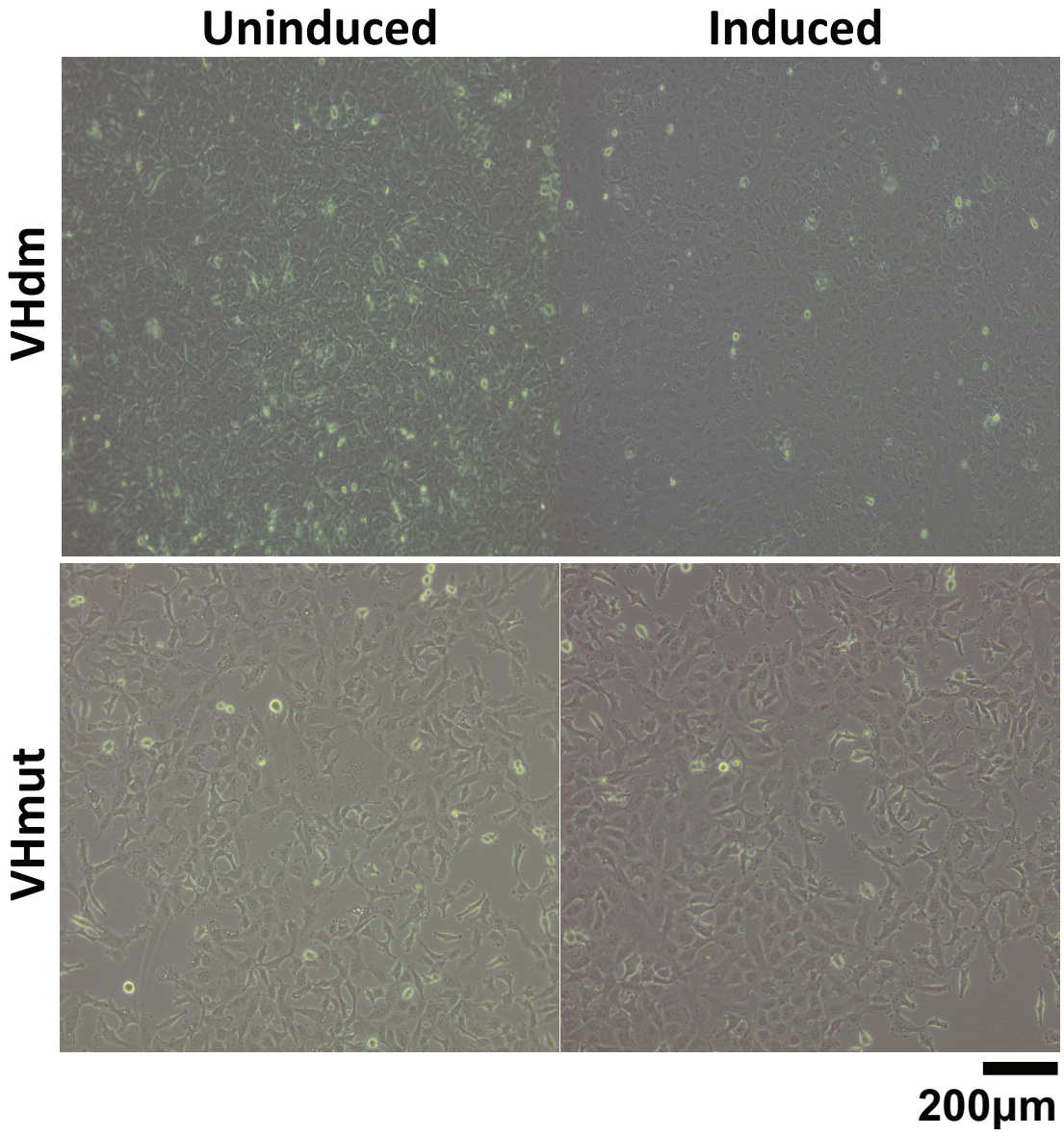

(continued from previous page)

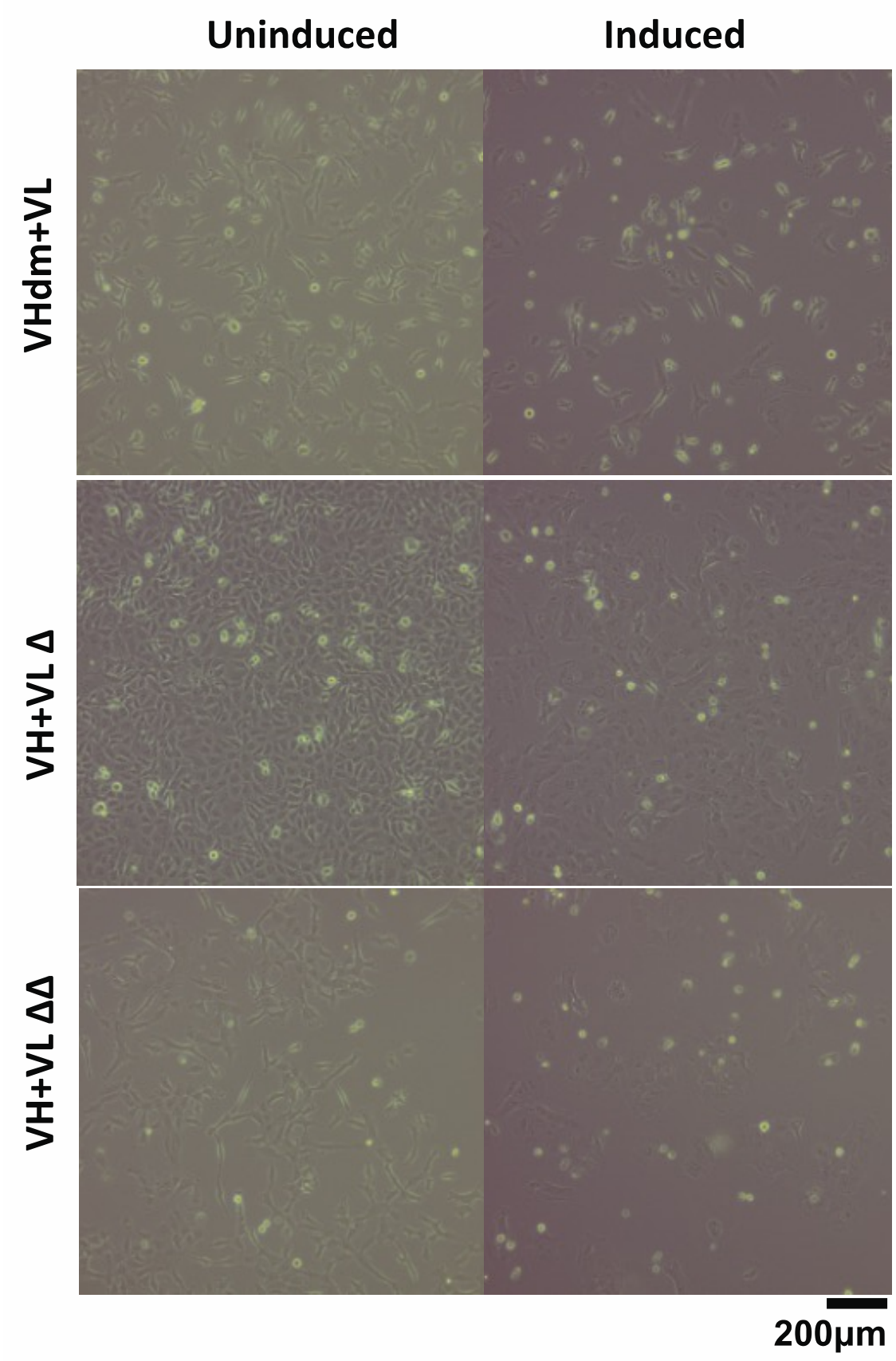

Appendix J

Clone Type	Clones	Total replicates	Conditions	Average Cell Cycle Distribution (%)			
				Sub G1	G1	S	G2/M
Parent	N/A	8	Uninduced	0.5	62.1	10.3	26.8
		8	Induced	0.5	65.4	11.9	21.9
		4	Etoposide	3.2	49.0	18.6	29.0
VH + VL	ABC	12	Uninduced	0.4	66.3	7.3	25.9
		12	Induced	45.3	32.3	16.7	5.6
VH-Only	ABC	12	Uninduced	1.8	62.7	9.2	20.6
		12	Induced	8.9	67.3	15.2	8.5
VL-Only	ABC	10	Uninduced	0.7	56.4	16.7	25.9
		10	Induced	1.5	55.9	16.7	25.1
VH+VL Δ	AB	5	Uninduced	1.6	74.1	7.7	16.6
		5	Induced	12.1	75.4	8.7	3.8
VH+VL ΔΔ	A	5	Uninduced	0.3	59.6	12.6	27.5
		5	Induced	7.0	76.1	7.7	9.2
VHdm + VL	ABC	12	Uninduced	0.4	58.2	8.8	32.6
		12	Induced	9.5	44.8	28.8	10.7
VHmut-Only	ABC	8	Uninduced	0.5	49.7	11.3	36.1
		8	Induced	0.5	51.6	12.6	33.8
VH-Only Δ	AB	8	Uninduced	1.3	60.7	11.3	25.8
		8	Induced	11.5	57.5	20.5	10.5
VHdm-Only	A	1	Uninduced	3.8	76.2	9.3	10.8
		1	Induced	16.2	2.0	71.8	10.0

Cell Cycle data

The full set of averaged cell cycle population data (derived from figure 4.7) are represented, indicating the number of clones and replicates tested. All measurements were performed after 48 hours in repective growth conditions (etoposide treatment was applied for the last 8 hours of the experiment). Column headings describe the respective cell cycle phases occupied by cells from each clone when expresion of the AIDA fragments is induced with tetracycline.

Appendix K

Luciferase reporter assay data

The full set of raw and averaged firefly and renilla luciferase assay data is shown, including the firefly:renilla ratios and the relative fold activity of each sample

Reaction		Firefly Luiferase Readings (Fluorescence Units)			Renilla Luciferase Reading			Firefly:Renilla Readings			Average	Fold Activity
		1	2	3	1	2	3	1	2	3		
Untransfected		397.68	513.23	310.04	515.97	489.17	561.94	0.77	1.05	0.55	0.79	N/A
Empty Vector		688.15	638.44	566.16	1065.62	1074.63	1139.33	0.65	0.59	0.50	0.58	1.00
VH#Y6	VL#204	17803.80	16994.19	18680.96	539.15	344.04	509.71	33.02	49.40	###	39.69	68.56
	VL#I21	5475.65	5356.51	5557.93	406.96	477.21	373.76	13.45	11.22	###	13.18	22.77
	VL#819	1179.03	944.53	1161.43	482.47	568.27	525.56	2.44	1.66	2.21	2.11	3.64
	VL#826	965.76	763.37	701.35	471.57	475.92	351.22	2.05	1.60	2.00	1.88	3.25
	VL#827	2238.65	2297.11	2222.37	422.12	541.82	474.63	5.30	4.24	4.68	4.74	8.19
VH#Y6dm	VL#204	4392.88	4587.90	5665.81	449.41	370.97	374.35	9.77	12.37	###	12.43	21.46
	VL#I21	2063.94	1888.17	2016.55	648.06	438.51	371.88	3.18	4.31	5.42	4.30	7.44
	VL#819	649.14	927.37	642.22	517.43	408.06	469.20	1.25	2.27	1.37	1.63	2.82
	VL#826	555.32	505.06	629.05	443.12	381.30	468.56	1.25	1.32	1.34	1.31	2.26
	VL#827	380.39	455.58	523.29	456.17	346.93	433.67	0.83	1.31	1.21	1.12	1.93
VH#Y6mut	VL#204	722.01	716.25	782.21	675.24	504.29	406.64	1.07	1.42	1.92	1.47	2.54
	VL#I21	409.50	625.75	758.29	420.27	466.73	392.98	0.97	1.34	1.93	1.41	2.44
	VL#819	468.78	422.35	574.43	356.98	559.86	525.18	1.31	0.75	1.09	1.05	1.82
	VL#826	465.15	443.56	466.90	494.86	363.85	489.32	0.94	1.22	0.95	1.04	1.79
	VL#827	463.08	446.22	595.79	490.19	505.13	540.28	0.94	0.88	1.10	0.98	1.69

Appendix L

Clonogenic Assay – Full data set

Clone	Plating Density	Growth Conditions	Plate 1	Plate 2	Plate 3	Average	Std Dev	Plating Efficiency (PE)	Surviving Fraction (SF)	%PE	%SF
VH+VL A	20 cell	Uninduced	25	11	14	16.67	7.37	0.89		89.1	0.2
	50 cell	Uninduced	37	50	46	44.33	6.66				
	100 cell	Uninduced	90	96	100	95.33	5.03				
	20 cell	Induced	0	0	0	0.00	0.00		0.00		
	50 cell	Induced	0	0	0	0.00	0.00				
	100 cell	Induced	2	0	0	0.67	1.15				
VH+VL B	20 cell	Uninduced	23	20	19	20.67	2.08	0.99		99.1	0
	50 cell	Uninduced	51	51	56	52.67	2.89				
	100 cell	Uninduced	92	81	93	88.67	6.66				
	20 cell	Induced	0	0	0	0.00	0.00		0.00		
	50 cell	Induced	0	0	0	0.00	0.00				
	100 cell	Induced	0	0	0	0.00	0.00				
VH+VL C	20 cell	Uninduced	18	14	7	13.00	5.57	0.71		71	0
	50 cell	Uninduced	37	39	39	38.33	1.15				
	100 cell	Uninduced	53	78	83	71.33	16.07				
	20 cell	Induced	0	0	0	0.00	0.00		0.00		
	50 cell	Induced	0	0	0	0.00	0.00				
	100 cell	Induced	0	0	0	0.00	0.00				
VL-Only A	20 cell	Uninduced	20	15	14	16.33	3.21	0.81		80.8	98.1
	50 cell	Uninduced	33	54	43	43.33	10.50				
	100 cell	Uninduced	66	71	85	74.00	9.85				
	20 cell	Induced	15	12	21	16.00	4.58		0.98		
	50 cell	Induced	39	46	35	40.00	5.57				
	100 cell	Induced	89	75	69	77.67	10.26				
VL-Only B	20 cell	Uninduced	24	22	19	21.67	2.52	1.08		107.7	94
	50 cell	Uninduced	63	51	51	55.00	6.93				
	100 cell	Uninduced	107	97	110	104.67	6.81				
	20 cell	Induced	23	20	23	22.00	1.73		0.94		
	50 cell	Induced	58	51	45	51.33	6.51				
	100 cell	Induced	99	96	78	91.00	11.36				
VL-Only C	20 cell	Uninduced	19	17	16	17.33	1.53	0.87		87	111
	50 cell	Uninduced	47	50	40	45.67	5.13				
	100 cell	Uninduced	81	84	84	83.00	1.73				
	20 cell	Induced	20	16	24	20.00	4.00		1.11		
	50 cell	Induced	51	51	39	47.00	6.93				
	100 cell	Induced	88	98	104	96.67	8.08				
Parent	20 cell	Uninduced	12	10	11	11.00	1.00	0.67		66.6	102.8
	50 cell	Uninduced	26	39	42	35.67	8.50				
	100 cell	Uninduced	78	68	74	73.33	5.03				
	20 cell	Induced	14	23	13	16.67	5.51		1.03		
	50 cell	Induced	31	31	29	30.33	1.15				
	100 cell	Induced	56	59	69	61.33	6.81				
VH-Only A	20 cell	Uninduced	11	19	16	15.33	4.04	0.80		79.6	59.5
	50 cell	Uninduced	45	37	44	42.00	4.36				
	100 cell	Uninduced	88	67	79	78.00	10.54				
	20 cell	Induced	6	10	20	12.00	7.21		0.59		
	50 cell	Induced	30	15	16	20.33	8.39				
	100 cell	Induced	48	45	31	41.33	9.07				
VH-Only B	20 cell	Uninduced	24	12	15	17.00	6.24	0.98		98	81.5
	50 cell	Uninduced	49	55	60	54.67	5.51				
	100 cell	Uninduced	112	96	91	99.67	10.97				
	20 cell	Induced	17	11	20	16.00	4.58		0.82		
	50 cell	Induced	38	46	32	38.67	7.02				
	100 cell	Induced	80	94	73	82.33	10.69				
VH-Only C	20 cell	Uninduced	24	13	18	18.33	5.51	0.97		97.1	87.4
	50 cell	Uninduced	57	51	(spilled)	54.00	4.24				
	100 cell	Uninduced	108	87	80	91.67	14.57				
	20 cell	Induced	20	14	15	16.33	3.21		0.87		
	50 cell	Induced	44	44	44	44.00	0.00				
	100 cell	Induced	89	82	84	85.00	3.61				

Clonogenic Assay – Full data set continued

Clone	Plating Density	Growth Conditions	Plate 1	Plate 2	Plate 3	Average	Std Dev	Plating Efficiency (PE)	Surviving Fraction (SF)	%PE	%SF
VHmut-Only A	20 cell	Uninduced	15	13	17	15.00	2.00	0.69		68.9	97.7
	50 cell	Uninduced	27	38	33	32.67	5.51				
	100 cell	Uninduced	68	64	67	66.33	2.08				
	20 cell	Induced	16	13	10	13.00	3.00		0.98		
	50 cell	Induced	33	24	39	32.00	7.55				
	100 cell	Induced	72	74	73	73.00	1.00				
VHmut-Only B	20 cell	Uninduced	21	22	25	22.67	2.08	0.93		92.8	89.9
	50 cell	Uninduced	37	39	43	39.67	3.06				
	100 cell	Uninduced	98	81	78	85.67	10.79				
	20 cell	Induced	17	17	16	16.67	0.58		0.90		
	50 cell	Induced	38	44	46	42.67	4.16				
	100 cell	Induced	85	68	92	81.67	12.34				
VHdm-Only A	20 cell	Uninduced	6	11	9	8.67	2.52	0.55		55.4	114
	50 cell	Uninduced	36	35	34	35.00	1.00				
	100 cell	Uninduced	68	48	43	53.00	13.23				
	20 cell	Induced	17	14	9	13.33	4.04		1.14		
	50 cell	Induced	33	24	33	30.00	5.20				
	100 cell	Induced	59	73	57	63.00	8.72				
VHdm+VL A	20 cell	Uninduced	8	13	10	10.33	2.52	0.60		59.8	32
	50 cell	Uninduced	30	35	28	31.00	3.61				
	100 cell	Uninduced	75	63	59	65.67	8.33				
	20 cell	Induced	3	5	5	4.33	1.15		0.32		
	50 cell	Induced	9	12	9	10.00	1.73				
	100 cell	Induced	11	21	15	15.67	5.03				
VHdm+VL B	20 cell	Uninduced	20	17	17	18.00	1.73	0.91		90.9	35.8
	50 cell	Uninduced	47	40	48	45.00	4.36				
	100 cell	Uninduced	109	91	78	92.67	15.57				
	20 cell	Induced	5	4	9	6.00	2.65		0.36		
	50 cell	Induced	18	20	17	18.33	1.53				
	100 cell	Induced	33	23	37	31.00	7.21				
VHdm+VL C	20 cell	Uninduced	20	12	8	13.33	6.11	0.68		67.7	71.4
	50 cell	Uninduced	30	41	32	34.33	5.86				
	100 cell	Uninduced	69	81	53	67.67	14.05				
	20 cell	Induced	4	11	14	9.67	5.13		0.71		
	50 cell	Induced	24	28	25	25.67	2.08				
	100 cell	Induced	43	53	40	45.33	6.81				
VH+VL Δ A	20 cell	Uninduced	24	28	20	24.00	4.00	1.09		109	52.2
	50 cell	Uninduced	62	53	49	54.67	6.66				
	100 cell	Uninduced	101	92	100	97.67	4.93				
	20 cell	Induced	9	8	15	10.67	3.79		0.52		
	50 cell	Induced	33	31	34	32.67	1.53				
	100 cell	Induced	55	47	54	52.00	4.36				
VH+VL Δ B	20 cell	Uninduced	10	16	10	12.00	3.46	0.57		57.3	105.8
	50 cell	Uninduced	26	34	28	29.33	4.16				
	100 cell	Uninduced	49	61	50	53.33	6.66				
	20 cell	Induced	8	12	23	14.33	7.77		1.06		
	50 cell	Induced	31	30	21	27.33	5.51				
	100 cell	Induced	61	55	51	55.67	5.03				
VH+VL ΔΔ A	20 cell	Uninduced	14	14	18	15.33	2.31	0.90		89.9	17.4
	50 cell	Uninduced	50	50	45	48.33	2.89				
	100 cell	Uninduced	102	91	96	96.33	5.51				
	20 cell	Induced	2	4	3	3.00	1.00		0.17		
	50 cell	Induced	8	8	7	7.67	0.58				
	100 cell	Induced	17	19	14	16.67	2.52				

Appendix M

Tripartite GFP assay full data set

Data set from the expanded tripartite GFP reconstitution assay. The measurements were performed in duplicate.

				1	2
Antigen	**GFP1-9**	**VH-GFP11**	**VL-GFP10**	**% GFP+**	**% GFP+**
None	None	None	None	0.17	0.12
LMO2	GFP1-9	VH#576	VL#204	16.6	19.9
			VL#I21	16.4	15.6
			VL#819	13.8	11.5
			VL#826	8.53	7.9
			VL#827	2.02	1.99
		VH#Y6	VL#204	42.5	37.3
			VL#I21	26.9	24.2
			VL#819	6.08	6.07
			VL#826	4.8	5.22
			VL#827	0.72	0.83
KRAS		VH#576	VL#204	16.1	13.9
			VL#I21	10.4	11.1
			VL#819	10.7	13.6
			VL#826	6.02	7
			VL#827	1.26	1.36
		VH#Y6	VL#204	51.6	50.5
			VL#I21	38.3	41.4
			VL#819	11.2	9.09
			VL#826	6.3	7.16
			VL#827	16.1	13.9
		VH#Y6dm	VL#204	29.1	31
			VL#I21	34.5	34
			VL#819	11.2	8.81
			VL#826	6.04	6.55
			VL#827	1.27	1.34
		VH#Y6mut	VL#204	6.77	7.27
			VL#I21	7.45	7.15
			VL#819	5.06	5.11
			VL#826	5.41	5.46
			VL#827	1	0.94